UNIVERSITY OF CALIFORNIA, SAN DIEGO

Mechanoelectric Feedback in Ventricular Myocardium

A dissertation submitted in partial satisfaction of the
requirements for the degree Doctor of Philosophy in
Bioengineering

by

Frederick J. Vetter

Committee in charge:

Professor Andrew D. McCulloch, Chair
Professor Scott B. Baden
Professor James W. Covell
Professor Mark H. Ellisman
Professor Gregory K. Feld

1999

The dissertation of Frederick J. Vetter is approved, and it is acceptable in quality and form for publication on microfilm:

Chair

University of California, San Diego

1999

TABLE OF CONTENTS

LIST OF SYMBOLS

a , b	ellipsoidal geometry semi-major and semi-minor radii
α , γ	mechanosensitive conductance parameters
b_i , C	passive material parameters
D_{ij}	conductivity tensor components
d	focus in prolate spheroidal coordinates
E_{ij}	Lagrangian Green's strain tensor components
η	fiber angle
$\tilde{f}$	applied forces vector
β	mechanosensitive channel constant conductance
G_{ms}	mechanosensitive channel saturation conductance
$g_{ms}(\cdot)$	stretch-dependent current conductance
h	wall thickness
h_I , h_S	imaged and sectioned wall thickness
I_i	strain invariant
I_{ms}	stretch-dependent current
$\mathbf{K}$	global tangent stiffness matrix
$\mathbf{K}_e$	element stiffness matrix
$\mathbf{L}$, $\mathbf{U}$	lower- and upper-triangular factors of $\mathbf{K}$
$\mathbf{M}$	preconditioning matrix
$\mathbf{N}_e$	Boolean connectivity matrix
N^e	number of finite elements
N^P	number of processors
p	hydrostatic pressure
R	ratio of unconstrained to constrained residuals
S_i	finite element arc length
σ_{ij}	Cauchy stress tensor components

T_{ij}	second Piola-Kirchhoff stress tensor components
$\tilde{u}$	solution vector
$\tilde{u}^i$	approximation of $\tilde{u}$ at iteration i
V_m	cellular transmembrane voltage
V_r	mechanosensitive channel reverse potential
$\tilde{v}^i$	subspace basis vector
W	strain energy function
y_k	minimizer of residual norm
$(x_1,\ x_2,\ x_3)$	rectangular Cartesian coordinates
$(\lambda,\ \mu,\ \theta)$	prolate spheroidal coordinates
$(\xi_1,\ \xi_2,\ \xi_3)$	isoparametric finite element coordinates

LIST OF FIGURES

LIST OF TABLES

ACKNOWLEDGEMENTS

This dissertation is the result of nearly six years of bioengineering study at the University of California San Diego. I conducted the research described herein as a member of the Cardiac Mechanics Research Group in the Department of Bioengineering under the supervision of Dr. Andrew McCulloch. The first chapter describes ventricular anatomy, mechanics and electrophysiology, and mechanoelectric feedback. Chapter II details the development of a three-dimensional finite element model of the rabbit ventricular geometry and fiber architecture. Parts of Chapters I and II have been published in *Progress in Biophysics and Molecular Biology* (vol. 69:157-184, 1998). In Chapter III the model is used to investigate passive ventricular mechanics of the rabbit heart; this chapter is being prepared for submission to a biomedical engineering journal. Chapter IV describes a modeling study of electrical propagation through unloaded and deformed myocardium. In Chapter V, which is also being prepared for submission, possible mechanisms of mechanoelectric feedback are investigated through modeling studies of the effect of regional myocardial deformation on action potential morphology.

I thank the members of my Doctoral Committee for their contributions to the success of this effort. Dr. Andrew McCulloch provided the overall guidance for my project and was instrumental in securing the various required resources. Dr. Scott Baden introduced me to parallel computing and was extremely helpful in relating abstract theory to my particular problem. Drs. James Covell and Greg Feld kept me focused on the scientific questions of cardiac function, thus preventing me from developing "just another mouse trap." Dr. Mark Ellisman was invaluable as an objective scientific observer, requiring me to clearly communicate the importance of questions to be answered and the contributions of my research efforts.

I have been fortunate to draw on the expertise of many people to complete this work. Rish Pavelec provided me with the hearts from which I collected the raw data for the anatomic model described in Chapter II. Drs. Alistair Young, Peter

Hunter, and Ian LeGrice provided much needed advice during the development of the model. Dr. Kevin Costa was an invaluable source of information when I began using our finite element program. Dr. Ann Marie Gallagher was generous to discuss her experiments in detail, and to provide me with her raw data. Dr. Jack Rogers provided frequent and detailed answers to my (sometimes nonsensical) questions regarding the collocation-Galerkin finite element method. Dr. Andy Pollard was helpful with discussions about action potential models, and with Dr. Delilah Huelsing provided several computer implementations of the models. Mark Mitchiner, Kris Virtue, Mark Duffield, Drew Schaffner, Linh Vu, and Nathan Wiger kept our departmental computing system up and running. Drs. Bill Karlon and Walt Baxter provided helpful technical advice and sanity checks. Reza Mazhari was a fun officemate, and we share the same interest in the newsgroups. Sara Vaplon was helpful with data analysis methods, discussions of collagen structure and function, and her love of kids. Several undergraduate students collected fiber orientation data. Scott Moonly sacrificed his weekends to section tissue and repair lab equipment. Jessica Wagenseil, Stephanie Pao, Ji Lu, and Phil Baddour also collected data, developed experimental procedures, or implemented computer models. All the members of CMRG provided support, ideas, and helpful criticism during our Friday morning lab meetings.

My wife Carol has been my single enduring source of stability throughout this effort. Her professional and personal advice carried me through this project. Her support and that of my family never wavered over the last six years.

My first three years of study were supported by the Department of Bioengineering under the NIH Predoctoral Training Grant. National Science Foundation Grant BES-9634974 supported my remaining years, and the supercomputer resources were provided through the National Biomedical Computational Resource NIH RR08065.

VITA

April 23, 1960	Born, Bakersfield, California
1984	B. S. Electrical Engineering, University of California, Davis
1984-1986	Systems Engineer, Signal Science Inc., Santa Clara California
1988	M. S. Electrical Engineering, University of California, Davis
1989	M. B. A. University of California, Davis
1993-1996	Fellow, NIH Training Grant, University of California, San Diego
1994	M. S. Bioengineering, University of California, San Diego
1999	Doctor of Philosophy University of California, San Diego

PUBLICATIONS

Manuscripts:

Vetter F. J. and McCulloch A. D. Three-Dimensional Analysis of Regional Cardiac Function: A Model of Rabbit Ventricular Anatomy. Progress in Biophysics and Molecular Biology, 69(2-3):157-184 (1998)

Abstracts:

Vetter F. J., Rogers J. M., and McCulloch A. D. A Finite Element Model of Passive Mechanics and Electrical Propagation in the Rabbit Ventricles. Computers in Cardiology 1998 vol. 25, pp. 705–708, September 13-16, 1998, Cleveland OH. IEEE Press, 1998

McCulloch A. D. and Vetter F. J. Anatomically Accurate Finite Element Model of Cardiac Electromechanical Interactions. First International Interdisciplinary Conference on Cardiovascular Medicine, Surgery, Science, and Mechanics, June 6-9, 1997 Washington, DC

Vetter F. J. and McCulloch A. D. A Finite Element Model of the Rabbit Ventricular Geometry. Annals of Biomedical Engineering, 24(Suppl. 1):S-44 (Sep/Oct 1996).

FIELDS OF STUDY

Major Field: Bioengineering

Studies in Applied Mathematics.
Professor Audrey A. Terras, University of California, San Diego

Studies in Biomechanics.
Professor Andrew D. McCulloch, University of California, San Diego

Studies in Physiology.
Professor K.-L. Paul Sung, University of California, San Diego

ABSTRACT OF THE DISSERTATION

Mechanoelectric Feedback in Ventricular Myocardium

by

Frederick J. Vetter
Doctor of Philosophy in Bioengineering
University of California, San Diego, 1999
Professor Andrew D. McCulloch, Chair

The influence of three-dimensional diastolic strain on action potential morphology in intact myocardium was investigated in a series of integrative modeling studies. Action potential morphology is known to be altered by stretch of the ventricles — a process known as mechanoelectric feedback. The mechanisms governing this process are not well understood, and experimental investigations are complicated by the three-dimensional anatomy and anisotropy of the heart. Our hypothesis was that nonuniform three-dimensional diastolic strains in the intact myocardium contribute significantly to nonuniform alterations in action potential morphology.

The first objective of this dissertation was to investigate three-dimensional distributions of stress and strain in the passively inflated rabbit left ventricle. A high-order finite element model of the rabbit ventricles was developed that represented the geometry of the heart to within ± 0.55 millimeters and the fiber orientation to within ± 18.6 degrees. We estimated material properties of the passive rabbit ventricular myocardium using the ventricular model and the finite element method on a scalable parallel processing computer. Simulations of passive left ventricular inflation to 25 mm Hg pressure required 5.3 hours. Predicted epicardial fiber and cross fiber strains were within the accuracy of experimental measurements. The results suggest that transmural fiber strain is relatively uniform and cross fiber strain increases from epicardium to endocardium. Predicted Cauchy stress was generally

higher in the fiber direction than the cross fiber direction. Rabbit myocardium may be more stiff than that of the canine or rat.

The second objective of this dissertation was to investigate possible mechanisms governing mechanoelectric feedback in the intact myocardium. Previous theories based on experimental observations and models of mechanoelectric coupling have focused on changes in length of the myofiber or sarcomere as the primary governing mechanical stimulus. Our results suggest that fiber strain alone cannot account for the transmural variation in action potential amplitude in response to stretch. A model of mechanosensitive conductance based on fiber and cross fiber strain produced both the reduction in epicardial action potential amplitude and corresponding transmural gradient. Mechanoelectric feedback may thus be governed by deformation other than changes in fiber length.

Chapter I

Introduction

The physiology of the heart depends on cellular ionic mechanisms that govern the electrical propagation and mechanical contraction and relaxation in myocardium. While much is known about these mechanisms at the cellular level, relating how these mechanisms interact regionally to alter electrical function in the ventricles is greatly complicated by the three-dimensional anatomy of the heart.

The structure of the heart is three-dimensional. The stresses and strains developed throughout the cardiac cycle depend on the thickness, curvatures, and fiber orientation in tissue, all of which vary regionally. The left ventricular endocardium and subendocardium display larger deformations than the outer regions of the wall. In addition, the material properties are anisotropic: myocardium is generally more stiff in the fiber direction than in the cross fiber direction. Electrical properties of myocardium are also anisotropic. The action potential is conducted faster in the direction of the myofiber than in the transverse plane. Duration of the action potential diminishes in the transverse fiber direction, but is unchanged when propagating parallel to the fibers. The velocity of the propagating wave slows when the wavefront has a negative curvature (i.e., is curved away from the direction of propagation), but is accelerated with a positive curvature. Alterations in action potential duration and velocity may lead to reentrant arrhythmia, and possibly degenerate into fibrillation. Thus the mechanics and electrophysiology of the

heart are greatly influenced by the three-dimensional geometry, fiber orientation, and anisotropy of intact myocardium.

Excitation-contraction coupling, the process by which an electrical stimulus initiates calcium influx to the cardiac myocyte resulting in mechanical contraction, is typically considered to be the process that governs beat-to-beat function in the heart. There is evidence, however, that a feedback pathway exists, whereby the electrical characteristics of myocardium are altered by the mechanical state of the tissue. This phenomena of mechanoelectric feedback may play a significant role in the regulation of normal electrical function and the genesis of arrhythmias.

The discovery of mechanosensitive ion channels [32, 183] in myocardium has led to speculation that these cellular structures are responsible for the mechanical sensitivity of electrical processes in the intact heart. Relating how these structures affect electrical function, however, is complicated by the three-dimensional anatomy of the heart. The studies presented in this dissertation investigated regional mechanics, electrical characteristics, and their interaction in the intact ventricular myocardium. Our hypothesis was that nonuniform three-dimensional diastolic strains in the intact myocardium contribute significantly to nonuniform alterations in action potential morphology.

I.A Ventricular Structure

I.A.1 Geometry

From the perspective of engineering mechanics, the ventricles are three-dimensional thick-walled pressure vessels with substantial variations in wall thickness and curvature both regionally and temporally throughout the cardiac cycle. The ventricular walls in the normal heart are thickest at the equator and base of the left ventricle and thinnest at the left ventricular apex and right ventricular free wall [13]. There are also variations in the principal dimensions of the left ventricle with species, age, phase of the cardiac cycle, and disease. But, in general, the ratio

of wall thickness to radius is too high to be treated accurately by all but the most sophisticated thick-wall shell theories [163].

Ventricular geometry has been studied in most quantitative detail in the dog heart [108, 159]. Geometric models have been very useful in the analysis, especially the use of confocal and nonconfocal ellipses of revolution to describe the epicardial and endocardial surfaces of the left and right ventricular walls. The canine left ventricle is reasonably modeled by a thick ellipsoid of revolution truncated at the base. The right ventricle wraps about 180 degrees around the heart wall circumferentially and extends longitudinally roughly two-thirds of the distance from the base to the apex. Using a truncated ellipsoidal model, left ventricular geometry in the dog can be defined by the major and minor radii of two surfaces, the left ventricular endocardium, and a surface defining the free wall epicardium and the septal endocardium of the right ventricle. Streeter and Hanna (1973) described the position of the basal plane using a truncation factor f_b defined as the ratio between the longitudinal distances from equator-to-base and equator-to-apex. Hence, the overall longitudinal distance from base to apex is $(1 + f_b)$ times the major radius of the ellipse. Since variations in f_b between diastole and systole are relatively small (0.45 to 0.51), they suggested a constant value of 0.5.

I.A.2 Myofiber Architecture

The cardiac ventricles have a complex three-dimensional muscle fiber architecture [161, 168]. Myocytes are approximately 120 μm long [52] and are connected such that in the normal heart wall there is a predominant fiber axis that is approximately tangent with the wall (within 10 degrees in most regions, except near the apex and papillary muscle insertions) [161]. Each ventricular myocyte is connected via gap junctions at intercalated disks to an average of 11.3 ± 2.2 neighbors [145]. From the sixteenth century studies of Vesalius up to 1942 [170, 131], investigators dissected discrete bundles of fibrous swirls, but modern histological techniques have shown that in the plane of the wall the muscle fiber angle makes a smooth transmu-

species	epi (°)	endo (°)	range (°)	h (mm)	source
rat	-49	51	100	—	[112]
guinea pig ED	-67	63	130	—	[67]
rabbit	-60	50	110	2	[51]
macaque	-65	65	130	6	[161]
dog ES	-59	68	127	12.1	[160]
dog ES	-40	49	89	—	[162]
dog unloaded	-80	54	134	—	[108]
dog ED	-63	52	115	9.3	[160]
dog ED	-63	49	112	—	[162]
dog ED	-70	34	104	—	[67]
pig	-51	70	121	13	[65]
pig ES	-79	54	133	—	[158]
human	-56	49	105	—	[118]
human	-57	49	106	12.6	[119]
mean ± SD	-61.4 ± 10.9°	54.1 ± 9.5°	115.4 ± 14°		

Table I.1: Left ventricular epicardial and endocardial fiber orientation and wall thickness for several species. ES: end-systole, ED: end-diastole. Fiber orientations for "dog unloaded" are from a fitted finite element model [108].

ral transition from epicardium to endocardium [55]. Similar patterns have been described for humans [119], dogs [162], macaques [137], pigs [158], rabbits [51], guinea pigs [67], and rats [112]. In man the muscle fiber angle typically varies continuously from about -60 degrees (i.e. 60 degrees clockwise from the circumferential axis) at the epicardium to about $+50$ degrees at the endocardium. Fiber orientation is relatively well conserved across species, with mean epicardial and endocardial fiber angles of -61.4 and 54.1 degrees, respectively (Table I.1).

Except at the junction between the right ventricular free wall, septum, and endocardium near the papillary muscle insertions, regional variations in ventricular

myofiber orientations are generally smooth [157]. A detailed study in the dog that mapped fiber angles throughout the entire right and left ventricles described the same general transmural pattern in all regions including the septum and right ventricular free wall, but with distinct regional variations [108]. Transmural differences in fiber angle were about 120–140 degrees in the left ventricular free wall, larger in the septum (160–180 degrees), and smaller in the right ventricular free wall (100–120 degrees). There are also small increases in LV fiber orientation from end-diastole to systole (4–23 degrees), with greatest changes at the epicardium and apex [160, 162]. Recent studies utilizing diffusion tensor MRI have validated the technique as a useful tool for reconstructing fiber orientation of the intact ventricle, and show promise for measuring the laminar sheet structure [147].

Collagen is the major structural protein in connective tissues but only comprises 2–5% of the myocardium by weight, compared with the myocytes which make up 90% [175]. The interstitial collagen matrix has a hierarchical organization and has been classified according to conventions established for skeletal muscle into endomysium, perimysium, and epimysium [22, 132]. The endomysium is associated with individual cells and includes a fine weave surrounding the cell and transverse structural connections connecting adjacent myocytes, with attachments localized near the z-line of the sarcomere. The perimysium groups cells together and includes large coiled fibers typically 1–3 microns in diameter composed of smaller collagen fibrils (40–50 nm) [133]. Perimysial collagen fibers wrap layers of cells into laminar sheets 3–4 cells thick which radially traverse the ventricular wall [84]. Finally, a thick epimysial collagen sheath surrounds the entire myocardium forming the protective epicardium (visceral pericardium) and endocardium.

I.B Passive Left Ventricular Mechanics

I.B.1 Experimental Investigations

The distribution of wall stress in the myocardium is fundamentally important because it affects ventricular pumping performance, myocardial oxygen demand, coronary blood flow, vulnerability to injury, myocyte growth and remodeling, and action potential shape and propagation [100, 101]. No reliable methods have been developed to measure the three-dimensional stress tensor in the intact heart wall primarily because of its large deformations and the tissue injury caused by implanted transducers [69]. However, methods have been developed to measure regional distributions of two- and three-dimensional deformations in the resting and beating canine, rat, and mouse heart using ultrasonic crystals [111, 171] and biplane video imaging or radiography of closely spaced material markers [172, 173, 113, 102]. MRI tagging methods have been used to measure three-dimensional ventricular strain distributions non-invasively [186, 3, 103]. These experiments have shown substantial regional and transmural strain heterogeneity even in the healthy heart, and provide data to validate models of ventricular mechanics.

Distributions of stress in the heart are governed by the three-dimensional structure of the ventricular walls, the material properties of the myofibers, and the collagen matrix in the relaxed and actively contracting states, and the boundary conditions imposed by cavity pressures and structures such as the valve annulus, chordae tendineae, pericardium and lungs. Many of these factors have been measured in the laboratory, including geometry and myocardial fiber architecture [159, 160, 108], laminar myofiber sheet orientations [84, 27], and passive and active uniaxial mechanical properties of isolated cardiac muscle [122, 167]. Although fully triaxial material testing still presents significant difficulties, biaxial stress-strain testing has been performed in freshly excised specimens of rabbit [90] and canine LV myocardium [185, 109], epicardium [70], and pericardium [82].

I.B.2 Mechanics Models

Theoretical models are needed to understand cardiac mechanics in terms of regional stress and strain distributions because methods to directly measure regional forces in the intact ventricle have not been entirely successful [69, 184] and triaxial material tests to determine the three-dimensional constitutive properties of myocardium do not yet exist. An accurate model should include the three-dimensional ventricular geometry; fiber and connective tissue architecture; the nonlinear, history-dependent constitutive properties of the myocardium during systole and diastole; and the pressure and displacement boundary conditions. Other important factors include the effects of blood perfusion and residual stress [99, 25, 56].

Many investigators have used the finite element method as a parametric framework for analysis of regional function in the heart as a three-dimensional continuum [11, 187, 125]. The finite element method provides an efficient and accurate means to both develop detailed anatomical continuum models and conduct numerical analyses of biological phenomena. High-order finite element models are typically very compact — they can represent a large number of physical parameters using relatively few model variables ("degrees of freedom" or DOF). Two significant capabilities of the finite element method when applied to cardiac modeling are the ability to represent and analyze irregularly shaped physical domains that may undergo large elastic deformations, and the provision for nonuniform domain discretization.

An accurate and mathematically compact structural model of the ventricular geometry and fiber architecture is prerequisite for simulating the effect of heterogeneous three-dimensional mechanics on the electrical behavior of intact myocardium. Nielsen et al. (1991) developed the first fully three-dimensional finite element model of the canine ventricular geometry and nonuniform fiber distribution. Their model clearly demonstrates the compactness of the finite element formulation by representing over 1,300 measured geometric coordinates with 240 DOF and 8,690 fiber orientation measurements with 396 DOF. This model provided the foundation

for the practical solution of large-scale cardiac stress analyses [26]. The model was recently extended to include the laminar sheet structure of myocardium [83], a feature that will be useful in the study of microstructural influences on mechanical deformation and electrical propagation in myocardium.

Costa et al. (1996) have developed and rigorously validated novel nonlinear finite element methods for the three-dimensional analysis of ventricular wall stress. The Galerkin finite element formulation includes important characteristics of ventricular mechanics such as large deformations, nonlinear elasticity, curvilinear coordinates, three-dimensional anisotropy with respect to continuously varying myofiber axes, muscle contraction, and pressure and displacement boundary conditions [56]. Stress and strain solutions that are converged to within 0.2% can be obtained for a model of the diastolic left ventricle with 16–32 tricubic Hermite elements, and computations can be completed in 1–2 hours on a Silicon Graphics R4400 workstation [26].

Comparing the results of transversely isotropic models [57] with three-dimensional strains measured in the isolated and intact dog heart [172, 113] has shown that these models generally agree very well with the observed strains. Although the present models approximate regional diastolic strains and most components of the strain tensor during systole fairly well, they do not accurately predict the transmural distributions of transverse shear strain components measured during systole [24, 110, 173, 172]. The only other models to include complete results on three-dimensional strains have also demonstrated this limitation [10]. Costa (1996) provided theoretical and experimental evidence that incorporating the effects of myocardial laminae [188, 84, 154] in the models with an appropriate choice of orthotropic material parameters may overcome this limitation. Among other findings, these models have shown that there is substantial regional heterogeneity of ventricular mechanics even under normal conditions [26], with the notable exception of the fiber strain distribution which is comparatively uniform despite significant variations in fiber stress and the strains in other directions [113]. One mechanism of

this fiber strain uniformity is the torsional deformation that results from the helical fiber orientations and the anisotropy of the resting and active myocardium [57].

I.C Cardiac Electrophysiology

I.C.1 Experimental Investigations

The time course of the cardiac action potential is governed by ionic currents via transmembrane channels, pumps, and exchangers which determine the excitability and refractoriness of the tissue. Electrical excitation in the ventricles is nonuniform [40]. Facilitated by the His-Purkinje system, endocardial excitation propagates radially to the epicardium, though the apical and central regions are activated earlier than the base. With respect to the myofibers, propagation is generally 2–4 times faster in the longitudinal than transverse direction [73, 37]. Gotoh et al. (1997) have demonstrated that fiber orientation can significantly affect action potential duration. On the epicardial surface of excised porcine RV tissue, they found that action potentials propagating parallel to the myofibers show no change in duration with distance from the stimulation site. Action potentials propagating transverse to the fiber direction, however, showed a significant decrease in duration with distance. Developing an understanding of cardiac activation and recovery patterns has been difficult because of the geometric and structural complexity of the heart and the fine spatial scale of the activation patterns relative to the whole organ. At the level of the laminar sheets, LeGrice et al. (1995) proposed that the intrinsic conduction velocity transverse to the myofiber is 2–3 times greater in the plane of the sheet than perpendicular to it. Experimental confirmation of this hypothesis is lacking, however, due to the inherent difficulty of measuring conduction patterns and activation times in three-dimensional tissue preparations. Wavefront geometry also plays a role in the speed of the propagating wave, increasing the velocity when the wavefront is curved toward the direction of propagation. When the wavefront curved away from the direction of propagation, the velocity decreases and the wave

may vanish above a critical radius of curvature [43, 16, 15].

Optical methods using potentiometric dyes have been successfully utilized to measure activation patterns in thin (two-dimensional) slices of isolated tissue and on the surface of intact hearts [42]. Davidenko et al. (1992) and Pertsov et al. (1993) reported stable spiral waves of activation in thin slices of sheep and dog epicardium. In three dimensions, though, these reentrant patterns degenerate to polymorphic tachycardia [54] and fibrillation [49].

At the cellular level, significant differences in the transient outward current between the epicardial and endocardial myocytes have been suggested as a reason for the different action potential morphologies in these regions [2]. Cardiomyocytes isolated from the rabbit display a higher action potential plateau amplitude and transient outward current density [44], but shorter action potential duration [23], in the epicardial cells compared to the endocardial cells. Cells isolated from the midmyocardial layers (M cells) of the canine LV show much longer action potential duration at low basic cycle lengths, and have a significantly smaller slow component of the delayed rectifier potassium current than either epicardial or endocardial cells [93]. In addition, early and delayed afterdepolarizations develop more readily in midmyocardial tissue [150, 149]. Hence regional differences in electrophysiology at the cellular level may manifest themselves as nonuniform phenomena at the organ level.

I.C.2 Ionic and Propagation Models

Using the formalism established by Hodgkin and Huxley for nerve cells [64], investigators have incorporated the experimental results from voltage-clamp studies of cardiac cells into increasingly sophisticated models of action potential [130, 7]. Highly detailed models of guinea pig ventricular action potential include background and leakage currents, ionic currents through voltage-gated channels, pumps and exchangers, and intracellular calcium transport between the cytoplasm, sarcoplasmic reticulum and intracellular buffers [94, 95, 191]. These models can simulate many

physiological phenomena, and they describe the underlying mechanisms of early- and delayed-afterdepolarizations and post-extrasystolic potentiation in the single myocyte [96]. Similarly detailed models of the cardiac action potential have also been derived for atrial, sinoatrial node, and Purkinje fiber cells [28, 91, 38, 39]. A model of the canine midmyocardial ventricular action potential including detailed intracellular calcium cycling has most recently been proposed by Winslow et al. (1999), whose analyses suggest that upregulation of the sodium-calcium exchanger protein is sufficient to account for alterations in the calcium transient and action potential duration observed in the failing canine heart.

The most general continuum models of cardiac electrical propagation fall within bidomain theory, which models the intracellular space and the interstitium as two anisotropic domains separated by the cell membrane [138, 123]. Bidomain models are essential for investigating many critical problems such as defibrillation which involve nonhomogeneous distributions of extracellular potential [21, 124, 63]. If the anisotropy of cellular and interstitial conductivity are assumed to be the same (a monodomain formulation), then the problem may be expressed as a three-dimensional extension of the continuous reaction-diffusion equation from cable theory:

$$C_m \frac{\partial}{\partial t} V_m = \nabla \cdot \mathbf{D} \nabla V_m - I_{ion}$$

where C_m is the membrane capacity, V_m and I_{ion} are the transmembrane voltage and ionic current, respectively, $\mathbf{D}$ is the conductivity tensor, and ∇ is the gradient operator. The conductivity tensor is anisotropic, simulating faster conduction in the fiber direction than transversely. With suitable choices for the nonlinear ionic current (I_{ion}), which models the membrane kinetics, this continuum system admits spiral waves in two dimensions or scrolls in three dimensions corresponding to reentrant activation [35, 179]. The majority of continuum models have used the FitzHugh-Nagumo (FHN) equations [116, 29]. In this reaction-diffusion system, the ionic currents are approximated by a phenomenological relation with parameters chosen to approximate the basic excitation and refractory properties of myocardium.

Using three-dimensional FHN models, Winfree (1994) has shown that rotors are scroll waves organized about vortex filaments that can assume complex topologies. Nonuniform anisotropy due to the heterogeneous cardiac muscle fiber orientation has been studied in these continuous systems [115]. Courtemanche and Winfree (1991) also reported propagation models using the Beeler-Reuter membrane model for the ionic currents. These simulations showed the spontaneous fractionation of reentrant activation waves due to the effects of nonuniform diastolic interval on refractory period. Although continuum models ignore the discrete effects of cell-to-cell coupling on macroscopic propagation [139, 155], cellular discontinuities can be simulated by appropriate modifications to the diffusion model [72].

To model electrical propagation in a nonuniformly anisotropic continuum, a collocation-Galerkin finite element method was developed by Rogers and McCulloch (1994). The finite element formulation demonstrated significant improvements over finite difference methods in its spatial and temporal convergence [134, 30]. To permit anisotropic propagation with respect to a fiber axis that varies spatially within a single finite element, the equations are transformed to a local orthonormal coordinate system with one axis that is always aligned with the fiber direction. The collocation method is used to assemble the partial differential equations into a system of ordinary differential equations (ODEs) that are satisfied exactly at collocation points in each finite element. The boundary conditions are handled using a Galerkin approach to overcome the limitations of collocation techniques over irregular boundaries [50]. The resulting system of ODEs is solved through time using an adaptive Runge-Kutta scheme [148]. With a modification of FHN kinetics, these new methods were used to identify a mechanism for spiral wave drift and scroll wave breakup in tissue with nonuniform muscle fiber angles [136].

Besides continuum models, numerical simulations of cardiac electrical activity may utilize cellular automata or resistively coupled network models. Cellular automata are simple, flexible and computationally efficient, but their rule-based propagation and discrete membrane potential waveforms preclude an accurate repre-

sentation of the electrotonic interactions between neighboring regions of myocardium [178, 4]. Resistively coupled network models have been used to simulate intercellular coupling more realistically [87]. They have been useful for investigating the effects of anisotropic extracellular coupling on membrane capacitance charging factors, safety factors, and propagation velocities. But accordingly, they are more complex and computationally expensive than cellular automata or continuum models. Resistive networks may be helpful for deriving new macroscopic models, but it is still impractical to extend them to the whole heart.

I.D Mechanoelectric Feedback

The cardiac cycle is initiated by an electrical stimulus resulting in fiber shortening, causing contraction; known as excitation-contraction coupling, this process was, until recently, considered to be "one-way". Experimental results, however, have demonstrated that a feedback pathway exists whereby the electrical characteristics of myocardium are altered by the mechanical state of the tissue. Mechanoelectric feedback, sometimes called back-coupling or contraction-excitation feedback [106, 80], is the little understood process where a change in the mechanical state of myocardium affects the electrical characteristics, particularly the diastolic (rest) transmembrane potential of the contractile myocytes and action potential morphology. Mechanoelectric feedback may play a significant role in the regulation of normal electrical function and the genesis of arrhythmias [46, 45, 33], and is thought to be governed by the activity of mechanosensitive channels, alterations in intracellular calcium cycling, or a combination of these [18].

I.D.1 Experimental Investigations

In isolated canine hearts, action potential amplitude and duration and the susceptibility to premature depolarizations are altered by diastolic ventricular dilatation [189, 60, 48, 62]. Increases in left ventricular diastolic volume have been

shown to decrease action potential duration and increase dispersion of repolarization in the isolated rabbit heart [190]. In contrast, decreasing the load on contracting myofibers increases action potential duration in strips of frog ventricular myocardium [79]. Using transient (50 millisecond) stretch pulses, Zabel et al. (1996) reported stretch-induced depolarizations or repolarizations of varying magnitude and stretch-induced arrhythmias at different epicardial regions of the diastolic left ventricle of the isolated rabbit heart; they suggested the origin of the stretch-induced response is not randomly located, but occurs at the location of highest stretch. In the anesthetized canine, Lekven et al. (1979) showed a transmurally nonuniform reduction in unipolar potential in response to increases in left ventricular diameter. Infusion of 0.5 to 2.5 liters of warm blood into the jugular vein resulted in an 11% increase in LV end-diastolic diameter and a corresponding 27% decrease in endocardial potential and a 15% decrease in epicardial potential.

In man, alterations of action potential duration or refractoriness have been observed during pulmonary valvuloplasty, transient aortic occlusion, and afterload reduction [88, 165, 6]. Taggart et al. (1992) reported shortened action potential duration during brief (1–3 beats) aortic occlusion in patients undergoing routine cardiac surgery for coronary artery disease. Their measurements showed no significant difference in action potential duration shortening at 90%, 70%, and 30% repolarization, and they later speculated that reduction in action potential duration during the first beat was due to altered calcium cycling (since the first beat after occlusion was not preceded with enhanced diastolic stretch of the LV) [166]. Shortening of the duration during the subsequent 1–2 beats, though, were thought to be caused by both altered calcium cycling and mechanosensitive channel activity, as the later beats occured during increased diastolic stretch (the LV volume being increased by additional filling after the first beat). Patients undergoing balloon valvuloplasty for pulmonary stenosis showed significantly shortened action potential duration accompanied by early afterdepolarizations during acute RV outflow tract occlusion, but after successful valvuloplasty the duration and QT interval increased

[88].

I.D.2 Mechanoelectric Feedback and Arrhythmogenesis

Mechanoelectric feedback may be arrhythmogenic. Several animal studies have shown that transient stretch of the ventricle may induce electrical activation [80, 86, 48, 61, 62] and possibly unsustained tachycardia [156, 62]. Others have shown that stretch increases the susceptibility to sustained arrhythmia in pathological hearts [174, 126, 20], but the effect of stretch on arrhythmia susceptibility in normal hearts is less clear [127, 19]. Increased LV volume in the isolated perfused rabbit heart decreases action potential amplitude and increases rest potential [189, 48]. Zabel et al. (1996) showed that a sustained 75% increase in LV volume resulted in a 28% decrease in action potential amplitude (Figure I.1). Franz et al. (1989) quantified the change in action potential duration at 20% (APD_{20}) and 90% (APD_{90}) repolarization in the isolated canine heart. They showed the action potential duration has a biphasic response to sustained increases in LV volume: APD_{20} decreased to 81% of baseline while APD_{90} increased by approximately 25% (Figure I.2). Hansen et al. (1991) quantified the transient increase in LV volume required to elicit a stretch-induced arrhythmia in the isolated, blood-perfused canine heart (Figure I.3). After pacing the heart at the apex for eight beats, they applied a 50 millisecond volume pulse to the LV 300 milliseconds after the last paced beat. A stretch-induced arrhythmia was generated with a 90% probability when the volume pulse was 21.3 ± 8.5 milliliters. They subsequently added one, three, or ten micromolar of gadolinium chloride ($GdCl_3$) to the perfusate and constructed a dose-response curve indicating the effects of gadolinium on the probability of eliciting a stretch-induced arrhythmia. The probability was reduced from 95% to approximately 10% with 10 μM gadolinium; the effect was reversible as the probability of eliciting a stretch-induced arrhythmia increased to approximately 89% after washout. Wang et al. (1994) studied the sensitivity to stretch in normal and failing canine hearts (Figure I.4). Using a protocol similar to that of Hansen et al. (1991),

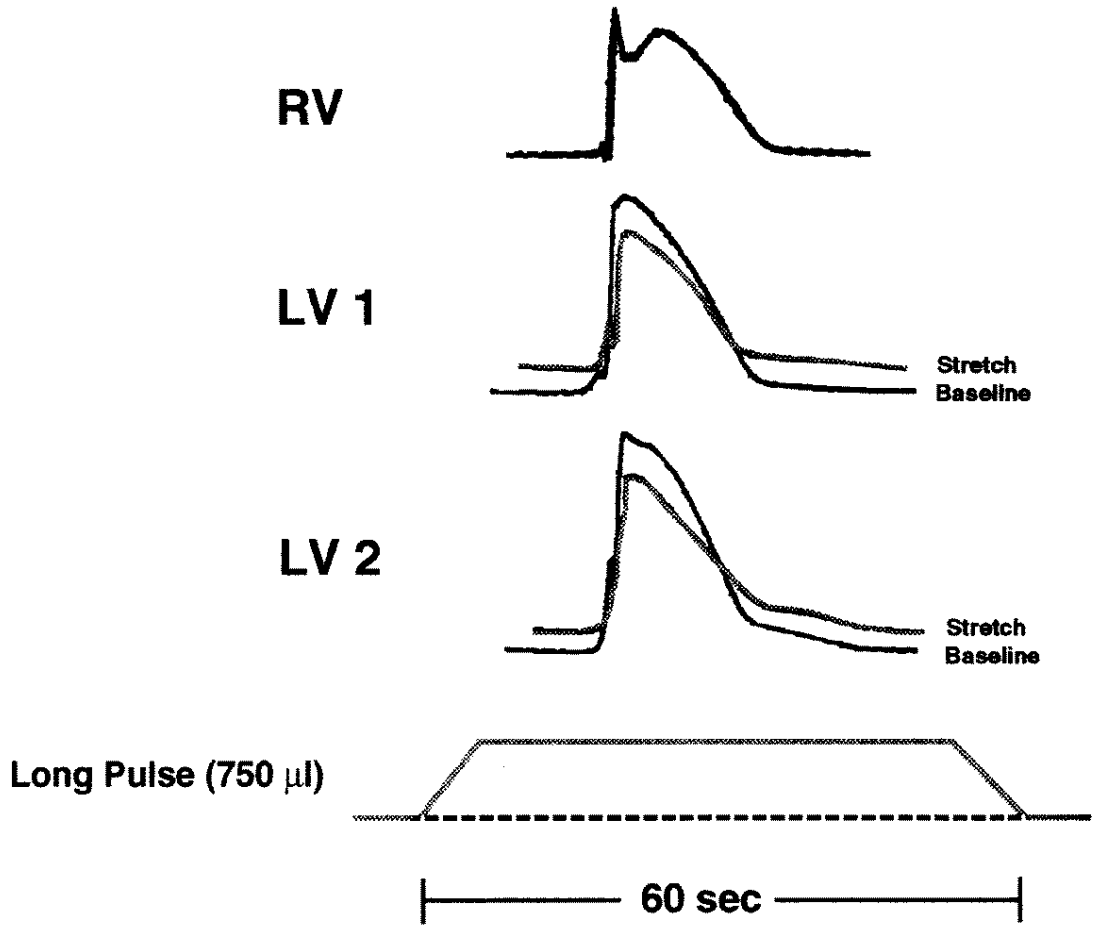

Figure I.1: Decrease in epicardial LV monophasic action potential amplitude to 72% of baseline in response to a 75% increase in LV volume in the isolated rabbit heart. From [189].

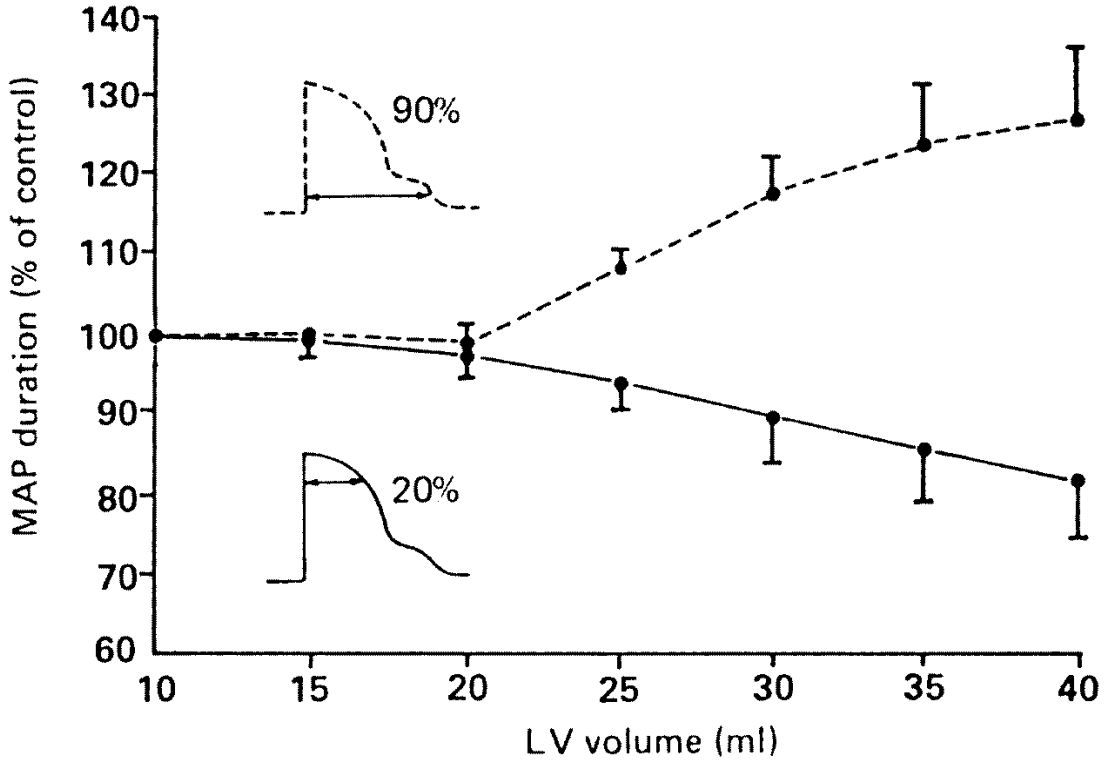

Figure I.2: Alterations in action potential duration in response to sustained increases in LV volume in the isolated canine heart. From [47].

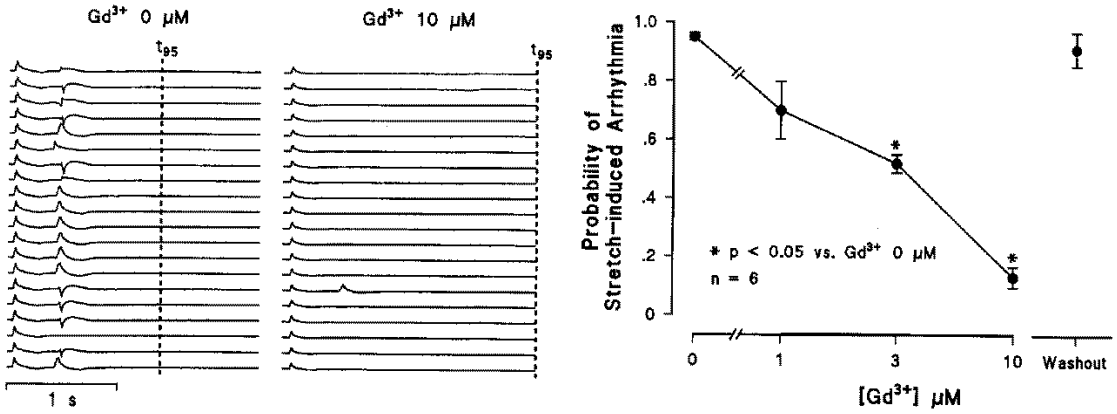

Figure I.3: Gadolinium reduces the probability of eliciting a stretch-induced arrhythmia in the isolated canine heart. The probability decreased from 95% to approximately 10% with 10 μM gadolinium. After washout the probability increased to approximately 89%. From [61].

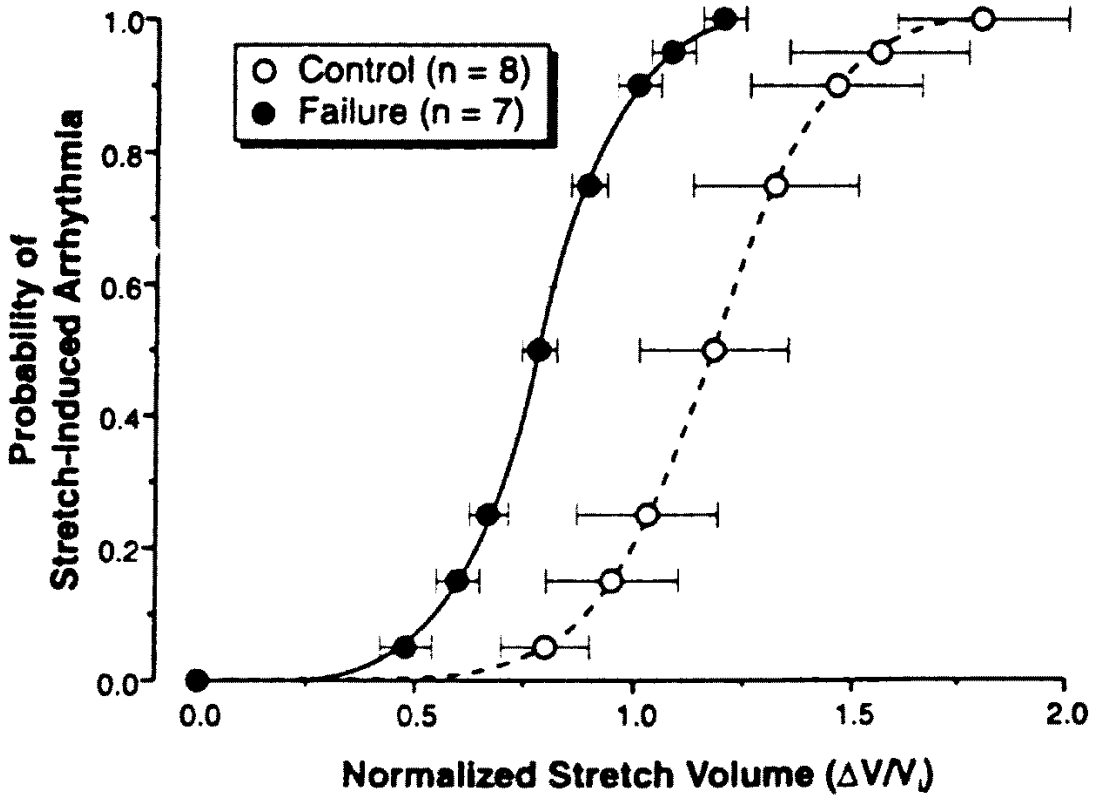

Figure I.4: Congestive heart failure increases sensitivity to stretch in the isolated canine heart. Fractional volume increase required to elicit a stretch-induced arrhythmia is 118% in normal hearts and 78% in failing hearts. From [174].

they determined the volume pulse required to elicit a stretch-induced arrhythmia with a 50% probability in normal canine hearts. The protocol was repeated using chronically dilated hearts that had been paced to failure over a period of three weeks. In the normal hearts, a 118% increase in LV volume elicited a stretch-induced arrhythmia with 50% probability. The failure hearts, with an increased end-diastolic diameter of 26%, required only a 78% LV volume increase to achieve the same probability of a stretch-induced arrhythmia, suggesting that chronically dilated hearts have a higher sensitivity to LV stretch.

Ischemia and sustained stretch increase dispersion of repolarization in the rabbit [78, 190] which may produce a favorable environment for the occurrence of

reentry [77]. Ischemic regions in myocardium show greater stretch or fiber lengthening than non-ischemic regions at end-diastole [89, 41] and lengthening during systole [169]. Van Leuven et al. (1994) found that ischemia increases the nonuniformity of end-systolic circumferential strain in the canine: perfused tissue showed depressed shortening during systole while adjacent ischemic tissue showed paradoxical circumferential lengthening. In the isolated rabbit heart, Kurz et al. (1993) found dispersion of APD_{70} increases from 17.7 to 77.8 milliseconds after five minutes of global ischemia. Thus ischemia enhances the heterogeneity of both mechanical and electrical processes in the heart. Similarly, stretch also increases mechanical and electrical heterogeneity: at the epicardium of the isolated, passively inflated canine heart the principal extension increases from 6.4% at the base to 20.7% at the apex in response to a 75% increase in LV volume [102]. Dispersion of APD_{90} increases from 27 to 38 milliseconds in the isolated rabbit heart after increasing LV volume by 1 milliliter [190]. Thus stretch, like ischemia, increases the spatial heterogeneity of myocardial deformation and action potential morphology.

Conduction velocity has been shown to decrease in stretched Purkinje fibers [120]. Sideris et al. (1994) found that increased left ventricular systolic pressure lengthened the duration of the QRS complex in the canine, and speculated this may be caused by either reduced conduction velocity or altered path length in the dilated ventricle. Shortening of the action potential duration or refractory period will increase the excitable gap in ventricular myocardium (the region of fully excitable tissue between the front of an oncoming depolarizing excitation wave and the tail of the preceding repolarizing wave [17]). This may oppose the effect of class III antiarrhythmic drugs used to terminate reentry by prolonging the refractory period and reducing (or eliminating) the excitable gap [176]. Reduced efficacy of the class III agent d-sotalol was reported by Reiter et al. (1994) in the dilated rabbit ventricle.

These observations suggest variations in regional mechanics may alter dispersion of repolarization or conduction velocity so as to enhance the onset or maintenance of arrhythmia. Franz (1996) suggests that dyskinetic wall motion during

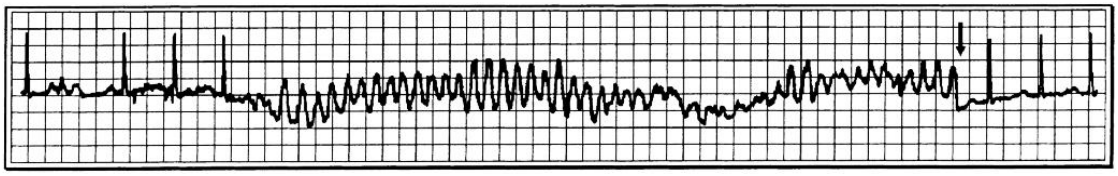

Figure I.5: Chest thump as an anti-arrhythmic intervention. Patient goes into ventricular tachycardia then fibrillation. A chest thump (arrow) reverts to normal sinus rhythm. Adapted from [5].

ischemia may lead to late-systolic regional stretch and stretch-induced depolarizations resulting in premature ventricular excitations. It has recently been suggested that *commotio cordis* may be a manifestation of mechanoelectric feedback [76]. *Commotio cordis* is a mechanical jar or shock to the heart creating a functional, but non-structural, injury leading to arrhythmia and likely resulting in death [97]. Maron et al. (1995) studied the deaths of 25 children and young adults (aged 3–19 years) that resulted from blunt impact to the chest. They speculated that the impact was delivered during an electrically vulnerable phase of ventricular excitation; a subsequent study by Link et al. (1998) using a swine model of *commotio cordis* found a significant occurrence of ventricular fibrillation when the chest impact preceded the peak of the T wave by 30 to 15 milliseconds. Alterations to cardiac rhythmicity due to chest impact are not necessarily catastrophic, however, as a "chest thump" may restore normal heart rhythm in patients with cardiac arrest or ventricular tachycardia [9, 104, 5] (Figure I.5).

I.D.3 Possible Mechanisms of Mechanoelectric Feedback

Alterations in Intracellular Calcium Cycling

In isolated guinea pig ventricular myocytes, increasing sarcomere length does not affect resting membrane potential or action potential amplitude but significantly decreases the action potential duration and magnitude of the intracellular calcium transient [177]. Changes in intracellular calcium cycling are believed to alter

action potential duration through changes in the transmembrane current associated with the sodium-calcium exchanger [71]. The sodium-calcium exchanger is electrogenic, extruding one calcium ion from the cell while absorbing three sodium ions into the cytoplasm, and thus gives rise to a depolarizing transmembrane current. The driving potential of the exchanger is the difference between the transmembrane potential and the Nernst potential of the exchanger: $V_m - E_{NaCa}$. The direction of exchange, however, can be reversed during the action potential; when V_m is positive to E_{NaCa} the exchanger will operate in the "reverse mode" and cause calcium influx and extrude sodium. The exchanger operates in the reverse mode during the upstroke and early plateau phase of the action potential. The duration of the reverse mode is difficult to predict because the exchanger driving potential is dependent upon the transmembrane flux and potential differences of the sodium and calcium ions, which are constantly changing during electrical excitation [114]. Stretched cardiac tissue increases the calcium affinity of troponin-C [1]. In turn, more calcium binds to myofilaments which may shorten the time course of the calcium transient, lengthen the reverse mode duration of the exchanger, and reduce calcium-dependent ion currents resulting in an attenuated depolarizing current, shortening the action potential duration. Conversely, in contracting myocardium the troponin-C affinity for calcium is decreased, and calcium is released from the myofilaments into the cytoplasm. The sarcoplasmic rise in calcium concentration causes the exchanger to extrude calcium during repolarization, creating an inward depolarizing current that tends to lengthen action potential duration [166].

Mechanosensitive Channels

Mechanosensitive channels have been identified in a number of cell types including neurons, yeast, and hair cells [183]. Mechanosensitive channels that deactivate (sometimes called stretch-inactivated channels) have been identified, but not in cardiac tissue [105]. The discovery of mechanosensitive ion channels in myocardium [32, 153] has led to speculation that these cellular structures are responsible for

the mechanical sensitivity of electrical processes in the intact heart. Ruknudin et al. (1993) identified five distinct mechanosensitive channels in cardiac myocytes that are cation selective. In cardiac ventricular cells, mechanosensitive channels have been identified with reverse potentials ranging from -70 to 10 mV and conductivities of 20 to 200 pS [68, 140, 31, 146, 14, 32]. The sarcolemmal density of the channels is estimated to range from 0.1 to 1 channels per μm^2 [140, 152]. Though these channels are primarily cation selective, anion-selective channels with similar characteristics have also been identified in atrial tissue [58]. Cardiac mechanosensitive channels show increases in their open probability in response to stretch, but the physics of the gating mechanisms are unknown. It is unclear whether the channels are activated by tension in the sarcolemma or stresses in the cytoskeletal proteins (or a combination of these) [59, 142]. Mechanosensitive channel activity has been measured in absence of a cytoskeleton in membrane patches from *Escherichia coli* embedded in artificial bilayers [8, 36]. In contrast, results from a series of patch-clamp experiments by Ruknudin et al. (1991) suggest that mechanosensitive channels are in series with some component of the cytoskeleton, possibly spectrin or fondrin [142]. Other experiments suggest the conductivity of a mechanosensitive channel may be affected by curvature of the membrane [12, 98]. Most recently it has been suggested that mechanosensitive channels may not be located in the cell membrane, but in the intracellular organelles [144].

Myocardial stretch is thought to activate mechanosensitive channels, producing a stretch-dependent depolarizing current in electrically quiescent tissue. Over the time course of the action potential, the stretch-dependent current will change direction from inward to outward at membrane potentials positive to the channel reverse potential; this current reversal will tend to shorten action potential duration during the plateau phase. During late repolarization the membrane potential will again drop below the reverse potential resulting in a depolarizing current that lengthens the action potential duration. Experimental confirmation for this biphasic response of the action potential duration has been shown in the intact canine and

rabbit ventricles [47, 189] and in atrial tissue [107].

Gadolinium, a blocker of mechanosensitive channels [182], reversibly suppresses stretch-induced arrhythmias in isolated canine hearts [156, 62]. In the presence of extracellular calcium, mechanical stimulation of chick embryo cardiomyocytes can cause waves of calcium-induced calcium release [152] that are prevented by 20 mM gadolinium. Gadolinium also, however, blocks L-type calcium channels and the rapid component of the delayed rectifier potassium current [81, 66, 117], so its use as an anti-arrhythmic agent is limited.

I.D.4 Mechanoelectric Feedback Models

The first model of a stretch-dependent current due to mechanosensitive channel activity was proposed by Sachs (1994). He chose a simple Boltzman relationship for the stretch-dependent current conductance, modeling the conductance as an exponential function of the change in sarcomere length. With this model he was able to qualitatively reproduce experimentally observed changes in action potential morphology measured in stretched Purkinje fibers, ventricular cells, and the whole heart. The Sachs model has recently been extended by Kohl et al. (1998) to include the effects of different ion species that may constitute the stretch-dependent current. Experimental data to validate such a detailed model is lacking, however, motivating other investigators to propose less complicated models of the stretch-dependent current.

Using a linear model of the stretch-dependent current, Riemer et al. (1998) examined the influence of the conductance and reverse potential of a mechanosensitive channel in two models of ventricular action potential. With a model of the frog ventricular action potential they found that action potential duration consistently shortens with reverse potentials of -20 and -50 mV; a guinea pig model also shows shorter duration action potentials with a -50 mV reverse potential, but the duration lengthens with a -20 mV reverse potential. Rice et al. (1998) also used a linear stretch-dependent current model to simulate the effect of circumferential lengthen-

ing during end-systole in an ischemic region on the LV using magnetic resonance imaging with cardiac tagging. They found that the minimum stretch-dependent conductance needed to generate an action potential decreases as the number of abnormally stretched cells increases, suggesting that a very small number of cells could generate stretch-induced action potentials possibly resulting in a reentrant arrhythmia. The linear current models proposed by Riemer et al. (1998) and Rice et al. (1998) used a time-independent, fixed amount of stretch — presumably representing the change in either sarcomere or myofiber length.

Knudsen et al. (1997) have developed a FHN-like phenomenological model of mechanoelectric feedback, with separate fast and slow excitation kinetics coupled to an additional time-dependent variable representing the myofiber length change during contraction. This four variable system provides a simple description of coupled excitation, recovery, and one-dimensional deformation, but the model variables cannot be directly related to physiological parameters in the heart.

Changes in sarcomere or myofiber length may not be the only mechanical parameter influencing stretch-dependent alterations in action potential morphology. Lekven et al. (1979) showed that step increases in end-diastolic left ventricular diameter reduced epicardial action potential amplitude by 14.7%, while endocardial action potential amplitude was reduced by 27.8%. Omens et al. (1991) have demonstrated a significant transmural cross fiber strain gradient exists in the passively inflated isolated dog heart. Thus the nonuniform transmural alteration of action potential amplitude in response to stretch may also be due in part to the transmural cross fiber strain gradient.

I.E Objectives of the Dissertation

The overall objective of this dissertation was to quantify the relationship between three-dimensional diastolic strains in the ventricle and the regional response of action potential morphology in the presence of mechanosensitive channels. We

hypothesized that nonuniform alterations in action potential amplitude are due in part to the mechanosensitive channel response to deformation other than changes in sarcomere or myofiber length. We integrated theoretical models of ventricular anatomy, passive mechanics, electrical propagation, and cellular transmembrane ionic currents to explore how cellular electrophysiology might be altered by regional variations in diastolic ventricular mechanics.

The first objective was to determine the three-dimensional strains in the passively inflated rabbit left ventricle. Similar to the approach developed by Nielsen et al. (1991), we developed a finite element model of the rabbit ventricular geometry and fiber orientation. Chapter II details the methods used to acquire the geometric and fiber angle measurements which were the basis for the finite element model of the ventricular anatomy. The model was used to predict the three-dimensional strains in the passively inflated rabbit left ventricle (Chapter III) using specialized parallel computational algorithms developed to allow for the rapid estimation of the myocardial material properties which govern material deformation.

The second objective of this work was to investigate possible mechanical stimuli governing the activation of mechanosensitive channels in deformed myocardium. As described in Chapter V, we added a stretch-dependent current in parallel to the ionic currents of a ventricular action potential model. We investigated different mechanical coupling parameters to simulate mechanosensitive conductance modulated by either fiber strain, cross fiber strain, or a combination of the two.

The text of this chapter, in part, is a reprint of the material as it appears in *Progress in Biophysics and Molecular Biology*, F. J. Vetter and A. D. McCulloch, 69(2-3):157-184 (1998). I was the primary researcher and author and the co-author(s) listed in this publication directed and supervised the research which forms the basis for this chapter.

References

[1] D. G. Allen and J. C. Kentish. Calcium concentration in the myoplasm of skinned ferret ventricular muscle following changes in muscle length. *J Physiol*, 407:489–503, Dec 1988.

[2] C. Antzelevitch, S. Sicouri, A. Lukas, V. V. Nesterenko, D.-W. Liu, and J. M. Di Diego. Regional differences in the electrophysiology of ventricular cells: Physiological and clinical implications. In D. P. Zipes and J. Jalife, editors, *Cardiac Electrophysiology: From Cell to Bedside*, chapter 23, pages 228–245. W. B. Saunders, Philadelphia, second edition, 1995.

[3] H. Azhari, J. L. Weiss, W. J. Rogers, C. O. Siu, E. A. Zerhouni, and E. P. Shapiro. Noninvasive quantification of principal strains in normal canine hearts using tagged MRI images in 3-D. *Am J Physiol*, 264(Heart Circ. Physiol. 33):H205–H216, Jan 1993.

[4] A. H. Bailie, R. H. Mitchell, and J. M. Anderson. A computer model of re-entry in cardiac tissue. *Comput Biol Med*, 20(1):47–54, 1990.

[5] J. S. Barrett. Chest thumps and the heart beat. *N Engl J Med*, 284(7):393, 18 February 1971.

[6] Y. Bashir, J. F. Sneddon, S. O'Nunain, V. E. Paul, S. Gibson, D. E. Ward, and A. J. Camm. Comparative electrophysiological effects of captopril or hydralazine combined with nitrate in patients with left ventricular dysfunction and inducible ventricular tachycardia. *Br Heart J*, 67(5):355–360, May 1992.

[7] G. W. Beeler and H. Reuter. Reconstruction of the action potential of ventricular myocardial fibres. *J Physiol*, 268(1):177–210, Jun 1977.

[8] C. Berrier, A. Coulombe, C. Houssin, and A. Ghazi. A patch-clamp study of ion channels of inner and outer membranes and of contact zones of *E. coli*, fused into giant liposomes: Pressure-activated channels are localized in the inner membrane. *FEBS Lett*, 259(1):27–32, 18 December 1989.

[9] J. L. Bierfeld, V. Rodriguez-Viera, J. M. Aranda, C. A. Jr, R. Lazzara, and B. Befeler. Terminating ventricular fibrillation by chest thump. *Angiology*, 30(10):703–707, Oct 1979.

[10] P. H. Bovendeerd, T. Arts, J. M. Huyghe, D. H. van Campen, and R. S. Reneman. Dependence of local left ventricular wall mechanics on myocardial fiber orientation: A model study. *J Biomech*, 25(10):1129–1140, Oct 1992.

[11] P. H. M. Bovendeerd, J. M. Huyghe, T. Arts, D. H. van Campen, and R. S. Reneman. Influence of endocardial-epicardial crossover of muscle fibers on left ventricular wall mechanics. *J Biomech*, 27(7):941–951, Jul 1994.

[12] C. L. Bowman and J. W. Lohr. Curvature-sensitive mechanosensitive ion channels and osmotically-evoked movements of the patch membrane (abstract). *Biophys J*, 70(2):A365, Feb 1996. Abstract Supplement for the Biophysical Society 40rd Annual Meeting, February 17–21, 1996, Baltimore, Maryland.

[13] J. W. B. Bradfield, G. Beck, and R. J. Vecht. Left ventricular apical thin point. *Br Heart J*, 39(7):806–809, Jul 1977.

[14] J. O. Bustamante, A. Ruknudin, and F. Sachs. Stretch-activated channels in heart cells: Relevance to cardiac hypertrophy. *J Cardiovasc Pharmacol*, 17(Suppl. 2):S110–S113, 1991.

[15] C. Cabo, A. M. Pertsov, W. T. Baxter, J. M. Davidenko, R. A. Gray, and J. Jalife. Wave-front curvature as a cause of slow conduction and block in isolated cardiac muscle. *Circ Res*, 75(6):1014–1028, Dec 1994.

[16] C. Cabo, A. M. Pertsov, J. M. Davidenko, W. T. Baxter, R. A. Gray, and J. Jalife. Vortex shedding as a precursor of turbulent electrical activity in cardiac muscle. *Biophys J*, 70(3):1105–1111, Mar 1996.

[17] C. Cabo and A. L. Wit. Cellular electrophysiologic mechanisms of cardiac arrhythmias. *Cardiology Clinics*, 15(4):517–38, Nov 1997.

[18] S. C. Calaghan and E. White. The role of calcium in the response of cardiac muscle to stretch. *Prog Biophys Mol Biol*, 71:59–90, 1999.

[19] H. Calkins, W. L. Maughan, D. A. Kass, K. Sagawa, and J. H. Levine. Electrophysiological effect of volume load in isolated canine hearts. *Am J Physiol*, 256(Heart Circ. Physiol. 25):H1697–H1706, Jun 1989.

[20] H. Calkins, W. L. Maughan, H. F. Weisman, S. Sugiura, K. Sagawa, and J. H. Levine. Effect of acute volume load on refractoriness and arrhythmia development in isolated, chronically infarcted canine hearts. *Circulation*, 79(3):687–697, Mar 1989.

[21] A. W. Cates and A. E. Pollard. A model study of intramural dispersion of action potential duration in the canine pulmonary conus. *Ann Biomed Eng*, 26(4):567–576, July-August 1998.

[22] J. B. Caulfield and T. K. Borg. The collagen network of the heart. *Laboratory Investigation*, 40(3):364–372, Mar 1979.

[23] S. J. Cook, J. P. Chamunorwa, M. K. Lancaster, and S. C. O'Neill. Regional differences in the regulation of intracellular sodium and in action potential configuration in rabbit left ventricle. *Pflügers Archiv. European Journal of Physiology*, 433(4):515–522, Feb 1997.

[24] K. D. Costa. *The Structural Basis of Three-Dimensional Ventricular Mechanics*. PhD thesis, University of California, La Jolla, California, 1996.

[25] K. D. Costa, P. J. Hunter, J. M. Rogers, J. M. Guccione, L. K. Waldman, and A. D. McCulloch. A three-dimensional finite element method for large elastic deformations of ventricular myocardium: I — cylindrical and spherical polar coordinates. *J Biomech Eng*, 118(4):452–463, Nov 1996.

[26] K. D. Costa, P. J. Hunter, J. M. Rogers, J. M. Guccione, L. K. Waldman, and A. D. McCulloch. A three-dimensional finite element method for large elastic deformations of ventricular myocardium: II — prolate spheroidal coordinates. *J Biomech Eng*, 118(4):464–472, Nov 1996.

[27] K. D. Costa, K. May-Newman, D. Farr, W. G. O'Dell, A. D. McCulloch, and J. H. Omens. Three-dimensional residual strain in midanterior canine left ventricle. *Am J Physiol*, 273(Heart Circ. Physiol. 42):H1968–H1976, 1997.

[28] M. Courtemanche, R. J. Ramirez, and S. Nattel. Ionic mechanisms underlying human atrial action potential properties: insights from a mathematical model. *Am J Physiol*, 275(Heart Circ. Physiol. 44):H301–H321, Jul 1998.

[29] M. Courtemanche, W. Skaggs, and A. T. Winfree. Stable three-dimensional action potential circulation in the FitzHugh-Nagumo model. *Physica D*, 41(2):173–182, Mar 1990.

[30] M. Courtemanche and A. T. Winfree. Re-entrant rotating waves in a Beeler-Reuter based model of two-dimensional cardiac electrical activity. *International Journal of Bifurcation and Chaos in Applied Sciences and Engineering*, 1(2):431–444, Jun 1991.

[31] W. Craelius. Stretch-activation of rat cardiac myocytes. *Exp Physiol*, 78(3):411–423, May 1993.

[32] W. Craelius, V. Chen, and N. El-Sherif. Stretch activated ion channels in ventricular myocytes. *Bioscience Reports*, 8(5):407–414, Oct 1988.

[33] B. Crozatier. Stretch-induced modifications of myocardial performance: from ventricular function to cellular and molecular mechanisms. *Cardiovasc Res*, 32(1):25–37, Jul 1996.

[34] J. M. Davidenko, A. V. Pertsov, R. Salomonsz, W. T. Baxter, and J. Jalife. Stationary and drifting spiral waves of excitation in isolated cardiac muscle. *Nature*, 355(6358):349–351, January 23 1992.

[35] J. M. Davidenko, R. Salomonsz, A. M. Pertsov, W. T. Baxter, and J. Jalife. Effects of pacing on stationary reentrant activity: Theoretical and experimental study. *Circ Res*, 77(6):1166–1179, Dec 1995.

[36] A. H. Delcour, B. Martinac, J. Adler, and C. Kung. Voltage-sensitive ion channel of *Escherichia coli*. *J Membr Biol*, 112(3):267–275, Dec 1989.

[37] C. Delgado, B. Steinhaus, M. Delmar, D. R. Chivalvo, and J. Jalife. Directional differences in excitability and margin of safety for propagation in sheep ventricular epicardial muscle. *Circ Res*, 67(1):97–110, Jul 1990.

[38] S. S. Demir, J. W. Clark, C. R. Murphey, and W. R. Giles. A mathematical model of a rabbit sinoatrial node cell. *Am J Physiol*, 266(Cell Physiol. 35):C832–C852, Mar 1994.

[39] D. DiFrancesco and D. Noble. A model of cardiac electrical activity incorporating ionic pumps and concentration changes. *Philos Trans R Soc Lond B Biol Sci*, 307(1133):353–398, January 10 1985.

[40] D. Durrer, R. T. van Dam, G. E. Freud, M. J. Janse, F. L. Meijler, and R. C. Arzbaecher. Total excitation of the isolated human heart. *Circulation*, 41(6):899–912, Jun 1970.

[41] C. H. Edwards II, J. S. Rankin, P. A. McHale, D. Ling, and R. W. Anderson. Effects of ischemia on left ventricular regional function in the conscious dog. *Am J Physiol*, 240(Heart Circ. Physiol. 9):H413–H420, Mar 1981.

[42] I. R. Efimov, D. T. Huang, J. R. M. Rendt, and G. Salama. Optical mapping of repolarization and refractoriness from intact hearts. *Circulation*, 90(3):1469–1480, Sep 1994.

[43] V. G. Fast and A. G. Kléber. Role of wavefront curvature in propagation of cardiac impulse. *Cardiovasc Res*, 33(2):258–271, Feb 1997.

[44] D. Fedida and W. R. Giles. Regional variations in action potentials and transient outward current in myocytes isolated from rabbit left ventricle. *J Physiol*, 442:191–209, Oct 1991.

[45] M. R. Franz. Stretch-activated arrhythmias. In D. P. Zipes and J. Jalife, editors, *Cardiac Electrophysiology: From Cell to Bedside*, chapter 57, pages 597–606. W. B. Saunders, Philadelphia, second edition, 1995.

[46] M. R. Franz. Mechano-electrical feedback in ventricular myocardium. *Cardiovasc Res*, 32(1):15–24, Jul 1996.

[47] M. R. Franz, D. Burkhoff, D. T. Yue, and K. Sagawa. Mechanically induced action potential changes and arrhythmia in isolated and in situ canine hearts. *Cardiovasc Res*, 23(3):213–223, Mar 1989.

[48] M. R. Franz, R. Cima, D. Wang, D. Profitt, and R. Kurz. Electrophysiological effects of myocardial stretch and mechanical determinants of stretch-activated arrhythmias. *Circulation*, 86(3):968–978, Sep 1992. Published erratum appears in Circulation 1992 Nov, 86(5):1663.

[49] D. W. Frazier, P. D. Wolf, J. M. Wharton, A. S. Tang, W. M. Smith, and R. E. Ideker. Stimulus-induced critical point: Mechanism for electrical initiation of reentry in normal canine myocardium. *J Clin Invest*, 83(3):1039–1052, Mar 1989.

[50] E. O. Frind and G. F. Pinder. A collocation finite element method for potential problems in irregular domains. *Int J Numer Methods Eng*, 14(5):681–701, 1979.

[51] A. M. Gallagher, J. H. Omens, L. L. Chu, and J. W. Covell. Alterations in collagen fibrillar structure and mechanical properties of the healing scar following myocardial infarction. *Cardiovasc Pathobiol*, 2(1):25–36, 1997.

[52] W. R. Giles and Y. Imaizumi. Comparison of potassium currents in rabbit atrial and ventricular cells. *J Physiol*, 405:123–145, Nov 1988.

[53] M. Gotoh, T. Uchida, W. Fan, M. C. Fishbein, H. S. Karagueuzian, and P.-S. Chen. Anisotropic repolarization in ventricular tissue. *Am J Physiol*, 272(Heart Circ. Physiol. 41):H107–H113, Jan 1997.

[54] R. A. Gray, J. Jalife, A. V. Panfilov, W. T. Baxter, C. Cabo, J. M. Davidenko, and A. M. Pertsov. Nonstationary vortexlike reentrant activity as a mechanism of polymorphic ventricular tachycardia in the isolated rabbit heart. *Circulation*, 91(9):2454–2469, May 1995.

[55] R. A. Greenbaum, S. Y. Ho, D. G. Gibson, A. E. Becker, and R. H. Anderson. Left ventricular fibre architecture in man. *Br Heart J*, 45(3):248–263, Mar 1981.

[56] J. M. Guccione, K. D. Costa, and A. D. McCulloch. Finite element stress analysis of left ventricular mechanics in the beating dog heart. *J Biomech*, 28(10):1167–1177, Oct 1995.

[57] J. M. Guccione, A. D. McCulloch, and L. K. Waldman. Passive material properties of intact ventricular myocardium determined from a cylindrical model. *J Biomech Eng*, 113(1):42–55, Feb 1991.

[58] N. Hagiwara, H. Masuda, M. Shoda, and H. Irisawa. Stretch-activated anion currents of rabbit cardiac myocytes. *J Physiol*, 456:285–302, Oct 1992.

[59] O. P. Hamill and D. W. McBride, Jr. Rapid adaptation of single mechanosensitive channels in *Xenopus* oocytes. *Proc Natl Acad Sci USA*, 89(16):7462–7466, 15 August 1992.

[60] D. E. Hansen. Mechanoelectrical feedback effects of altering preload, afterload, and ventricular shortening. *Am J Physiol*, 264(Heart Circ. Physiol. 33):H423–H432, Feb 1993.

[61] D. E. Hansen, M. Borganelli, G. P. Stacy, Jr., and L. K. Taylor. Dose-dependent inhibition of stretch-induced arrhythmias by gadolinium in isolated canine ventricles. Evidence for a unique mode of antiarrhythmic action. *Circ Res*, 69(3):820–831, Sep 1991.

[62] D. E. Hansen, C. S. Craig, and L. M. Hondeghem. Stretch-induced arrhythmias in the isolated canine ventricle. Evidence for the importance of mechanoelectrical feedback. *Circulation*, 81(3):1094–1105, Mar 1990.

[63] C. S. Henriquez, A. L. Muzikant, and C. K. Smoak. Anisotropy, fiber curvature, and bath loading effects on activation in thin and thick cardiac tissue preparations: Simulations in a three-dimensional bidomain model. *J Cardiovasc Electrophysiol*, 7(5):424–444, May 1996.

[64] A. L. Hodgkin and A. F. Huxley. A quantitative description of membrane current and its application to conduction and excitation in nerve. *J Physiol*, 117:500–544, 1952.

[65] J. W. Holmes and J. W. Covell. Collagen fiber orientation in myocardial scar tissue. *Cardiovasc Pathobiol*, 1(1):15–22, 1996.

[66] K. Hongo, C. Pascarel, O. Cazorla, F. Gannier, J. Y. Le Guennec, and E. White. Gadolinium blocks the delayed rectifier potassium current in isolated guinea-pig ventricular myocytes. *Exp Physiol*, 82(4):647–656, Jul 1997.

[67] W. Hort. Makroskopische und mikrometrische untersuchungen am myokard verschieden stark gefüllter linker kammern. *Virchows Archiv für Pathologische Anatomie und Physiologie und für Klinische Medizin*, 333:523–564, 1960.

[68] H. Hu and F. Sachs. Mechanically activated currents in chick heart cells. *J Membr Biol*, 154(3):205–216, Dec 1996.

[69] R. M. Huisman, G. Elzinga, N. Westerhof, and P. Sipkema. Measurement of left ventricular wall stress. *Cardiovasc Res*, 14(3):142–153, Mar 1980.

[70] J. D. Humphrey and F. C. P. Yin. Biaxial mechanical behavior of excised epicardium. *J Biomech Eng*, 110(4):349–351, Nov 1988. Published erratum appears in J. Biomech. Eng. 1989 Aug, 111(3):227.

[71] N. C. Janvier and M. R. Boyett. The role of Na-Ca exchange current in the cardiac action potential. *Cardiovasc Res*, 32(1):69–84, Jul 1996.

[72] J. P. Keener. Wave propagation in myocardium. In L. Glass, P. Hunter, and A. McCulloch, editors, *Theory of Heart: Biomechanics, Biophysics, and Nonlinear Dynamics of Cardiac Function*, chapter 17, pages 405–436. Springer-Verlag, New York, 1991.

[73] S. B. Knisley and B. C. Hill. Effects of bipolar point and line stimulation in anisotropic rabbit epicardium: Assessment of the critical radius of curvature for longitudinal block. *IEEE Trans Biomed Eng*, 42(10):957–966, Oct 1995.

[74] Z. Knudsen, A. V. Holden, and J. Brindley. Qualitative modeling of mechanoelectrical feedback in a ventricular cell. *Bull Math Biol*, 59(6):1155–1181, Nov 1997.

[75] P. Kohl, K. Day, and D. Noble. Cellular mechanisms of cardiac mechanoelectric feedback in a mathematical model. *Canadian Journal of Cardiology*, 14(1):111–119, Jan 1998.

[76] P. Kohl, P. Hunter, and D. Noble. Stretch-induced changes in heart rate and rhythm: clinical observations, experiments and mathematical models. *Prog Biophys Mol Biol*, 71:91–138, 1999.

[77] C. S. Kuo, C. P. Reddy, K. Munakata, and B. Surawicz. Mechanism of ventricular arrhythmias caused by increased dispersion of repolarization. *Eur Heart J*, 6 Suppl. D:63–70, Nov. 1985.

[78] R. W. Kurz, R. Xiao-Lin, and M. R. Franz. Increased dispersion of ventricular repolarization and ventricular tachyarrhythmias in the globally ischaemic rabbit heart. *Eur Heart J*, 14(11):1561–1571, Nov. 1993.

[79] M. J. Lab. Transient depolarisation and action potential alterations following mechanical changes in isolated myocardium. *Cardiovasc Res*, 14(11):624–637, Dec 1980.

[80] M. J. Lab. Contraction-excitation feedback in myocardium: Physiological basis and clinical relevance. *Circ Res*, 50(6), Jun 1982.

[81] A. Lacampagne, F. Gannier, J. Argibay, D. Garnier, and J. Y. Le Guennec. The stretch-activated ion channel blocker gadolinium also blocks L-type calcium channels in isolated ventricular myocytes of the guinea-pig. *Biochimica et Biophysica Acta*, 1191(1):205–208, April 20 1994.

[82] M. C. Lee, Y. C. Fung, R. Shabetai, and M. M. LeWinter. Biaxial mechanical properties of human pericardium and canine comparisons. *Am J Physiol*, 253(Heart Circ. Physiol. 22):H75–H82, Jul 1987.

[83] I. J. LeGrice, P. J. Hunter, and B. H. Smaill. Laminar structure of the heart: A mathematical model. *Am J Physiol*, 272(Heart Circ. Physiol. 41):H2466–H2476, May 1997.

[84] I. J. LeGrice, B. H. Smaill, L. Z. Chai, S. G. Edgar, J. B. Gavin, and P. J. Hunter. Laminar structure of the heart: Ventricular myocyte arrangement and connective tissue architecture in the dog. *Am J Physiol*, 269(Heart Circ. Physiol. 38):H571–H582, Aug 1995.

[85] J. Lekven, K. Chatterjee, J. V. Tyberg, and W. W. Parmley. Reduction in ventricular endocardial and epicardial potentials during acute increments in left ventricular dimensions. *American Heart Journal*, 98(2):200–206, Aug 1979.

[86] B. B. Lerman, D. Burkhoff, D. T. Yue, M. R. Franz, and K. Sagawa. Mechanoelectrical feedback: Independent role of preload and contractility in modulation of canine ventricular excitability. *J Clin Invest*, 76(5):1843–1850, Nov 1985. Published erratum appears in J. Clin. Invest. 1986 Jun, 77(6):2053.

[87] M. D. Lesh, M. Pring, and J. F. Spear. Cellular uncoupling can unmask dispersion of action potential duration in ventricular myocardium. A computer modeling study. *Circ Res*, 65(5):1426–1440, Nov 1989.

[88] J. H. Levine, T. Guarnieri, A. H. Kadish, R. I. White, H. Calkins, and J. S. Kan. Changes in myocardial repolarization in patients undergoing balloon valvuloplasty for congenital pulmonary stenosis: evidence for contraction-excitation feedback in humans. *Circulation*, 77(1):70–77, Jan. 1988.

[89] W. Y. W. Lew. Influence of ischemic zone size on nonischemic area function in the canine left ventricle. *Am J Physiol*, 252(Heart Circ. Physiol. 21):H990–H997, May 1987.

[90] D. H. S. Lin and F. C. P. Yin. A multiaxial constitutive law for mammalian left ventricular myocardiumin steady-state barium contracture or tetanus. *J Biomech Eng*, 120(4):504–517, Aug 1998.

[91] D. S. Lindblad, C. R. Murphey, J. W. Clark, and W. R. Giles. A model of the action potential and underlying membrane currents in a rabbit atrial cell. *Am J Physiol*, 271(Heart Circ. Physiol. 40):H1666–H1696, Oct 1996.

[92] M. S. Link, P. J. Wang, N. G. Pandian, S. Bharati, J. E. Udelson, M. Y. Lee, M. A. Vecchiotti, B. A. VanderBrink, G. Mirra, B. J. Maron, and N. A. M. Estes, III. An experimental model of sudden death due to low-energy chest-wall impact (commotio cordis). *N Engl J Med*, 338(25):1805–1811, June 18 1998.

[93] D. W. Liu and C. Antzelevitch. Characteristics of the delayed rectifier current (I_{Kr} and I_{Ks}) in canine ventricular epicardial, midmyocardial, and endocardial myocytes: A weaker I_{Ks} contributes to the longer action potential of the M cell. *Circ Res*, 76(3):351–365, Mar 1995.

[94] C.-H. Luo and Y. Rudy. A model of the ventricular cardiac action potential: Depolarization, repolarization, and their interaction. *Circ Res*, 68(6):1501–1526, Jun 1991.

[95] C.-H. Luo and Y. Rudy. A dynamic model of the cardiac ventricular action potential. I. Simulations of ionic currents and concentration changes. *Circ Res*, 74(6):1071–1096, Jun 1994.

[96] C.-H. Luo and Y. Rudy. A dynamic model of the cardiac ventricular action potential. II. Afterdepolarizations, triggered activity, and potentiation. *Circ Res*, 74(6):1097–1113, Jun 1994.

[97] B. J. Maron, L. C. Poliac, J. A. Kaplan, and F. O. Mueller. Blunt impact to the chest leading to sudden death from cardiac arrest during sports activities. *N Engl J Med*, 333(6):337–342, Aug 1995.

[98] B. Martinac, J. Adler, and C. Kung. Mechanosensitive ion channels of *E. coli* activated by amphipaths. *Nature*, 348(6298):261–263, 15 November 1990.

[99] K. May-Newman, J. H. Omens, R. S. Pavelec, and A. D. McCulloch. Three-dimensional transmural mechanical interaction between the coronary vasculature and passive myocardium in the dog. *Circ Res*, 74(6):1166–1178, Jun 1994.

[100] A. D. McCulloch. Cardiac biomechanics. In J. D. Bronzino, editor, *Biomedical Engineering Handbook*, chapter 31, pages 418–439. CRC Press: IEEE Press, Boca Raton, 1995.

[101] A. D. McCulloch and J. H. Omens. Factors affecting the regional mechanics of the diastolic heart. In L. Glass, P. Hunter, and A. McCulloch, editors, *Theory of Heart: Biomechanics, Biophysics, and Nonlinear Dynamics of Cardiac Function*, chapter 5, pages 87–119. Springer-Verlag, New York, 1991.

[102] A. D. McCulloch, B. H. Smaill, and P. J. Hunter. Regional left ventricular epicardial deformation in the passive dog heart. *Circ Res*, 64(4):721–733, Apr 1989.

[103] C. C. Moore, W. G. O'Dell, E. R. McVeigh, and E. A. Zerhouni. Calculation of three-dimensional left ventricular strains from biplanar tagged MR images. *Journal of Magnetic Resonance Imaging*, 2(2):165–175, March-April 1992.

[104] T. Morgera, N. Baldi, D. Chersevani, G. Medugno, and F. Camerini. Chest thump and ventricular tachycardia. *PACE*, 2(1):69–75, Jan 1979.

[105] C. E. Morris and W. J. Sigurdson. Stretch-inactivated ion channels coexist with stretch-activated ion channels. *Science*, 243(4892):807–809, February 10 1989.

[106] S. Naidu and F. Kavaler. Interaction of sarcomere length and excitation-contraction coupling in ventricular myocardium. *Bulletin of the New York Academy of Medicine*, 47(10):1231, Oct 1971.

[107] S. A. Nazir and M. J. Lab. Mechanoelectric feedback in the atrium of the isolated guinea-pig heart. *Cardiovasc Res*, 32(1):112–119, Jul 1996.

[108] P. M. F. Nielsen, I. J. LeGrice, B. H. Smaill, and P. J. Hunter. Mathematical model of geometry and fibrous structure of the heart. *Am J Physiol*, 260(Heart Circ. Physiol. 29):H1365–H1378, Apr 1991.

[109] V. P. Novak, F. C. P. Yin, and J. D. Humphrey. Regional mechanical properties of passive myocardium. *J Biomech*, 27(4):403–412, Apr 1994.

[110] J. H. Omens and J. W. Covell. Transmural distribution of myocardial tissue growth induced by volume-overload hypertrophy in the dog. *Circulation*, 84(3):1235–1245, Sep 1991.

[111] J. H. Omens, D. D. Farr, A. D. McCulloch, and L. K. Waldman. Comparison of two techniques for measuring two-dimensional strain in rat left ventricles. *Am J Physiol*, 271(Heart Circ. Physiol. 40):H1256–H1261, Sep 1996.

[112] J. H. Omens, D. A. MacKenna, and A. D. McCulloch. Measurement of strain and analysis of stress in resting rat left ventricular myocardium. *J Biomech*, 26(6):665–676, Jun 1993.

[113] J. H. Omens, K. D. May, and A. D. McCulloch. Transmural distribution of three-dimensional strain in the isolated arrested canine left ventricle. *Am J Physiol*, 261(Heart Circ. Physiol. 30):H918–H928, Sep 1991.

[114] L. H. Opie. *The Heart: Physiology, from Cell to Circulation.* Lippincott-Raven, Philadelphia, third edition, 1998.

[115] A. V. Panfilov and J. P. Keener. Generation of reentry in anisotropic myocardium. *J Cardiovasc Electrophysiol*, 4(4):412–421, Aug 1993.

[116] A. V. Panfilov and J. P. Keener. Re-entry in an anatomical model of the heart. *Chaos, Solitons, and Fractals*, 5(3/4):681–689, March/April 1995.

[117] C. Pascarel, K. Hongo, O. Cazorla, E. White, and J. Y. Le Guennec. Different effects of gadolinium on I_{KR}, I_{KS} and I_{K1} in guinea-pig isolated ventricular myocytes. *Br J Pharmacol*, 124(2):356–360, May 1998.

[118] E. S. Pearlman, K. T. Weber, and J. S. Janicki. Quantitative histology of the hypertrophied human heart. *Federation Proceedings*, 40(7):2042–2047, May 15 1981.

[119] E. S. Pearlman, K. T. Weber, J. S. Janicki, G. G. Pietra, and A. P. Fishman. Muscle fiber orientation and connective tissue content in the hypertrophied human heart. *Laboratory Investigation*, 46(2):158–164, Feb 1982.

[120] Z. J. Penefsky and B. F. Hoffman. Effects of stretch on mechanical and electrical properties of cardiac muscle. *Am J Physiol*, 204(3):433–438, 1963.

[121] A. M. Pertsov, J. M. Davidenko, R. Salomonsz, W. T. Baxter, and J. Jalife. Spiral waves of excitation underlie reentrant activity in isolated cardiac muscle. *Circ Res*, 72(3):631–650, Mar 1993.

[122] J. G. Pinto and Y. C. Fung. Mechanical properties of the heart muscle in the passive state. *J Biomech*, 6(6):597–616, Nov 1973.

[123] R. Plonsey and R. C. Barr. Current flow patterns in two-dimensional anisotropic bisyncytia with normal and extreme conductivities. *Biophys J*, 45(3):557–571, Mar 1984.

[124] A. E. Pollard, K. W. Spitzer, and M. J. Burgess. Contributions of the specialized conduction system to the activation sequence in the canine pulmonary conus. *Am J Physiol*, 273(Heart Circ. Physiol. 42):H446–H463, Jul 1997.

[125] R. A. Province, M. G. Fishler, and N. V. Thakor. Effects of defibrillation shock energy and timing on 3-D computer model of heart. *Ann Biomed Eng*, 21(1):19–31, 1993.

[126] M. P. Pye and S. M. Cobbe. Arrhythmogenesis in experimental models of heart failure: the role of increased load. *Cardiovasc Res*, 32(2):248–257, Aug 1996.

[127] M. J. Reiter, D. P. Synhorst, and D. E. Mann. Electrophysiological effects of acute ventricular dilatation in the isolated rabbit heart. *Circ Res*, 62(3):554–562, Mar 1988.

[128] M. J. Reiter, Z. Zetelaki, C. J. Kirchhof, L. Boersma, and M. A. Allessie. Interaction of acute ventricular dilatation and d-sotalol during sustained reentrant ventricular tachycardia around a fixed obstacle. *Circulation*, 89(1):423–431, Jan 1994.

[129] J. J. Rice, R. L. Winslow, J. Dekanski, and E. McVeigh. Model studies of the role of mechano-sensitive currents in the generation of cardiac arrhythmias. *J Theor Biol*, 190(4):295–312, February 21 1998.

[130] T. L. Riemer, E. A. Sobie, and L. Tung. Stretch-induced changes in arrhythmogensis and excitability in experiementally based heart cell models. *Am J Physiol*, 275(Heart Circ. Physiol. 44):H431–H442, 1998.

[131] J. S. Robb and R. C. Robb. The normal heart: Anatomy and physiology of the structural units. *American Heart Journal*, 23:455–467, 1942.

[132] T. F. Robinson, L. Cohen-Gould, and S. M. Factor. Skeletal framework of mammalian heart muscle. Arrangement of inter- and pericellular connective tissue structures. *Laboratory Investigation*, 49(4):482–498, Oct 1983.

[133] T. F. Robinson, M. A. Geraci, E. H. Sonnenblick, and S. M. Factor. Coiled perimysial fibers of papillary muscle in rat heart: morphology, distribution, and changes in configuration. *Circ Res*, 63(3):577–592, Sep 1988.

[134] J. M. Rogers, M. S. Courtemenche, and A. D. McCulloch. Finite element methods for modelling impulse propagation in the heart. In A. V. Panfilov and A. V. Holden, editors, *Computational Biology of the Heart*, chapter 7, pages 217–234. J. Wiley & Sons Ltd., West Sussex, England, 1997.

[135] J. M. Rogers and A. D. McCulloch. A collocation-Galerkin finite element model of cardiac action potential propagation. *IEEE Trans Biomed Eng*, 41(8):743–757, Aug 1994.

[136] J. M. Rogers and A. D. McCulloch. Nonuniform muscle fiber orientation causes spiral wave drift in a finite element model of cardiac action potential propagation. *J Cardiovasc Electrophysiol*, 5(6):496–509, Jun 1994.

[137] M. A. Ross and D. D. Streeter, Jr. Nonuniform subendocardial fiber orientation in the normal macaque left ventricle. *European Journal of Cardiology*, 3(3):229–247, Oct 1975.

[138] B. J. Roth. How the anisotropy of the intracellular and extracellular conductivities influences stimulation of cardiac muscle. *J Math Biol*, 30(6):633–646, 1992.

[139] Y. Rudy and W. Quan. A model study of the effects of the discrete cellular structure on electrical propagation in cardiac tissue. *Circ Res*, 61(6):815–823, Dec 1987.

[140] A. Ruknudin, F. Sachs, and J. O. Bustamante. Stretch-activated ion channels in tissue-cultured chick heart. *Am J Physiol*, 264(Heart Circ. Physiol. 33):H960–H972, Mar 1993.

[141] A. Ruknudin, M. J. Song, and F. Sachs. The ultrastructure of patch-clamped membranes: A study using high voltage electron microscopy. *J Cell Biology*, 112(1):125–134, Jan 1991.

[142] F. Sachs. Stretch-sensitive ion channels: An update. In D. P. Corey and S. D. Roper, editors, *Sensory Transduction*, volume 47 of *Society of General Physiologists Series*, chapter 15, pages 241–260. Rockefeller University Press, New York, 1992. Society of General Physiologists, 45th annual symposium, Marine Biological Laboratory, Woods Hole, Massachusetts, 5–8 September 1991.

[143] F. Sachs. Modeling mechanical-electrical transduction in the heart. In V. C. Mow, F. Guilak, R. M. Hochmuth, and R. Tran-Son-Tay, editors, *Cell Mechanics and Cellular Engineering*, chapter 18, pages 308–328. Springer-Verlag, New York, 1994.

[144] F. Sachs. Mechanosensitive channels: Lost in space (abstract). *Biophys J*, 76(1):A3, Jan 1998. Abstract Supplement for the Biophysical Society 43rd Annual Meeting, February 13–17, 1999, Baltimore, Maryland.

[145] J. E. Saffitz, H. L. Kanter, K. G. Green, T. K. Tolley, and E. C. Beyer. Tissue-specific determinants of anisotropic conduction velocity in canine atrial and ventricular myocardium. *Circ Res*, 74(6):1065–1070, Jun 1994.

[146] N. Sasaki, T. Mitsuiye, and A. Noma. Effects of mechanical stretch on membrane currents of single ventricular myocytes of guinea-pig heart. *Japanese Journal of Physiology*, 42(6):957–970, 1992.

[147] D. F. Scollan, A. Holmes, R. Winslow, and J. Forder. Histological validation of myocardial microstructure obtained from diffusion tensor magnetic resonance imaging. *Am J Physiol*, 275(Heart Circ. Physiol. 44):H2308–2318, Dec. 1998.

[148] L. F. Shampine. *Numerical Solution of Ordinary Differential Equations*. Chapman & Hall, New York, 1994.

[149] S. Sicouri and C. Antzelevitch. Afterdepolarizations and triggered activity develop in a select population of cells (M cells) in canine ventricular myocardium: the effects of acetylstrophanthidin and Bay K 8644. *PACE*, 14(11 Part 2):1714–1720, Nov 1991.

[150] S. Sicouri and C. Antzelevitch. Drug-induced afterdepolarizations and triggered activity occur in a discrete subpopulation of ventricular muscle cells (M cells) in the canine heart: quinidine and digitalis. *J Cardiovasc Electrophysiol*, 4(1):48–58, Feb 1993.

[151] D. A. Sideris, S. T. Toumanidis, K. Kostopoulos, A. Pittaras, G. S. Spyropoulos, E. B. Kostis, and S. D. Moulopoulos. Effect of acute ventricular pressure changes on QRS duration. *J Electrocardiol*, 27(3):199–202, Jul 1994.

[152] W. Sigurdson, A. Ruknudin, and F. Sachs. Calcium imaging of mechanically induced fluxes in tissue-cultured chick heart: Role of stretch-activated ion channels. *Am J Physiol*, 262(Heart Circ. Physiol. 31):H1110–H1115, Apr 1992.

[153] W. J. Sigurdson, C. E. Morris, B. L. Brezden, and D. R. Gardner. Stretch activation of a K^+ channel in molluscan heart cells. *Journal of Experimental Biology*, 127:191–209, Jan 1987.

[154] B. H. Smaill and P. J. Hunter. Structure and function of the diastolic heart. In L. Glass, P. Hunter, and A. McCulloch, editors, *Theory of Heart: Biomechanics, Biophysics, and Nonlinear Dynamics of Cardiac Function*, chapter 1, pages 1–29. Springer-Verlag, New York, 1991.

[155] M. S. Spach, W. T. Miller, III, D. B. Geselowitz, R. C. Barr, J. M. Kootsey, and E. A. Johnson. The discontinuous nature of propagation in normal canine cardiac muscle. Evidence for recurrent discontinuities of intracellular resistance that affect the membrane currents. *Circ Res*, 48(1):39–54, Jan 1981.

[156] G. P. Stacy, Jr., R. L. Jobe, L. K. Taylor, and D. E. Hansen. Stretch-induced depolarizations as a trigger of arrhythmias in isolated canine left ventricles. *Am J Physiol*, 263(Heart Circ. Physiol. 32):H613–H621, Aug 1992.

[157] D. D. Streeter, Jr. Gross morphology and fiber geometry of the heart. In R. M. Berne, editor, *Handbook of Physiology, Section 2: The Cardiovascular System*, volume 1, chapter 4, pages 61–112. American Physiological Society, Bethesda, Maryland, 1979.

[158] D. D. Streeter, Jr. and D. L. Bassett. An engineering analysis of myocardial fiber orientation in pig's left ventricle in systole. *Anat Rec*, 155(4):503–512, Aug 1966.

[159] D. D. Streeter, Jr. and W. T. Hanna. Engineering mechanics for successive states in canine left ventricular myocardium: I. Cavity and wall geometry. *Circ Res*, 33:639–655, Dec 1973.

[160] D. D. Streeter, Jr. and W. T. Hanna. Engineering mechanics for successive states in canine left ventricular myocardium: II. Fiber angle and sarcomere length. *Circ Res*, 33:656–664, Dec 1973.

[161] D. D. Streeter, Jr., W. E. Powers, M. A. Ross, and F. Torrent-Guasp. Three-dimensional fiber orientation in the mammalian left ventricular wall. In J. Baan, A. Noordergraaf, and J. Raines, editors, *Cardiovascular System Dynamics*, chapter 9, pages 73–84. MIT Press, Cambridge, Mass., 1978.

[162] D. D. Streeter, Jr., H. M. Spotnitz, D. P. Patel, J. Ross, Jr., and E. H. Sonnenblick. Fiber orientation in the canine left ventricle during diastole and systole. *Circ Res*, 24(3):339–347, Mar 1969.

[163] L. A. Taber. On a nonlinear theory for muscle shells: Part II — Application to the beating left ventricle. *J Biomech Eng*, 113(1):63–71, Feb 1991.

[164] P. Taggart, P. Sutton, M. J. Lab, M. Runnalls, W. O'Brien, and T. Treasure. Effect of abrupt changes in ventricular loading on repolarization induced by transient aortic occlusion in humans. *Am J Physiol*, 263(Heart Circ. Physiol. 32):H816–H823, Sep 1992.

[165] P. Taggart, P. M. Sutton, T. Treasure, M. Lab, W. O'Brien, M. Runnalls, R. H. Swanton, and R. W. Emanuel. Monophasic action potentials at discontinuation of cardiopulmonary bypass: evidence for contraction-excitation feedback in man. *Circulation*, 77(6):1266–1275, Jun 1988.

[166] P. Taggart and P. M. I. Sutton. Cardiac mechano-electric feedback in man: clinical relevance. *Prog Biophys Mol Biol*, 71:139–154, 1999.

[167] H. E. ter Keurs, W. H. Rijnsburger, R. van Heuningen, and M. J. Nagelsmit. Tension development and sarcomere length in rat cardiac trabeculae: Evidence of length-dependent activation. *Circ Res*, 46(5):703–714, May 1980.

[168] F. Torrent-Guasp. *The Cardiac Muscle*. Publications of the Juan March Foundation. Editorial Graficas Torroba, Madrid, Spain, 1973. Translation of El musculo cardiaco.

[169] S. L. Van Leuven, L. K. Waldman, A. D. McCulloch, and J. W. Covell. Gradients of epicardial strain across the perfusion boundary during acute myocardial ischemia. *Am J Physiol*, 267(Heart Circ. Physiol. 36):H2348–H2362, Dec 1994.

[170] A. Vesalius. *The Epitome of Andreas Vesalius*. M.I.T. Press, Cambridge, Mass., 1969. Translated from the Latin by L. R. Lind.

[171] F. J. Villarreal, L. K. Waldman, and W. Y. Lew. Technique for measuring regional two-dimensional finite strains in canine left ventricle. *Circ Res*, 62(4):711–721, Apr 1988.

[172] L. K. Waldman, Y. C. Fung, and J. W. Covell. Transmural myocardial deformation in the canine left ventricle: Normal in vivo three-dimensional finite strains. *Circ Res*, 57(1):152–163, Jul 1985.

[173] L. K. Waldman, D. Nosan, F. Villarreal, and J. W. Covell. Relation between transmural deformation and local myofiber direction in canine left ventricle. *Circ Res*, 63(3):550–62, Sep 1988.

[174] Z. Wang, L. K. Taylor, W. D. Denney, and D. E. Hansen. Initiation of ventricular extrasystoles by myocardial stretch in chronically dilated and failing canine left ventricle. *Circulation*, 90(4):2022–2031, Oct 1994.

[175] K. T. Weber. Cardiac interstitium in health and disease: The fibrillar collagen network. *J Am Coll Cardiol*, 13(7):1637–1652, Jun 1989.

[176] D. W. Whalley, D. J. Wendt, and A. O. Grant. Basic concepts in cellular cardiac electrophysiology: Part II: Block of ion channels by antiarrhythmic drugs. *PACE*, 18(9 Part I):1686–1704, Sep 1995.

[177] E. White, J.-Y. Le Guennec, J. M. Nigretto, F. Gannier, J. A. Argibay, and D. Garnier. The effects of increasing cell length on auxotonic contractions; membrane potential and intracellular calcium transients in single guinea-pig ventricular myocytes. *Exp Physiol*, 78(1):65–78, Jan 1993.

[178] M. R. Wilby, M. J. Lab, and A. V. Holden. Dynamical model of signal propagation in the heart. *J Theor Biol*, 168(4):399–406, Jun 1994.

[179] A. T. Winfree. Varieties of spiral wave behavior: An experimentalist's approach to the theory of excitable media. *Chaos*, 1(3):303–334, 1991.

[180] A. T. Winfree. Persistent tangled vortex rings in generic excitable media. *Nature*, 371(6494):233–236, September 15 1994.

[181] R. L. Winslow, J. Rice, S. Jafri, E. Marbán, and B. O'Rourke. Mechanisms of altered excitation-contraction coupling in canine tachycardia-induced heart failure, II model studies. *Circ Res*, 84:571–586, 19 March 1999.

[182] X.-C. Yang and F. Sachs. Block of stretch-activated ion channels in Xenopus oocytes by gadolinium and calcium ions. *Science*, 243(4894 Part 1):1068–1071, February 24 1989.

[183] X. C. Yang and F. Sachs. Mechanically sensitive, nonselective cation channels. *Exs*, 66:79–92, 1993.

[184] F. C. Yin. Ventricular wall stress. *Circ Res*, 49(4):829–842, Oct 1981.

[185] F. C. P. Yin, R. K. Strumpf, P. H. Chew, and S. L. Zeger. Quantification of the mechanical properties of noncontracting canine myocardium under simultaneous biaxial loading. *J Biomech*, 20(6):577–589, 1987.

[186] A. A. Young and L. Axel. Three-dimensional motion and deformation of the heart wall: estimation with spatial modulation of magnetization — a model-based approach. *Radiology*, 185(1):241–247, Oct 1992.

[187] A. A. Young, C. M. Kramer, V. A. Ferrari, L. Axel, and N. Reichek. Three-dimensional left ventricular deformation in hypertrophic cardiomyopathy. *Circulation*, 90(2):854–867, Aug 1994.

[188] A. A. Young, I. J. LeGrice, M. A. Young, and B. H. Smaill. Extended confocal microscopy of myocardial laminae and collagen network. *Journal of Microscopy*, 192(Pt 2):139–150, Nov 1998.

[189] M. Zabel, B. S. Koller, F. Sachs, and M. R. Franz. Stretch-induced voltage changes in the isolated beating heart: Importance of the timing of stretch and implications for stretch-activated ion channels. *Cardiovasc Res*, 32(1):120–130, July 1996.

[190] M. Zabel, S. Portnoy, and M. R. Franz. Effect of sustained load on dispersion of ventricular repolarization and conduction time in the isolated intact rabbit heart. *J Cardiovasc Electrophysiol*, 7(1):9–16, Jan 1996.

[191] J. Zeng, K. R. Laurita, D. S. Rosenbaum, and Y. Rudy. Two components of the delayed rectifier K^+ current in ventricular myocytes of the guinea pig type: Theoretical formulation and their role in repolarization. *Circ Res*, 77(1):140–152, June 1995.

Chapter II

Structural Model of the Rabbit Ventricular Anatomy

II.A Introduction

The dynamic pumping function of the heart depends on cellular ionic mechanisms which give rise to the cardiac action potential, the crossbridge interactions that develop myofilament tension, and intracellular calcium fluxes that regulate contraction. To understand how these processes govern the mechanics and electrophysiology of the intact myocardium requires knowledge of the three-dimensional geometry and structure of the whole heart. Normal myocardium is heterogeneous [4]. The normal heart exhibits nonhomogeneous distributions of stress, strain, electrical activation and repolarization [7, 32, 6]. These heterogeneities are frequently exaggerated in pathological conditions such as myocardial ischemia [18, 30, 31, 20]. Three-dimensional models provide a way to investigate how regional mechanics and electrical propagation depend on local properties.

Although many important variables can be experimentally measured in cardiac cells or in the whole heart, practical methods for measuring their three-dimensional variations throughout the myocardium are highly limited. Hence, there is a need for three-dimensional models of myocardial electrical and mechanical func-

tion based on the underlying biophysics of the cell and a realistic representation of regional ventricular geometry and fiber architecture.

Hunter and Smaill (1988) have detailed how a continuum approach could be used to achieve these goals in practice. Continuum models must be represented in a manner suitable for efficient and accurate computation. The finite element method is capable of formulating and solving nonlinear continuum problems on irregular and anisotropic physical structures and thus provides a framework for the development and use of practical continuum models. In this chapter we develop a new high-order finite element model of the rabbit ventricular geometry and fiber angle architecture suitable for studying the regional mechanics and electrical properties of intact myocardium.

II.B Methods

The computational procedures outlined here closely follow those developed by Nielsen et al. (1991), though we have chosen the rabbit because many of the most suitable experiments for validating three-dimensional models of this kind have been conducted in this species [2, 3, 5, 8, 9, 10, 11, 15, 16, 19, 21, 24, 33, 34, 35]. An electrophysiological model of a 9-gram rabbit heart will have about one thirtieth the number of degrees of freedom of a comparably converged model of the dog heart, since the space constant for conduction is similar for both species (about 1 mm) [17, 23]. Nonetheless, with appropriately timed extrastimuli, the rabbit model is still large enough to admit the complex reentrant dynamics that can also be evoked in larger species [1, 12, 27].

II.B.1 Experimental Preparation

New Zealand white rabbits (3.8–4.1 kg) were anesthetized with 50 mg/kg ketamine hydrochloride and 4 mg/kg xylazine hydrochloride and ventilated with oxygen and 1.5% halothane. A sternotomy was performed, the aorta clamped, and

3 mg/kg heparin sodium injected into the left ventricle (LV). The heart was arrested in diastole using a hyperkalemic cardioplegic solution (29.5 mM KCl).

The heart was immediately excised, the pulmonary vessels removed and the chordae tendineae cut to prevent valve closure during fixation. The aorta was cannulated and the heart suspended in Ringers lactate solution, then perfused in the unloaded state with 10% buffered formalin phosphate at 80 mm Hg for 3–4 minutes. The heart was stored in 10% buffered formalin phosphate until sectioned.

II.B.2 Tissue Processing

The right and left ventricular cavities were filled with a quick-setting dental rubber (polyvinylsiloxane). Two 25 gauge needles were inserted in orthogonal directions at the apex in the short-axis plane; the needles prevent the heart from moving relative to the surrounding rubber. The whole heart was placed in a custom-built rigid tube and plunger assembly. The open volume between the heart and tube was also filled with dental rubber. Three hemispherical notches (machined parallel to the tube axis on the inner surface) provide a "tongue-in-groove" key that prevented the heart and surrounding rubber from rotating within the tube. On the face of the tube are four crosshair fiducial markers (visible in each panel of Figure II.1) used for later registering the images of the short-axis slices.

After a setting time of 3–5 minutes, successive short-axis digital images (640 x 480 pixels, 0.13 mm/pixel) of the tissue, rubber, and fiducial markers were acquired as 2–3 mm thick slices of the rubber and tissue were cut from the face of the tube (Figure II.1). From these images the geometric contours of the tissue-rubber interface were segmented and the geometric coordinates of the fiducial markers are recorded using standard image processing software (NIH Image). The last slice contained the LV apex and geometric minimum of the epicardium. These points were highlighted with small white dots of titanium dioxide and their geometric coordinates also recorded. With tissue slice thickness information, the geometric contours and fiducial markers constitute a three-dimensional geometric representation of the

right and left ventricular epicardial and endocardial surfaces.

Myocardial fiber measurements were collected from blocks of tissue cut from the slices in a radial direction. Each block was mounted on a cryostage and serially sectioned in the plane tangent to the epicardium (shown schematically in Figure II.3(a)). Measurements of the local myocardial fiber angle relative to the slice plane were made at four central locations in images of unstained 20-μm sections from the epicardial tangent plane (Figure II.3(b)). Selected sections from a block of the inferior septum are shown in Figure II.4. High magnification (67×) images of the sections showed an average sarcomere length (Figure II.2) of 2.06 $\pm$ 0.12 μm (n = 133), consistent with the intact myocardium in diastasis [28], suggesting there was minimal systematic dilation or shrinkage in this preparation.

II.B.3 Image Registration and Coordinate Transformations

The heart and tube assembly had to be removed from the imaging apparatus to cut successive short-axis slices. Since the assembly could not be replaced exactly in the previous imaging position, a reference image was chosen and a translation-rotation transformation determined for each of the other images to register the fiducial markers. After applying these transformations to the contours of the tissue-rubber interface, the geometric coordinates of the cardiac surfaces were consistent with a global "measurement" coordinate system (Figure II.5(a)).

To develop the mathematical model, it is convenient to define a "model" coordinate system relative to features of the heart (Figure II.5(b)). Since no anatomical features have the same geometric position from one heart to the next, we chose to locate the x_1-axis of the model coordinate system on a line through the LV apex and the LV cavity centroid in the slice nearest the equator. The origin of the model coordinate system is located at the origin of the best-fit ellipsoid to the LV cavity contours; this best-fit ellipsoid also gives the focus position d in the transformation

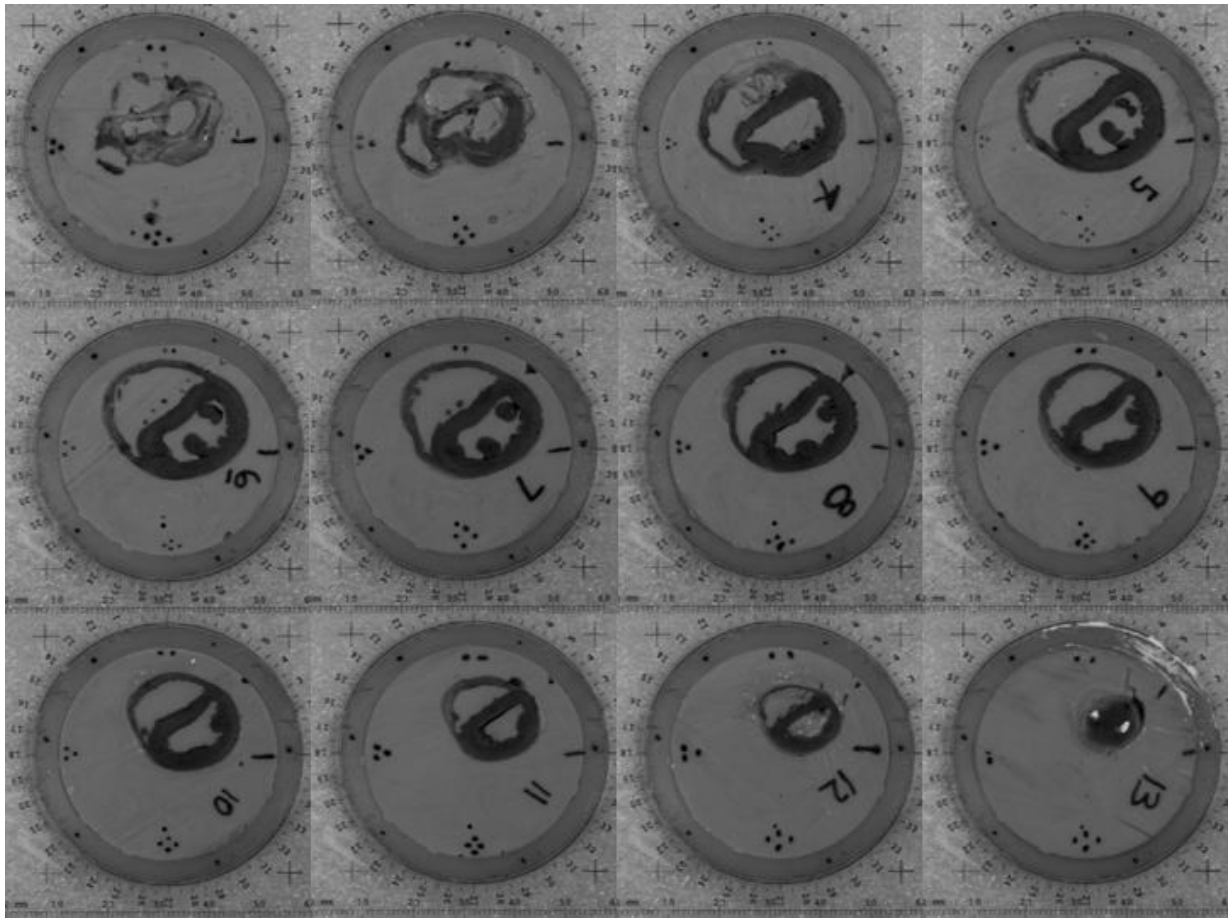

Figure I.1: Successive serial images of the short-axis slices of myocardium cast in dental rubber. After each image was captured, 2–3 mm of the tissue/rubber plug were pressed out of the tube and sliced off, exposing the myocardium and rubber for the next image. Successive images are shown in rows starting at the base (upper left) and ending at the apex (lower right).

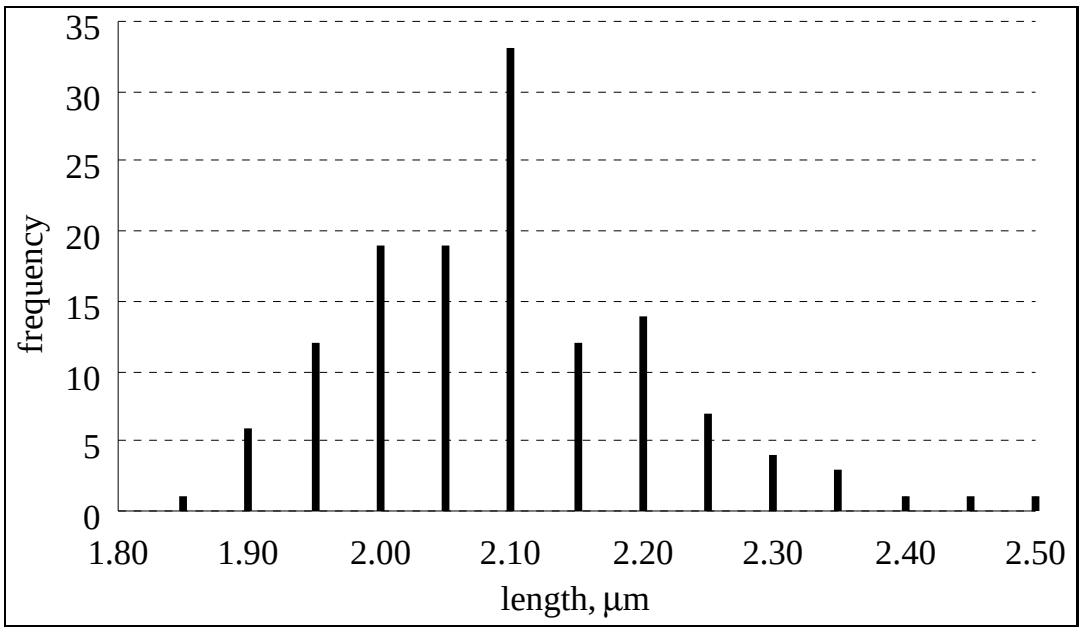

Figure II.2: Frequency of sarcomere lengths (n = 133) from cryosections collected from the LV, RV, and septum. Mean ± SD : 2.06 $\pm$ 0.12 μm.

from prolate spheroidal to rectangular Cartesian coordinates:

$$\begin{aligned} x_1 &= d \cosh\lambda \cos\mu \\ x_2 &= d \sinh\lambda \sin\mu \cos\theta \\ x_3 &= d \sinh\lambda \sin\mu \sin\theta \end{aligned} \tag{II.1}$$

The x_2-axis of the model system was located at the bisection of the line from the right ventricular (RV) cavity corners in the same nearest-equatorial slice.

II.B.4 Surface and Fiber Fitting

Before fitting, the three-dimensional geometric coordinates were converted to prolate spheroidal coordinates, which enables the surface fits to be reduced to one dimension [22]. The circumferential θ coordinate of the six nodes on the vertical RV boundary was fitted (6 DOF) to the extremal geometric coordinates in this region. The longitudinal μ coordinate of the 20 basal nodes was fitted (20 DOF) to the geometric contours of the first slice of myocardium. Finally, using the method of Nielsen

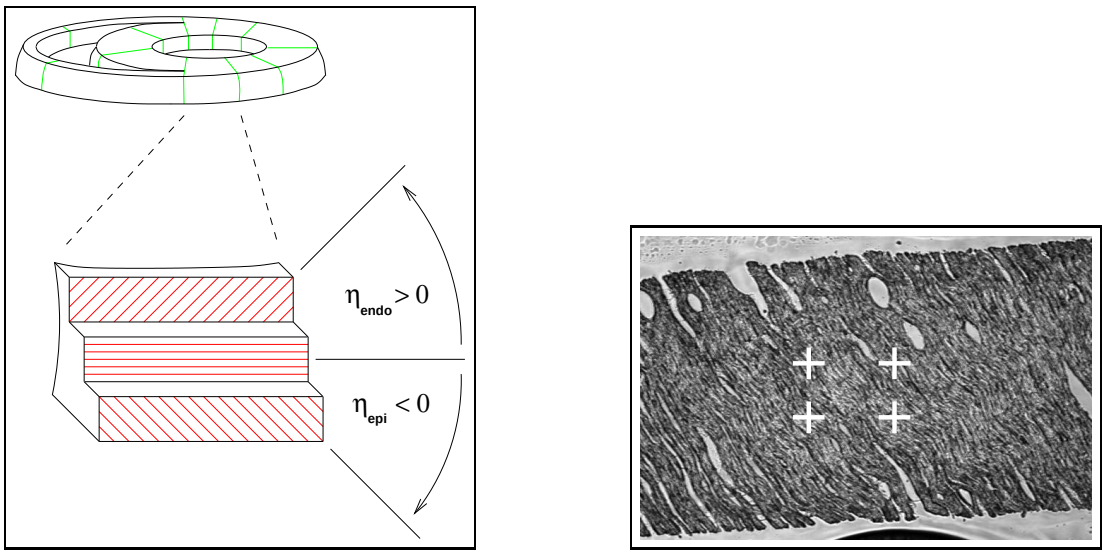

(a) Tissue slice and block schematic

(b) Unstained tissue cryosection

Figure II.3: (a) Schematic of a block cut from a tissue slice, showing the transmural variation in fiber angle η. (b) Micrograph (6.68×) of unstained cryosectioned tissue showing fiber orientations. White crosses indicate the typical locations of the four fiber angle measurements. Angles were measured with respect to the lower edge of the tissue. In the section shown the average measured fiber angle was −61 degrees.

et al. (1991), the radial λ coordinate of the nodes defining the four two-dimensional finite element meshes (48 total elements), one each for the left ventricular endocardium, the epicardium, and right ventricular free and septal walls, was simultaneously fitted (226 DOF) to the coordinates of the cardiac surfaces using a constrained linear least-squares method. The constraints imposed on the fit ensure derivative symmetry at the left ventricular apex and the epicardial geometric minimum, and derivative equality at the right ventricular free and septal wall boundaries.

Owing to the sparsity of geometric coordinates in the apical (last) slice, the radial positions of the nodes at the LV apex and epicardial geometric minimum were not fitted; instead, these nodal variables were assigned the geometric coordinates of the titanium oxide dots at these locations. The remaining radial coordinates

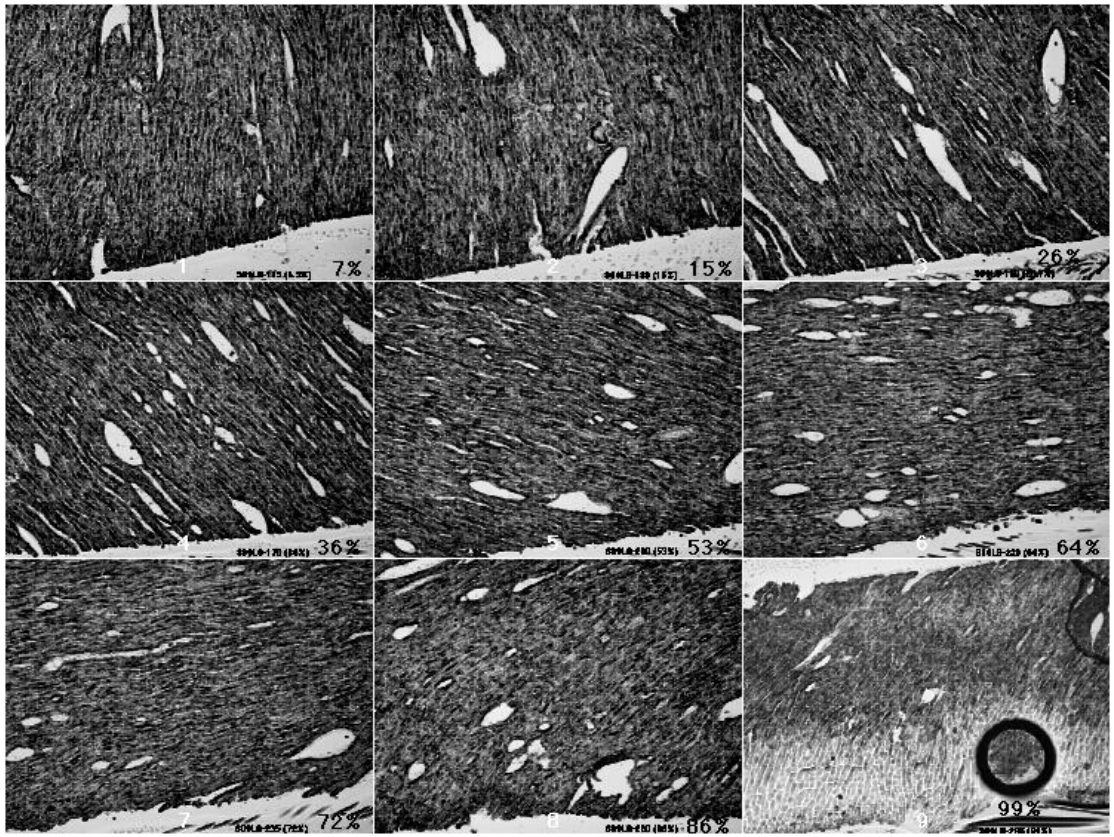

Figure I.4: Typical images (6.68×) of serial cryosections of unstained tissue from the inferior septum. Normalized transmural wall depth of the sections (from left to right, starting at upper left): 7, 15, 26, 36,35 64, 72, 86, and 99%. Total thickness of the block was 3.66 mm. Average measured fiber angle in the first section is −104 degrees; in the last section this average is +43 degrees.

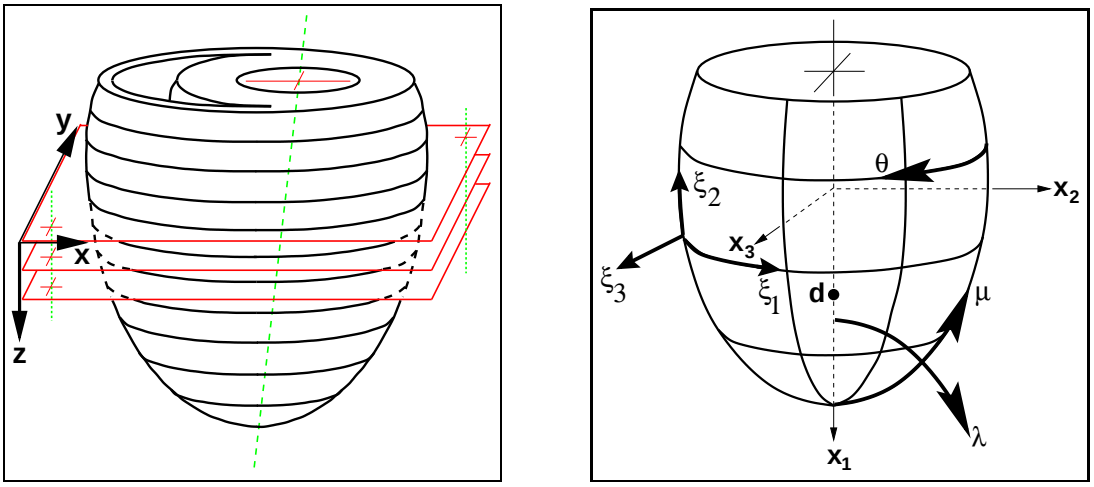

(a) Measurement coordinate system

(b) Model coordinate system

Figure II.5: Schematic diagrams of the "measurement" and "model" coordinate systems. (a) Locations of the individual slices are represented by planes, which are parallel to each other but not perpendicular to the long-axis of the LV cavity. (b) The rectangular Cartesian "model" coordinate system (x_1, x_2, x_3) is collinear with the long-axis of the LV cavity. The prolate spheroidal coordinate system (λ, μ, θ) is convenient for modeling cardiac geometry. The curvilinear parametric coordinates (ξ_1, ξ_2, ξ_3), used in fitting and subsequent analysis, are the local finite element coordinates.

were fitted to 8,351 geometric coordinates, interpolated with bicubic Hermite basis functions [22, 13] to provide derivative continuity on the surfaces. To generate the single three-dimensional volumetric mesh from the four two-dimensional meshes, additional nodes were defined in the LV midwall, and the two-dimensional surface elements were connected transmurally by defining nodal interconnections through the myocardial walls. The final three-dimensional mesh of 36 elements (552 total DOF) defines the geometry of the ventricular model and was used to fit the fiber angle measurements.

The geometric coordinates of the first and last serial tissue section of each

block were mapped onto the geometric model to define the location of the measured fiber angles relative to the model. The measured fiber angles were then mapped to the appropriate transmural positions in the model, and corrected for the difference between the plane of the tissue slices (to which the measured angles were referenced) and the curvilinear local finite element circumferential plane (the ξ_1–ξ_3 plane, to which the angles are referenced in the model). This correction is required because the plane of the tissue slices is not, in general, parallel to the ξ_1–ξ_3 plane in the three-dimensional elements. Redundant nodes at the RV boundary (like those used by Nielsen et al. (1991)) allow for the abrupt change in fiber angle in these regions. Fitted fiber angles at the nodes along the RV endocardial circumferential boundary were constrained to be equal to those at the corresponding nodes in the apical midwall — again owing to the sparsity of measurements in this region. The same constraint was applied to a single node at the RV endocardial boundary at the base. Over 14,300 local fiber angle measurements from 3,592 serial sections were fitted (184 DOF) using bilinear-cubic Hermite basis functions.

II.C Results

The fitted three-dimensional finite element model of the ventricular geometry and fiber angles is shown in Figure II.6 and II.7. The root mean squared errors (RMSE) of the geometric and fiber fits are summarized by region in Table II.1. Over 22,500 measurements are represented by 736 degrees of freedom with a RMSE of ± 0.55 mm in the geometric surfaces and ± 19 degrees in the fiber angles. The RV free wall had the highest error of ± 0.72 mm and the LV wall had the error of ± 0.35 mm. Fitting errors for the fiber angle distribution were highest for the apex (± 31 degrees) and lowest for the septum (± 11.9 degrees).

Gross anatomical information can be extracted from the model (Table II.2). The volumes of the LV free wall, septum, RV free wall, and apex are calculated from the three-dimensional element volumes representing those regions in the ac-

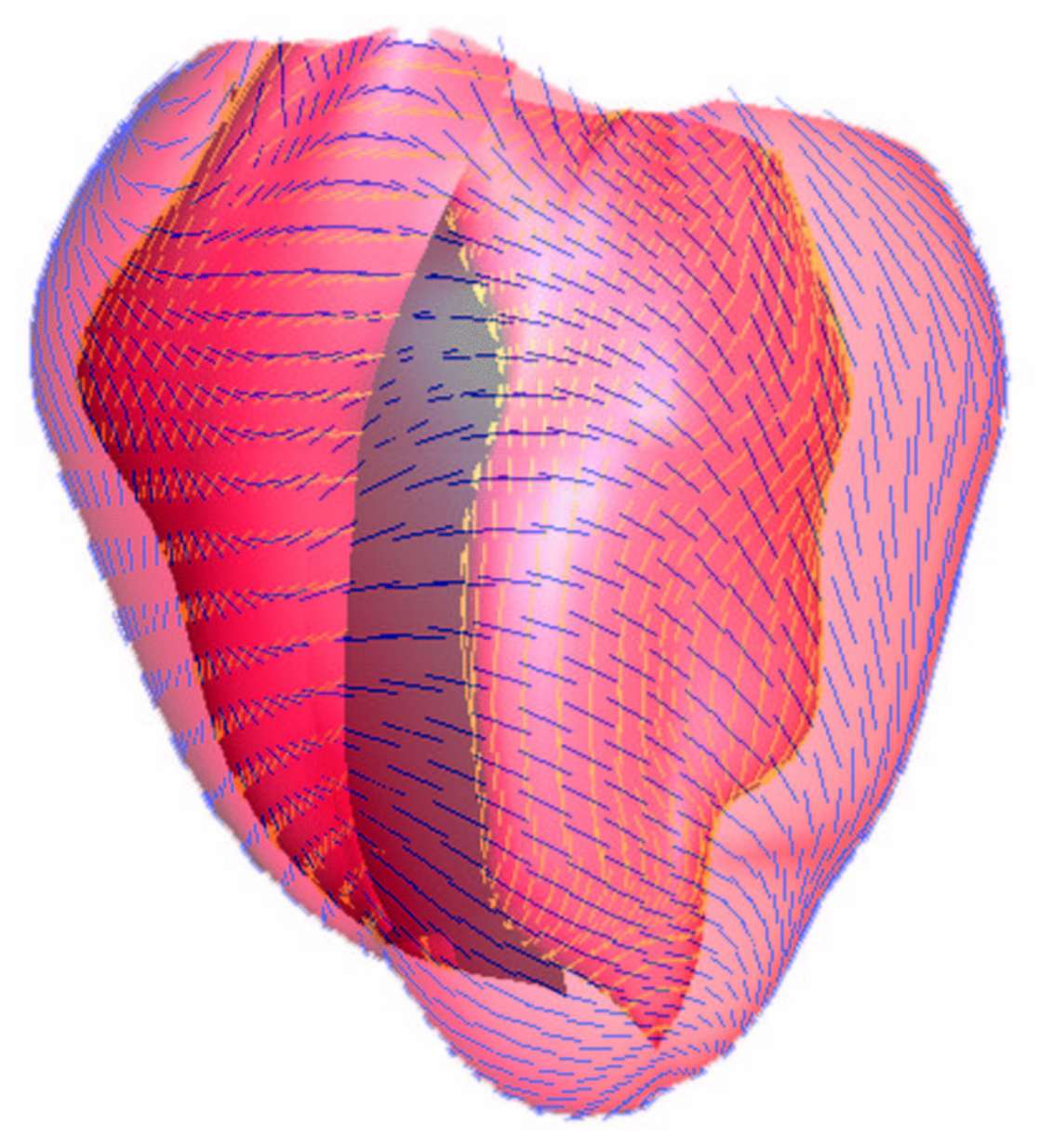

Figure II.6: Anterior view of the fitted three-dimensional finite element model showing interpolated fiber angles superposed on epicardial and endocardial surfaces.

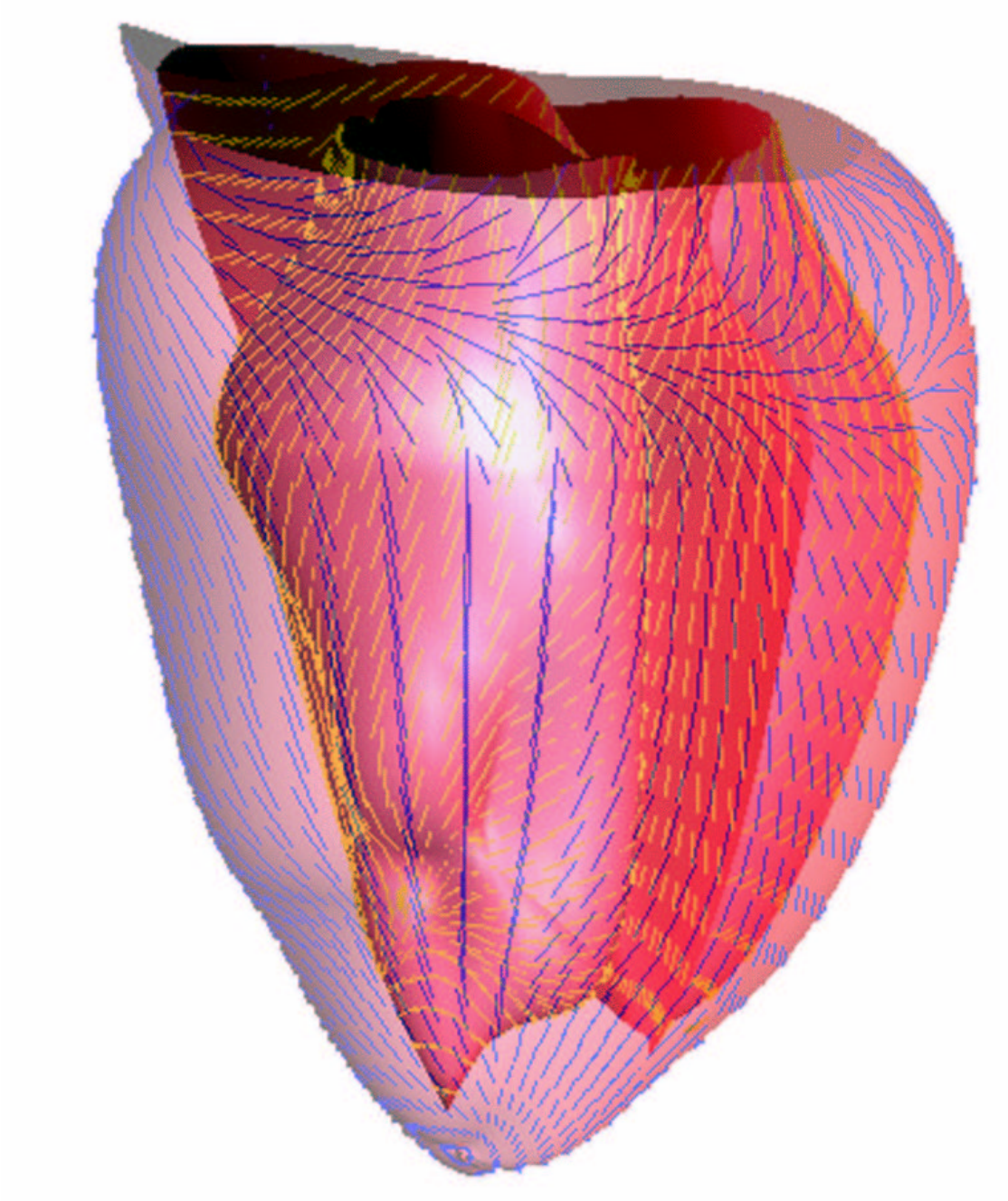

Figure II.7: Posterior lateral view of the fitted three-dimensional finite element model showing interpolated fiber angles superposed on epicardial and endocardial surfaces.

heart region	geometry # points	RMSE (mm)	fibers # sections	RMSE (deg.)	number of elements
LVFW	3200	0.35	1569	15.4	12
RVFW	3157	0.72	599	18.3	6
Septum	1514	0.47	852	11.9	6
Apex	480	0.61	572	31.1	12
overall	8351	0.55	3592	18.6	36

Table II.1: Root mean squared errors (RMSE) in the fitted finite element geometry (552 DOF) and fiber distribution (184 DOF) models.

tual heart. The average thickness of the same elements was used to determine wall thickness. The total myocardial volume in the model was 6.61 milliliters and the LV and RV cavities had volumes of 2.49 and 1.75 milliliters, respectively. The transmural fiber distributions were the interpolated values along a line in the equatorial plane at the circumferential midpoint of each region, except the apex, where the angles are interpolated from the longitudinal midpoint of the apical elements in the lateral wall. The fitted fiber distribution errors are all below 20 degrees except at the apex, where gradients of measured fiber angles were primarily monotonic, but demonstrated distinct transition from a positive transmural gradient to a negative

heart region	volume (ml)	average wall thickness (mm)	transmural fiber angle distribution (degrees)	
			epicardium	endocardium
LV free wall	3.42	4.98	−71.0	59.6
septal wall	1.36	4.88	−45.1	51.5
RV free wall	1.35	1.69	−78.2	28.0
apex	0.48	3.49	−29.6	69.3

Table II.2: Anatomical information from the finite element model.

gradient in the anterior region (Figure II.8).

II.D Discussion

The methods used to collect the geometric and fiber orientation data provided a means to check for systematic error in the transmural location of the measured fiber angles. Wall thickness throughout the heart was estimated in two ways for each block of tissue sectioned. First the radial thickness of each block was measured from the short-axis slices (Figure II.1) at the epicardial and endocardial endpoints of the desired transmural sectioning path. The distance between these points was designated the "imaged thickness," h_I, and is accurate to within pixel resolution of images (0.013 mm). After sectioning a secondary measure of wall thickness was computed by multiplying the number of sections by the thickness of each section; the local wall thickness computed in this manner was designated the "sectioned thickness" or h_S.

Assuming for the moment that each tissue block had no curvature in the longitudinal direction (i.e., the heart is cylindrical), then a plot of the sectioned thickness versus the imaged thickness would be linear if the measurements were perfect. In reality, the longitudinal curvature of the wall will introduce error in the imaged thickness. The sectioned thickness measurement will be erroneous due to differences in the desired sectioning path from the actual path, trabeculae on the endocardial surface, and differences between the sectioning plane and the epicardial tangent plane.

Since both of the thickness measures have some uncertainty, a total least-squares fit [26] of the imaged thickness to the sectioned thickness was computed for 136 tissue blocks in this heart. As shown in Figure II.9, the relationship between the two thickness measures is somewhat linear and the systematic error (0.045 mm) is significantly less than the RMS error of the geometric fit of the model ($\pm$0.55 mm). This suggests that mapping the normalized depths along the sectioning paths

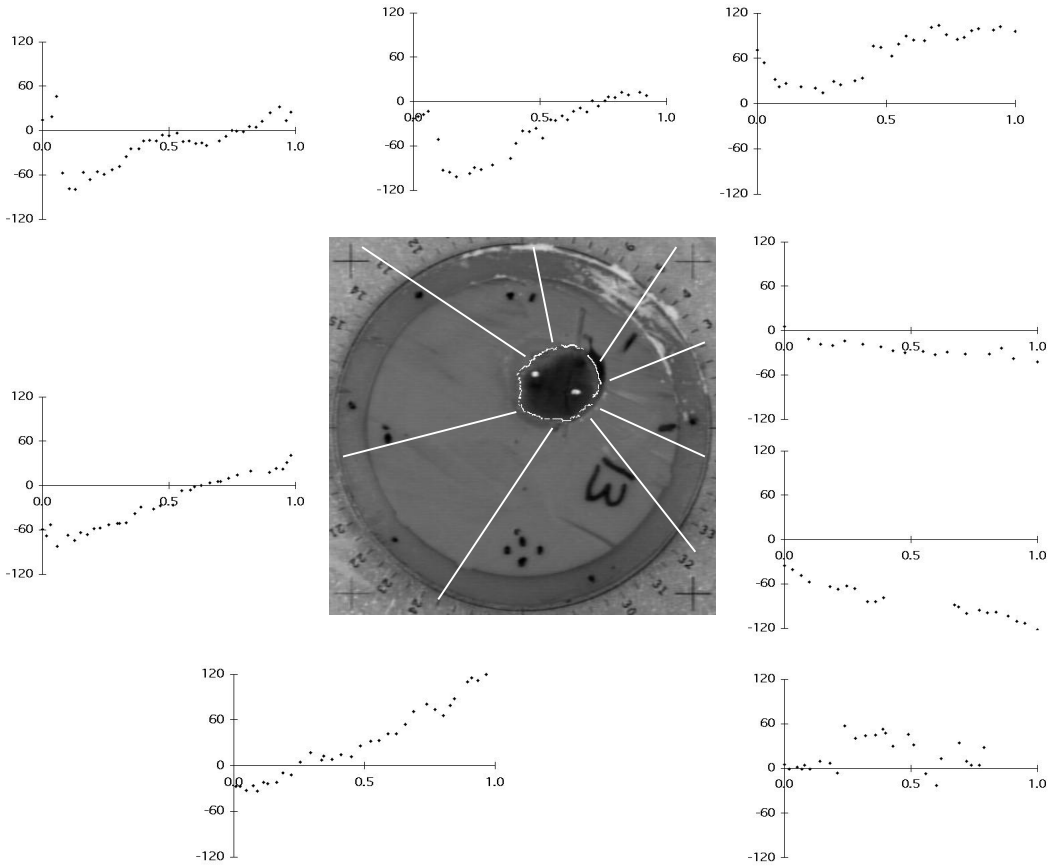

Figure II.8: Measured, uncorrected fiber angles from eight apical tissue blocks. The white contour outlines tissue-rubber boundary. White dots at lower right and upper left are lowest points the LV and RV cavities, respectively. White lines indicate direction of the transmural sectioning path which ended at the lower right dot. Plot axes are fiber angle (vertical scale: -120 to $+120$ degrees) vs. normalized wall depth (horizontal scale: 0.0 is epicardium, 1.0 is endocardium). Note the negative transmural gradient in the plots on the right.

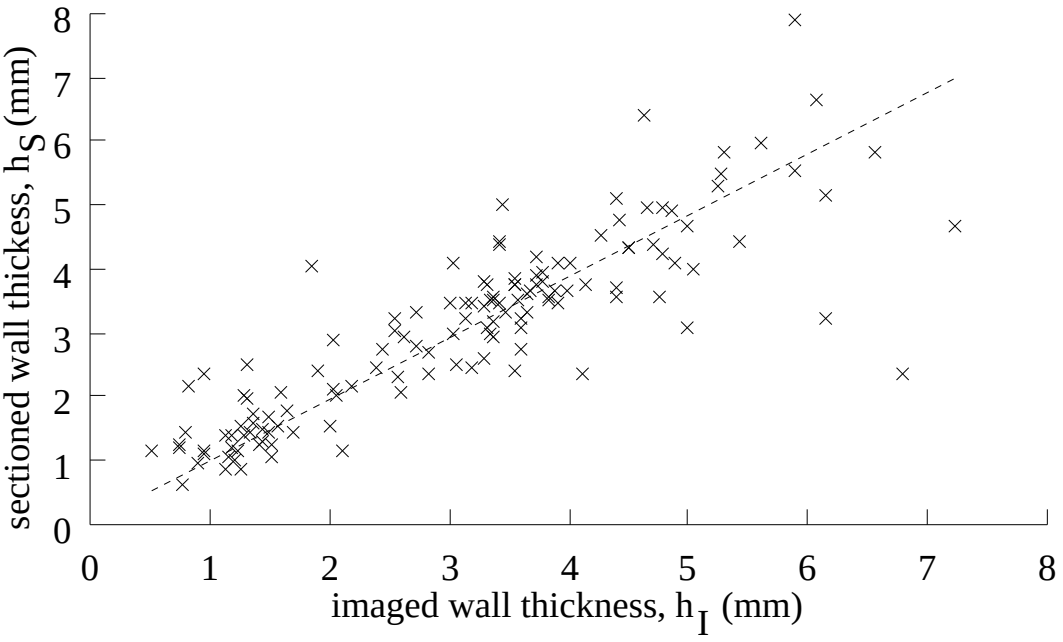

Figure II.9: Total least squares fit of the wall thickness as measured by image surface points and the number of collected transmural sections. Equation of the fitted line is $h_S = 0.962345\, h_I + 0.044811$.

to the fitted geometric model does not introduce any systematic deviation from the true location of the measured fiber angles.

The RV and LV cavity volumes, 2.49 and 1.75 ml, are somewhat smaller than the end-diastolic volumes of 3.38 and 3.29 ml reported for the rabbit [25]. In addition, the larger RV volume implies the RV was probably distended while being filled with dental rubber.

The positive to negative shift in the transmural gradient of the fiber orientation at the apex (Figure II.8) was unexpected. We attribute this change in transmural fiber gradient direction to the transition of fibers from subepicardium to subendocardium where the imbrication angle of the fibers is greatest [29]. Using higher-order interpolation functions in the longitudinal direction, together with a nodal imbrication angle parameter in the basal and apical regions, should reduce the fitted fiber distribution errors.

	LVFW	RVFW	Septum	Apex	total
geometry (mm)	0.80	0.75	1.27	1.29	1.10
fiber (deg.)	20.5	28.5	17.8	34.2	24.1

Table II.3: RMSE by region for the simplified model using trilinear Lagrange interpolation of the fitted coordinate values and fiber angles.

A comparison of the measured fiber angles and the fitted transmural distributions is shown in Figure II.10. The fitted fiber distributions are in close agreement with the measured angles and the fitted distributions in the canine [22]. The epicardial angles are nearly identical in the lateral, anterior septal, and posterior walls. At the endocardium of the RV, however, the canine model has a fiber orientation close to zero degrees, but in the rabbit the same angles approach 40 degrees. In the anterior septum a similar transmural trend is present in both models, but the rabbit model orientation is shifted approximately 30 degrees more positive relative to the canine model.

The high-order finite element model presented here can be simplified by omitting the derivatives and interpolating only the fitted geometric value and fiber angle parameters using trilinear Lagrange basis functions. Although this approach increases the total RMSE of the geometric model to ± 1.10 mm and the fiber distribution RMSE to ± 24.1 degrees (detailed by region in Table II.3), for some applications the simplified computations may justify the reduced accuracy. The fitted geometric coordinate values and fiber angles are listed in Tables II.4, II.5, and II.6.

The text of this chapter, in part, is a reprint of the material as it appears in *Progress in Biophysics and Molecular Biology*, F. J. Vetter and A. D. McCulloch, 69(2-3):157-184 (1998). I was the primary researcher and author and the co-author(s) listed in this publication directed and supervised the research which forms the basis for this chapter.

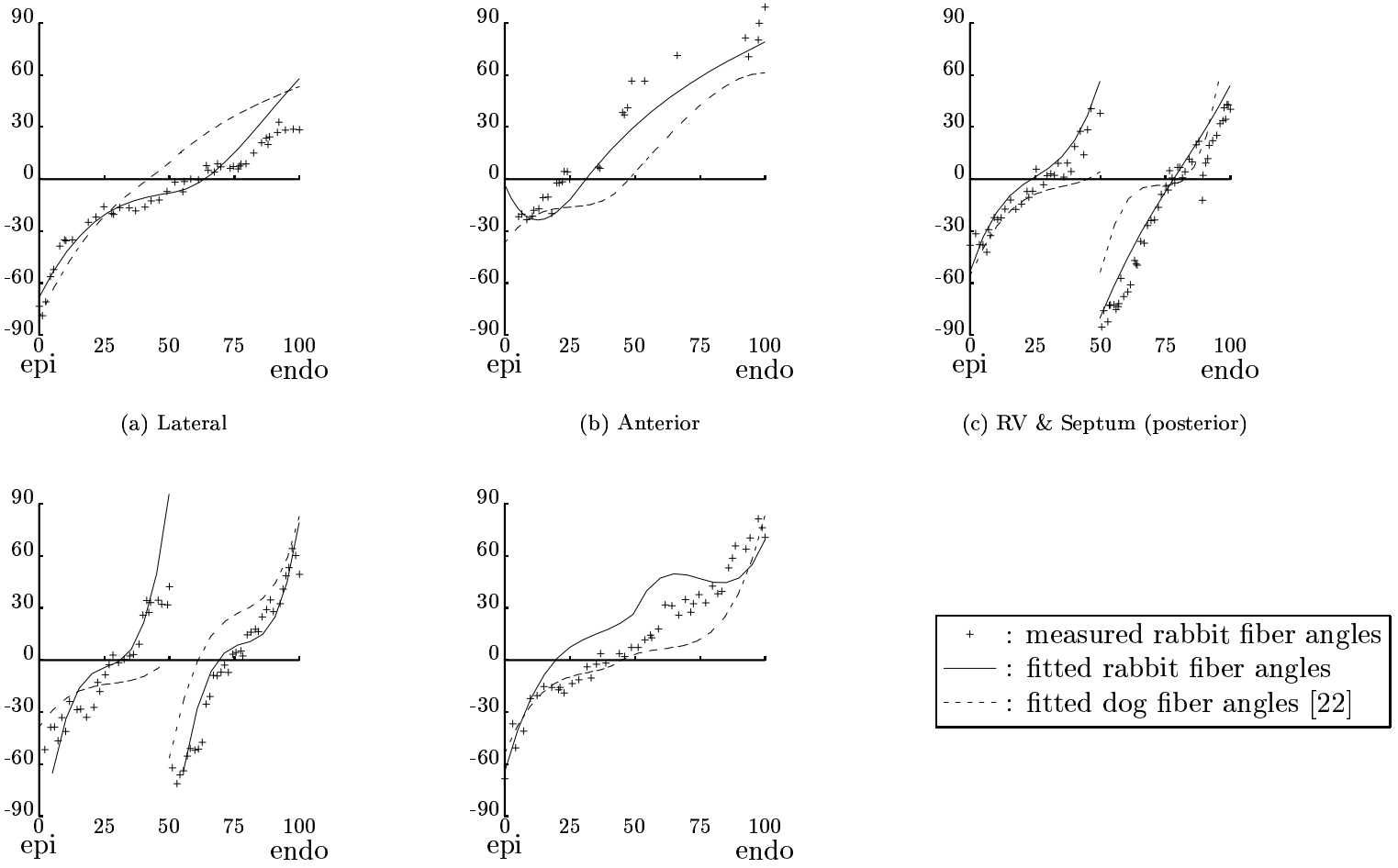

(a) Lateral

(b) Anterior

(c) RV & Septum (posterior)

(d) RV & Septum (anterior)

(e) Posterior

Figure I.10: Measured and fitted fiber angles for the rabbit (crosses and solid lines) and fitted fiber angles for the dog. Horizontal axes are normalized wall depth (%); vertical axes are fiber angle (degrees).

	epicardium				LV midwall				LV endocardium			
Region	μ	θ	λ	η	μ	θ	λ	η	μ	θ	λ	η
base	118.81	50.751	0.85587	163.38	123.80	50.751	0.68504	5.9867	129.16	50.751	0.44017	−8.0727
	116.90	125.00	0.77879	53.824	121.51	125.00	0.62236	33.294	12.12	125.00	0.46593	100.37
	129.64	250.00	0.71123	−72.463	133.09	250.00	0.51355	23.546	6.354	250.00	0.31586	42.909
	124.41	283.16	1.0629	−43.435	125.80	28.79	0.98015	−4.2603	137.32	281.91	0.36250	78.118
mid	90.00	70.898	0.84819	−37.142	90.00	70.898	0.73965	69.169	90.00	70.898	0.35657	63.359
	90.00	125.00	0.77315	−91.549	90.00	125.00	0.63522	−16.048	90.00	125.00	0.49729	75.354
	90.00	250.00	0.69948	−44.937	90.00	250.00	0.58290	−0.50420	90.00	250.00	0.46632	39.603
	90.00	307.74	0.92556	39.571	90.00	307.74	0.85618	−24.452	90.00	307.74	0.50333	118.50
	27.00	55.378	0.88807	−23.196	27.00	55.378	0.85321	3.6419	27.00	55.378	0.57724	34.932
	40.00	125.00	0.70523	−8.129	40.00	125.00	0.49725	34.972	40.00	125.00	0.28926	69.780
	40.00	250.00	0.64705	−37.802	40.00	250.00	0.48005	34.253	40.00	250.00	0.31305	123.66
	40.00	335.48	0.89627	−94.723	40.00	335.48	0.86512	41.523	40.00	335.48	0.60243	45.200
apex	0.00	–	0.91900	6.8298	0.00	–	0.86950	8.3762	0.00	–	0.82000	45.147

Table I.4: Fitted prolate spheroidal geometric coordinates (λ, μ, θ) and fiber angles (η) in the left ventricular wall and apex, excluding derivatives. Focus $d = 13.29$ mm. Coordinate values μ, θ and fiber angle η are in degrees; the λ coordinate is dimensionless. See text for discussion.

	epicardium				RV endocardium			
Region	μ	θ	λ	η	μ	θ	λ	η
base	124.41	283.16	1.0629	−43.435	125.80	282.79	0.98015	−14.542
	121.42	301.81	1.1687	120.17	122.88	300.00	1.1474	−24.761
	121.96	343.23	1.0802	−149.31	122.82	343.23	0.96135	181.460
	118.81	50.751	0.85587	163.38	123.80	50.751	0.68504	−41.311
mid	90.00	307.74	0.92556	39.571	90.00	307.74	0.85618	−45.051
	90.00	336.00	1.0315	−117.54	90.00	336.00	0.94621	97.764
	90.00	4.3166	1.1208	−71.218	90.00	4.3166	1.0505	15.674
	90.00	70.898	0.84819	−37.142	90.00	70.898	0.73965	97.036
	40.00	335.48	0.89627	−94.723	40.00	335.48	0.86512	41.523
	35.00	357.00	0.88674	−142.13	35.00	357.00	0.79233	7.0367
	31.00	20.429	0.88346	40.636	31.00	20.429	0.83939	−4.3418
	27.00	55.378	0.88807	−32.496	27.00	55.378	0.85321	3.6419

Table I.5: Fitted prolate spheroidal geometric coordinates (λ, μ, θ) and fiber angles (η) in the right ventricular free wal, excluding derivatives. Focus $d = 13.29$ mm. Coordinate values μ, θ and fiber angle η are in degrees; the λ coordinate is dimensionless. See text for discussion.

	RV endocardium				LV endocardium			
Region	μ	θ	λ	η	μ	θ	λ	η
base	125.80	282.79	0.98015	−4.2603	137.32	281.91	0.36250	78.118
	125.56	300.00	0.94373	22.499	130.45	319.23	0.72481	−63.278
	129.11	343.23	0.78889	−73.139	133.80	343.23	0.54247	−47.308
	123.80	50.751	0.68504	−30.118	129.16	50.751	0.44017	−8.0727
mid	90.00	307.74	0.85618	−86.681	90.00	307.74	0.50333	118.50
	90.00	336.00	0.69423	−121.24	90.00	336.00	0.25560	81.181
	90.00	4.3166	0.47084	−31.668	90.00	4.3166	0.18885	46.254
	90.00	70.898	0.73965	−129.46	90.00	70.898	0.35657	63.359
	40.00	335.48	0.86512	−55.216	40.00	335.48	0.60243	45.200
	35.00	357.00	0.79233	−53.720	35.00	357.00	0.53948	55.272
	31.00	20.429	0.83939	−192.93	31.00	20.429	0.52467	−4.6942
	27.00	55.378	0.85321	−60.695	27.00	55.378	0.57724	34.932

Table I.6: Fitted prolate spheroidal geometric coordinates (λ, μ, θ) and fiber angles (η) in the septum, excluding derivatives. Focus $d = 13.29$ mm. Coordinate values μ, θ and fiber angle η are in degrees; the λ coordinate is dimensionless. See text for discussion.

References

[1] M. A. Allessie, M. J. Schalij, C. J. Kirchhof, L. Boersma, M. Huybers, and J. Hollen. Experimental electrophysiology and arrhythmogenicity. Anisotropy and ventricular tachycardia. *Eur Heart J*, 10 Suppl. E:2–8, Sept. 1989.

[2] T. D. Barrett, B. A. MacLeod, and M. J. A. Walker. A model of myocardial ischemia for the simultaneous assessment of electrophysiological changes and arrhythmias in intact rabbits. *Journal of Pharmacological and Toxicological Methods*, 37(1):27–36, Feb. 1997.

[3] W. F. Bluhm and W. Y. W. Lew. Sarcoplasmic reticulum in cardiac length-dependent activation in rabbits. *Am J Physiol*, 269(Heart Circ. Physiol. 38):H965–H972, 1995.

[4] D. L. Brutsaert. Nonuniformity: A physiologic modulator of contraction and relaxation of the normal heart. *J Am Coll Cardiol*, 9(2):341–348, Feb. 1987.

[5] S. J. Cook, J. P. Chamunorwa, M. K. Lancaster, and S. C. O'Neill. Regional differences in the regulation of intracellular sodium and in action potential configuration in rabbit left ventricle. *Pflügers Archiv. European Journal of Physiology*, 433(4):515–522, Feb 1997.

[6] D. Durrer, R. T. van Dam, G. E. Freud, M. J. Janse, F. L. Meijler, and R. C. Arzbaecher. Total excitation of the isolated human heart. *Circulation*, 41(6):899–912, Jun 1970.

[7] I. R. Efimov, B. Ermentrout, D. T. Huang, and G. Salama. Activation and repolarization patterns are governed by different structural characteristics of ventricular myocardium: Experimental study with voltage-sensitive dyes and numerical simulations. *J Cardiovasc Electrophysiol*, 7(6):512–530, Jun 1996.

[8] M. R. Franz, R. Cima, D. Wang, D. Profitt, and R. Kurz. Electrophysiological effects of myocardial stretch and mechanical determinants of stretch-activated arrhythmias. *Circulation*, 86(3):968–978, Sep 1992. Published erratum appears in Circulation 1992 Nov, 86(5):1663.

[9] A. M. Gillis, E. Kulisz, and H. J. Mathison. Cardiac electrophysiological variables in blood-perfused and buffer-perfused, isolated, working rabbit heart. *Am J Physiol*, 271(Heart Circ. Physiol. 40):H784–H789, Aug. 1996.

[10] R. A. Gray, J. Jalife, A. V. Panfilov, W. T. Baxter, C. Cabo, J. M. Davidenko, and A. M. Pertsov. Nonstationary vortexlike reentrant activity as a mechanism of polymorphic ventricular tachycardia in the isolated rabbit heart. *Circulation*, 91(9):2454–2469, May 1995.

[11] M. N. Hicks, M. A. McIntosh, K. A. Kane, A. C. Rankin, and S. M. Cobbe. The electrophysiology of rabbit hearts with left ventricular hypertrophy under normal and ischaemic conditions. *Cardiovasc Res*, 30(2):181–186, Aug. 1995.

[12] B. C. Hill, A. J. Hunt, and K. R. Courtney. Reentrant tachycardia in a thin layer of ventricular subepicardium: Effects of d-sotalol and lidocaine. *J Cardiovasc Pharmacol*, 16(6):871–880, Dec. 1990.

[13] P. J. Hunter, A. D. McCulloch, P. M. F. Nielsen, and B. H. Smaill. A finite element model of passive ventricular mechanics. In R. L. Spilker and B. R. Simon, editors, *Computational Methods in Bioengineering*, volume 9, pages 387–397. American Society of Mechanical Engineers, New York, NY, November/December 1988.

[14] P. J. Hunter and B. H. Smaill. The analysis of cardiac function: A continuum approach. *Prog Biophys Mol Biol*, 52(2):101–164, 1988.

[15] S. B. Knisley. Transmembrane voltage changes during unipolar stimulation of rabbit ventricle. *Circ Res*, 77(6):1229–1239, Nov 1995.

[16] S. B. Knisley and T. C. Baynham. Line stimulation parallel to myofibers enhances regional uniformity of transmembrane voltage changes in rabbit hearts. *Circ Res*, 81(2):229–241, Aug. 1997.

[17] S. B. Knisley and B. C. Hill. Effects of bipolar point and line stimulation in anisotropic rabbit epicardium: Assessment of the critical radius of curvature for longitudinal block. *IEEE Trans Biomed Eng*, 42(10):957–966, Oct 1995.

[18] R. W. Kurz, X.-L. Ren, and M. R. Franz. Dispersion and delay of electrical restitution in the globally ischaemic heart. *Eur Heart J*, 15(4):547–554, Apr. 1994.

[19] W. Y. Lew, Y. Nishikawa, and H. Su. Cardiac myocyte function and left ventricular strains after brief ischemia and reperfusion in rabbits. *Circulation*, 90(4):1942–1950, Oct. 1994.

[20] W. Y. W. Lew. Influence of ischemic zone size on nonischemic area function in the canine left ventricle. *Am J Physiol*, 252(Heart Circ. Physiol. 21):H990–H997, May 1987.

[21] D. H. S. Lin and F. C. P. Yin. A multiaxial constitutive law for mammalian left ventricular myocardiumin steady-state barium contracture or tetanus. *J Biomech Eng*, 120(4):504–517, Aug 1998.

[22] P. M. F. Nielsen, I. J. LeGrice, B. H. Smaill, and P. J. Hunter. Mathematical model of geometry and fibrous structure of the heart. *Am J Physiol*, 260(Heart Circ. Physiol. 29):H1365–H1378, Apr 1991.

[23] T. Osaka, I. Kodama, N. Tsuboi, J. Toyama, and K. Yamada. Effects of activation sequence and anisotropic cellular geometry on the repolarization phase of action potential of dog ventricular muscles. *Circulation*, 76(1):226–236, July 1987.

[24] L. M. Owens, T. A. Fralix, E. Murphy, W. E. Cascio, and L. S. Gettes. Correlation of ischemia-induced extracellular and intracellular ion changes to cell-to-cell electrical uncoupling in isolated blood-perfused rabbit. *Circulation*, 94(1):10–13, July 1 1996.

[25] M. R. Pinsky, S. Perlini, P. L. Solda, P. Pantaleo, A. Calciati, and L. Bernardi. Dynamic right and left ventricular interactions in the rabbit: simultaneous measurement of ventricular pressure-volume loops. *Journal of Critical Care*, 11(2):65–76, June 1996.

[26] D. S. Riggs, J. A. Guarnieri, and S. Addelman. Fitting straight lines when both variables are subject to error. *Life Sciences*, 22(13–15):1305–1360, April 3–17 1978.

[27] M. J. Schalij, W. J. E. P. Lammers, P. L. Rensma, and M. A. Allessie. Anisotropic conduction and reentry in perfused epicardium of rabbit left ventricle. *Am J Physiol*, 263(Heart Circ. Physiol. 32):H1466–H1478, Nov. 1992.

[28] E. H. Sonnenblick, J. Ross, Jr., J. W. Covell, H. M. Spotnitz, and D. Spiro. The ultrastructure of the heart in systole and diastole. Changes in sarcomere length. *Circ Res*, 21(4):423–431, Oct. 1967.

[29] D. D. Streeter, Jr. Gross morphology and fiber geometry of the heart. In R. M. Berne, editor, *Handbook of Physiology, Section 2: The Cardiovascular System*, volume 1, chapter 4, pages 61–112. American Physiological Society, Bethesda, Maryland, 1979.

[30] S. L. Van Leuven, L. K. Waldman, A. D. McCulloch, and J. W. Covell. Gradients of epicardial strain across the perfusion boundary during acute myocardial ischemia. *Am J Physiol*, 267(Heart Circ. Physiol. 36):H2348–H2362, Dec 1994.

[31] F. J. Villarreal, W. Y. Lew, L. K. Waldman, and J. W. Covell. Transmural myocardial deformation in the ischemic canine left ventricle. *Circ Res*, 68(2):368–381, Feb. 1991.

[32] L. K. Waldman, D. Nosan, F. Villarreal, and J. W. Covell. Relation between transmural deformation and local myofiber direction in canine left ventricle. *Circ Res*, 63(3):550–62, Sep 1988.

[33] M. W. Watkins, A. Higashiyama, Z. Chen, and M. M. LeWinter. Rapid shortening during relaxation increases activation and improves systolic performance. *Circulation*, 94(6):1475–1482, September 15 1996.

[34] M. W. Watkins, B. K. Slinker, Y. Goto, and M. M. LeWinter. 2,3-Butanedione monoxime increases contractile efficiency in the rabbit ventricle. *Am J Physiol*, 263(Heart Circ. Physiol. 32):H1811–H1818, Dec 1992.

[35] M. Zabel, B. S. Koller, F. Sachs, and M. R. Franz. Stretch-induced voltage changes in the isolated beating heart: Importance of the timing of stretch and implications for stretch-activated ion channels. *Cardiovasc Res*, 32(1):120–130, July 1996.

Chapter III

Three-Dimensional Stress and Strain in Passive Rabbit Left Ventricle

III.A Abstract

To determine regional stress and strain distributions in rabbit ventricular myocardium, an anatomically accurate finite element model was used to solve the equations of stress equilibrium during passive filling of the left ventricle. Computations were conducted on a scalable parallel processing computer and performance was found to scale well with the number of processors used, so that simulations previously requiring approximately 60 minutes were completed in just over five minutes. Epicardial strains from the model analysis showed good agreement with experimental measurements when material properties were chosen such that cross fiber strain was more heterogeneous than fiber strain, which is also consistent with experimental observations in other species. Regional curvature of the wall rather than wall thickness had a greater influence on the circumferential stress; however, variations in regional circumferential and longitudinal wall stress were not predicted reliably using more simplified analytical models.

III.B Introduction

The three-dimensional geometry and fiber orientation of the intact myocardium plays an important role in the diastolic mechanics of the ventricles. Previous models of passive mechanics have simulated the canine and rat left ventricles [12, 5, 61, 40, 38]. Yet no models have analyzed stress and strain in the rabbit ventricles even though this species is a popular model for two-dimensional mechanics, mechanoenergetics, and electrical propagation [21, 49, 83, 26, 27, 45].

We used an anatomic model of the rabbit left and right ventricular geometry and fiber structure to estimate the distributions of stress and strain in intact rabbit ventricular myocardium. Deformation of the model showed good agreement with the epicardial strains measured on the rabbit heart when material properties were chosen such that cross fiber strain was more heterogeneous than fiber strain, and reproduced the transmural heterogeneity of cross fiber strains similar to that observed in the dog.

III.B.1 LV Mechanics

The rabbit is an important experimental preparation for the investigation of arrhythmogenesis [27], cellular electrophysiology [50], energetics [83], material properties [49], and coupled mechanoelectrical interactions [88, 20]. Two-dimensional epicardial strains were measured in the LV by Gallagher et al. (1997) to study the changes collagen fiber structure and mechanics of the cardiac scar after infarction. They measured LV volume and fiber, cross fiber, and shear strains on the anterolateral epicardium of isolated hearts from a control group, and from groups at three and 14 days post infarction under passive LV pressure loads of 0 to 30 mm Hg. In the control group, fiber strain was consistently larger than cross fiber strain and accompanied by a small negative shear strain, characteristics similar to epicardial strains measured in rat, canine, and porcine hearts [61, 62, 34]. The wide use of the rabbit as an experimental model, then, can potentially provide a foundation for

integrating the results from a number of diverse experiments into a single unified model of cardiac function.

Although the rabbit is an important and valuable experimental model, no theoretical model of three-dimensional rabbit LV mechanics has been developed. Theoretical models are necessary because methods to directly measure regional forces in the intact ventricle have not been entirely successful [36, 86] and triaxial material tests to determine the three-dimensional constitutive properties of myocardium do not yet exist. Hence theoretical models serve as a means to calculate myocardial stresses using material descriptions validated with experimentally measured strains [30, 61]. Unfortunately, three-dimensional strains have not been measured in the rabbit LV, but have been described in the canine and porcine LV [62, 34]. Given the similar characteristics of the two-dimensional epicardial strains measured in the three species, it seems reasonable to assume the additional three-dimensional strain components in the rabbit should be qualitatively the same as those in the canine and pig.

Despite experimental evidence that left ventricular wall mechanics are three-dimensional [81], only a few fully three-dimensional mechanics models exist. Huyghe et al. (1992) have developed an axisymmetric quasi-linear viscoelastic finite element model of the canine LV incorporating ventricular torsion, transmural fiber anisotropy, and intracoronary blood in the wall. Bovendeerd et al. (1996) have studied the effects of ischemia on the border zone mechanics, stroke work, and global deformation using a three-dimensional LV model featuring the dependence of active fiber stress on time, strain, and strain rate. Both of these models have been used to simulate a full cardiac cycle.

Mechanics models based on simplified LV geometries have been useful for gaining basic insights into the importance of the thick LV wall geometry, torsional deformation, large elastic deformation, and transverse shear strains [55, 30, 16, 37]. These models, however, cannot account for the complex three-dimensional variations in wall thickness, curvature, or fiber orientation in the analysis of stress or

strain in the ventricle. Furthermore, simplified models do not allow for interactions between the left and right ventricles, the pericardium, or coronary blood flow. Hence more sophisticated models of the ventricles, incorporating a realistic three-dimensional geometry and fiber architecture, a constitutive law reflecting the nonlinear anisotropic elastic properties of myocardium, and boundary conditions that impose physiologically realistic constraints under normal or diseased conditions are required for studying the heterogeneous regional mechanics of intact myocardium.

III.B.2 Computational Approaches

Advances in computing hardware and software have made large-scale three-dimensional models of cardiac mechanics feasible. New designs of scalable parallel processing computers have brought about machines with potentially thousands of processors, each with hundreds of megabytes of core random access memory, and internal message-passing networks with low latency and high bandwidth [1, 74]. Complementing these hardware improvements is the recent development of a standard portable message-passing library definition, which allows researchers to design and implement software that is easily ported to a wide range of stand-alone workstations, heterogeneous computing networks, and scalable parallel processing platforms [54]. Thus, cost effective facilities (e.g., a network of workstations) can be exploited during the development phase of a large-scale modeling effort and more scarce resources may be used later to solve the computationally intensive problems.

III.C Methods

To estimate the material properties of the intact rabbit left ventricle, we first refined the anatomic model of the rabbit ventricles and chose a constitutive law relating the strain energy in the myocardium to three-dimensional strains. Boundary conditions were determined that allowed for realistic material deformation under physiologic constraints and provided a stable convergence to a numerical solution.

Algorithms previously validated on a serial computer [11, 12] were implemented on a scalable parallel processing computer to reduce simulation run time. Estimated material parameters were iteratively determined by comparing the two-dimensional epicardial strains predicted by the model to those obtained in healthy hearts by Gallagher et al. (1997). Myocardial stresses resulting from the finite element model were compared with the stresses predicted by analytical models based on a simplified geometric and equilibrium assumptions.

III.C.1 Anatomic Model

The anatomic model of the rabbit ventricular geometry and fiber architecture (Chapter II) was modified to serve as a computational domain for model of passive LV inflation simulating the control group experiments of Gallagher et al. (1997). The discontinuous fitted fiber orientations allowed by extra nodes at the junction of the the RV septal and free wall surfaces (Section II.B.4) were removed to avoid numerical difficulties by assigning the average fiber orientation at the redundant nodes along the junction to a single node, and removing the redundant nodes. A small apical hole ($\mu = 1$ degree) was introduced to eliminate redundant nodes in this region. The mesh was converted from prolate spheroidal to rectangular Cartesian coordinates so that the deforming model could admit translations at the apex. This conversion required two circumferential refinements of the finite element mesh on the left ventricular free wall to maintain the geometry in the region of the LV papillary muscle insertions. The resulting 48-element mesh was used as the computational domain for simulating passive inflation of the left ventricle.

The finite element model used tricubic Hermite interpolation functions with four point Gaussian quadrature integration in each of the local finite element directions. Because no analytic solution exists for this problem, convergence of the finite element mesh was determined asymptotically: the 48-element model was inflated to 5 mm Hg, and regions of highest strain energy were refined until the overall strain energy of the deformed mesh changed by less than 0.5%. This resulted in a 174-

node model (9 circumferential × 5 longitudinal × 2 transmural elements) suitable for modeling the three-dimensional deformation of rabbit ventricular myocardium. The LV of the 90-element model (3,783 degrees of freedom) was inflated from 0 to 25 mm Hg in 5-mm Hg increments, with 5 load steps per increment (6 load steps for the 5-10 mm Hg increment). The right ventricle was unloaded throughout the simulation to approximate the experimental protocol followed by Gallagher et al. (1997).

III.C.2 Constitutive Law

Previous analyses modeled the myocardium as a transversely isotropic, hyper-elastic material with an exponential strain energy function [30, 61] and a Lagrange multiplier that contributes a hydrostatic pressure p to the stress to satisfy the kinematic incompressibility constraint:

$$\begin{aligned} W &= \tfrac{1}{2}C\left(e^{Q}-1\right)-\tfrac{1}{2}p\left(I_3-1\right) \\ Q &= b_1E_{ff}^2+b_2\left(E_{rr}^2+E_{cc}^2+2E_{rc}^2\right)+2b_3\left(E_{fr}^2+E_{fc}^2\right) \end{aligned} \tag{III.1}$$

where the Lagrangian strains E_{ij} are referred to the local fiber coordinate system consisting of fiber (f), cross fiber (c), and radial (r) coordinate directions. The third strain invariant I_3 is unity for an incompressible material.

For the rabbit ventricular myocardium, Lin and Yin (1998) recently proposed a constitutive law that is a function of the principal strain invariants. Using thin slabs of rabbit myocardium from LV midwall, they measured material deformation in response to a range of applied loads and determined representative material parameters by fitting an exponential form of the strain energy function to data obtained from uniaxial and biaxial tests. Their strain energy function has the form:

$$\begin{aligned} W &= C\left(e^{Q}-1\right) \\ Q &= b_1\left(I_1-3\right)^2+b_2\left(I_1-3\right)\left(I_4-1\right)+b_3\left(I_4-1\right)^2 \end{aligned} \tag{III.2}$$

where I_1 is the first strain invariant and I_4 they define as:

$$I_4=\tilde{n}\cdot\mathbf{C}\cdot\tilde{n}$$

where $\mathbf{C}$ is the right Cauchy-Green deformation tensor and $\tilde{n}$ is a unit vector along the muscle fibers in the undeformed state.

With the Lagrange multiplier formulation of the constitutive law (Equation III.1) the hydrostatic pressure terms are unknowns, resulting in a system of equations with mixed dependent variables (nodal displacements and hydrostatic pressures). The kinematic incompressibility constraint is treated explicitly as an additional equation in the augmented lagrangian finite element formulation [24]. This makes the problem difficult to solve numerically unless a memory-intensive direct solution method is used (Section III.C.4), although more effective variations have been proposed [24]. Instead, we used a newly developed formulation of the constitutive law which corrects the strain energy for changes in myocardial volume using a bulk modulus parameter b_4 [59]:

$$W = \frac{1}{2}C\left(e^{Q} - 1\right) - b_4\left(\det\left[\mathbf{C}\right] - 2\sqrt{\det\left[\mathbf{C}\right]} + 1\right) \tag{III.3}$$

where $\det\left[\mathbf{C}\right]$ is the determinant of the right Cauchy-Green deformation tensor [75], b_4 is a penalty weight applied to correct the strain energy for changes in myocardial volume, and Q is defined in Equation III.1. By using this compressible constitutive formulation, the large bulk modulus compared with the other coefficients acts as a penalty factor. The material parameters C, b_1, b_2, and b_3 in Equation III.3 were estimated so that the Lagrangian Green's strain components E_{ff}, E_{cc}, and E_{fc} agreed with epicardial strain measurements from the isolated, arrested rabbit heart [21]. Initially the material parameters were set to values used in previous simulations of canine LV passive inflation [12], with b_4 equal to 200 kPa [87]. A simulation of LV passive inflation was conducted and the results compared to the experimentally measured components of strain. Material parameters were modified according to a heuristic procedure based on the discrepancies in strains: parameters b_1 or b_2 were modified according the differences in the fiber or cross fiber strain, respectively, between the model and the experimental data. Parameter b_3 was similarly modified according to differences in shear strain. The material constant C was modified to

scale the response over the range of applied LV pressures. The parameters that best reproduced the values and slopes of the experimentally measured strain-pressure relations were accepted as best estimates of myocardial material parameters.

III.C.3 Boundary Conditions

Boundary conditions were specified by constraining the various finite element degrees of freedom (either the nodal position coordinates or their partial derivatives with respect to the local finite element arc lengths) to remain unchanged from their initial values. Changes to nodal positions and circumferential and transmural derivatives at the base of the epicardium and right ventricular endocardium were prohibited. Constraints at the base were chosen that simulated the effects of the relatively stiff annuli of the valves: the LV endocardium was constrained to move only in the basal plane, allowing cavity expansion but not longitudinal displacement in the x_3 direction [29]. At the apex all derivatives in the posterior direction and nodal coordinates were unconstrained. Constraints to the longitudinal and transmural derivatives at the apex prevented spurious solutions with unrealistically large deformations along the boundary of the small apical hole, and were imposed only to improve the behavior of the model and not as an attempt to achieve any type of symmetry or regionally uniform response. Referring to the coordinate systems in Figure II.5(b), the boundary used here are expressed mathematically as:

$$
\begin{aligned}
\text{epicardial base:} \quad u &= \partial u/\partial S_1 = \partial u/\partial S_3 = \partial^2 u/\partial S_1 \partial S_3 \\
&= \partial^3 u/\partial S_1 \partial S_2 \partial S_3 = 0 \quad \text{for } u \in \{x_1, x_2, x_3\} \\
\text{LV endocardial base:} \quad x_1 &= \partial x_1/\partial S_1 = \partial x_1/\partial S_3 \\
&= \partial^2 x_1/\partial S_1 \partial S_3 = 0 \\
\text{RV endocardial base:} \quad u &= \partial u/\partial S_1 = \partial u/\partial S_3 \\
&= \partial^2 u/\partial S_1 \partial S_3 = 0 \quad \text{for } u \in \{x_1, x_2, x_3\} \\
\text{LV endocardial apex: } \partial u/\partial S_1 &= \partial u/\partial S_2
\end{aligned}
$$

$$= \partial u/\partial S_3 = \partial^2 u/\partial S_1 \partial S_3 = \partial^2 u/\partial S_2 \partial S_3$$
$$= \partial^3 u/\partial S_1 \partial S_2 \partial S_3 = 0 \quad \text{for } u \in \{x_1, x_2\}$$

III.C.4 Computational Approaches

The finite element method is a powerful numerical technique used to approximate the solution to a (large) system of nonlinear partial differential equations [22]. The system of equations, arising from a discretized mathematical description of the physical problem to be solved, is represented by the matrix equation:

$$\mathbf{K}\tilde{u} = \tilde{f} \tag{III.4}$$

where $\tilde{f}$ is the vector of forces applied to the system and $\tilde{u}$ is the vector of unknown nodal displacements to be determined. The $n \times n$ global tangent stiffness matrix $\mathbf{K}$ (or simply the global stiffness matrix if the material is linear) is assembled from [58]:

$$\mathbf{K} = \sum_{N^e} \mathbf{N}_e \mathbf{K}_e \mathbf{N}_e^T \tag{III.5}$$

where N^e is the number of elements in the mesh, $\mathbf{N}_e$ is the $n \times m$ Boolean mesh connectivity matrix, and $\mathbf{K}_e$ is the $m \times m$ element stiffness matrix, each of which is computed by mapping the discretized equations from the physical space to an isoparametric finite element space.

Most finite element schemes follow the same sequence of operations to solve a nonlinear problem: the element stiffness matrices $\mathbf{K}_e$ are sequentially computed and assembled into the global tangent stiffness matrix $\mathbf{K}$. Since the system of equations is nonlinear, the element stiffness matrices, and thus the global tangent stiffness matrix, are functions of the solution vector $\tilde{u}$ and special techniques such as the Newton-Raphson method (outlined in Figure III.1) must be used to solve the matrix equation. The Newton-Raphson method (or Full Newton method) iteratively approximates the solution and re-computes (updates) the global tangent stiffness matrix after each iteration [23]. In the *modified* Newton-Raphson method, the matrix is not updated after each iteration, but is instead updated only when

some convergence criterion is not met. After computing the vector of applied forces the global system of nonlinear equations (Equation III.4) is solved, often via a direct method which factors the matrix $\mathbf{K}$ into a pair of lower- and upper-triangular matrices, $\mathbf{K} = \mathbf{LU}$, through a series of scalings and row (or column) exchanges. The solution vector $\tilde{u}$ is then computed by a forward substitution step $\mathbf{L}\tilde{c} = \tilde{f}$ to compute $\tilde{c}$, and a back substitution step $\mathbf{U}\tilde{u} = \tilde{c}$ to compute $\tilde{u}$. Direct methods often require significant additional memory for storing the $\mathbf{L}$ and $\mathbf{U}$ matrices since fill-in will likely destroy the sparse structure of the original matrix [22].

III.C.5 Parallel Strategy and Implementation

In simulations involving nonlinear high-order models of the ventricle, evaluation of the element stiffness matrices is the most costly step in terms of time required to obtain the final solution. This additional computational cost is due primarily to the complex geometry of the elements and the nonlinear constitutive relation of myocardium [52]. Any element stiffness matrix, however, can be computed independently of the other element stiffness matrices in the mesh — a fact that may be exploited using a data parallel implementation on a scalable parallel processing computer [84].

Computational approaches implemented on a scalable parallel processing (SPP) platform differ from the serial approach outlined above to exploit data parallel operations inherent in the finite element method. The computation of a particular element stiffness matrix is assigned to one of the available processors. Assuming that N^P processors are available, the finite element mesh has N^e elements, and the computation of each $\mathbf{K}_e$ is assigned to a separate processor (i.e., $N^P{=}N^e$), the time required to compute the N^e element stiffness matrices will be reduced by $1/N^e$; this ignores, however, the time required for interprocessor communication so a smaller reduction will be realized [46]. After the computation of all the element stiffness matrices is complete, the global tangent stiffness matrix is assembled and the solution is obtained using Equation III.4 by a direct method.

$R_p = W_p = \Delta\tilde{u}_p = 0$

`Do until converged`

Form element stiffness matrices

`Compute` $\mathbf{K}_e$ `for all elements`

`Assemble` $\mathbf{K}_e$ `into` $\mathbf{K}$

Form right hand side vector $\tilde{f}$*, solve equations*

`Solve` $\mathbf{K}\tilde{u}$ `=` $\tilde{f}$ `with direct solver`

`Compute residual vector,` $\tilde{r}$ `=` $\mathbf{K}\tilde{u}$ `-` $\tilde{f}$

Compute convergence indicators

`Compute strain energy,` W`, and change,` $\Delta W = W - W_p$

`Compute change in solution vector,` $\Delta\tilde{u}$

`Compute ratio of unconstrained/constrained residuals,` R

Check for convergence

`If (`$R < \epsilon$ `and` $\Delta\tilde{u} < \epsilon$`) or` $\Delta W < \epsilon$

Converged, exit

`Else`

Not converged, continue iterating

$R_p = R,\ \Delta\tilde{u}_p = \Delta\tilde{u},\ W_p = W$

Figure III.1: Outline of the Newton-Raphson method utilizing a direct solver.

The cost of explicitly assembling the global tangent stiffness matrix is that the matrix must be small enough to fit into core memory on a processor, thus limiting the size of the matrix and the problem to be solved. This limitation may be overcome using a multiple-instruction multiple-data (MIMD) programming model where, for example, the available processors are partitioned into two groups: one group to compute the element stiffness matrices and the other group to solve the system $\mathbf{K}\tilde{u} = \tilde{f}$. This scheme, however, is highly inefficient as the computational load would be extremely unbalanced; one processor group would be idle while waiting for the other to complete its task. An additional drawback is that separate algorithms must be designed and implemented for the two groups of processors. Alternatively, a single-instruction multiple-data (SIMD) programming model allows the global tangent stiffness matrix to be partitioned across processors with blocks of rows assigned to individual processors. Software currently available could then solve the system directly by factoring the matrix in a preprocessing step [43]. This approach, though, complicates the implementation of the algorithm since individual degrees of freedom (DOFs) in the element stiffness matrices must be mapped and then communicated to the processor maintaining the rows where the DOF assembles into the global stiffness matrix.

A more natural partitioning scheme utilizes the known mesh topology contained in the Boolean connectivity matrix, $\mathbf{N}_e$. If an element stiffness matrix is instead saved on the processor where it is originally computed, existing mapping information between the local element DOFs and the global DOFs can be utilized during operations involving the global tangent stiffness matrix. In this approach, known as the element-by-element formulation [35], the global stiffness matrix $\mathbf{K}$ is not explicitly assembled: instead each processor maintains its assigned element stiffness matrix (or matrices) and is responsible for providing any information in $\mathbf{K}$ derived from $\mathbf{K}_e$. For example, to compute the matrix-vector product $\mathbf{K}\tilde{u}$, each processor maps the relevant components in the vector $\tilde{u}$ to the columns of the individual $\mathbf{K}_e$ matrices via the $\mathbf{N}_e$ matrix to compute a partial product [58]. The

resulting partial products are then summed (or *reduced*) across all the processors to form $\mathbf{K}\tilde{u}$:

$$\mathbf{K}\tilde{u} = \sum_{N^e} \left(\mathbf{N}_e \mathbf{K}_e \mathbf{N}_e^T \tilde{u} \right) \tag{III.6}$$

The lack of an explicit representation of the global stiffness matrix, though helpful in reducing memory requirements, introduces another problem: since no $\mathbf{K}$ matrix exists, $\mathbf{K}$ cannot be factored, thus precluding the use of a direct method to solve the global system of equations.

An iterative method was chosen to overcome this difficulty. [It is important at ths point to distinguish between the two iterative approaches that were utilized: the iterations of the Newton-Raphson method were part of the process to determine the solution for the nonlinear system (Equation III.4). The iterative methods described here solve the linear systems that arise as approximations within each Newton-Raphson iteration.] Such a method will perturb an initial guess of the solution $\tilde{u}$ based on some search criteria. Several iterative methods exist, though few are applicable to general systems of equations. For example, the conjugate gradient method requires a symmetric positive definite matrix [3]. The Chebyshev Iteration method can solve nonsymmetric systems, but requires good *a priori* estimates of the extremal eigenvalues of the matrix [25]. Both the quasi-minimal residual (QMR) and generalized minimal residual (GMRES) methods are applicable to nonsymmetric matrices. While the QMR method requires matrix-vector products with both the system matrix and its transpose, the GMRES method requires only a single matrix-vector product [3]. As part of the iterative solution the GMRES method generates a sequence of subspace basis vectors $\tilde{v}^i$ via a modified Gram-Schmidt orthogonalization process and constructs an estimate of the solution as a linear combination of the initial guess $\tilde{u}^0$ and the subspace basis vectors:

$$\tilde{u}^i = \tilde{u}^0 + y_1 \tilde{v}^1 + \cdots + y_i \tilde{v}^i$$

where the coefficients y_k minimize the residual norm $\|\tilde{f} - \mathbf{K}\tilde{u}^i\|$. Note that the cost of computing each subspace basis vector $\tilde{v}^i$ increases linearly with each iteration be-

cause the Gram-Schmidt orthogonalization process uses all the current basis vectors in the subspace to generate the new basis vector [3].

For an $n \times n$ matrix $\mathbf{K}$, the GMRES method is guaranteed to converge (using exact arithmetic) to the solution after n iterations:

$$\tilde{u} = \tilde{u}^0 + y_1\tilde{v}^1 + \cdots + y_n\tilde{v}^n$$

but this requires computing and storing all n subspace basis vectors. An effective modification to the GMRES method, known as the *restarted* GMRES method, generates only k subspace basis vectors, $k \ll n$, and is much less memory intensive. If convergence has not been achieved after k iterations, the algorithm clears all accumulated information and restarts the iterations using $\tilde{u}^k$ as the initial guess of the true solution. A significant drawback to the restarted GMRES method is that no guidelines exist for the appropriate choice of the vector subspace dimension k. If the subspace dimension is too small the algorithm may "stagnate" and fail to converge; if the dimension is too large then the computational cost and storage requirements for the subspace basis vectors is excessive. Hence an appropriate choice of the vector subspace dimension simply "requires skill and experience" [3].

The restarted GMRES method requires little additional memory beyond the system matrix $\mathbf{K}$ since the $\mathbf{LU}$ factors of $\mathbf{K}$ are never computed [3]; however, additional storage of four work space vectors and the k basis vectors is necessary [17]. The savings in memory gained by utilizing iterative methods is somewhat offset, however, by the slow rate of convergence of iterative methods compared to direct methods.

The convergence rate of nearly all iterative methods is highly dependent on the condition number of the matrix [3]. Iterative methods demonstrate peak performance when the matrix is strictly diagonally dominant; i.e., close to the identity matrix [68]. The convergence rate of an iterative method can be significantly accelerated by left preconditioning the matrix with its approximate inverse:

$$\mathbf{MK}\tilde{u} = \mathbf{M}\tilde{f}$$

that is, we desire a preconditioner $\mathbf{M}$ such that the matrix-matrix product is close to the identity matrix: $\mathbf{MK} \approx \mathbf{I}$. Many schemes exist for computing a preconditioner $\mathbf{M}$, but the simplest and most easily parallelized is to simply choose the main diagonal of the system matrix, $[\mathbf{M}]_{ii} = [\mathbf{K}]_{ii}^{-1}$, as the preconditioner, also known as the point Jacobi preconditioner [3].

The restarted GMRES method has been successfully used in a finite element setting by many investigators [85, 71, 44, 4, 42, 78]; van Gijzen [80] gives an excellent description of the restarted GMRES method in a finite element context. We chose the restarted GMRES method as implemented in the Parallel Iterative Methods (PIM) package [17]. Unlike other implementations of iterative methods [43, 39, 69], the PIM package places no restrictions on the underlying data structure of the system matrix, requiring instead that the user develop additional support routines for matrix-vector products, preconditioning, inner-products, vector norms, and global accumulations. For the simulations conducted here, the restarted GMRES method used 100 subspace basis vectors (determination of this number is described in the following Section), a solution tolerance of 10^{-9}, and a maximum of 10 restarts. Yeckel and Derby (1997) have shown it is not always advantageous to solve the linear system to a high degree of precision as long as the nonlinear Newton iteration converges to an acceptable tolerance. We adopted their strategy and allowed the Newton iteration to advance even when the restarted GMRES method had executed the maximum number of restarts. All components of the solution vector $\tilde{u}$ were initially set to unity. The solution was accepted when the change in strain energy was less than 10^{-6}.

Material parameters of the passively inflated rabbit LV were estimated using the recently proposed form of the constitutive law (Equation III.1). An element-by-element approach was implemented on a SPP platform to reduce run time, and a modified Newton-Raphson method was used to solve the nonlinear system of equations, utilizing the restarted GMRES method to solve the linear systems of equations during each modified Newton-Raphson iteration. The strategy imple-

mented here (shown schematically in Figure III.2) requires only that the diagonal preconditioner, the solver residual vector, and partial products of the element stiffness matrices with either the diagonal preconditioner or intermediate solver vectors be globally reduced and broadcast to all processors. This approach was expected to be highly scalable because additional finite elements could simply be assigned to additional processors. We computed speedup as the run time on a single processor divided by the run time on P processors. This definition of speedup is technically incorrect; speedup is defined as the ratio of the serial run time of the *best sequential algorithm* to the run time of the parallel algorithm executed on P processors [46]. The best sequential algorithm for this problem utilizes a direct solver but was too large to fit into main memory, thus serial performance was significantly degraded by the use of virtual memory. Our implementation used the Message Passing Interface library [54] on the Cray T3E (272 processors running at 300 MHz, each with 128 Mb of main memory) at the San Diego Supercomputer Center (Appendix III.H).

The computational procedure followed here is diagrammed in Figure III.3. The problem and solution parameters were defined on a laboratory workstation (SGI Indigo^2). The contents of the global data structures were then written to a binary file (approximately 8.7 Mb), which was then transferred to the Cray T3E via the UNIX file transfer protocol (`ftp`). On the T3E, the parallel version of the program was launched on 45 processors, each of which read the binary file and loaded the global data into memory. Assigning static global data in this manner obviated several one-to-all broadcasts, greatly simplifying the problem definition on the SPP platform. When the `SOLVE` command was issued, each processor determined which of the element stiffness matrices it was to compute and store; the solution algorithm then proceeded as outlined in Figure III.2. Each of the 45 processors computed and stored two element stiffness matrices and carried a copy of the current global solution vector $\tilde{u}$. When the restarted GMRES algorithm required an evaluation of the matrix-vector product $\mathbf{K}\tilde{u}$, each processor mapped the subset of relevant components in the global solution vector to the appropriate columns in the element stiffness matrix

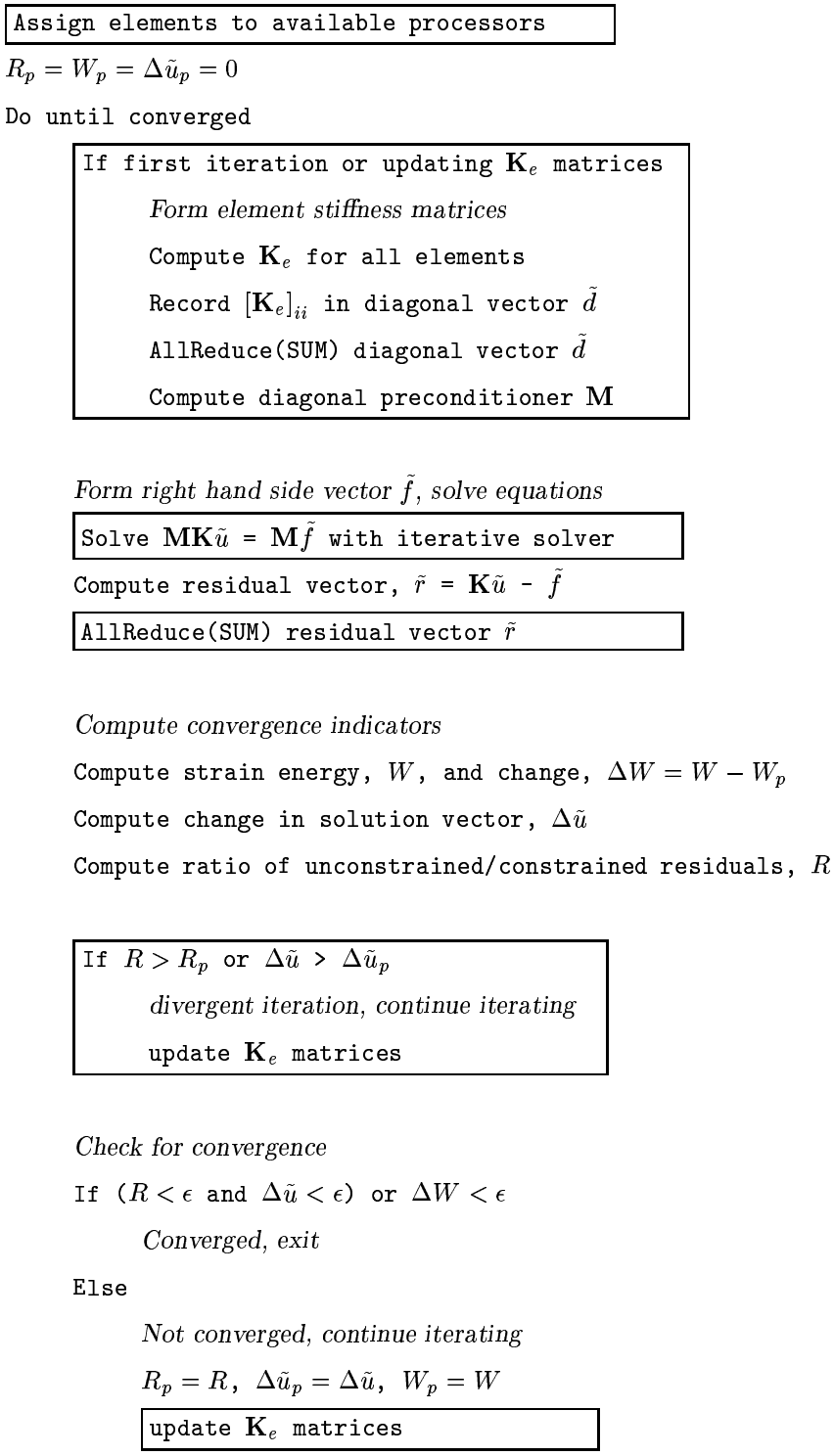

Figure III.2: Outline of the modified Newton-Raphson method utilizing an iterative solver executed on a SPP platform. Differences from Figure III.1 are boxed.

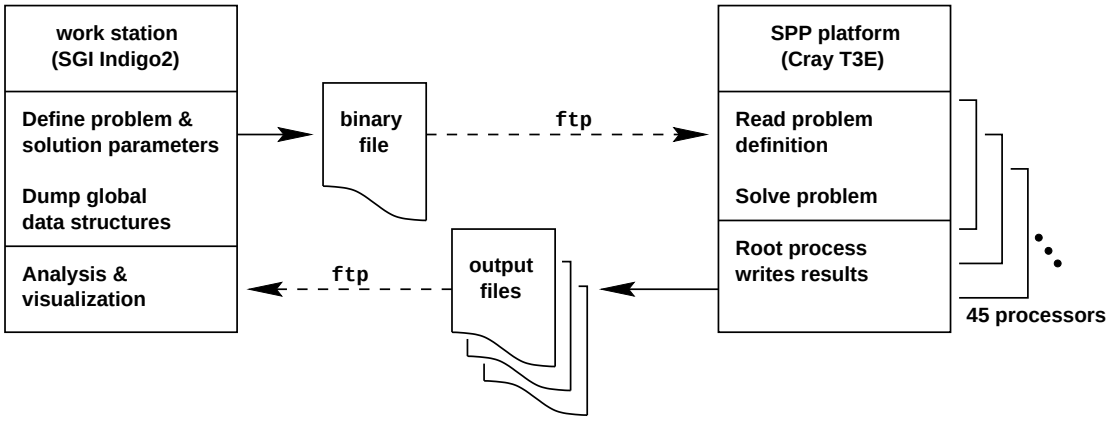

Figure III.3: Schematic diagram of the computational procedure to solve the passive LV inflation problem.

$\mathbf{K}_e$ (Equation III.6) and executed the multiplication. The resulting 45 vectors of partial products were summed (by the `AllReduce(SUM)` actions in Figure III.2) to form the full matrix-vector product $\mathbf{K}\tilde{u}$. The current iterate was then updated by the restarted GMRES algorithm to form the subsequent approximation to the global solution $\tilde{u}$. After the global solution was obtained, the root processor wrote the deformed nodal parameters and displacements, cavity pressure, and global residual vector to output files (approximately 860 Kb per load step). If the simulation was to continue to higher LV pressures the `SOLVE` procedure was repeated, otherwise the program was terminated normally on all processors. When the simulation was completed the output files were transferred to a laboratory workstation for analysis and visualization.

III.C.6 Regional Wall Stress and Geometry

Because of the irregular three-dimensional geometry and fiber architecture of the model heterogeneous distributions of stress were expected. We investigated the extent to which local geometric factors such as wall thickness and curvature were predictive of these variations. In simple (thin-walled) global equilibrium analyses these factors together with chamber pressure are the sole determinants of circum-

ferential and longitudinal stress. We therefore used a popular analytic formulae [56] to investigate the sources of heterogeneity.

The regional left ventricular wall thickness and circumferential and longitudinal curvatures were computed using the passively inflated finite element model (10 mm Hg LV pressure) at 18 locations along the equator at the epicardium, midwall, and endocardium. These geometric parameters were used to compute regional wall stress using a model that assumes a simplified thick-walled ellipsoidal geometry for the LV [56]. Using the simplified model, the circumferential and longitudinal wall stresses are computed from:

$$T_{11} = \frac{Pb}{h}\left(1 - \frac{b^2}{2a^2} - \frac{h}{2b} + \frac{h^2}{8a^2}\right) \quad \text{(III.7)}$$

$$T_{22} = \frac{Pb}{2h}\left(1 - \frac{h}{2b}\right)^2 \quad \text{(III.8)}$$

where T_{11} and T_{22} are the circumferential and longitudinal components of the second Piola-Kirchhoff stress tensor, respectively, a and b are the semi-major and semi-minor axes of the ellipsoidal geometry of the LV, and h is the ventricular wall thickness. These expressions of wall stress are derived based on the assumptions of an axisymmetric ellipsoidal geometry and that the local stress depends only on the geometric parameters of the ventricle and the cavity pressure (i.e., the LV is linearly elastic). The effects of the geometric parameters on computed stresses were examined by using the regional values of each parameter. To quantify the influence of the regional variation of the individual parameters on the computed stresses, stresses were also computed using the mean value of each parameter instead of the regional values.

III.D Results

III.D.1 Validation: Canine LV Passive Inflation

A high-order finite element model of the canine LV (described elsewhere [12]) with 960 DOFs served to validate the parallel implementation of the finite

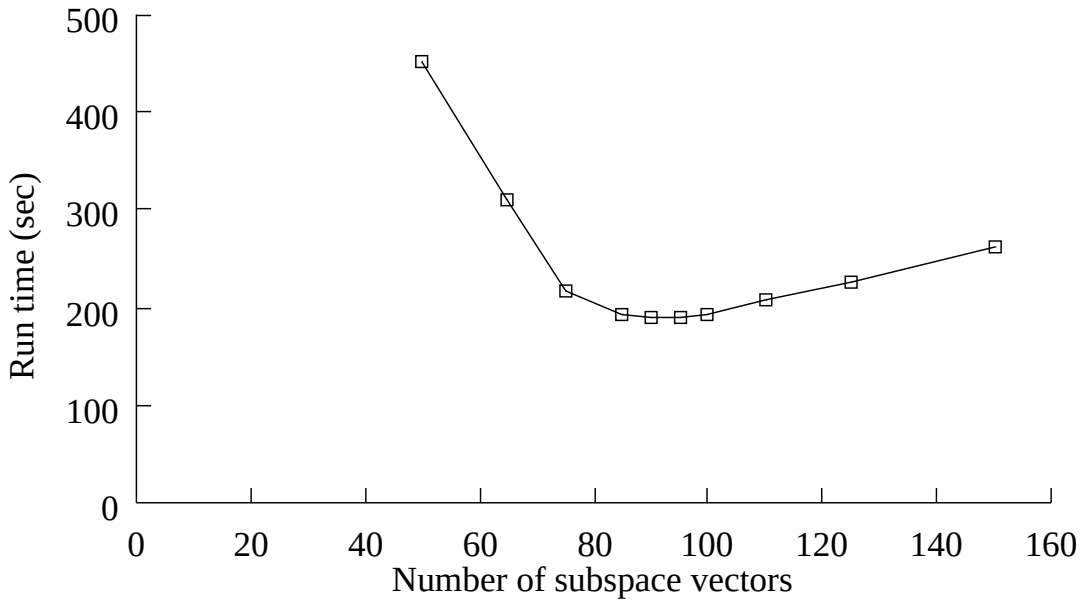

Figure III.4: Run time for the first load step of the passively inflated canine LV simulation as a function of the restarted GMRES vector subspace dimension. When the dimension ranged from 85 to 100 vectors, the run time varied by 4.02 seconds with 90 vectors providing the minimum run time of 189.60 seconds.

element procedures. Using the constitutive law in Equation III.3 with $b_1 = 1.76$, $b_2 = 18.5$, $b_3 = 1.63$, and $b_4 = 30$, the LV was inflated to 7.5 mm Hg in four successive load steps, using either a Full Newton method or a modified Newton-Raphson method. Left diagonal preconditioning reduced the condition number of the global tangent stiffness matrix from 550×10^6 to 3,570; without preconditioning the restarted GMRES method never reduced the residuals and always failed to converge. The restarted GMRES subspace had 100 basis vectors, approximately the number resulting in the minimum run time (Figure III.4). The solution was identical to that reported previously [12]. The resulting run times and speedup are shown in Figure III.5. On 16 processors run time was reduced to 8.7 minutes using the Full Newton method, or to 5.2 minutes using a modified Newton-Raphson method. With the Full Newton method speedup was 13.9 (87% efficiency), but only 10.6 with the modified Newton-Raphson method (66% efficiency). The Full

Newton method required 23 evaluations of the global tangent stiffness matrix **K** and 116 restarted GMRES iterations whereas the modified Newton-Raphson method required 6 evaluations of **K** and 383 restarted GMRES iterations.

III.D.2 Rabbit LV Passive Inflation

Computation

Twelve simulations (4176 DOFs) were conducted to determine the best estimates of the material parameters; the results presented here are from the simulation using the best estimates. The number of iterations and execution times for each LV pressure range are shown in Table III.1. The L_2 norm of the restarted GMRES residual vector, the sum of unconstrained DOF residuals, and the change in strain energy is shown for the first 11 Newton iterations of load step 1 in Figure III.6. During this sequence of iterations, the norm of the restarted GMRES residual vector never reached the solution tolerance of 10^{-9}, thus the maximum allowed 10 restarts were used during each Newton iteration. On 45 processors this simulation required 237.5 CPU hours and ran for approximately 5.3 hours. On each processor data storage required 14.4 Mb of main memory and the program required 9.84 Mb of main memory.

Global Deformation of the Ventricles

A cross-section of the unloaded and deformed ventricles at 25 mm Hg LV pressure (Figure III.7, LEFT) show the LV volume increased substantially, apex displaced 2.18 mm in the longitudinal direction, flattening the septal wall. At 5 and 25 mm Hg pressure the septum was displaced 2.0 and 3.7 mm toward the RV at the equator. The RV cavity maintained a volume of at least 1 milliliter throughout the pressure range and the LV cavity volume was was within 10% of the experimentally measured volumes at non-zero pressures (Figure III.7, RIGHT). A problem occured along the apical boundary of the RV cavity at nonzero LV pressures, where the model

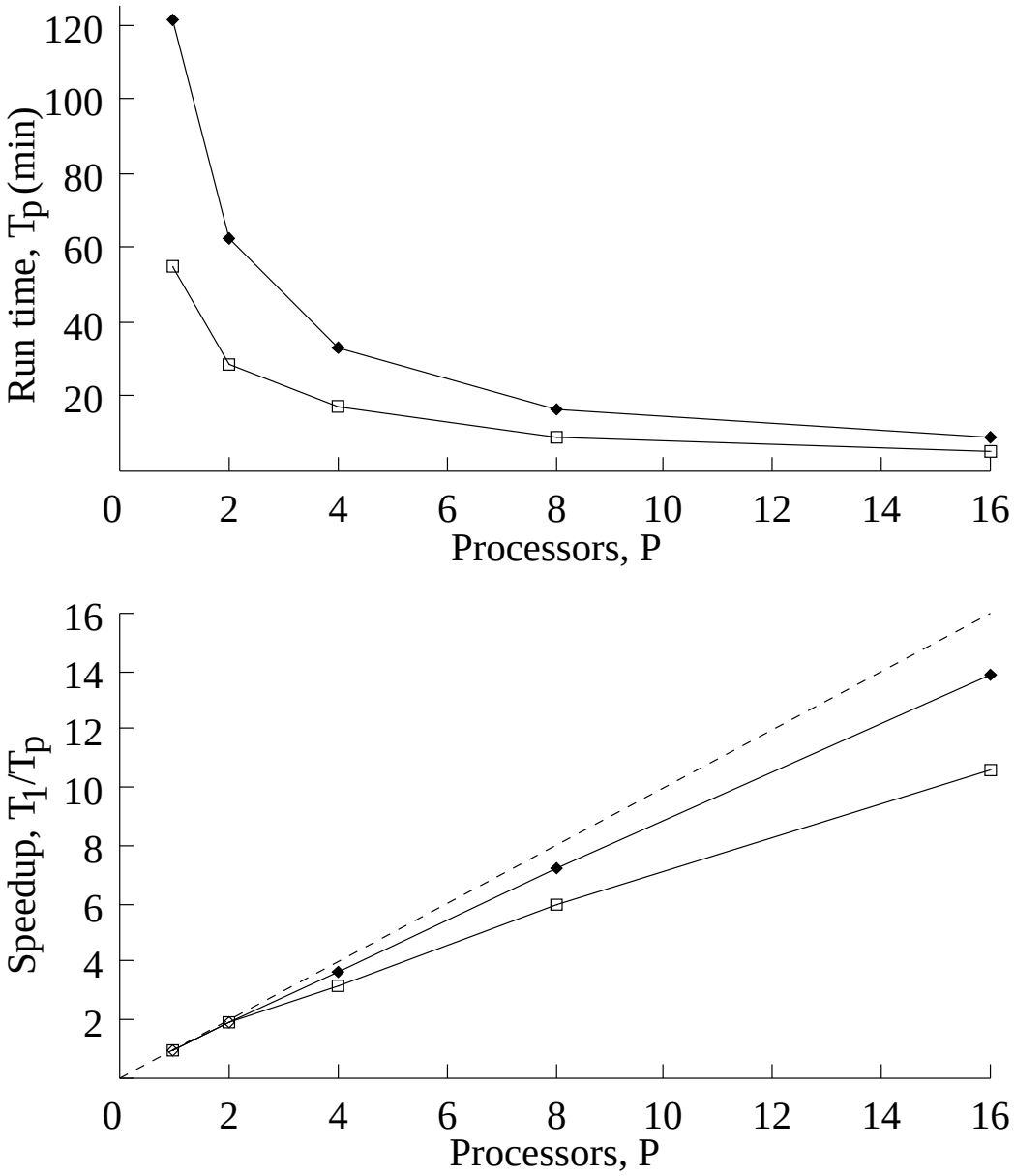

Figure III.5: Run time and speedup for the 16 element canine LV simulation [12] using either a modified Newton-Raphson (boxes) or Full Newton (diamonds) method. Dashed line is ideal speedup.

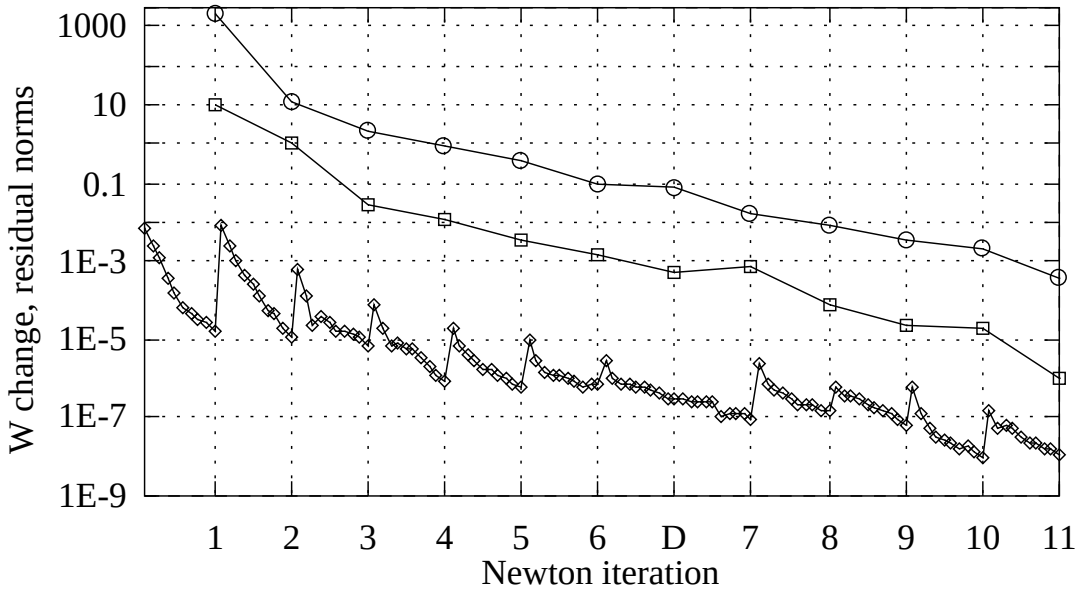

Figure III.6: The L_2 norm of the restarted GMRES residual vector (diamonds), sum of unconstrained DOF residuals (circles), and change in strain energy (boxes) during load step 1 of model rabbit LV inflation to 5 mm Hg pressure. Numbers on horizontal axis denote end of the Newton iteration. The iteration following number 6 was divergent ("D").

LV pressure (mm Hg):	0 to 5	5 to 10	10 to 15	15 to 20	20 to 25
Load step 1:	11	17	13	15	13
2:	10	11	11	10	7
3:	11	11	11	9	9
4:	13	13	10	10	9
5:	11	10	8	10	7
6:		9			
total Newton iterations:	56	71	53	54	45
run time (seconds):	4155	5484	3771	3830	2990

Table III.1: Number of Newton iterations and run time required to simulate the passive inflation of the rabbit LV from 0 to 25 mm Hg.

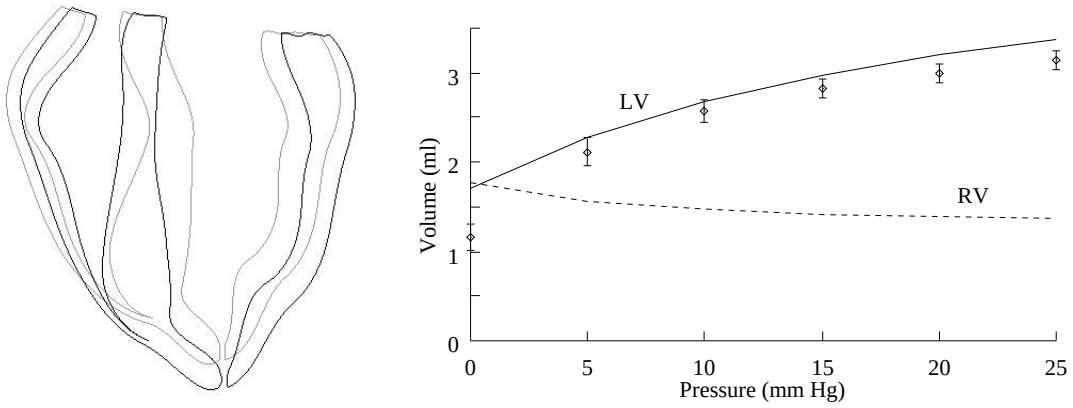

Figure III.7: LEFT: Anterior view of the unloaded (gray) and deformed (black) ventricular cross-sections at 25 mm Hg. RIGHT: Measured LV cavity volume (symbols ± SEM) [21] and LV and RV volumes from the model.

converged to an incompatible displacement solution, admitting a non-physiologic change to the node positions allowing the intraventricular septum to penetrate the RV free wall. The most dramatic instance is shown in the lower left region of Figure III.8 where at 25 mm Hg LV pressure the septal surface is intersecting the the free wall surface resulting in the impossible situation of the septum and RV free wall occupying the same physical space.

Epicardial and Transmural Strains

When parameters of the strain energy function had the the values $C = 1.76,\ b_1 = 50.0,\ b_2 = 5.0,\ b_3 = 1.63,\ b_4 = 200$, the model showed good agreement with epicardial strains measured on the anterolateral wall (Figure III.9) [21]. The fiber and cross fiber strains are well within the error of the experimental measurements, but the magnitude of the fiber-cross fiber shear strain is larger than that of experiment by an average of 12%, indicating the elastic stiffness of the model in the tangent plane (parameter b_3 in Equation III.3) was lower than that in the actual rabbit LV myocardium. This is further highlighted in the principal strain profiles and direction of the first principal strain (Figure III.10, top), where the first principal

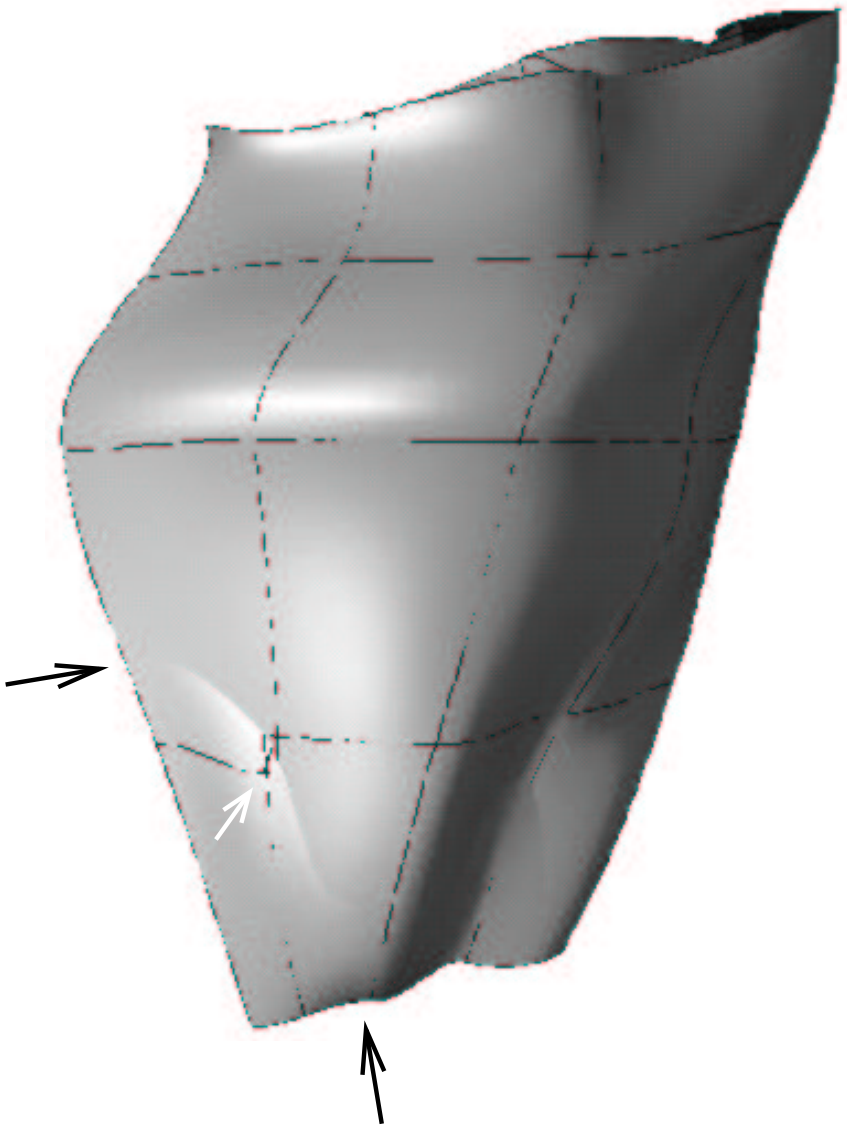

Figure III.8: Model surfaces representing the RV endocardium at 25 mm Hg LV pressure. The incompatible displacement solution allowed the surface of the intraventricular septum to penetrate the RV free wall. Black arrows indicate endpoints on the line of intersection between the two surfaces. White arrow indicates a node on the septal surface that has penetrated the RV wall.

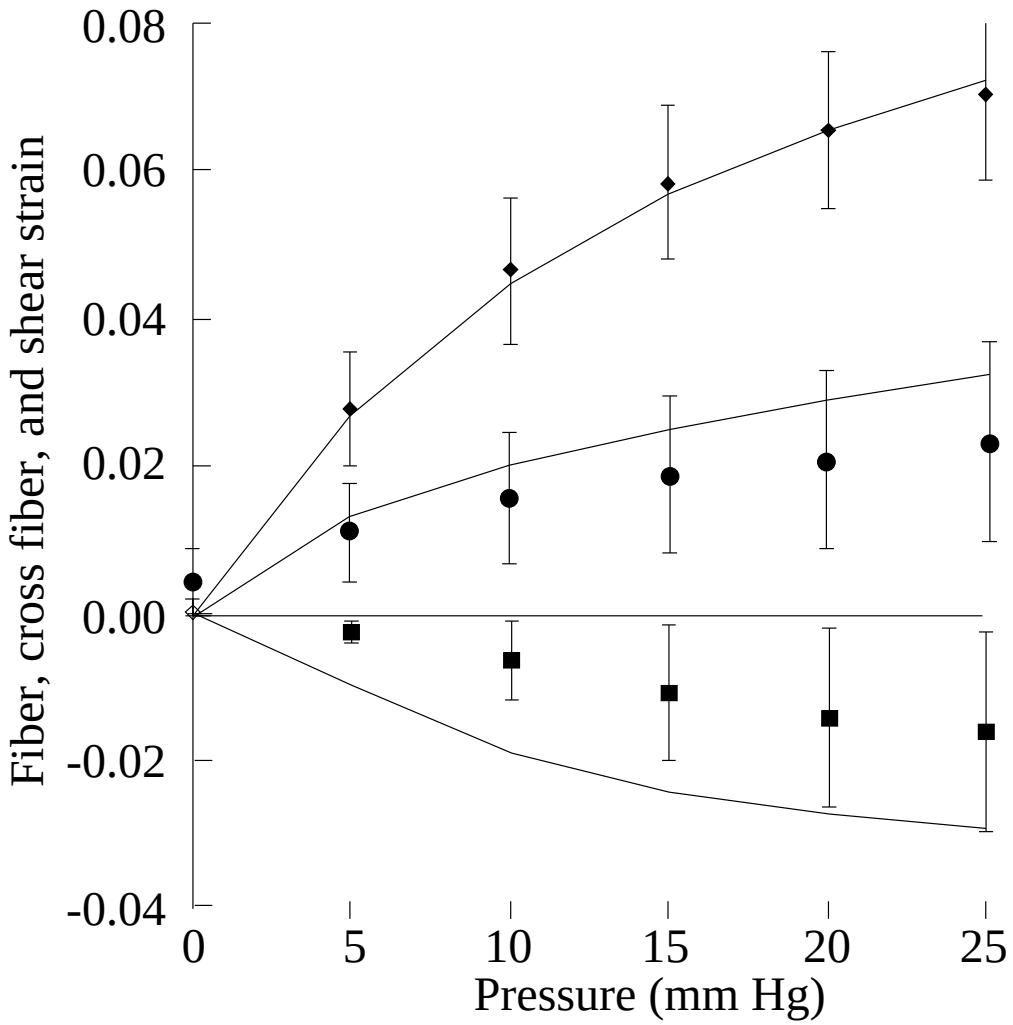

Figure III.9: Epicardial strain profiles from the anterolateral wall. Simulations (solid lines) show good agreement with experimental fiber (diamonds), cross fiber (circles), and shear (boxes) strains [21]. Error bars are ± SEM.

strain is consistently larger than experiment, the maximum difference occuring at 25 mm Hg pressure where the strain computed from the experimental data is 0.075 but the model predicted 0.088. Similarly, the second principal strain is consistently lower than experiment with the largest discrepancy at 10 mm Hg pressure (measured: 0.014; model: 0.0098). The direction of the first principal strain in the model closely followed that computed from the experimental measurements (Figure III.10, bottom), and in both cases the direction was more negative than the local epicardial fiber angle (in the experimental hearts the mean local epicardial fiber angle is -60 degrees, in the model the angle was -52 degrees). The largest error is at 5 mm Hg pressure where angle computed from the experimental data is -68 degrees, but the model yielded -78 degrees. In addition, variations of the principal direction with increasing LV pressure differ slightly: the experimental data show the direction becoming monotonically more longitudinal with increasing LV pressure; in the model the change in direction shifted from negative to positive at pressures above 15 mm Hg (see inset in the bottom plot of Figure III.10).

At 25 mm Hg LV pressure, fiber strain was nearly uniform transmurally over the entire LV wall, varying from 0.012 to 0.093 at the subepicardium and from 0.04 to 0.14 at the subendocardium (Figure III.11). Conversely, cross fiber strain shows a much larger transmural variation: -0.022 to 0.22 strain at the subepicardium and -0.016 to 0.43 at the subendocardium. The compressive strains are isolated to a single region near the LV posterior papillary insertion (the lighter regions in the lower right portion of the cross fiber strain maps in Figure III.11). More detailed maps (with narrowed scales) are shown in Appendix III.G along with epicardial strains with respect to cardiac coordinates.

The transmural variation in strain at 10 mm Hg from the same anterolateral region (Figure III.12) shows that both circumferential and radial strains increase in magnitude toward the endocardium, similar to strains measured in the passively inflated (8 ± 4 mm Hg) canine LV [62]. The radial strain is negative because the wall thinned under pressure loading with the greatest amount occuring at the suben-

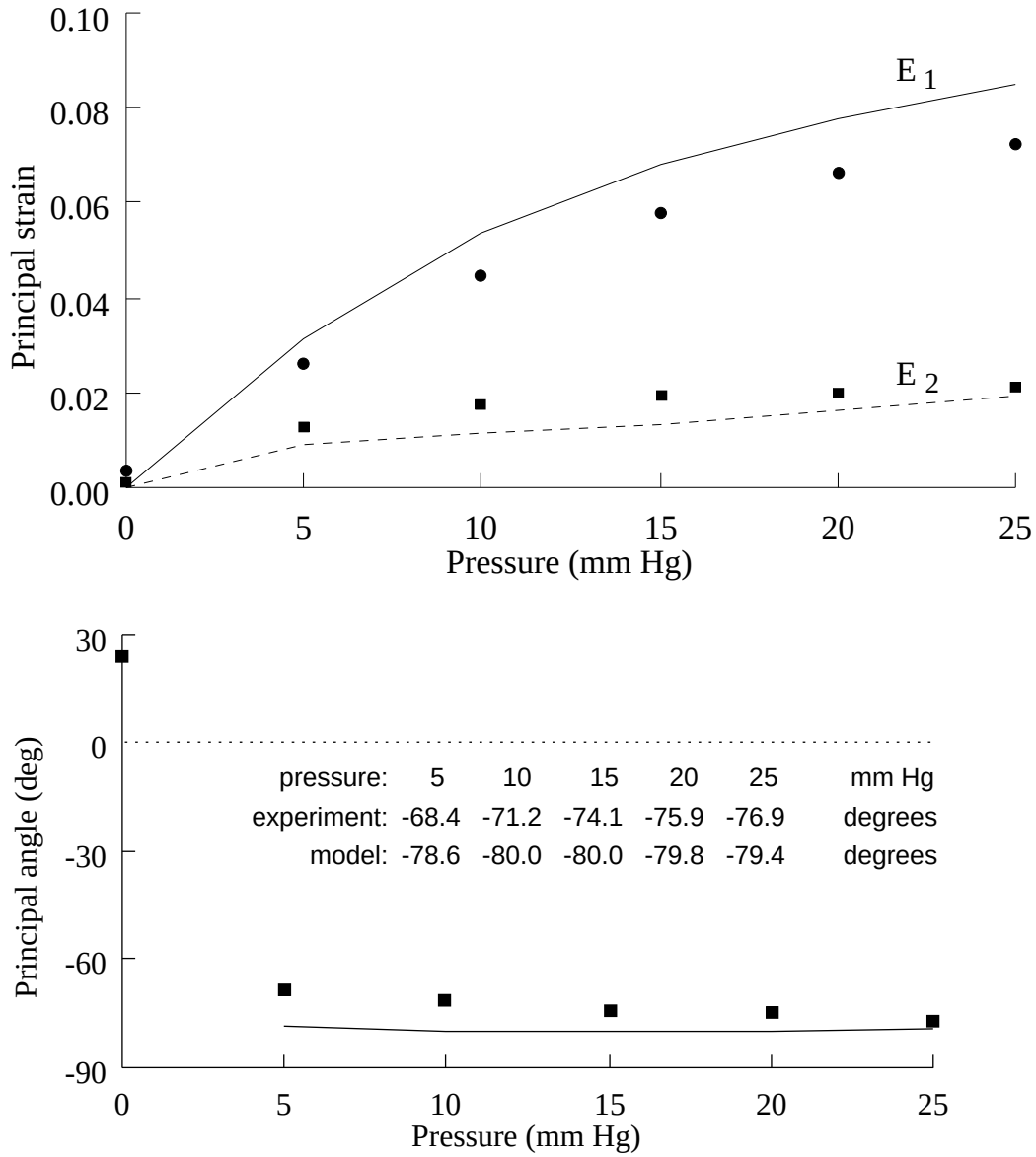

Figure III.10: Principal strain profiles (TOP) and angle (BOTTOM) from the anterolateral wall. Simulation (solid line) shows good agreement with experimental strains (symbols) [21].

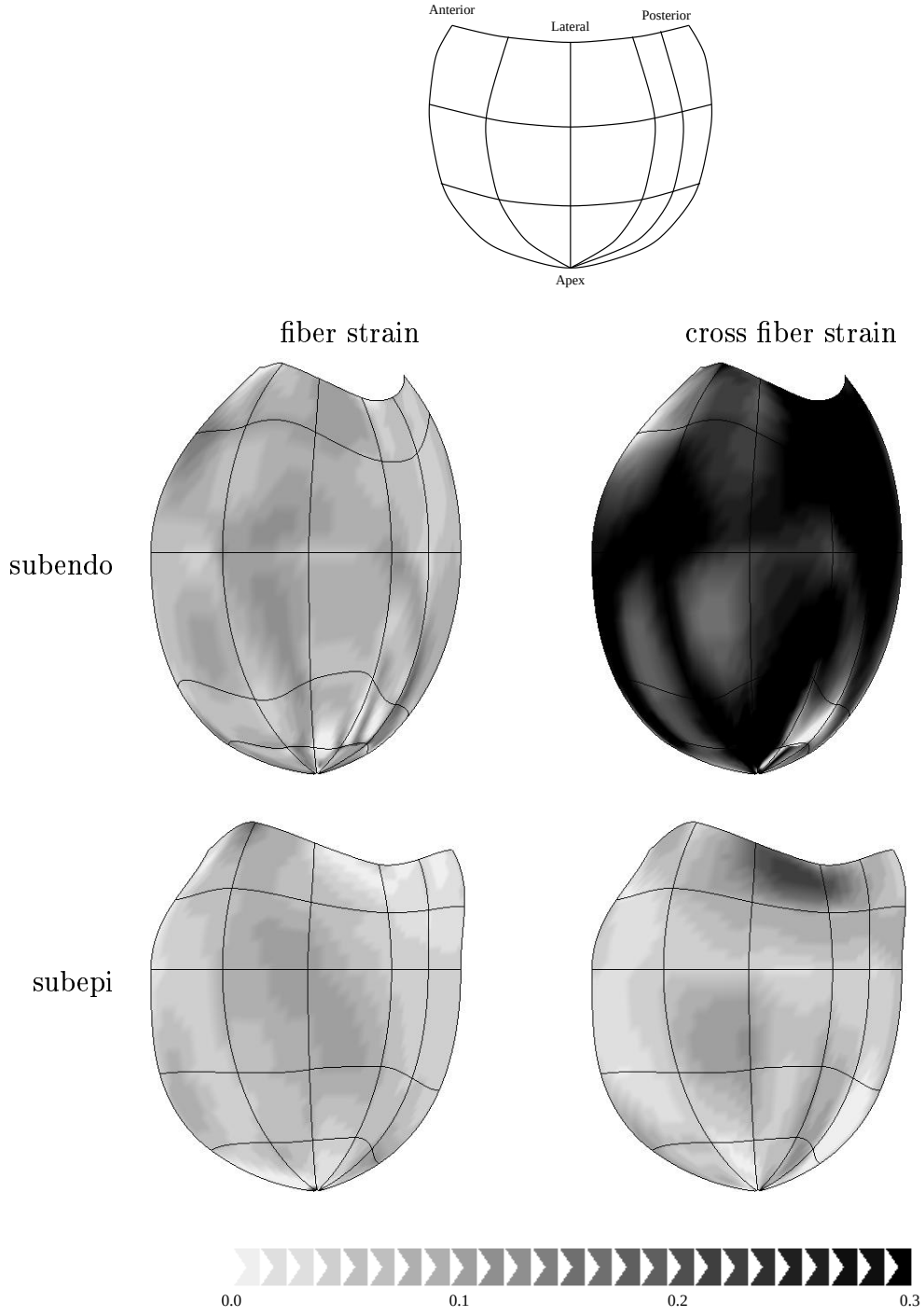

Figure III.11: Hammer maps of fiber and cross fiber strain in the LV free wall at 25 mm Hg pressure.

docardium. The longitudinal strain, however, remains relatively uniform through the wall (0.045 $\pm$ 0.012) Overall, the circumferential-longitudinal shear strain is small and negative through the wall (-0.018 $\pm$ 0.011) but becomes positive at 95% wall depth, with a value of 0.011 at the endocardium. The circumferential-radial shear is almost uniformly negative through the the wall (-0.086 $\pm$ 0.031) and the longitudinal-radial shear rapidly becomes most negative (-0.081) at 60% wall depth, then sharply increases to a maximum (+0.218) at the endocardial surface.

Regional LV Wall Stress

Over the lateral wall and apex, Cauchy stress resolved in the fiber direction was on average higher than that in the cross fiber direction; for the region shown in Figure III.13 the mean fiber stress was 2.91 $\pm$ 3.93 kPa and the mean cross fiber stress was 1.47 $\pm$ 3.51 kPa. At the midventricle fiber stress tended to be larger than cross fiber stress transmurally. At the epicardium and midwall, cross fiber stress is more uniform than the fiber stress, although fiber stress tended to be larger. The apex and papillary insertions at the subendocardium show the greatest magnitude and regional variability in both directions, where negative stresses occurred predominately at the regions of negative curvature.

Circumferential and longitudinal stresses computed from the finite element and simplified models have very weak correlations (Figure III.14). Most notable is that 44% of the circumferential stresses are opposite in sign (i.e., in either quadrants II or IV in the top plot of Figure III.14). To a lesser extent the same disagreement exists for the longitudinal wall stress, where 26% of the values are opposite in sign. Table III.2 lists the average stress from the finite element model, the equations for the simplified model, and the simplified model equations using either the mean value of wall thickness or radii of the ellipsoidal geometry. The simplified model underestimated the finite element model circumferential stresses by 25% when used with the regional values of wall thickness and curvatures. Longitudinal stresses computed using the simplified model overestimate those from the finite element

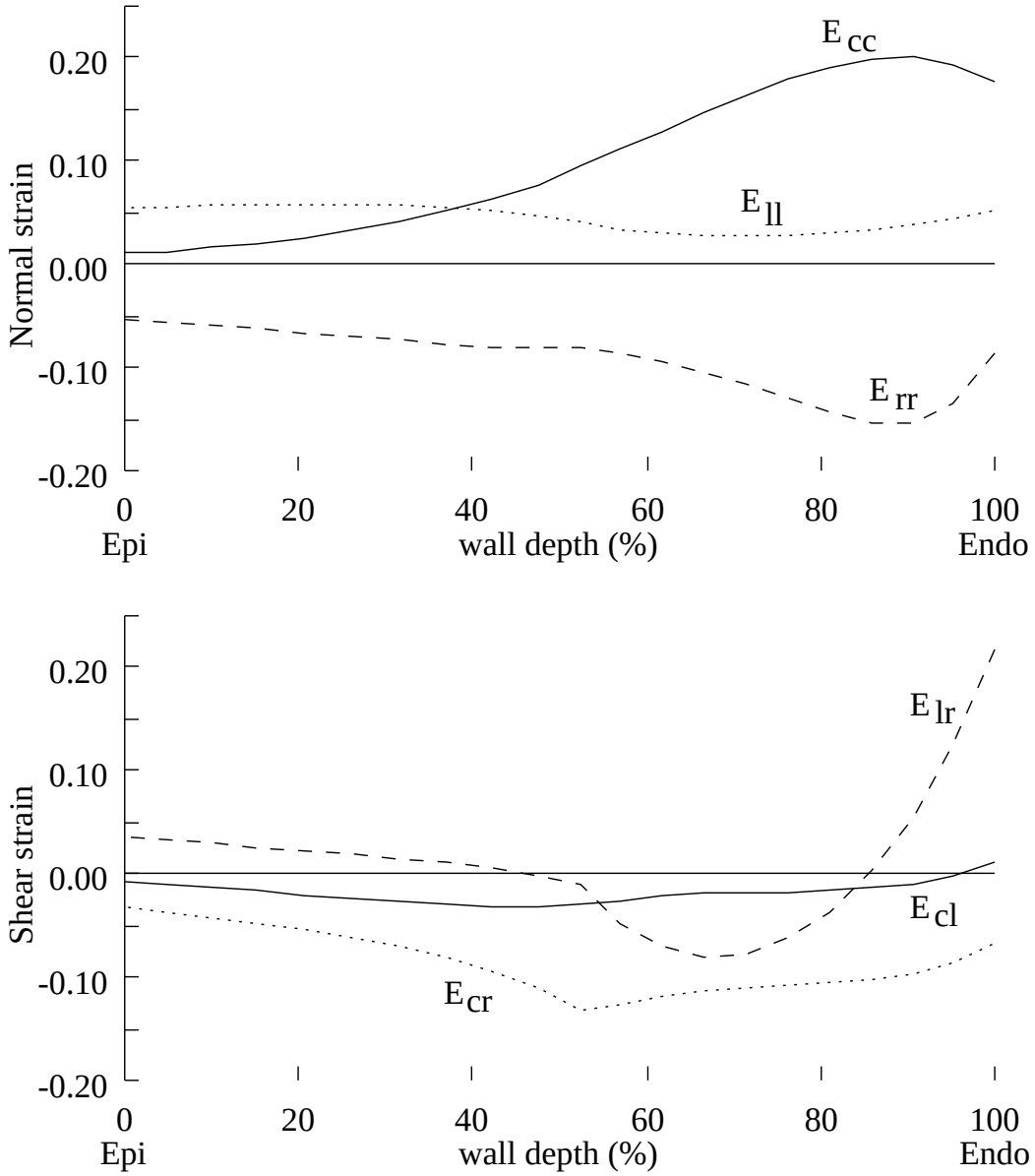

Figure III.12: Transmural normal and shear strains with respect to cardiac coordinates at 10 mm Hg LV pressure. TOP: Circumferential (E_{cc}), longitudinal (E_{ll}), and radial (E_{rr}) strains. BOTTOM: Circumferential-longitudinal fiber (E_{cl}), circumferential-radial (E_{cr}), and longitudinal-radial (E_{lr}) shear strains.

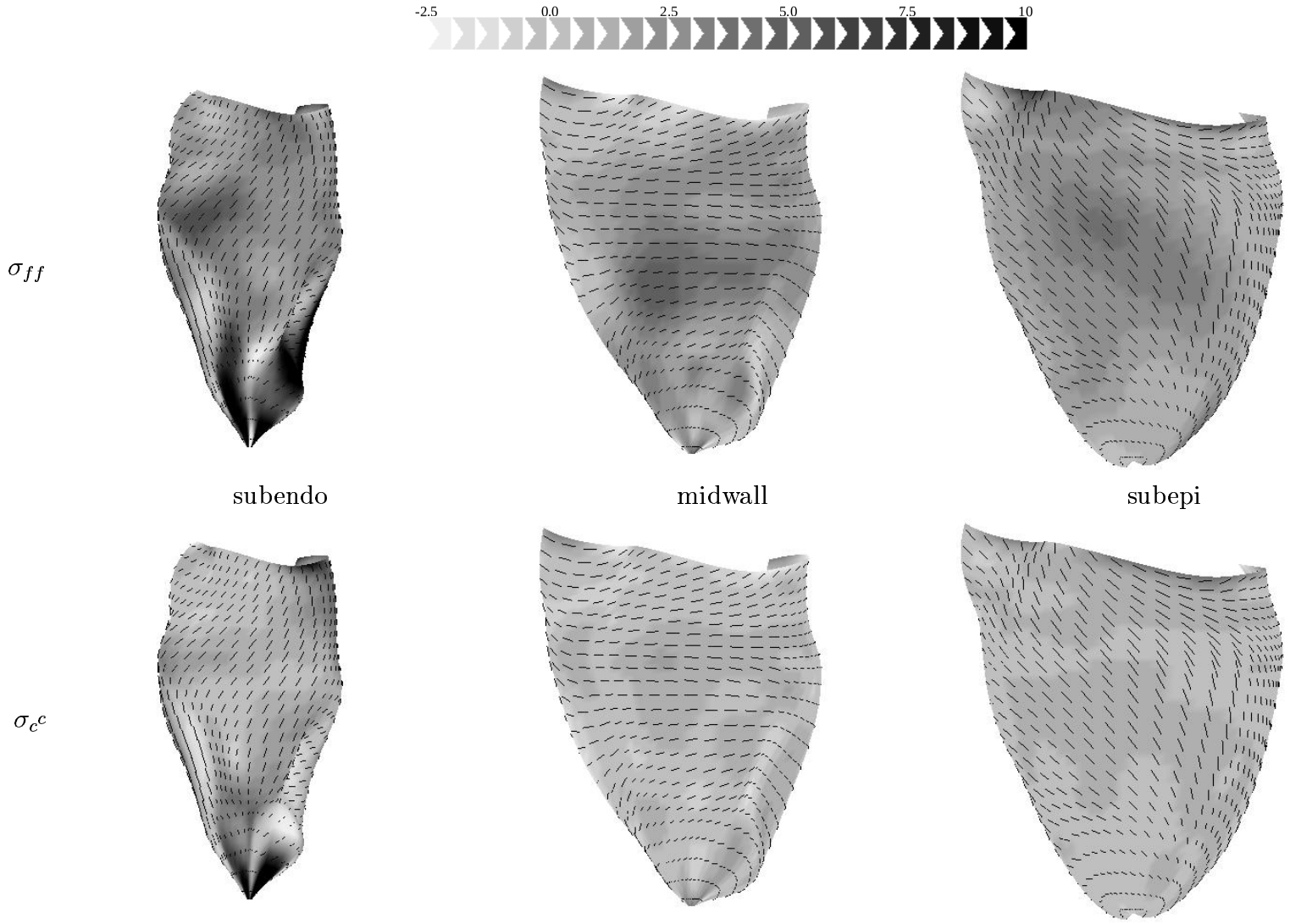

Figure II.13: Cauchy stress (kPa) resolved in fiber (TOP) and cross fiber (BOTTOM) directions in the LV free wall and apex at 10 mm Hg pressure. Black lines indicate local myofiber orientation.

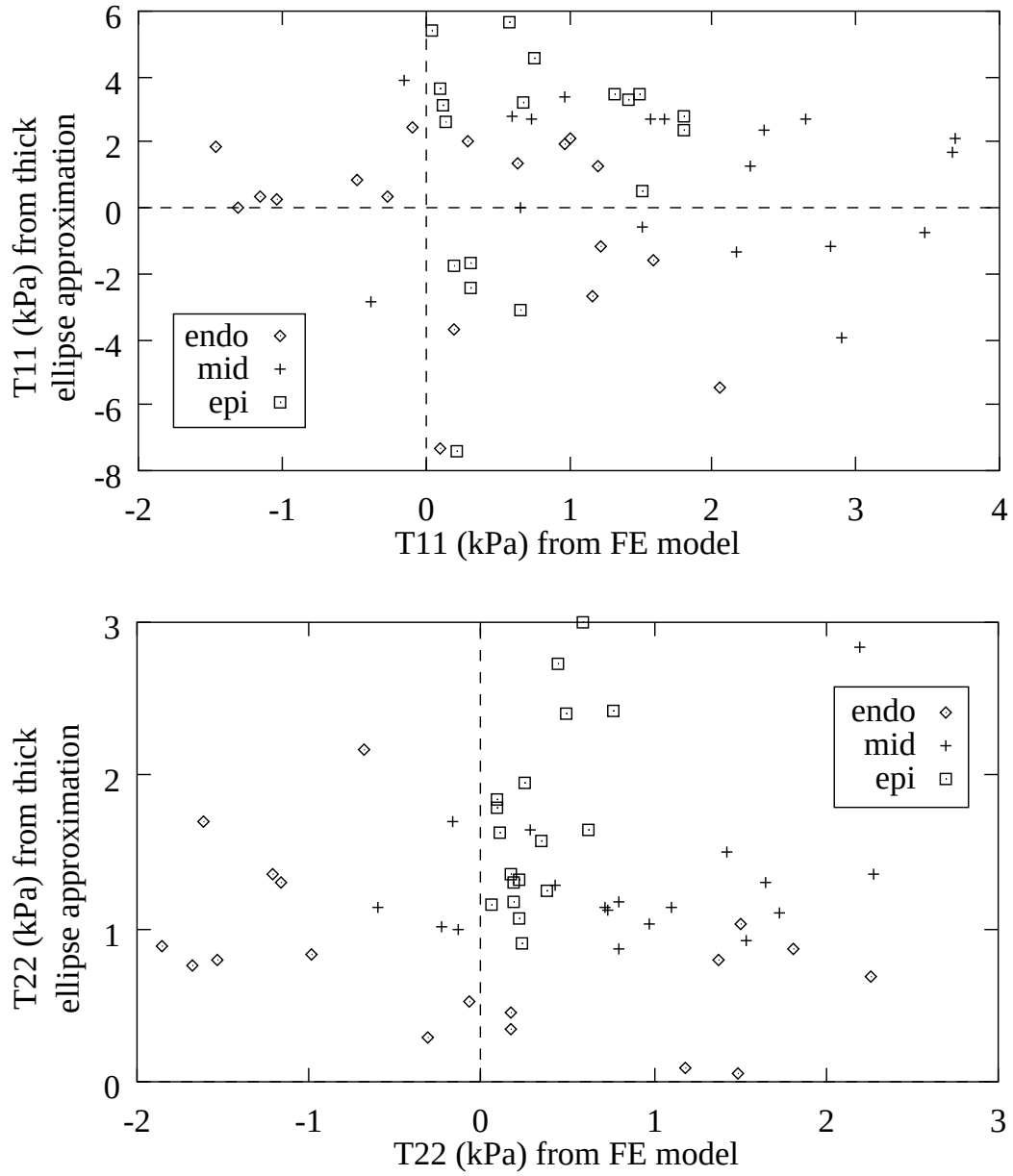

Figure III.14: Circumferential stress from Equation III.7 (TOP) and longitudinal stress from Equation III.8 (BOTTOM) at 10 mm Hg LV pressure plotted against stresses predicted by the finite element model.

	T_{11} (kPa)	% error	r^2
finite element model	0.952 ± 1.20		
simplified model	0.712 ± 2.95	-25.2	6.60×10^{-5}
mean wall thickness	0.622 ± 2.99	-34.7	4.32×10^{-7}
mean semi-minor radius	-0.662 ± 6.35	-165.5	4.81×10^{-3}
mean semi-major radius	2.147 ± 0.57	125.5	0.131
	T_{22} (kPa)	% error	r^2
finite element model	0.368 ± 0.99		
simplified model	1.318 ± 0.65	258.2	9.19×10^{-4}
mean wall thickness	1.313 ± 0.65	256.8	4.90×10^{-3}
mean semi-minor radius	1.479 ± 0.14	301.9	0.0390

Table III.2: Regional circumferential (TOP) and longitudinal (BOTTOM) stresses computed from the the finite element (FE) model, the simplified thick-walled ellipsoid model, and the simplified thick-walled ellipsoid model using the mean value of either wall thickness (h) or the semi-minor (b) or semi-major (a) radius of the ellipsoid. LV pressure was 10 mm Hg.

model by at least 250%. The magnitude of the error in both stress components generally increased using either the mean wall thickness or curvatures.

III.E Discussion

Simulations of passive left ventricular inflation were conducted using a realistic model of the rabbit ventricles. Material parameters of a transversely isotropic, hyper-elastic constitutive law were found that predicted epicardial strains in the anterolateral wall which were consistent with experiment, and suggest that transmural strain characteristics in the rabbit ventricle are qualitatively similar to those found in the canine ventricle. These results further the understanding of the passive mechanics of the intact rabbit ventricular myocardium, and may be important when interpreting the results of experimental investigations in electrical propagation [27], mechanoenergetics [83], or coupled mechanical and electrical interactions [20, 88, 89]. High-order finite element models have been used previously to investigate ventricular mechanics. Some assume an axisymmetric geometry which cannot model regional variations in stress due to local variations in wall thickness or curvature [40, 41]. Others have assumed constant transmural variation in fiber orientation or lack the right ventricle [12, 6]. A high-order finite element model of the canine left and right ventricles has been developed [57] but its use in modeling ventricular mechanics has been limited [10]. The model used here features an anatomically accurate left and right ventricular geometry and a realistic nonuniform transmural variation in fiber orientation. The element-by-element approach to solving the nonlinear system of governing equations was shown to be highly scalable on a parallel processing computer, achieving near-linear speedups for a similar passive inflation problem in the canine LV. Previous simulations requiring 60 minutes to complete on a laboratory workstation were completed here in just over 5 minutes, a 90% reduction in run time [12]. More importantly, larger and more detailed models can be utilized to obtain new insights regarding myocardial processes and interactions that are not possible

to measure with current experimental techniques.

III.E.1 Computational Approach

In validation runs involving the canine LV simulations, differences in the parallelism of the underlying algorithms is highlighted by comparing the timing results of the Full Newton and modified Newton-Raphson algorithms. The Full Newton method required nearly four times as many evaluations of the global tangent stiffness matrix than did the modified Newton-Raphson method. Evaluation of the global tangent stiffness matrix was an efficient data parallel operation since it required only local data (i.e., information available on the individual processor) to evaluate the element stiffness matrices and no interprocessor communication. The restarted GMRES method, on the other hand, relied heavily on interprocessor communication since partial matrix-vector products must be globally reduced at each iteration. For this phase of the solution procedure the Full Newton method required only 116 restarted GMRES iterations, less than one-third of 363 iterations required by the modified Newton-Raphson method. Hence the Full Newton method spent proportionally more time executing fully data parallel operations, whereas the modified Newton-Raphson method had a much larger number of synchronization points. Even so, the modified Newton-Raphson method had a shorter run time suggesting that, for this particular problem, evaluation of the global tangent stiffness matrix was more computationally expensive than the interprocessor communication overhead. For a problem where the reverse situation exists using the Full Newton method would likely provide shorter run times.

The left diagonal preconditioner utilized here was relatively simple to implement and effective for our problem. Without preconditioning the restarted GMRES method never reduced the residuals and always failed to converge. More elaborate parallel preconditioners exist, however, and would likely accelerate convergence of the restarted GMRES method at the cost of a more complicated implementation [67]. Yeckel and Derby (1997) have shown that symmetric left and right diagonal

preconditioning is sometimes more effective for accelerating restarted GMRES convergence in computational fluid dynamics problems. Preconditioners based on the individual element stiffness matrices of trilinear brick elements have been shown to be more effective than diagonal scaling, producing preconditioned systems with substantially lower condition numbers [82].

III.E.2 Regional LV Mechanics

During diastole, passive filling of the left ventricle increases cavity volume and distends the ventricular wall. The deformation of the myocardium during filling is highly dependent upon the passive material properties of the myocardium, which are known to vary across species [61]. Characterizing the passive material properties of myocardium is complicated by the complex myofiber arrangement, anisotropy, and nonlinear constitutive relations of the myocardium. Attempts to quantify passive myocardial material properties, however, have been successful in a few cases. Using an exponential form of the constitutive law, Guccione et al. (1991) have determined the material properties of passive myocardium in the canine using a cylindrical model of the LV. These material parameters have proven to be effective in reproducing left ventricular strains in the fiber, cross fiber, and radial (transmural) directions in a more realistic prolate spheroidal, high-order finite element description of the the canine LV [12]. The circumferential-radial and longitudinal-radial components of shear strain, however, did not agree with experimental measurements, suggesting the myocardium may be orthotropic, thus requiring a more detailed mathematical description [10]. Validated orthotropic constitutive laws have not yet been developed, and the transversely isotropic description of three-dimensional passive myocardium has performed sufficiently well in the past [12, 33].

The longitudinal strain measured in canine LV increases from approximately 0.04 at the epicardium to 0.12 and the subendocardium [62]; in the model, however, longitudinal strain is relatively uniform through the wall. The small positive circumferential-longitudinal shear strain at 95% wall depth indicated the ven-

tricular torsion changes direction (from left-handed to right-handed) at the subendocardium, also at odds with experimental findings. Similarly, the circumferential-radial shear is almost uniformly negative through the the wall and the longitudinal-radial shear undergoes a sudden change in magnitude at the inner half of the wall, neither of which has been observed in the canine or porcine heart [62, 34]. The differences in these strain components suggest the that the computed stresses are also in error, though the inaccuracy is difficult to quantify since each component of the three-dimensional stress tensor will depend on all the components of the strain tensor [75].

Despite these shortcomings, the model accurately predicts epicardial deformation on the anterolateral wall under passive loading. The stiffness in the fiber direction is much greater than in the cross fiber direction, characteristics similar to those in the canine and rat LV [62, 61]. Transmurally, the relatively uniform fiber strain and highly nonuniform cross fiber and radial strains are similar to those found in the canine, but transmural three-dimensional strains have yet to be measured in the intact rabbit ventricle so implications of this result must be derived cautiously. Transmural strains have yet to be measured in the rabbit heart, but advances in magnetic resonance (MR) imaging with cardiac tagging may provide a means of measuring these strains. MR studies have obtained 156×313 μm image resolution in the short-axis plane of the rabbit heart, sufficient to establish and track tags with 1 mm spacing through the LV wall [73, 2]. Displacement data acquired in this manner should prove adequate for nonhomogeneous analysis of transmural strain [53].

The stress-strain relations for the rat [61] and dog [30] using the incompressible form of the strain energy law (Equation III.1), rabbit [49], and the model using the parameters estimated here (Table III.3) are shown in Figure III.15. It has been previously shown that the rat myocardium is significantly less stiff than that of the canine, and that both materials are stiffer in the fiber direction than in the cross fiber direction [62]. The material parameters proposed here also suggest

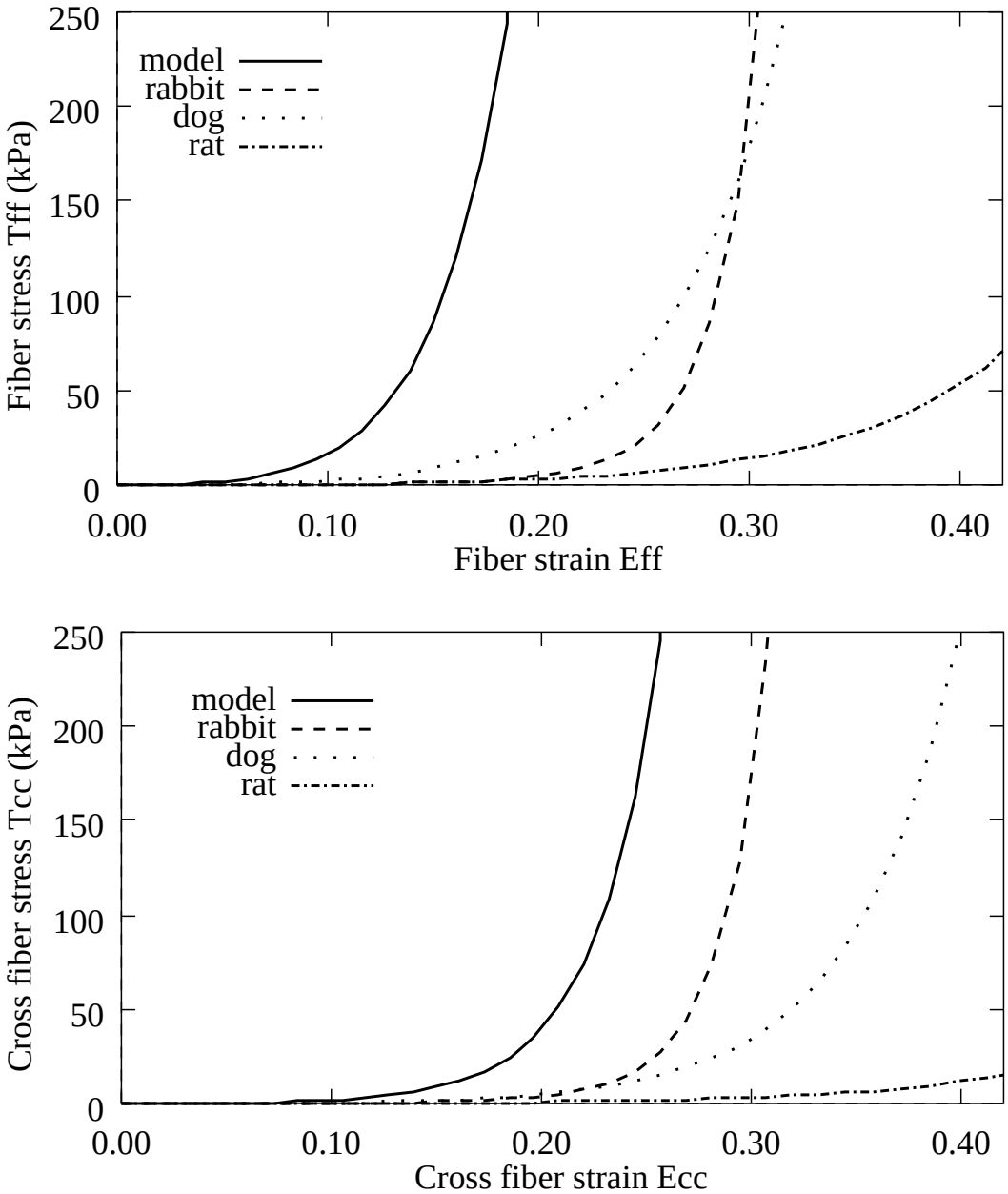

Figure III.15: Equibiaxial fiber and cross fiber stress-strain curves from models of the dog [12], rat [61], rabbit [49] and the model.

	C (kPa)	b_1	b_2	b_3	b_4 (kPa)	W form	reference
rat	2.2	9.2	2.0	3.7		III.1	[61]
dog	0.88	18.5	3.58	1.63		III.1	[12]
rabbit	0.103	9.13	2.32	0.08		III.2	[49]
model	0.88	50.0	5.0	1.63	200	III.3	

Table III.3: Material parameters used in Equations III.1, III.2, or III.3 to generate the stress-strain curves shown in Figure III.15.

that rabbit myocardium is stiffer in the fiber direction than in the cross fiber direction. In addition, our results suggest rabbit myocardium is more stiff than canine myocardium (note the solid lines are steeper than the dotted lines in Figure III.15).

Gallagher et al. (1997) noted that strains they measured were lower than those observed in other species, and the material parameters determined here suggest intact myocardium of the rabbit may be more stiff than that in the rat and canine. These results, however, are not completely consistent with the the material description of the rabbit myocardium proposed by Lin and Yin (1998), which show nearly equal stiffness in the fiber and cross fiber directions, and a generally more compliant material at strains below 20%. This discrepancy may be due in part to differences in the experimental preparations: strains obtained from LV passive inflation may be affected by the myocardial laminae, but in thin slabs of tissue this effect would be minimized because the sheets lie transmurally in the ventricle. The specimens used by Lin and Yin were excised at the midwall where the sheets run approximately normal to the epicardial plane [47]. In addition, the passive inflation protocol used by Gallagher et al. (1997) produced maximal fiber strain on the order of 10%. The thin slabs used in the equibiaxial tests conducted by Lin and Yin were subjected to 30% strain in the fiber or cross fiber direction. This may have made the tissue more compliant due to strain softening [19, 18], resulting in the stress-strain curves being shifted to the right (Figure III.15).

Omens and coworkers (1993) used an analysis similar to that of Guccione

et al. (1991) to describe normal strains in the passively inflated rat LV. They were able to minimize the least-squares difference between measured and predicted mid-wall strains, and show that the fiber to cross fiber stiffness ratio is lower in the rat than that in the canine at low loads (2.50 in rat and 5.24 in canine at 0–5 mm Hg LV pressure), but the ratios become nearly equal at higher loads (1.63 and 1.39, respectively, at 10–20 mm Hg). From these results they hypothesized the perimysial collagen structure in the rat may be significantly different than in the canine. A subsequent study showed that in canine myocardium the perimysial collagen fiber has a larger diameter and is less tortuous than in the more compliant rat myocardium, suggesting that the microstructural parameters of the perimysial collagen are the most important determinants of tissue stiffness [51]. In light of these studies, the results presented here suggest that similar variations may exist in the microstructural parameters of the perimysial collagen fibers in the rabbit myocardium. Relative to the canine myocardium, perimysial collagen fibers in the rabbit myocardium may have a larger diameter and smaller tortuosity, thus contributing to the greater stiffness of the rabbit tissue.

The inter-species differences in myocardial stiffness may have important implications when comparing the results of studies on mechanoelectric feedback. Many experimental preparations have utilized isolated canine or rabbit hearts to correlate mechanical stretch with the probability of eliciting a stretch-induced depolarization [20, 76, 31, 32]. Lekven et al. (1979) have shown that sustained increase in LV end-diastolic diameter in the canine heart causes a nonuniform transmural reduction in unipolar potential amplitude. In the isolated rabbit heart, Zabel et al. (1996) have investigated the relationship between increases in LV cavity volume and the change in amplitude of stretch-induced depolarization and repolarization. None of these studies quantified the direction or magnitude of myocardial deformation, but instead reported global changes in LV cavity diameter or volume. Assuming the stretch-induced response is related to the material deformation and not stress [70], the inter-species variations in myocardial stiffness discussed above suggest that

different stresses must be applied to myocardium of different species to elicit the same electrophysiological response. This supposition does not account for other differences in the electrophysiological environment that may exist across species. Even so, given a uniform experimental preparation and, for example, the same passive inflation protocol, we would expect the stretch-induced electrical response at a particular LV pressure to vary across species based on the differences in myocardial stiffness.

The global deformation of the model LV reproduces the experimentally measured volumes within 10% [21], except at the unloaded state (Figure III.7). The initial volume of the model was 1.71 milliliters whereas the experimental volume was 1.17 ± 0.39 milliliters. The disagreement may be due to two factors, one related to the model and the other to the experimental technique. The model omits the LV papillary muscles, and surfaces representing the LV endocardium do not have sufficient spatial resolution to capture the detailed variations on the endocardium [57]; thus it is likely that the model has a higher LV volume than an actual heart. The balloons used to experimentally measure the LV cavity volumes may not completely fill the narrow spaces around the endocardial trabeculae and papillary muscles, resulting in a lower LV volume. These two factors combined may be the cause of the large discrepancy in the unloaded LV volume.

As the pressure load in the LV increased, the intraventricular septum flattened and moved toward the RV, consistent with observations of septal motion in the isolated working rabbit heart made by Santamore et al. (1976). The septal displacement in the model (2.0 to 3.7 mm), however, is somewhat less than the the 5.9 to 6.8 mm they reported. This may be due to the restriction of longitudinal septal motion caused by the basal boundary conditions or an insufficient description of the material parameters.

Similar to the strain, Cauchy stress resolved in fiber and cross fiber directions varied regionally throughout the LV and apex, but without the transmural uniformity of fiber strain or the distinct positive transmural gradient of cross fiber

strain. Negative stresses tended to located in the highly-curved regions near the papillary insertions at the subendocardium, though cross fiber stress was also negative at the midwall near the posterior papillary. The largest variations in both fiber and cross fiber stress occurred at the subendocardium, where the largest stress were at the apex, though it is unknown if this is indicative of actual stresses in the heart. The apex is the thinnest region in the LV [8] and may be a site of high stress, but this has not been experimentally measured. Throughout the entire LV wall and apex the mean fiber stress was higher than the mean cross fiber stress, suggesting that fiber orientation may play a significant role in the stress distribution in intact myocardium. Aside from this, however, there were no other apparent correlations between stress and fiber orientation, so it may be possible that highly detailed representations of myofiber orientation are not required for stress analysis in the LV, and thus models incorporating an approximate fiber distribution but with highly resolved geometric features like wall thickness and curvature may be sufficient [12].

Correlations of the circumferential and longitudinal components of LV wall stress computed from the finite element model and the model based on a simplified LV geometry are extremely weak (Figure III.14). The estimates of longitudinal wall stress, T_{22}, computed from the simplified model show essentially no agreement with the finite element model stresses, except that the estimated stresses are all tensile. The simplified model provides a reasonable estimate (error of -25.2%) of the circumferential wall stress, T_{11}, of the finite element model using the regional values of wall thickness and ellipsoidal radii. Using the mean value of wall thickness (h), the semi-major axis radius (a), or the semi-minor axis radius (b) introduces more error into the estimated wall stress, but the mean wall thickness has the smallest effect, increasing the magnitude of the error by less than 10%. This suggests the regional curvature of the ventricular wall may be a more dominant determinant of regional circumferential stress than regional wall thickness.

III.E.3 Limitations

Though this model was anatomically detailed in terms of the geometry and fiber orientations, many features of the heart are still lacking. The model does not include the imbrication angle of the myofibers [77]. By including the imbrication angle in simulations of passive LV inflation, Bovendeerd and coworkers (1994) found that shear deformation was significantly reduced in the basal and apical regions of the ventricle. The model lacks the myocardial laminar sheet structure which was first quantified by LeGrice et al. (1995) and most recently by Costa et al. (1997), who showed that sliding and deformation of the myocardial laminae may contribute significantly to systolic thickening of the LV wall and suggested an orthotropic (rather than transversely isotropic) constitutive law may better describe the material properties of LV myocardium. The unloaded reference state for the model contained no residual stress, though residual stress is known to exist in the unloaded heart [13, 66, 60] and reduces transmural cross fiber strain gradients [79, 30]. Thus the cross fiber strains reported here may be overestimated.

Numerically optimized material parameters, obtained by minimizing the sum of squared differences between experimental and model-predicted variables, have been determined previously by Guccione et al. (1991) using a cylindrical model of the LV. They verified that a global minimum had been obtained by repeating their optimization procedure from a wide range of initial parameter values and computing the variance of each parameter. Such an effort can potentially require a very large number of simulations, and the resulting solution may not be unique [28]. From a practical standpoint we chose not to numerically optimize the material parameters given that each simulation required approximately five hours (and over 230 CPU hours) to complete. We would expect the model to better reproduce the experimental strain measurements had the material parameters been numerically optimized instead of heuristically estimated. Nevertheless, using the estimated material parameters obtained after 12 simulations, the model reproduced the experimentally

measured fiber and cross fiber strains well within the experimental accuracy.

The incompatible displacement solution (Figure III.8) demonstrates that the model admits solutions that are not physically realistic. This occurs because the finite element solution minimizes the error of the unconstrained DOFs without regard to physical constraints not defined by the boundary conditions. The situation encountered here is an example of a finite element "contact problem" where two impenetrable surfaces come in contact and subsequently deform in response to the reaction forces the two surfaces impose on each other. The finite element simulation of the contact problem is an active area of research, and the contact deformation of relatively simple geometries can be adequately modeled [14, 64, 65, 9]. Current methods, however, may be unable to reproduce the contact deformation of highly irregular bodies with anisotropic, nonlinear material properties such as the heart [90].

Some effort was directed at resolving the incompatible displacement solution by simply applying a constant pressure to the RV cavity. With a constant 2.5 mm Hg pressure in the RV the surfaces did not come in contact throughout the entire 0–25 mm Hg range of LV pressure. Reducing the RV pressure to 1 mm Hg resulted in the incompatible displacement at LV pressures of 15 mm Hg and above. Results of these simulations were not presented because there is no evidence that the RV was pressure loaded in the experimental preparation [21].

For several reasons we do not expect that the model strains would differ significantly if the contact problem were solved properly. The surfaces penetrated in a small region relative to the overall size of the ventricular model. The penetrating surfaces were confined to the apical region of the RV cavity, distant from where the model strains were compared to experimentally measured strains. Finally, the penetrating surfaces are part of the intraventricular septum and the RV free wall: deformation of the thick septum is likely to be altered when the septum contacts the much thinner RV wall, but we expect this difference to be slight since the septum is much larger than the RV. This reasoning is based on the model deformations pre-

sented here; thus, if rabbit myocardium is found to be significantly more compliant than this model suggests, then our results must be interpreted accordingly.

III.F Conclusions

We have estimated the material properties of the intact rabbit myocardium using a three-dimensional model of the rabbit ventricles. Estimated material parameters were validated with epicardial strains measured previously in the passively inflated rabbit heart. On the epicardium, fiber strain was larger than cross fiber strain, a feature also observed in the dog and rat myocardium. Transmural strains, which were not validated due to the lack of experimental measurements in the rabbit, showed characteristics similar to those in the canine and porcine left ventricle. Cauchy stress in the lateral wall and apex was generally larger in the fiber direction than in the cross fiber direction. At the subendocardium and midwall, cross fiber stress was more uniform than fiber stress. Negative stresses were generally located on the subendocardium at or near regions of negative curvature, though negative cross fiber stress also appeared at the midwall near the posterior papillary insertion. The computational approach used a scalable parallel processing computer and was shown to be highly scalable, reducing the time required to obtain a solution by 90%. The model may serve as a means to integrate the diverse experimental results from the rabbit into a unified model of cardiac function.

III.G Appendix: Detailed Strain Maps

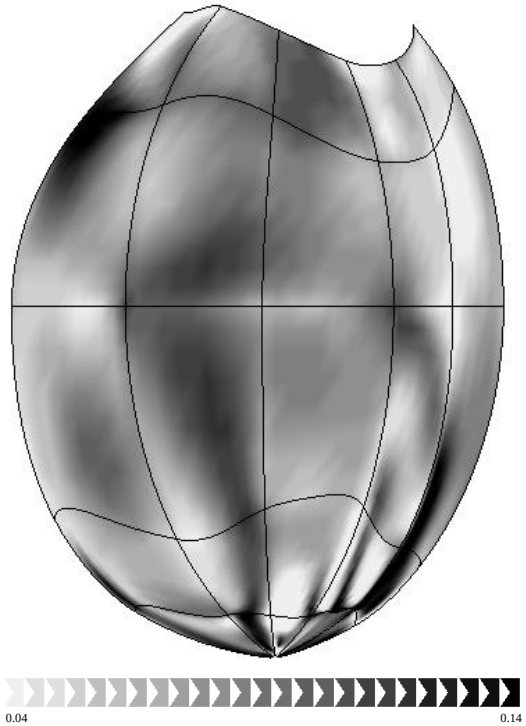

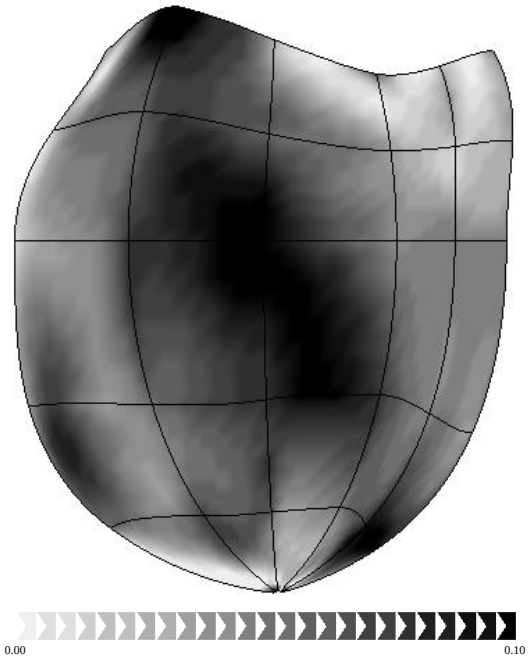

Subendocardial (TOP) and subepicardial (BOTTOM) fiber strain maps at 25 mm Hg. Note the different scales for each map.

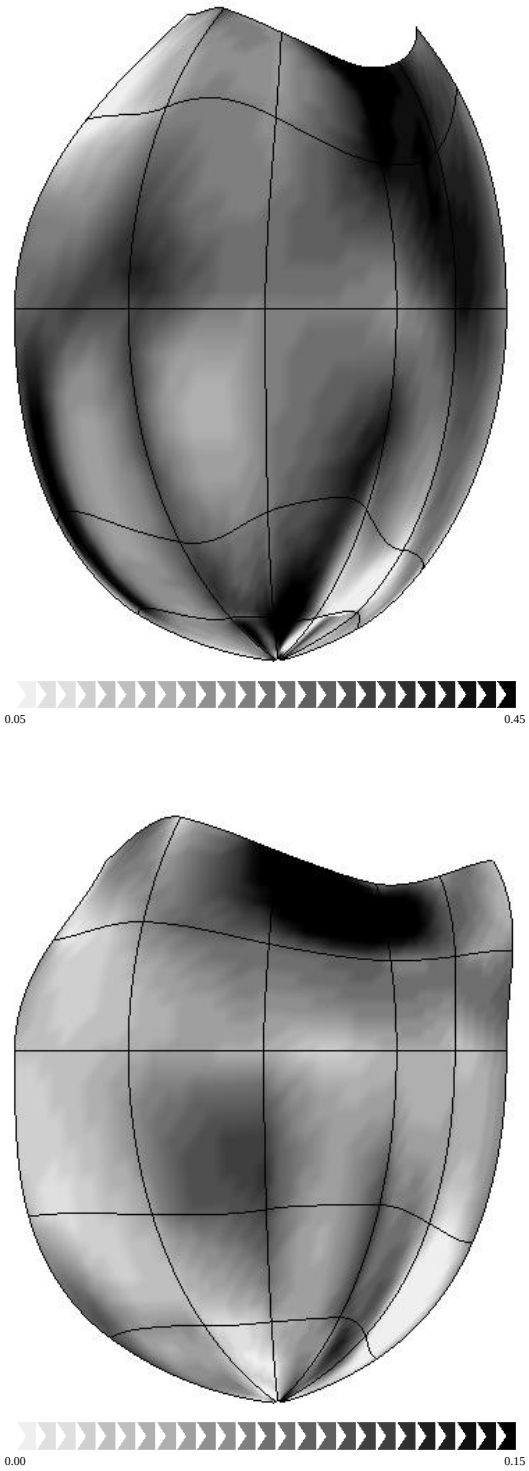

Subendocardial (TOP) and subepicardial (BOTTOM) cross fiber strain maps at 25 mm Hg. Note the different scales for each map.

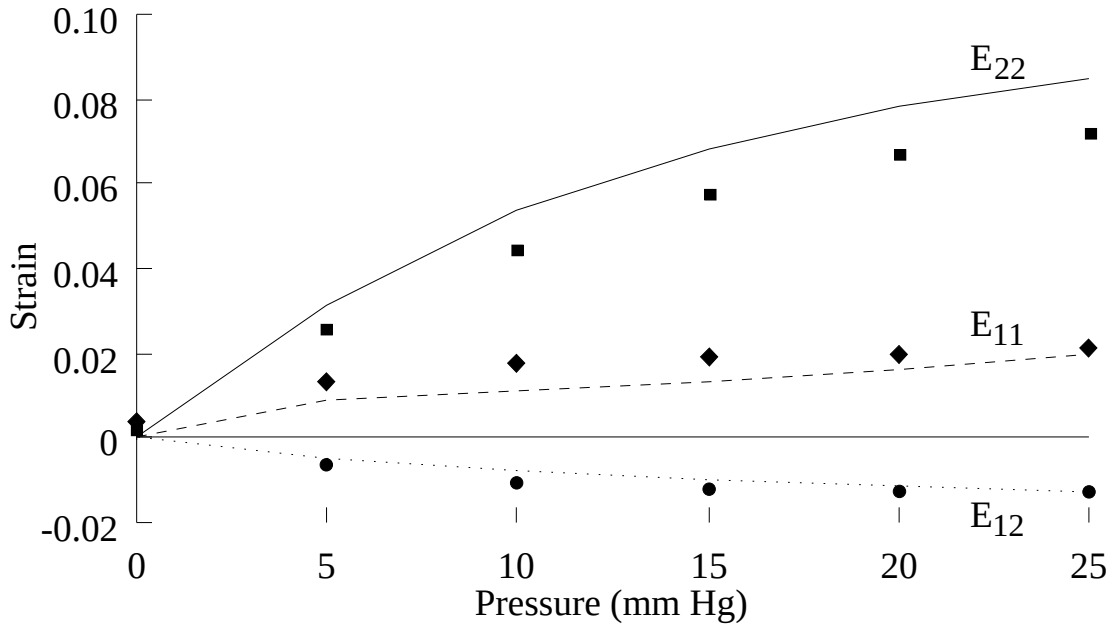

Figure III.16: Epicardial strain profiles from the anterolateral wall in cardiac coordinates. Simulations (solid lines) show good agreement with experimental circumferential (diamonds), longitudinal (boxes), and shear (circles) strains [21].

III.H Appendix: Computational Hardware and Software

Platform	SGI Indigo^2	Cray T3E [1]
address	`diablo.ucsd.edu`	`golden.sdsc.edu`
OS	IRIX64 6.2	unicosmk 2.0.3.39
Processor	195 MHz IP28	300 MHz Alpha 21164
FPU	MIPS R10010 rev. 0.0	
CPU	MIPS R10000 rev. 2.5	
main memory	192 Mb	128 Mb
data cache	32 Kb	8 Kb
instruction cache	32 Kb	8 Kb
secondary cache	1 Mb	96 Kb

Libraries: Y12 matrix subroutines (SGI and Cray) [63]

Parallel Iterative Methods 2.1 (SGI and Cray) [17]

UMFPACK 2.2 matrix subroutines (SGI and Cray) [15]

MPI (Cray)

```
mpt package version is:  1.1.0.0.5
mpt package creation date is:  Fri Aug 23 12:16:38 CDT 1996
mpt_level=mpt.1.1.0.0
mpi_level=mpi.1.0.9.4
mpi_mpp_level=mpi.1.0.1.0
libsma_level=libsma.2.0.1.4
libmpt_level=libmpt.1.0.1.0
product=mpt
pkgversion=1.1.0.0.5
```

Compilers and options:

SGI `f77`: Fortran 77, 4.0.2

```
FFLAGS = -mips2 -O2 -w0 -col120 -static -r8 -Olimit 2600
```

`cc`: C, 3.19

```
CFLAGS = -mips2 -O2 -lm
```

Cray `f90 -V` : Cray CF90 Version 3.0.0.0 10/28/97 11:37:13

```
FFLAGS = -DCOUPLED_ONLY -DGENSOL_ALLOC -DHAVE_UMFPACK -DMPI -N132 -e0v
```

`cc -V` : Cray Standard C Version 6.0.0.0 10/28/97 11:37:36

```
CFLAGS = -DCOUPLED_ONLY -DGENSOL_ALLOC -DHAVE_UMFPACK -DMPI -I. -c
```

References

[1] E. Anderson, J. Brooks, C. Grassl, and S. Scott. Performance of the CRAY T3E multiprocessor. White paper, Cray Research, `http://www.cray.com/products/systems/crayt3e/1200/performace.htm` or `http://www.sgi.com/t3e/performance.html`, 22 August 1997.

[2] E. Atalar and E. R. McVeigh. Optimum tag thickness for the measurement of motion by MRI. *IEEE Trans Med Imaging*, 13(1):152–160, Mar 1994.

[3] R. Barrett, M. Berry, T. F. Chan, J. Demmel, J. Donato, J. Dongarra, V. Eijkhout, R. Pozo, C. Romine, and H. Van der Vorst. *Templates for the Solution of Linear Systems: Building Blocks for Iterative Methods*. SIAM, Philadelphia, 1994.

[4] M. Behr, A. Johnson, J. Kennedy, S. Mittal, and T. Tezduyar. Computation of incompressible flows with implicit finite element implementations on the Connection Machine. *Comp Meth Appl Mech Eng*, 108(1–2):99–118, Sep 1993.

[5] P. H. Bovendeerd, T. Arts, T. Delhaas, J. M. Huyghe, D. H. van Campen, and R. S. Reneman. Regional wall mechanics in the ischemic left ventricle: numerical modeling and dog experiments. *Am J Physiol*, 270(Heart Circ. Physiol. 39):H398–H410, Jan 1996.

[6] P. H. Bovendeerd, T. Arts, J. M. Huyghe, D. H. van Campen, and R. S. Reneman. Dependence of local left ventricular wall mechanics on myocardial fiber orientation: A model study. *J Biomech*, 25(10):1129–1140, Oct 1992.

[7] P. H. M. Bovendeerd, J. M. Huyghe, T. Arts, D. H. van Campen, and R. S. Reneman. Influence of endocardial-epicardial crossover of muscle fibers on left ventricular wall mechanics. *J Biomech*, 27(7):941–951, Jul 1994.

[8] J. W. B. Bradfield, G. Beck, and R. J. Vecht. Left ventricular apical thin point. *Br Heart J*, 39(7):806–809, Jul 1977.

[9] A. B. Chaudhary and K.-J. Bathe. A solution method for static and dynamic analysis of three-dimensional contact problems with friction. *Computers and Structures*, 24(6):855–873, 1986.

[10] K. D. Costa. *The Structural Basis of Three-Dimensional Ventricular Mechanics*. PhD thesis, University of California, La Jolla, California, 1996.

[11] K. D. Costa, P. J. Hunter, J. M. Rogers, J. M. Guccione, L. K. Waldman, and A. D. McCulloch. A three-dimensional finite element method for large elastic deformations of ventricular myocardium: I — cylindrical and spherical polar coordinates. *J Biomech Eng*, 118(4):452–463, Nov 1996.

[12] K. D. Costa, P. J. Hunter, J. M. Rogers, J. M. Guccione, L. K. Waldman, and A. D. McCulloch. A three-dimensional finite element method for large elastic deformations of ventricular myocardium: II — prolate spheroidal coordinates. *J Biomech Eng*, 118(4):464–472, Nov 1996.

[13] K. D. Costa, K. May-Newman, D. Farr, W. G. O'Dell, A. D. McCulloch, and J. H. Omens. Three-dimensional residual strain in midanterior canine left ventricle. *Am J Physiol*, 273(Heart Circ. Physiol. 42):H1968–H1976, 1997.

[14] M. A. Crisfield. *Non-linear Finite Element Analysis of Solids and Structures*, volume 2: Advanced Topics. Wiley, New York, 1997.

[15] T. A. Davis and I. S. Duff. An unsymmetric-pattern multifrontal method for sparse LU factorization. *SIAM J Matrix Anal Appl*, 18(1):140–158, Jan 1997.

[16] H. Demiray. Large deformation analysis of some basic problems in biophysics. *Bull Math Biol*, 38(06):701–712, 1976.

[17] R. Dias da Cunha and T. Hopkins. A parallel implementation of the restarted GMRES iterative algorithm for nonsymmetric systems of linear equations. *Advances in Computational Mathematics*, 2(3):261–277, 1994.

[18] J. L. Emery, J. H. Omens, and A. D. McCulloch. Biaxial mechanics of the passively overstretched left ventricle. *Am J Physiol*, 272(5 Pt 2):H2299–H2305, May 1997.

[19] J. L. Emery, J. H. Omens, and A. D. McCulloch. Strain softening in rat left ventricular myocardium. *J Biomech Eng*, 119(1):6–12, Feb 1997.

[20] M. R. Franz, R. Cima, D. Wang, D. Profitt, and R. Kurz. Electrophysiological effects of myocardial stretch and mechanical determinants of stretch-activated arrhythmias. *Circulation*, 86(3):968–978, Sep 1992. Published erratum appears in Circulation 1992 Nov, 86(5):1663.

[21] A. M. Gallagher, J. H. Omens, L. L. Chu, and J. W. Covell. Alterations in collagen fibrillar structure and mechanical properties of the healing scar following myocardial infarction. *Cardiovasc Pathobiol*, 2(1):25–36, 1997.

[22] C. F. Gerald and P. O. Wheatley. *Applied Numerical Analysis*. Addison-Wesley, Reading, Mass., sixth edition, 1997.

[23] P. E. Gill, W. Murray, and M. H. Wright. *Practical Optimization*. Academic Press, New York, 1981.

[24] R. Glowinski and P. Le Tallec. *Augmented Lagrangian and operator-splitting methods in nonlinear mechanics*, volume 9 of *SIAM studies in applied mathematics*. Society for Industrial and Applied Mathematics, Philadelphia, 1989.

[25] G. H. Golub and C. F. Van Loan. *Matrix Computations*. Johns Hopkins University Press, Baltimore, second edition, 1993.

[26] Y. Goto, B. K. Slinker, and M. M. LeWinter. Similar normalized E_{max} and O_2 consumption-pressure-volume area relation in rabbit and dog. *Am J Physiol*, 255(Heart Circ. Physiol. 24):H366–H374, Aug 1988.

[27] R. A. Gray, J. Jalife, A. V. Panfilov, W. T. Baxter, C. Cabo, J. M. Davidenko, and A. M. Pertsov. Nonstationary vortexlike reentrant activity as a mechanism of polymorphic ventricular tachycardia in the isolated rabbit heart. *Circulation*, 91(9):2454–2469, May 1995.

[28] A. E. Green and J. E. Adkins. *Large Elastic Deformations*. Clarendon Press, Oxford, second edition, 1970.

[29] J. M. Guccione and A. D. McCulloch. Finite element modeling of ventricular mechanics. In L. Glass, P. Hunter, and A. McCulloch, editors, *Theory of Heart: Biomechanics, Biophysics, and Nonlinear Dynamics of Cardiac Function*, chapter 6, pages 121–144. Springer-Verlag, New York, 1991.

[30] J. M. Guccione, A. D. McCulloch, and L. K. Waldman. Passive material properties of intact ventricular myocardium determined from a cylindrical model. *J Biomech Eng*, 113(1):42–55, Feb 1991.

[31] D. E. Hansen, M. Borganelli, G. P. Stacy, Jr., and L. K. Taylor. Dose-dependent inhibition of stretch-induced arrhythmias by gadolinium in isolated canine ventricles. Evidence for a unique mode of antiarrhythmic action. *Circ Res*, 69(3):820–831, Sep 1991.

[32] D. E. Hansen, C. S. Craig, and L. M. Hondeghem. Stretch-induced arrhythmias in the isolated canine ventricle. Evidence for the importance of mechanoelectrical feedback. *Circulation*, 81(3):1094–1105, Mar 1990.

[33] J. W. Holmes and J. W. Covell. Collagen fiber orientation in myocardial scar tissue. *Cardiovasc Pathobiol*, 1(1):15–22, 1996.

[34] J. W. Holmes, J. A. Nuñez, and J. W. Covell. Functional implications of myocardial scar structure. *Am J Physiol*, 272(Heart Circ. Physiol. 41):H2123–H2130, May 1997.

[35] T. J. R. Hughes, I. Levit, and J. Winget. An element-by-element solution algorithm for problems of structural and solid mechanics. *Comp Meth Appl Mech Eng*, 36:241–254, 1983.

[36] R. M. Huisman, G. Elzinga, N. Westerhof, and P. Sipkema. Measurement of left ventricular wall stress. *Cardiovasc Res*, 14(3):142–153, Mar 1980.

[37] J. D. Humphrey and F. C. Yin. Constitutive relations and finite deformations of passive cardiac tissue II: stress analysis in the left ventricle. *Circulation Research*, 65(3):805–817, Sep 1989.

[38] P. J. Hunter and B. H. Smaill. The analysis of cardiac function: A continuum approach. *Prog Biophys Mol Biol*, 52(2):101–164, 1988.

[39] S. A. Hutchinson, L. V. Prevost, C. H. T. J. N. Shadidxi and, and R. S. Tuminaro. *Aztec User's Guide Version 2.0*. Sandia National Laboratories, Albuquerque, NM 87185, Jul 1998. Available from `http://www.cs.sandia.gov/CRF/pspapers/Aztec_ug_2.0.ps`.

[40] J. M. Huyghe, T. Arts, D. H. van Campen, and R. S. Reneman. Porous medium finite element model of the beating left ventricle. *Am J Physiol*, 262(Heart Circ. Physiol. 31):H1256–H1267, Apr 1992.

[41] J. M. Huyghe, D. H. van Campen, T. Arts, and R. M. Heethaar. A two-phase finite element model of the diastolic left ventricle. *J Biomech*, 24(7):527–538, 1991.

[42] Z. Johan, T. J. R. Hughes, K. K. Mathur, and S. L. Johnsson. A data parallel finite element method for computational fluid dynamics on the Connection Machine system. *Comp Meth Appl Mech Eng*, 99(1):113–134, Aug 1992.

[43] M. T. Jones and P. E. Plassmann. *BlockSolve95 Users Manual: Scalable Library Software for the Parallel Solution of Sparse Linear Systems*. Argonne National Laboratory, 9700 South Class Avenue, Argonne IL 60439, Jun 1997. Argonne National Laboratory Report 95/48 (revised June 1997). Available from `ftp://info.mcs.anl.gov/pub/BlockSolve95/manual.ps`.

[44] J. Kennedy, M. Behr, V. Kalro, and T. Tezduyar. Implementation of implicit finite element methods for incompressible flows on the CM–5. *Comp Meth Appl Mech Eng*, 119(1–2):95–111, Nov 1994.

[45] S. B. Knisley. Transmembrane voltage changes during unipolar stimulation of rabbit ventricle. *Circ Res*, 77(6):1229–1239, Nov 1995.

[46] V. Kumar, A. Grama, A. Gupta, and G. Karypis. *Introduction to Parallel Computing: Design and Analysis of Algorithms*. Benjamin/Cummings, Redwood City, CA, 1994.

[47] I. J. LeGrice, B. H. Smaill, L. Z. Chai, S. G. Edgar, J. B. Gavin, and P. J. Hunter. Laminar structure of the heart: Ventricular myocyte arrangement and connective tissue architecture in the dog. *Am J Physiol*, 269(Heart Circ. Physiol. 38):H571–H582, Aug 1995.

[48] J. Lekven, K. Chatterjee, J. V. Tyberg, and W. W. Parmley. Reduction in ventricular endocardial and epicardial potentials during acute increments in left ventricular dimensions. *American Heart Journal*, 98(2):200–206, Aug 1979.

[49] D. H. S. Lin and F. C. P. Yin. A multiaxial constitutive law for mammalian left ventricular myocardiumin steady-state barium contracture or tetanus. *J Biomech Eng*, 120(4):504–517, Aug 1998.

[50] D. S. Lindblad, C. R. Murphey, J. W. Clark, and W. R. Giles. A model of the action potential and underlying membrane currents in a rabbit atrial cell. *Am J Physiol*, 271(Heart Circ. Physiol. 40):H1666–H1696, Oct 1996.

[51] D. A. MacKenna, S. M. Vaplon, and A. D. McCulloch. Microstructural model of perimysial collagen fibers for resting myocardial mechanics during ventricular filling. *Am J Physiol*, 273(Heart Circ. Physiol. 42):H1576–H1586, Sep 1997.

[52] A. McCulloch, L. Waldman, J. Rogers, and J. Guccione. Large-scale finite element analysis of the beating heart. *Crit Rev Biomed Eng*, 20(5–6):427–449, 1992.

[53] A. D. McCulloch and J. H. Omens. Non-homogeneous analysis of three-dimensional transmural finite deformation in canine ventricular myocardium. *J Biomech*, 24(7):539–548, 1991.

[54] Message Passing Interface Forum. MPI: A message-passing interface standard. *Int J Supercomp Appl*, 8(3/4):169–416, Fall-Winter 1994.

[55] I. Mirsky. Ventricular and arterial wall stresses based on large deformation analyses. *Biophys J*, 13(11):1141–1159, Nov 1973.

[56] I. Mirsky. Elastic properties of the myocardium: a quantitative approach with physiological and clinical applications. In R. M. Berne, editor, *Handbook of Physiology, Section 2: The Cardiovascular System*, volume 1, chapter 14, pages 497–531. American Physiological Society, Bethesda, Maryland, 1979.

[57] P. M. F. Nielsen, I. J. LeGrice, B. H. Smaill, and P. J. Hunter. Mathematical model of geometry and fibrous structure of the heart. *Am J Physiol*, 260(Heart Circ. Physiol. 29):H1365–H1378, Apr 1991.

[58] B. Nour-Omid and B. N. Parlett. Element preconditioning using splitting techniques. *SIAM J Sci Stat Comput*, 6(3):761–770, Jul 1985.

[59] W. G. O'Dell and A. D. McCulloch. A novel numerical formulation for modeling tissue compressibility. *Proc ASME*, (in press), 1998.

[60] J. H. Omens and Y. C. Fung. Residual strain in rat left ventricle. *Circ Res*, 66(1):37–45, Jan 1990.

[61] J. H. Omens, D. A. MacKenna, and A. D. McCulloch. Measurement of strain and analysis of stress in resting rat left ventricular myocardium. *J Biomech*, 26(6):665–676, Jun 1993.

[62] J. H. Omens, K. D. May, and A. D. McCulloch. Transmural distribution of three-dimensional strain in the isolated arrested canine left ventricle. *Am J Physiol*, 261(Heart Circ. Physiol. 30):H918–H928, Sep 1991.

[63] O. Østerby and Z. Zlatev. *Direct Methods for Sparse Matrices*, volume 157 of *Lecture Notes in Computer Science*. Springer-Verlag, New York, 1983.

[64] P. Papadopoulos, R. E. Jones, and J. M. Solberg. A novel finite element formulation for frictionless contact problems. *Int J Numer Methods Eng*, 38(15):2603–2617, 15 August 1995.

[65] H. Parisch. A consistent tangent stiffness matrix for three-dimensional nonlinear contact analysis. *Int J Numer Methods Eng*, 28(8):1803–1812, Aug 1989.

[66] E. K. Rodriguez, J. H. Omens, L. K. Waldman, and A. D. McCulloch. Effect of residual stress on transmural sarcomere length distributions in rat left ventricle. *Am J Physiol*, 264(Heart Circ. Physiol. 33):H1048–H1056, Apr 1993.

[67] Y. Saad. Highly parallel preconditioners for general sparse matrices. In *Recent Advances in Iterative Methods*, volume 60 of *The IMA Volumes in Mathematics and its Applications*, pages 165–199. Springer-Verlag, New York, 1994. Papers from the IMA Workshop on Iterative Methods for Sparse and Structured Problems, held in Minneapolis MN, February 24–March 1, 1992.

[68] Y. Saad. *Iterative Methods for Sparse Linear Systems*. PWS Pub. Co., Boston, 1996.

[69] Y. Saad, G.-C. Lo, and S. Kuznetsov. *PSPARSLIB Users Manual: A Portable Library of parallel Sparse Iterative Solvers*. University of Minnesota, Department of Computer Science, 200 Union Street S.E., Minneapolis, MN 55455, Jan 1998. Available from `http://www.cs.umn.edu/Research/arpa/p_sparslib/psp/DOCS/manual.ps`.

[70] F. Sachs. Stretch-sensitive ion channels: An update. In D. P. Corey and S. D. Roper, editors, *Sensory Transduction*, volume 47 of *Society of General Physiologists Series*, chapter 15, pages 241–260. Rockefeller University Press, New York, 1992. Society of General Physiologists, 45th annual symposium, Marine Biological Laboratory, Woods Hole, Massachusetts, 5–8 September 1991.

[71] A. G. Salinger, Q. Xiao, Y. Zhou, and J. J. Derby. Massively parallel finite element computations of three-dimensional, time-dependent, incompressible flows in materials processing systems. *Comp Meth Appl Mech Eng*, 119(1–2):139–156, Nov 1994. Symposium on Parallel Finite Element Computations, Minneapolis, MN, USA; 25–27 Oct. 1993.

[72] W. P. Santamore, P. R. Lynch, G. Meier, J. Heckman, and A. A. Bove. Myocardial interaction between the ventricles. *J Appl Physiol*, 41(3):362–368, Sep 1976.

[73] D. F. Scollan, A. Holmes, R. Winslow, and J. Forder. Histological validation of myocardial microstructure obtained from diffusion tensor magnetic resonance imaging. *Am J Physiol*, 275(Heart Circ. Physiol. 44):H2308–2318, Dec. 1998.

[74] Silicon Graphics, Inc. CRAY T3E datasheets. Technical report, Silicon Graphics, Inc., `http://www.sgi.com/t3e/t3e_1200.html`, 1999.

[75] A. J. M. Spencer. *Continuum Mechanics*. Longman, New York, 1980.

[76] G. P. Stacy, Jr., R. L. Jobe, L. K. Taylor, and D. E. Hansen. Stretch-induced depolarizations as a trigger of arrhythmias in isolated canine left ventricles. *Am J Physiol*, 263(Heart Circ. Physiol. 32):H613–H621, Aug 1992.

[77] D. D. Streeter, Jr. Gross morphology and fiber geometry of the heart. In R. M. Berne, editor, *Handbook of Physiology, Section 2: The Cardiovascular System*, volume 1, chapter 4, pages 61–112. American Physiological Society, Bethesda, Maryland, 1979.

[78] T. Tezduyar, M. Behr, S. Mittal, and A. A. Johnson. Computation of unsteady incompressible flows with stabilized finite element methods: Space-time formulations, iterative strategies and massively parallel implementations. In P. Smolinski, editor, *New methods in Transient Analysis*, PVP-Vol. 246/AMD-Vol. 143, pages 7–24, New York, 1992. ASME. Presented at the Winter Annual Meeting of the American Society of Mechanical Engineers, Anaheim, California, November 8–13, 1992.

[79] S. Tsadok. Fiber and sheet strain distributions in ventricular myocardium referred to the stress-free state. Master's thesis, University of California, La Jolla, California, 1998.

[80] M. B. van Gijzen. An element-by-element solution algorithm for nonsymmetric linear systems of equations. In J. F. Dijksman and F. T. M. Nieuwstadt, editors, *Integration of Theory and Applications in Applied Mechanics*, pages 295–304, Boston, 1990. Kluwer Academic Publishers. Choice of papers presented at the First National Mechanics Congress, April 2-4, 1990, Rolduc, Kerkrade, the Netherlands.

[81] L. K. Waldman. Multidimensional measurement of regional strains in the intact heart. In L. Glass, P. Hunter, and A. McCulloch, editors, *Theory of Heart: Biomechanics, Biophysics, and Nonlinear Dynamics of Cardiac Function*, chapter 7, pages 145–174. Springer-Verlag, New York, 1991.

[82] A. J. Wathen. An analysis of some element-by-element techniques. *Comp Meth Appl Mech Eng*, 74(3):271–287, Sep 1989.

[83] M. W. Watkins, B. K. Slinker, Y. Goto, and M. M. LeWinter. 2,3-Butanedione monoxime increases contractile efficiency in the rabbit ventricle. *Am J Physiol*, 263(Heart Circ. Physiol. 32):H1811–H1818, Dec 1992.

[84] J. M. Winget and T. J. R. Hughes. Solution algorithms for nonlinear transient heat conduction analysis employing element-by-element iterative strategies. *Comp Meth Appl Mech Eng*, 52:711–815, 1985.

[85] A. Yeckel and J. J. Derby. Parallel computation of incompressible flows in materials processing: Numerical experiments in diagonal preconditioning. *Parallel Computing*, 23(9):1379–1400, Sep 1997.

[86] F. C. Yin. Ventricular wall stress. *Circ Res*, 49(4):829–842, Oct 1981.

[87] F. C. P. Yin, C. C. Chan, and R. M. Judd. Compressibility of perfused passive myocardium. *Am J Physiol*, 271(Heart Circ. Physiol. 40):H1864–H1870, Nov 1996.

[88] M. Zabel, B. S. Koller, F. Sachs, and M. R. Franz. Stretch-induced voltage changes in the isolated beating heart: Importance of the timing of stretch and implications for stretch-activated ion channels. *Cardiovasc Res*, 32(1):120–130, July 1996.

[89] M. Zabel, S. Portnoy, and M. R. Franz. Effect of sustained load on dispersion of ventricular repolarization and conduction time in the isolated intact rabbit heart. *J Cardiovasc Electrophysiol*, 7(1):9–16, Jan 1996.

[90] Z.-H. Zhong and J. Mackerle. Static contact problems — a review. *Engineering Computations*, 9:3–37, 1992.

Chapter IV

Three-Dimensional Propagation in Myocardium

IV.A Introduction

Little is known about how mechanical deformation affects the spread of electrical excitation in the intact heart. The three-dimensional anatomy of the ventricles is likely to play an important role in this process. Previous efforts have investigated either passive inflation [6] or three-dimensional propagation [12] in the left ventricle (LV), but the effects of three-dimensional deformation on propagation have not been explored. To address this issue, we have developed a high-order finite element model of the rabbit ventricular geometry and fiber architecture suitable for integrating the biophysics of the cell into the function of the whole organ.

IV.B Methods

A subset of the finite elements from the mechanics model were used as the domain for simulating three-dimensional electrical propagation through the myocardium. Two elements from the unloaded and deformed (15 mm Hg LV pressure) states in the anterolateral wall were further refined to generate a 512 element mesh

(8 circumferential × 8 longitudinal × 8 transmural) with elements approximately 1 mm on edge.

The myocardium was approximated as a continuum in which propagation is governed by the three-dimensional cable equation (Section IV.G). For a transversely isotropic medium the conductivity tensor models the preferential diffusion of the electrical excitation in the longitudinal direction of the myofiber as compared with the transverse direction [28]. The coefficients of the conductivity tensor (**D** in Equation IV.5) were estimated ($D_{11} = 1.71$, $D_{22} = D_{33} = 0.565$ mS/cm) to match the longitudinal and transverse propagation velocities found experimentally [17].

The ventricular action potential was simulated using the Beeler-Reuter ionic model [2] and initiated with a threshold stimulus applied to a small area on the LV endocardium for 4 milliseconds. The collocation-Galerkin finite element method was used to the solve discretized cable equation with no-flux boundary conditions [28]. Matrix factorization and back substitution used routines from the Y12M package [22]; the ODEs were integrated using the RKSUITE routine [30]. simulations were run on a SGI Octane workstation with a 225 MHz MIPS R10000 processor and 640 Mb of main memory (Appendix IV.F).

IV.C Results

Identical simulations (46,656 DOF) were conducted in the same region of the anterolateral wall using the ventricular geometry from either the unloaded or deformed states. To simulate 40 milliseconds of propagation in the unloaded state required 8.2 hours of CPU time; the deformed state required 14 hours. The execution time required for different phases of the solution is shown in Table IV.1. Data storage required 287.4 Mb of main memory.

Transmembrane potentials sampled at 0.5 milliseconds intervals on the epicardium directly opposite the stimulated endocardium are shown in Figure IV.1. In the deformed state the path length was reduced by 0.63 millimeters from the

			integration			
configuration	assembly	factor	membrane	back sub	RKSUITE	total
unloaded	34.3	1722.8	1430.3	25914.5	222.1	27566.9
deformed	34.2	1957.4	2367.7	45645.8	358.2	48371.7

Table IV.1: Execution time (seconds) required for different phases of the solution to the three-dimensional propagation problem. Integration time consists of the time required to update the membrane current model, back substitute the vector of collocation point variables with the factored mapping matrix, and update the numerical integrator (RKSUITE) variables. In the unloaded configuration the integration required 9,122 derivative evaluations; the deformed configuration required 15,160 evaluations.

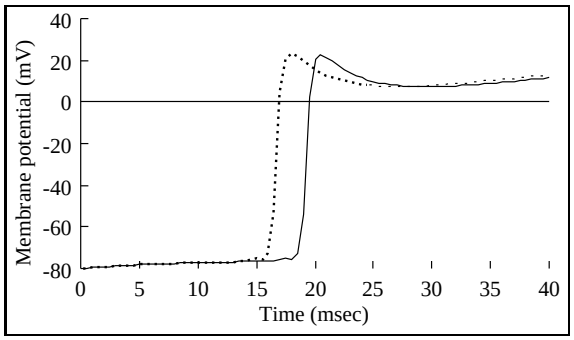

Figure IV.1: Transmembrane potentials at the same epicardial site in the unloaded (solid line) and deformed (dotted line) states.

unloaded state. Earlier activation in the deformed state was consistent with a shorter path length caused by radial thinning of the LV wall at higher cavity pressure.

The propagating wave arrived at the epicardial surface of the deformed geometry approximately 2.5 milliseconds earlier than on unloaded geometry (Figure IV.2). The transmural activation time, defined as the time in which the transmembrane voltage became greater than -40 mV, is shown for both configurations in Figure IV.3. In the early stages of the simulations ($t \leq 8$ milliseconds) the propagating wave radiates away from the simulated region in a somewhat elliptical

fashion.

IV.D Discussion

Simulations of electrical propagation through unloaded and deformed myocardium show that activation occurred earlier in the thinned tissue, suggesting that in the presence of uniform electrophysiological parameters myocardial geometry alone can affect activation time. Thus it is possible that LV cavity pressure, which will likely alter wall thickness, may be an important parameter in experimental studies of activation time and breakthrough patterns on the epicardial surface [10, 15].

We are unaware of any experimental studies on the effect of tissue thickness on activation time, and indeed interpreting the findings of such a study would be difficult given the current understanding of how stretch may activate mechanosensitive channels or alter intracellular calcium cycling [5]. Dominguez and Fozzard (1979) found that stretch increases conduction velocity in Purkinje fibers, but Reiter et al. (1994, 1988) showed dilatation has no affect on conduction velocity in a thin slab of ventricular tissue or the intact ventricle.

Analysis of the transmural activation times, however, implies this may be a limitation of the model. As the wave contacted the basal or apical boundaries (the top or bottom edges) the no-flux boundary conditions forced the wavefront to become perpendicular to the boundary. This accelerates the wave along the boundary, causing it to flatten and lose the elliptical shape. It may be possible to reduce the effect of the no-flux boundary conditions by using a highly refined mesh near the boundary of the computational domain. This may effectively isolate the perpendicular wavefront to a small region of the domain, possibly with minimal effect on the propagating wave in the central region. Another possible remedy would be to decouple the ionic reaction at the boundary, converting the two-dimensional finite element surfaces on the boundary into current sinks [28]. Although this has the

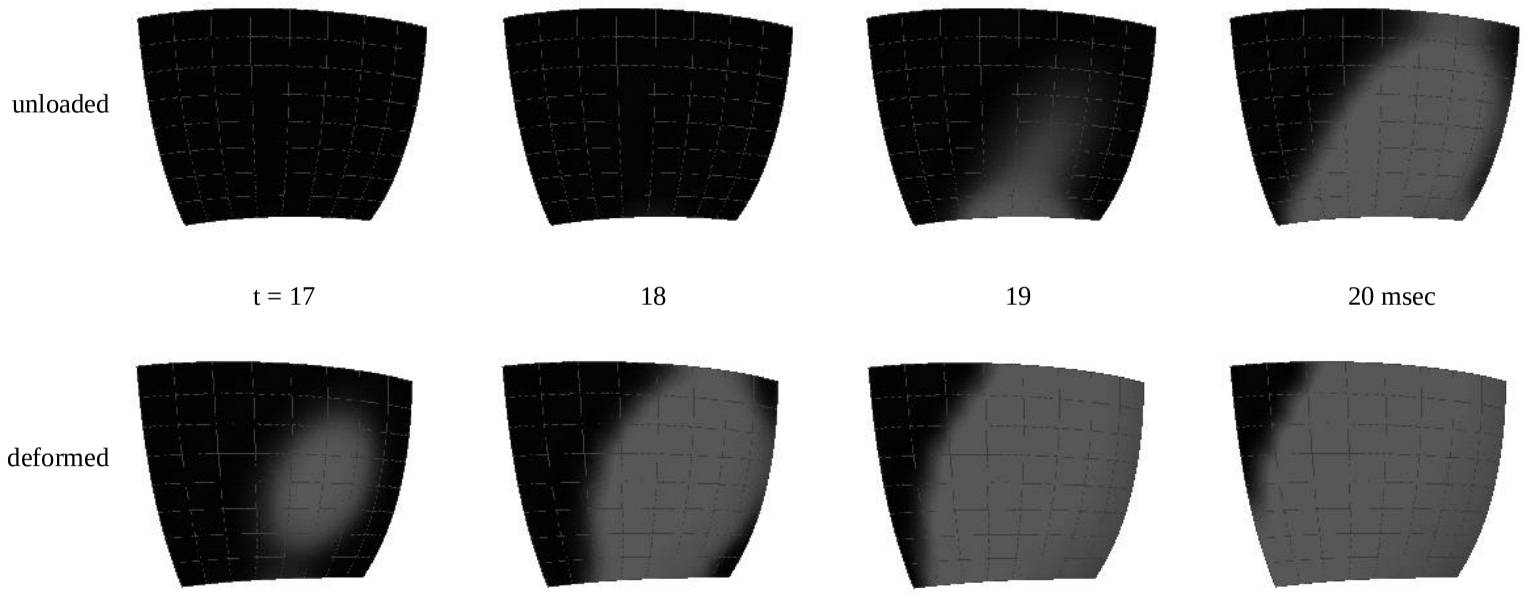

Figure IV.2: The epicardial surface of the three-dimensional geometric model in the unloaded and deformed (15 mm Hg LV pressure) states. The propagating electrical wave emerged on the epicardial surface approximately 2.5 milliseconds earlier in the deformed state.

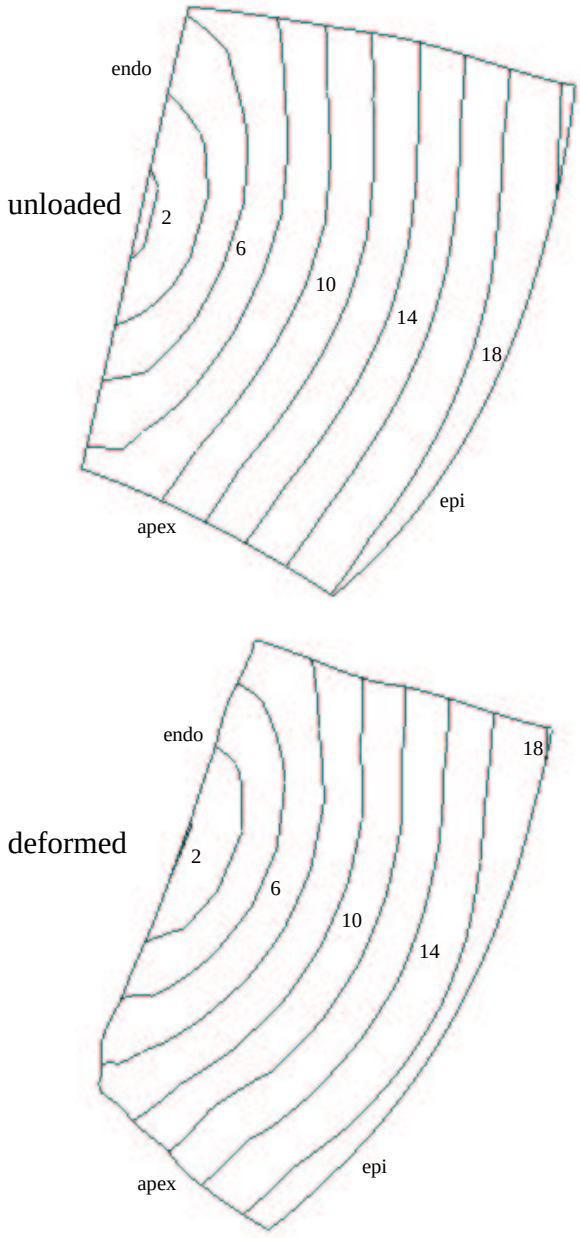

Figure IV.3: Transmural activation time (milliseconds) in the unloaded and deformed (15 mm Hg LV pressure) states. Contours are drawn at 2 millisecond intervals. Note the wavefront along the apical boundary appears to advance more rapidly than the wavefront near the midwall region.

opposite effect (the wave propagates with a reduced velocity along the boundary) it may provide satisfactory results for the problem under consideration. Finally, non-reflecting boundary conditions could be used in place of the no-flux conditions used here [16]. This approach has been used to successfully model undersea sound propagation [23], but its effectiveness on highly complex geometries with nonlinear reaction kinetics is not known. The slight depolarization of the rest potential (Figure IV.1) was due to an error in the implementation of the ionic model, which has been corrected.

Propagation in the deformed state required over 14 hours of CPU time to simulate 40 milliseconds, which was sufficient to investigate epicardial activation time. Such a short simulation time, however, precludes investigations into action potential duration, for example, because at least several hundred milliseconds must be simulated to capture the late repolarization phase. In addition, processes that may affect the rest state of the myocardium should be simulated with a quiescent period before any applied stimulus to allow the gating variables of the ionic model to equilibrate. For example, the rest potential will increase in the presence of a stretch-dependent current [26, 27, 31]. Thus a simulation of propagation in three-dimensional myocardium for 800 milliseconds may require 280 hours of CPU time if we simply extrapolate using the results here.

Our timing results indicate that propagation on realistic three-dimensional domains can be simulated feasibly within the processor speed and memory constraints of the current generation of laboratory workstations. Shorter solution times are always desirable, however, and may be possible using scalable vector or parallel processing computers.

IV.E Appendix: Parallel Collocation-Galerkin FE Method

A significant portion of the solution time for the propagation problems described in Chapter IV was spent integrating the system of ordinary differential equations (ODEs). We attempted to reduce the run time by parallelizing the integration phase of the solution.

The collocation-Galerkin finite element method integrates the ODEs at the finite element nodes, while computing the derivatives required by the numerical integrator at the collocation points. Since the number of unknowns is larger than the number of collocation points, Galerkin finite element equations are used with the boundary conditions to obtain enough additional equations to form a well-posed problem.

IV.E.1 Methods

The numerical integrator solves the problem:

$$\mathbf{G}_D \dot{\tilde{u}}_N = \mathbf{G}_K \tilde{u} + \mathcal{N}\left(\mathbf{G}_D \tilde{u}_N\right)$$

where $\mathbf{G}_K$ contains the spatial coupling terms of the discretized cable equation, $\mathbf{G}_D$ is the matrix that maps nodal parameters to collocation points, and $\mathcal{N}\left(\mathbf{G}_D \tilde{u}\right)$ is the nonlinear reaction kinetics of the system The $\mathbf{G}_K$ and $\mathbf{G}_D$ matrices are sparse. Evaluation of the derivatives needed by the integrator occurs at the collocation points:

$$\dot{\tilde{u}} = \mathbf{G}_K \tilde{u} + \mathcal{N}\left(\mathbf{G}_D \tilde{u}_N\right)$$

The vector of derivatives $\dot{\tilde{u}}$ is then mapped from the collocation points to the nodal parameters of the finite element mesh, $\dot{\tilde{u}}_N$, via the solution to the system:

$$\mathbf{G}_D \dot{\tilde{u}}_N = \dot{\tilde{u}}$$

With a serial (single processor) algorithm this operation can be performed relatively quickly: since the $\mathbf{G}_D$ matrix does not change over time (with static geometries like

those used here) the matrix can be factored once and repeatedly used in the forward and back substitution to compute the nodal parameters as the solution is advanced in time. As the timing results in Table IV.1 show, however, in three dimensions the most costly operation is the back substitution of the vector $\dot{\tilde{u}}$ into the factored $\mathbf{G}_D$ matrix: this step consumed 94% of the execution time for the three-dimensional simulations described in Chapter IV.

We implemented this algorithm using a MIMD programming model to simulate propagation of a wave generated by the FitzHugh-Nagumo (FHN) equations [11, 21]. The computation of the spatial coupling terms was assigned to a single processor, S, since the nonlinear reaction and spatial coupling computations are data independent. Computation of the nonlinear reaction terms was then executed on the remaining processors. These processors received the $\mathbf{G}_K\tilde{u}$ matrix-vector product via a one-to-all broadcast from processor S. The factorization of the $\mathbf{G}_D$ matrix was omitted; instead, we used the row-partitioning scheme implemented in the PETSc library [1] to distribute the $\mathbf{G}_D$ matrix across all the processors (except processor S). The nodal parameter vector was then computed in parallel using the PETSc implementation of the restarted GMRES iterative method. The restarted GMRES method used 500 basis vectors, was allowed a maximum of 2000 restarts, and an absolute error tolerance of 3.2×10^{-12} and a relative error tolerance of 10^{-12}; the error tolerances were determined by the guidelines in the PETSc documentation and through extensive experimentation. Our test problem was a flat two-dimensional plane with four bilinear elements (32 DOFs) utilizing modified FitzHugh-Nagumo kinetics [28]. All runs simulated 75 milliseconds. The components of the solution vector were initially set to unity, and not reset after the iterative method converged.

IV.E.2 Results

The time required to assemble the equations was less than 0.25 seconds for all simulations. The resulting run times and speedup for the parallel implementation are listed in Table IV.2. The time required to update the modified FHN

N processors	update	GMRES	total	speedup
2	1.70	31.52	33.22	1
3	1.68	57.97	59.65	0.557
4	1.70	97.03	98.73	0.336
5	1.70	83.70	85.40	0.389
6	1.70	126.20	127.90	0.260
7	1.70	133.50	135.20	0.246

Table IV.2: Run time and speedup for the parallel collocation-Galerkin finite element algorithm. Note that one processor was dedicated to computing the spatial coupling so that only N-1 processors were used for parallel iterative solution of the system of equations. The "update" column is the time required to update the ionic membrane model and the `RKSUITE` integrator overhead.

model was 0.005 seconds. It is apparent from the near linear increase in run time with additional processors that the algorithm with an iterative solver did not parallelize well. Essentially all of the increased run time was due to the execution of the parallel restarted GMRES iterative method. Although our test problem was quite small, these results suggest that a direct method may be more beneficial than an iterative method when solving the matrix equations with a static coefficient matrix and multiple right hand side vectors. Unfortunately, parallel direct methods currently available on scalable parallel processing architectures are designed only for dense matrices, imposing a significant restriction on the maximum problem size [3, 4]. To our knowledge, the only available parallel sparse direct method runs on parallel vector architectures and has not yet been implemented on scalable parallel machines [8].

IV.F Appendix: Computational Hardware and Software

Platform	SGI Octane
address	`lawson.ucsd.edu`
OS	IRIX64 6.5
Processor	225 MHz IP30
FPU	MIPS R10010 rev. 0.0
CPU	MIPS R10000 rev. 3.4
main memory	1664 Mb
data cache	32 Kb
instruction cache	32 Kb
secondary cache	1 Mb

Libraries: Y12 matrix subroutines [22]

UMFPACK 2.2 matrix subroutines [7]

RKSUITE 1.0 ODE integrator [30]

ODEPACK collection of ODE integrators [14]

Compilers and options:

`f77`: Fortran 77, 7.2.1

```
FFLAGS = -O2 -col120 -static -r8 -DRENDER_MESH -DCOLLOCATION -DGENSOL_ALLOC
```

`cc`: C, 7.2.1

```
CFLAGS = -O2 -DDOUBLE_REAL -lm -DRENDER_MESH -DCOLLOCATION
                                        -DGENSOL_ALLOC -I../include -I.
```

IV.G Appendix: Three-Dimensional Cable Equation

The charge on a capacitor is proportional to the potential difference across the gap, and is written as

$$q = CV \tag{IV.1}$$

where q is in coulombs, V is in volts, and C is the constant of proportionality (capacitance) in farads (1 farad = 1 coulomb/volt). Since current is the rate of change of charge with respect to time (coulombs/second), differentiating Equation IV.1 gives:

$$\frac{dq}{dt} = I_C = C\frac{dV}{dt}$$

the current-voltage relationship for a capacitor, with positive current defined as charge moving from the positive potential to the negative potential. Let I_m be the current per unit volume passing through the cell membrane (μA/cm^3); this current has two components: the capacitive current I_C and the ionic current I_{ion}.

$$I_m = I_{ion} + C_m\frac{dV_m}{dt}$$

Let $\tilde{J}$ be the intracellular current density (e.g., μA/cm^2) [29]. By the continuity of current, the divergence of $\tilde{J}$ must be equal to I_m:

$$\nabla \bullet \tilde{J} = I_m \tag{IV.2}$$

where ∇ is the gradient operator:

$$\nabla = \hat{\mathbf{i}}\frac{\partial}{\partial x} + \hat{\mathbf{j}}\frac{\partial}{\partial y} + \hat{\mathbf{k}}\frac{\partial}{\partial z}$$

The current density is related to the intracellular potential by Ohm's Law:

$$\tilde{J} = -\mathbf{D}\nabla\Phi_i \tag{IV.3}$$

where $\mathbf{D}$ is the intracellular conductivity tensor (mS/cm) and Φ_i is is the intracellular potential (mV). In three dimensions, the cable equation is written as [13]:

$$\nabla \bullet \mathbf{D}\nabla\Phi_i = S_v\left(I_{ion} + C_m\frac{dV_m}{dt}\right) \tag{IV.4}$$

where C_m is the membrane capacitance (μF/cm^2), S_v is the ratio of the cell surface to volume (1/cm), and I_{ion} and V_m are the transmembrane ionic current (μA/cm^2) and potential difference (mV), respectively.

For a monodomain formulation, the extracellular potential is assumed to be uniformly zero, thus the intracellular potential Φ_i becomes simply the transmembrane potential V_m. When the conductivity tensor $\mathbf{D}$ varies spatially, the spatial coupling term $\nabla \bullet \mathbf{D}\nabla V_m$ becomes:

$$\begin{aligned}
\mathbf{D}\nabla V_m &= \begin{bmatrix} D_{11} & D_{12} & D_{13} \\ D_{21} & D_{22} & D_{23} \\ D_{31} & D_{32} & D_{33} \end{bmatrix} \begin{bmatrix} \partial V_m/\partial x \\ \partial V_m/\partial y \\ \partial V_m/\partial z \end{bmatrix} \\
&= \begin{bmatrix} D_{11}\,\partial V_m/\partial x + D_{12}\,\partial V_m/\partial y + D_{13}\,\partial V_m/\partial z \\ D_{21}\,\partial V_m/\partial x + D_{22}\,\partial V_m/\partial y + D_{23}\,\partial V_m/\partial z \\ D_{31}\,\partial V_m/\partial x + D_{32}\,\partial V_m/\partial y + D_{33}\,\partial V_m/\partial z \end{bmatrix}
\end{aligned} \tag{IV.5}$$

$$\begin{aligned}
\nabla \bullet \mathbf{D}\nabla V_m = {} & D_{11}\frac{\partial^2 V_m}{\partial x^2} + \frac{\partial D_{11}}{\partial x}\frac{\partial V_m}{\partial x} + \\
& D_{12}\frac{\partial^2 V_m}{\partial y \partial x} + \frac{\partial D_{12}}{\partial x}\frac{\partial V_m}{\partial y} + \\
& D_{13}\frac{\partial^2 V_m}{\partial z \partial x} + \frac{\partial D_{13}}{\partial x}\frac{\partial V_m}{\partial z} + \\
& D_{21}\frac{\partial^2 V_m}{\partial x \partial y} + \frac{\partial D_{21}}{\partial y}\frac{\partial V_m}{\partial x} + \\
& D_{22}\frac{\partial^2 V_m}{\partial y^2} + \frac{\partial D_{22}}{\partial y}\frac{\partial V_m}{\partial y} + \\
& D_{23}\frac{\partial^2 V_m}{\partial z \partial y} + \frac{\partial D_{23}}{\partial y}\frac{\partial V_m}{\partial z} + \\
& D_{31}\frac{\partial^2 V_m}{\partial x \partial z} + \frac{\partial D_{31}}{\partial z}\frac{\partial V_m}{\partial x} + \\
& D_{32}\frac{\partial^2 V_m}{\partial y \partial z} + \frac{\partial D_{32}}{\partial z}\frac{\partial V_m}{\partial y} + \\
& D_{33}\frac{\partial^2 V_m}{\partial^2 z} + \frac{\partial D_{33}}{\partial z}\frac{\partial V_m}{\partial z}
\end{aligned}$$

If Equation IV.4 is written with respect to local fiber coordinates such that trans-

verse isotropy can be assumed, the conductivity tensor $\mathbf{D}$ is diagonal and constant with $D_{22} = D_{33}$, simplifying the spatial coupling to $\mathbf{D}\nabla^2 V_m$; rearranging:

$$\begin{aligned} C_m \frac{dV_m}{dt} &= \frac{1}{S_v}\mathbf{D}\nabla^2 V_m - I_{ion} \\ &= \frac{1}{S_v}\left(D_{11}\frac{\partial^2 V_m}{\partial x^2} + D_{22}\frac{\partial^2 V_m}{\partial y^2} + D_{33}\frac{\partial^2 V_m}{\partial z^2}\right) - I_{ion} \end{aligned} \tag{IV.6}$$

The ionic current I_{ion} is determined by one of the many transmembrane ionic current models [20, 2, 18, 19].

IV.H Appendix: Beeler-Reuter Equations

Fast inward sodium current:

$$I_{Na} = (G_{Na} \cdot m^3 \cdot h \cdot j + G_{NaC}) \cdot (V_m - E_{Na})$$

where $G_{Na} = 4$ and $G_{NaC} = 0.003$ mS/cm^2, and $E_{Na} = 50$ mV.

Slow inward current (calcium):

$$I_s = G_s \cdot d \cdot f \cdot (V_m - E_s)$$

where $E_s = -82.3 - 13.0287 \cdot \ln[Ca]_i$ and $G_s = 0.09$ mS/cm^2.

Time- and voltage-dependent outward current (potassium)

$$I_{x_1} = 0.8 \frac{\exp[0.04 \cdot (V_m + 77)] - 1}{\exp[0.04 \cdot (V_m + 35)]} \cdot x_1$$

Time-independent outward potassium current

$$I_{k_1} = 0.35 \left\{ \frac{4 \cdot \{\exp[0.04 \cdot (V_m + 85)] - 1\}}{\exp[0.08 \cdot (V_m + 53)] + \exp[0.04 \cdot (V_m + 53)]} + \frac{0.2 \cdot (V_m + 23)}{1 - \exp[-0.04 \cdot (V_m + 23)]} \right\}$$

Calcium concentration:

$$\frac{d[Ca]_i}{dt} = -10^{-7} I_s + 0.07 \cdot (10^{-7} - [Ca]_i)$$

where $[Ca]_i = 10^{-7}$ moles/liter at steady-state.

Gating variables:

$$\alpha_{x_1} = \frac{0.0005e^{0.083(V+50)}}{1+e^{0.057(V+50)}} \qquad \beta_{x_1} = \frac{0.0013e^{-0.06(V+20)}}{1+e^{-0.04(V+50)}}$$

$$\alpha_m = \frac{V+47}{1-e^{-0.1(V+47)}} \qquad \beta_m = 40e^{-0.056(V+72)}$$

$$\alpha_h = 0.126e^{-0.25(V+77)} \qquad \beta_h = \frac{1.7}{1+e^{-0.082(V+22.5)}}$$

$$\alpha_j = \frac{0.055e^{-0.25(V+78)}}{1+e^{-0.2(V+78)}} \qquad \beta_j = \frac{0.3}{1+e^{-0.1(V+32)}}$$

$$\alpha_d = \frac{0.095e^{-0.01(V-5)}}{1+e^{-0.072(V-5)}} \qquad \beta_d = \frac{0.07e^{-0.017(V+44)}}{1+e^{0.05(V+44)}}$$

$$\alpha_f = \frac{0.012e^{-0.008(V+28)}}{1+e^{0.15(V+28)}} \qquad \beta_f = \frac{0.0065e^{-0.02(V+30)}}{1+e^{-0.2(V+30)}}$$

References

[1] S. Balay, W. D. Gropp, L. C. McInnes, and B. F. Smith. *PETSc 2.0 Users Manual*, 1998. Available from `http://www.mcs.anl.gov/petsc`.

[2] G. W. Beeler and H. Reuter. Reconstruction of the action potential of ventricular myocardial fibres. *J Physiol*, 268(1):177–210, Jun 1977.

[3] C. Bendtsen. *ParSODES: A Parallel Stiff ODE Solver*. Danish Computer Centre for Research and Education, DTU, Bldg. 304 DK-2800 Lyngby, Denmark, 1996. Available from `http://www.netlib.org/ode/parsodes.tar.gz`.

[4] L. S. Blackford, J. Choi, A. Cleary, E. D'Azevedo, J. Demmel, I. Dhillon, J. Dongarra, S. Hammarling, G. Henry, A. Petitet, K. Stanley, D. Walker, and R. C. Whaley. *ScaLAPACK Users Guide*. SIAM, Philadelphia, PA, 1997.

[5] S. C. Calaghan and E. White. The role of calcium in the response of cardiac muscle to stretch. *Prog Biophys Mol Biol*, 71:59–90, 1999.

[6] K. D. Costa, P. J. Hunter, J. M. Rogers, J. M. Guccione, L. K. Waldman, and A. D. McCulloch. A three-dimensional finite element method for large elastic deformations of ventricular myocardium: II — prolate spheroidal coordinates. *J Biomech Eng*, 118(4):464–472, Nov 1996.

[7] T. A. Davis and I. S. Duff. An unsymmetric-pattern multifrontal method for sparse LU factorization. *SIAM J Matrix Anal Appl*, 18(1):140–158, Jan 1997.

[8] J. W. Demmel, J. R. Gilbert, and X. S. Li. *SuperLU Users Guide*, 1997. Available from `http://http.cs.berkeley.edu/~xiaoye/superlu.html`.

[9] G. Dominguez and H. A. Fozzard. Effect of stretch on conduction velocity and cable properties of cardiac Purkinje fibers. *Am J Physiol*, 237(3):C119–C124, Sep 1979.

[10] I. R. Efimov, B. Ermentrout, D. T. Huang, and G. Salama. Activation and repolarization patterns are governed by different structural characteristics of ventricular myocardium: Experimental study with voltage-sensitive dyes and numerical simulations. *J Cardiovasc Electrophysiol*, 7(6):512–530, Jun 1996.

[11] R. FitzHugh. Impulses and physiological states in theoretical models of nerve membrane. *Biophys J*, 1:445–466, Jul 1961.

[12] R. A. Gray, J. Jalife, A. V. Panfilov, W. T. Baxter, C. Cabo, J. M. Davidenko, and A. M. Pertsov. Nonstationary vortexlike reentrant activity as a mechanism of polymorphic ventricular tachycardia in the isolated rabbit heart. *Circulation*, 91(9):2454–2469, May 1995.

[13] D. M. Harrild and C. S. Henriquez. A finite volume model of cardiac propagation. *Ann Biomed Eng*, 25(2):315–334, March-April 1997.

[14] A. C. Hindmarsh. ODEPACK, a systematized collection of ODE solvers. In R. S. Stepleman, editor, *Scientific Computing: Applications of Mathematics and Computing to the Physical Sciences*, volume 1 of *IMACS Transactions on Scientific Computation*, pages 55–64. North-Holland, New York, 1983. Based on papers presented at the Tenth IMACS World Congress on System Simulation and Scientific Computation, held in Montreal, Canada, August 8-13, 1982.

[15] A. Kanai and G. Salama. Optical mapping reveals that repolarization spreads anisotropically and is guided by fiber orientation in guinea pig hearts. *Circ Res*, 77(4):784–802, Oct 1995.

[16] J. B. Keller and D. Givoli. Exact non-reflecting boundary conditions. *Journal of Computational Physics*, 82(1):172–192, May 1989.

[17] S. B. Knisley and B. C. Hill. Effects of bipolar point and line stimulation in anisotropic rabbit epicardium: Assessment of the critical radius of curvature for longitudinal block. *IEEE Trans Biomed Eng*, 42(10):957–966, Oct 1995.

[18] C.-H. Luo and Y. Rudy. A model of the ventricular cardiac action potential: Depolarization, repolarization, and their interaction. *Circ Res*, 68(6):1501–1526, Jun 1991.

[19] C.-H. Luo and Y. Rudy. A dynamic model of the cardiac ventricular action potential. I. Simulations of ionic currents and concentration changes. *Circ Res*, 74(6):1071–1096, Jun 1994.

[20] R. E. McAllister, D. Noble, and R. W. Tsien. Reconstruction of the electrical activity of cardiac Purkinje fibres. *J Physiol*, 251(1):1–59, Sep 1975.

[21] J. Nagumo, S. Arimoto, and S. Yoshizawa. An active pulse transmission simulating nerve axon. *Proc IRE*, pages 2061–2070, Oct 1962.

[22] O. Østerby and Z. Zlatev. *Direct Methods for Sparse Matrices*, volume 157 of *Lecture Notes in Computer Science*. Springer-Verlag, New York, 1983.

[23] J. S. Papadakis. Exact, nonreflecting boundary conditions for parabolic-type approximations in underwater acoustics. *Journal of Computational Acoustics*, 2(2):83–98, Jun 1994.

[24] M. J. Reiter, D. P. Synhorst, and D. E. Mann. Electrophysiological effects of acute ventricular dilatation in the isolated rabbit heart. *Circ Res*, 62(3):554–562, Mar 1988.

[25] M. J. Reiter, Z. Zetelaki, C. J. Kirchhof, L. Boersma, and M. A. Allessie. Interaction of acute ventricular dilatation and d-sotalol during sustained reentrant

ventricular tachycardia around a fixed obstacle. *Circulation*, 89(1):423–431, Jan 1994.

[26] J. J. Rice, R. L. Winslow, J. Dekanski, and E. McVeigh. Model studies of the role of mechano-sensitive currents in the generation of cardiac arrhythmias. *J Theor Biol*, 190(4):295–312, February 21 1998.

[27] T. L. Riemer, E. A. Sobie, and L. Tung. Stretch-induced changes in arrhythmogensis and excitability in experiementally based heart cell models. *Am J Physiol*, 275(Heart Circ. Physiol. 44):H431–H442, 1998.

[28] J. M. Rogers and A. D. McCulloch. A collocation-Galerkin finite element model of cardiac action potential propagation. *IEEE Trans Biomed Eng*, 41(8):743–757, Aug 1994.

[29] B. J. Roth. How the anisotropy of the intracellular and extracellular conductivities influences stimulation of cardiac muscle. *J Math Biol*, 30(6):633–646, 1992.

[30] L. F. Shampine. *Numerical Solution of Ordinary Differential Equations*. Chapman & Hall, New York, 1994.

[31] M. Zabel, B. S. Koller, F. Sachs, and M. R. Franz. Stretch-induced voltage changes in the isolated beating heart: Importance of the timing of stretch and implications for stretch-activated ion channels. *Cardiovasc Res*, 32(1):120–130, July 1996.

Chapter V

Mechanoelectric Feedback in Left Ventricular Myocardium

V.A Abstract

Mechanoelectric feedback has been described in isolated cells and intact ventricular myocardium, but the mechanical stimulus that governs mechanosensitive channel activity in intact tissue is unknown. To study the interaction of myocardial mechanics and electrophysiology in three dimensions, we used a finite element model of the rabbit ventricles to simulate electrical propagation through passively loaded myocardium. A stretch-dependent current was added in parallel to the ionic currents in the Beeler-Reuter ventricular action potential model. We investigated different mechanical coupling parameters to simulate stretch-dependent conductance modulated by either fiber strain, cross fiber strain, or a combination of the two. Electrical propagation was simulated using the collocation-Galerkin finite element method on a laboratory workstation. All three models of the stretch-dependent conductance resulted in reduced epicardial action potential amplitudes in response to increases in left ventricular cavity pressure, but only the conductance modulated by both fiber and cross fiber strain reproduced the epicardial and transmural changes in action potential amplitude similar to experimental observations in passively loaded rabbit

and working canine hearts. These results suggest that changes in action potential characteristics may be due not only to length changes along the long axis direction of the myofiber, but also to deformation in the plane normal to the long axis. This model provides a framework for investigating how cellular biophysics integrate into the function of the intact ventricles.

V.B Introduction

Little is known about how mechanical deformation affects the action potential characteristics in the intact ventricle. The three-dimensional anatomy of the ventricle and heterogeneity of regional strains are likely to affect the heterogeneity of electrical activation and repolarization. Under conditions of increased mechanical heterogeneity, mechanoelectric feedback may increase dispersion of repolarization or likelihood of unidirectional block and consequent risk of reentrant arrhythmia [49]. Previous efforts have investigated either passive inflation [35, 52, 51] or action potential changes [54, 16, 48, 15] in the left ventricle (LV), but the relationships between three-dimensional regional deformations and action potential morphology have not been explored.

Action potential characteristics are modified by left ventricular volume loading, and many investigators have hypothesized that mechanosensitive channels play the primary role in this process [54, 48, 16]. Though most investigations have assumed that changes in sarcomere or myofiber length is the governing mechanical stimulus, strain in the intact ventricle is nonuniform and deformation occurs in all dimensions [51, 35]. In the unloaded state, three-dimensional residual strains also exist and have been reported in the rat, rabbit, and canine left ventricle [34, 17, 8]. Regional left ventricular strains are altered under ischemic conditions or the presence of an infarct [50, 23, 18]. Thus, while fiber strain or changes in sarcomere length may be the primary modulator of mechanically induced changes in action potential morphology, the role of these other significant myocardial deformations has not been

examined.

In the isolated Langendorff-perfused rabbit heart, Franz et al. (1992) reported that resting potential increases at the epicardium and endocardium under sustained volume loading of the LV, while the action potential amplitude decreases. They also observed that the left ventricle can be mechanically paced by transient 50-millisecond volume pulses of approximately 700 microliters. In isolated buffer-perfused canine hearts, Hansen et al. (1991) measured the probability of eliciting a stretch-induced arrhythmia as a function of the magnitude of a 50-millisecond volume pulse; with a baseline volume of 20 milliliters the mean volume transient needed to cause a stretch-induced arrhythmia with at least 90% probability was 21.3 ± 8.5 milliliters. Zabel et al. (1996) showed the action potential amplitude decreased to $72.3 \pm 15\%$ of baseline when the left ventricle was stretched to 175% of the baseline volume. In another study they reported that dispersion of action potential duration increased with a sustained increase in LV volume [55]. In the anesthetized canine, Lekven et al. (1979) showed a transmurally nonuniform reduction in unipolar potential in response to increases in left ventricular diameter. Infusion of 0.5 to 2.5 liters of warm blood into the jugular vein resulted in an 11% increase in LV end-diastolic diameter and a corresponding 27% decrease in endocardial potential and a 15% decrease in epicardial potential.

One-dimensional models based on the change in sarcomere length or circumferential strain have been useful for describing the qualitative effects of mechanosensitive channels in the myocardium. Zabel et al. (1996) modeled cellular changes in action potential morphology observed in the rabbit heart using a stretch-dependent current model proposed by Sachs (1994), and found similarities between their model and observations of action potential changes at the epicardium of the isolated rabbit left ventricle. Riemer et al. (1998) examined the influence of the conductance and reverse potential of a mechanosensitive channel in two models of ventricular action potential. Using a model of the frog ventricular action potential, they found that action potential duration consistently shortens with reverse potentials of -20 and -50

mV; a guinea pig model also shows shorter duration action potentials with a -50 mV reverse potential, but the duration lengthens with a -20 mV reverse potential. Rice et al. (1998) simulated the effect of circumferential lengthening during end-systole in an ischemic region on the LV using magnetic resonance imaging with cardiac tagging. They found that the minimum stretch-dependent conductance needed to generate an action potential decreases as the number of abnormally stretched cells increases, suggesting that a very small number of cells could generate stretch-induced action potentials possibly resulting in a reentrant arrhythmia.

The objective of this study was to analyze the effect of regionally heterogeneous diastolic strains on action potential amplitude. We used a two-dimensional transmural plane from the model of the passively inflated rabbit ventricles as the computational domain. The corresponding strains were used as the mechanical stimuli. To investigate the possible effects of mechanical heterogeneity, two models of the a stretch-dependent conductance were used. The first model used a fixed, spatially uniform conductance to generate a stretch-dependent current of uniform magnitude over the two-dimensional plane. The second model used strains from the passive inflation model to generate a current modulated by the local strain in the deformed myocardium to investigate whether fiber strain or some other component of myocardial deformation is the primary mechanical stimulus. Transmembrane current from the latter model varied regionally due to local variations in strain.

V.C Methods

V.C.1 Anatomic Model

The finite element model of rabbit ventricular geometry and myofiber architecture was described in Chapter II. Briefly, bicubic Hermite surfaces were fitted to over 8,000 geometric coordinates measured from the epicardial and endocardial surfaces of a 9.0 gram New Zealand White rabbit heart. Over 14,000 fiber orientation measurements were collected from transmural serial sections of the same heart;

a mathematical description of the fiber angle orientation was formulated by fitting bilinear-cubic Hermite basis functions to the measured fiber angles. The resulting 36 element three-dimensional anatomic model of the ventricles has 552 degrees of freedom (DOF) and a root-mean-squared error (RMSE) of ± 0.55 mm. The fitted fiber angle functions have 182 DOF and a RMSE of ± 19 degrees.

The computational domain was based on the model used to analyze regional ventricular mechanics (Chapter III). Two finite elements from the anterolateral wall were isolated and refined in the circumferential, longitudinal, and transmural directions to generate a three-dimensional 729 node mesh (8 circumferential $\times$ 8 longitudinal $\times$ 8 transmural elements) with a spatial discretization of approximately 1 mm (Figure V.1). A two-dimensional transmural plane (8 longitudinal $\times$ 8 transmural elements, 81 nodes) was then extracted from the three-dimensional mesh to serve as the computational domain for the simulations described below. Cubic Hermite interpolation of the planar geometry used two Gauss points in either local finite element direction. Note that on the two-dimensional transmural plane the local finite element coordinate directions were defined such that the ξ_1 direction was oriented in the transmural direction (increasing from endocardium toward the epicardium) and the ξ_2 direction was oriented longitudinally (increasing from the apex toward the base).

V.C.2 Ionic and Stretch-Dependent Current Models

The Beeler-Reuter model of ventricular action potential was used to model ionic transmembrane currents [2]. Mechanoelectric feedback in the model was incorporated by defining an additional transmembrane current, in parallel with the others, to represent the current flowing through mechanosensitive channels. The magnitude of stretch-dependent conductance was governed by the reverse potential of the channel and a conductance modulated as a linear function of the material strain in the myocardium [37, 38]. The stretch-dependent current and conductance

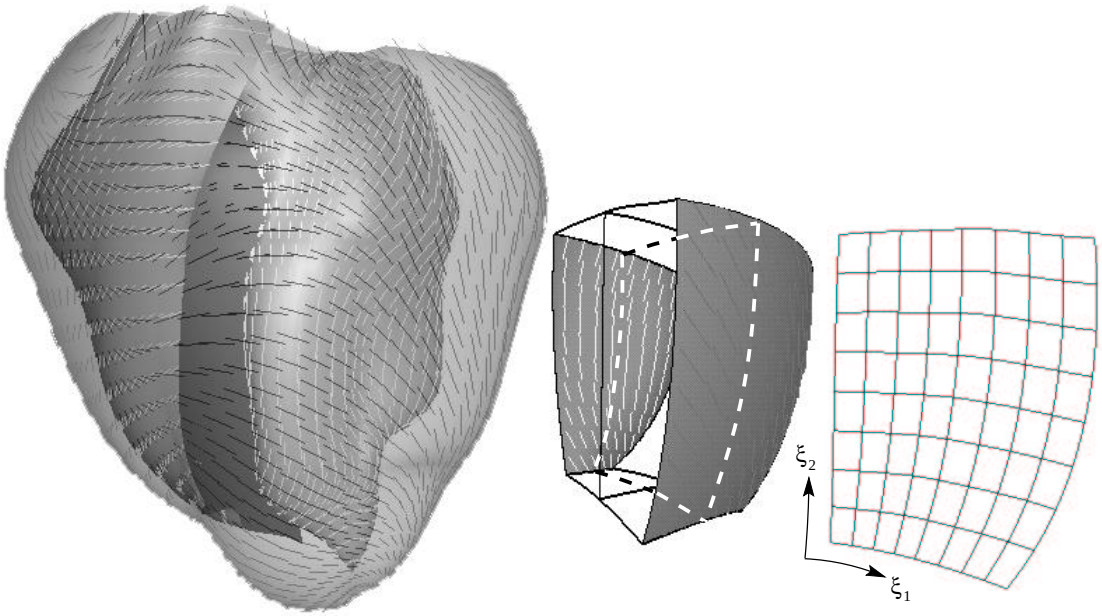

Figure V.1: Generation of the two-dimensional propagation domain from the three-dimensional anatomic model. Dashed line indicates boundaries of the two-dimensional plane within the three-dimensional mesh.

had the form:

$$I_{ms} = g_{ms}\,(V_m - V_r) \quad \text{(V.1)}$$

$$g_{ms} = G_{ms}\,(\alpha\,E + \beta) \quad \text{(V.2)}$$

where V_m is the transmembrane voltage (mV), I_{ms} is the stretch-dependent transmembrane current (μA/cm^2), G_{ms} is the saturation conductance of the mechanosensitive channel (μS/cm^2), E is the local value of either the fiber or cross fiber strain, and α is a dimensionless sensitivity parameter governing the magnitude of the mechanically modulated conductance. The scaling parameter β was constant throughout the tissue at any given mechanical state. We investigated the effects of a spatially uniform stretch-dependent conductance (i.e., $\alpha = 0$ and $\beta \neq 0$) and a stretch-dependent conductance that varied according to regional myocardial strain. For all the simulations conducted here we used a reverse potential (V_r) of -20 mV [9, 24].

Spatially Uniform Stretch-Dependent Conductance

We first characterized the electrophysiological response in terms of action potential amplitude to a spatially uniform stretch-dependent conductance, i.e., the change in action potential due to a constant stretch-dependent conductance in the two-dimensional plane. In this series of simulations the scaling parameter α was zero and the stretch-dependent conductance (g_{ms}) had a constant value of 5, 10, 20, 25, 27.5 or 30 μS/cm^2. No influence of the regional variations in any of the strain components was included. An additional simulation with no stretch-dependent current ($g_{ms} = 0$) served as a baseline for these simulations and the simulations described below.

Regionally Varying Stretch-Dependent Conductance

In addition to the above simulations we investigated the effect of realistic heterogeneous myocardial strains on action potential amplitude. We focused on

model	G_{ms}	E	α	β
$g_{ms}(E_{ff})$	200	E_{ff}	1.3995	0
$g_{ms}(E_{cc})$	200	E_{cc}	0.5045	0
$g_{ms}(E_{ff}, E_{cc})$	200	E_{cc}	0.1683	$\gamma\overline{E}_{ff}$

Table V.1: Different models of mechanosensitive conductance utilizing either fiber strain (E_{ff}), cross fiber strain (E_{cc}), or cross fiber and mean fiber strain ($\overline{E}_{ff}$) as the mechanical stimulus. The conductivity G_{ms} is in μS/cm^2, the strain E and sensitivity parameters α and γ are dimensionless, with $\gamma = 1.74265$ μS/cm^2. The values of the sensitivity parameters were chosen such that the maximum value of the stretch-dependent conductance g_{ms} was 30 μS/cm^2 at 15 mm Hg pressure.

three specific forms of the stretch-dependent conductance, modulated by either regional fiber strain, cross fiber strain, or a combination of the two. Table V.1 shows the different parameters used in each of the three models for g_{ms}, where E_{ff} is the fiber strain, E_{cc} is the cross fiber strain, and $\overline{E}_{ff}$ is the mean fiber strain (referred to the unloaded state) over the two-dimensional surface. The values of the sensitivity parameter α and scaling parameter γ were chosen such that at a left ventricular cavity pressure of 15 mm Hg the maximum value of g_{ms} was 30 μS/cm^2 over the two-dimensional surface. The fiber or cross fiber strains used as the mechanical stimulus for this conductance model were the resulting strains from the simulations of passive LV inflation (Chapter III). The strains on the two-dimensional plane are shown in Figure V.2; the minimum fiber strain at at 5 mm Hg LV pressure was 0.016. The minimum cross fiber strain at 5 mm Hg was 0.015. Note that the fiber strain was more homogeneous (varying from 0.036 to 0.097 at 15 mm Hg) than the cross fiber strain which showed a substantial positive transmural gradient from epicardium to endocardium (0.026 to 0.289 at 15 mm Hg).

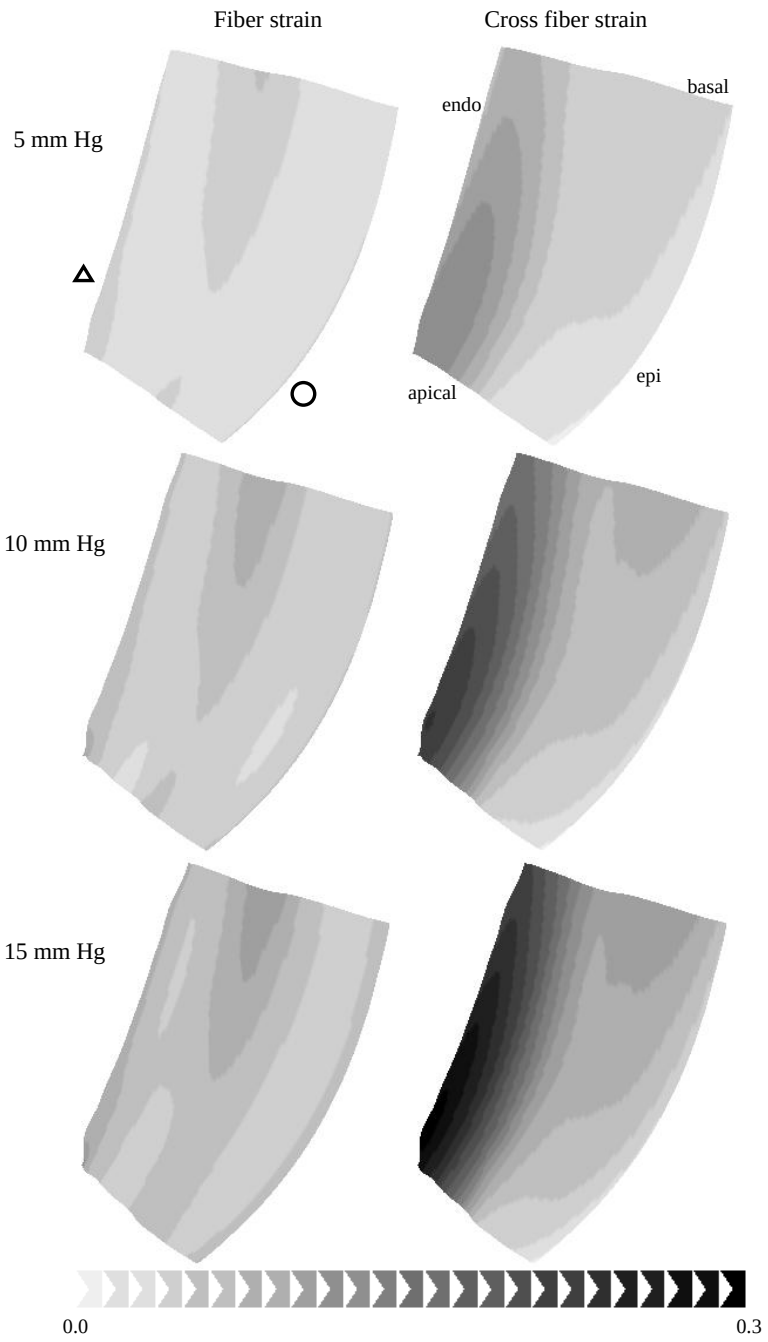

Figure V.2: Maps of fiber and cross fiber strain on the two-dimensional surface. The fiber strain was nearly uniform over the plane, but the cross fiber strain shows a positive transmural gradient from epicardium to endocardium. Symbols △ and ◯ identify endocardial and epicardial locations where action potential amplitude ratios were computed.

V.C.3 Two-Dimensional Propagation

The myocardium was approximated as a continuum in which propagation is governed by the two-dimensional cable equation (Appendix IV.G). For a transversely isotropic medium the conductivity tensor models the preferential conductivity of the electrical excitation in the longitudinal direction of the myofiber as compared with the transverse direction [41]. The coefficients of the conductivity tensor were estimated using a three-dimensional geometry (Chapter IV). The conductivity in the transmural plane was assumed to be constant and approximated with an isotropic conductivity tensor with values of the conductivity transverse to the long axis of the myofiber.

The collocation-Galerkin finite element method was used to solve the discretized cable equation with no-flux boundary conditions [41]. In all the simulations, the time and voltage dependent variables of the ionic current model were brought to their quiescent state by simulating the first 400 milliseconds with no applied stimulus. At 400 milliseconds the ventricular action potential was initiated with a 4 millisecond threshold stimulus applied to the nodes along the most basal edge of the two-dimensional transmural plane. All runs simulated 900 milliseconds. The time history of transmembrane voltage was recorded at 100 microsecond intervals for later analysis and visualization. The ordinary differential equations describing the state variables in the Beeler-Reuter model were integrated using an implicit Adams method with relative and absolute error tolerances of 10^{-4} [22]. The resting transmembrane potential was defined as the value 5 milliseconds before the stimulus was applied, and the action potential amplitude was defined as the difference between the maximal voltage during the plateau phase (the "dome" voltage) and the resting transmembrane potential, similar to experimental protocols using monophasic action potential electrode recordings [14]. Action potential duration at 90% repolarization (APD_{90}) was calculated as the time elapsed from the maximum rate of action potential upstroke to the point of 90% repolarization from the action potential

amplitude. Dispersion of action potential duration was calculated as the absolute value of difference in APD_{90} at the locations of maximum and minimum mechano-sensitive conductance on the plane. The ratio of the loaded (left ventricular pressure of 5, 10, or 15 mm Hg) to baseline (no stretch-dependent current) action potential amplitudes were computed at points on the endocardium and epicardium located approximately 4.25 mm from the stimulus region (identified by the symbols $\triangle$ and $\bigcirc$ in Figure V.2). All simulations were run on a SGI Octane workstation with a 225 MHz MIPS R10000 processor and 1664 Mb of main memory (Appendix V.G). Each simulation solved for 2,592 degrees of freedom and typically required 20 minutes to complete. The program and data required 28.3 Mb and 17.7 Mb of main memory, respectively.

V.D Results

V.D.1 Spatially Uniform Stretch-Dependent Conductance

The resting potential and action potential amplitude for the baseline and five spatially uniform stretch-dependent conductance simulations are shown in Table V.2. The baseline ($g_{ms} = 0$) resting transmembrane potential was -84.6 mV, the maximum amplitude was 16.3 mV at the peak of the upstroke and 15.5 during the plateau phase (Figure V.3); the action potential duration at 90% repolarization (APD_{90}) was 287.3 milliseconds. When the conductance ranged from 5 to 30 $\mu S/cm^2$ the maximum amplitude of both the upstroke and plateau decreased; with a conductance of 25 $\mu S/cm^2$ the upstroke and plateau amplitudes decreased to 65% and 69% of baseline, respectively. APD_{90} increased nonlinearly with the conductance. The action potential failed to propagate when the conductance was 30 $\mu S/cm^2$. The resting potential decreased linearly with increasing conductance:

$$V_{rest} = 0.467\, g_{ms} - 84.9\ ,\ r^2 = 0.9985 \qquad \text{(V.3)}$$

g_{ms}	0	5	10	20	25	27.5	30
V_{rest}	-84.6	-82.6	-80.4	-75.8	-73.3	-72.0	-70.6
amplitude	100.0	96.1	92.0	81.9	69.3	48.0	—
APD_{90}	287.3	288.3	289.7	293.7	300.0	—	—

Table V.2: Resting potential and action potential amplitude and duration for a spatially uniform stretch-dependent conductance. Conductance (g_{ms}) is in $\mu S/cm^2$, resting potential (V_{rest}) and amplitude in millivolts, action potential duration (APD_{90}) in milliseconds. Amplitude for the $g_{ms} = 27.5$ $\mu S/cm^2$ simulation was computed from the maximum potential of the upstroke.

During repolarization the action potentials generated from a non-zero stretch conductance crossed over the baseline action potential between 669 and 693 milliseconds (Figure V.3). Crossover time was inversely proportional to conductance: the earliest crossover occured with $g_{ms} = 25$ $\mu S/cm^2$, and the latest with $g_{ms} = 5$ $\mu S/cm^2$. The potential at which the crossover occurred ranged from -57 to -37 mV. The lowest conductance (5 $\mu S/cm^2$) had the most negative crossover potential (-57 mV), and the crossover potential became less negative with increasing conductances. The crossover potential was always more negative than the reverse potential of the mechanosensitive channel.

V.D.2 Regionally Varying Stretch-Dependent Conductance

Variations of the stretch-dependent conductance for the three g_{ms} models are listed in Table V.3. All three models showed an increase in mean conductance with increasing left ventricular pressure. In none of the simulations was propagation blocked. Recall that the maximum conductance at 15 mm Hg for the three models was fixed at 30 $\mu S/cm^2$ (Section V.C.2). For the range of pressures simulated, the lowest mean and minimum conductances were always produced by the $g_{ms}(E_{cc})$ model, and the largest produced by the $g_{ms}(E_{ff}, E_{cc})$ model.

Figures V.4 through V.6 show the locations of the maximum (□) and min-

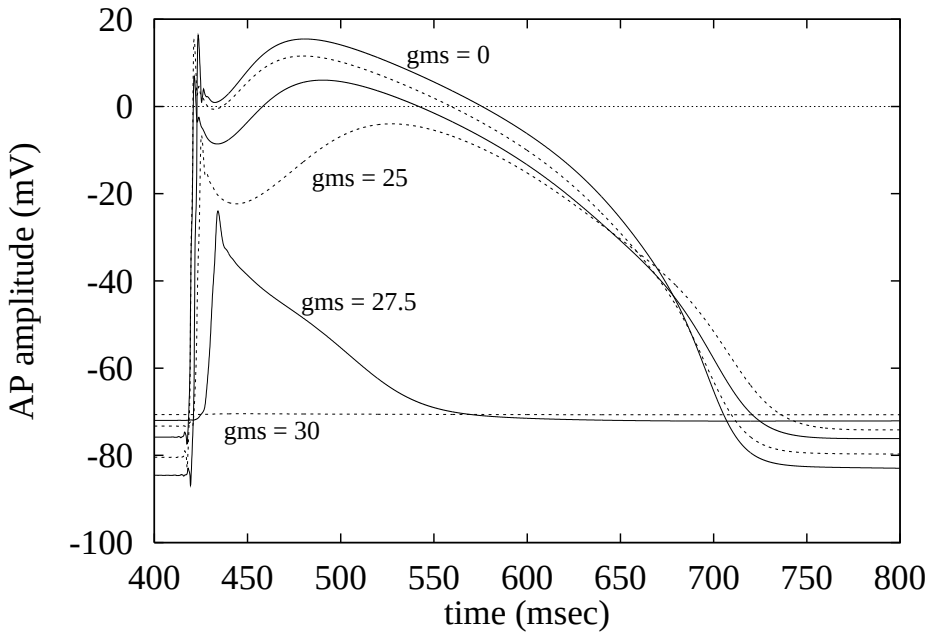

Figure V.3: Action potentials from the endocardial surface using a spatially uniform stretch current (i.e., $\alpha = 0$ in Equation V.2). For the traces shown the stretch-dependent conductance g_{ms} was 0, 10, 20, 25, 27.5, or 30 μS/cm^2. The trace for g_{ms} = 5 μS/cm^2 is not shown for clarity.

LV	$g_{ms}(E_{ff})$		
pressure	min	max	mean ± SD
5 mm Hg	3.66	13.96	7.12 ± 2.25
10 mm Hg	7.39	24.03	12.81 ± 3.42
15 mm Hg	9.63	30.00	16.46 ± 4.09

LV	$g_{ms}(E_{cc})$		
pressure	min	max	mean ± SD
5 mm Hg	0.84	12.86	5.98 ± 3.38
10 mm Hg	1.33	23.24	10.58 ± 6.09
15 mm Hg	1.52	30.00	13.59 ± 7.85

LV	$g_{ms}(E_{ff}, E_{cc})$		
pressure	min	max	mean ± SD
5 mm Hg	9.58	13.59	11.30 ± 1.13
10 mm Hg	16.19	23.50	19.28 ± 2.03
15 mm Hg	20.51	30.00	24.53 ± 2.62

Table V.3: Variations of stretch-dependent conductance (mean ± SD μS/cm^2) with LV pressure of the different stretch conductance models.

	$g_{ms}(E_{ff})$	$g_{ms}(E_{cc})$	$g_{ms}(E_{ff}, E_{cc})$
5 mm Hg	8.3	7.2	4.6
10 mm Hg	1.2	10.2	5.5
15 mm Hg	1.1	11.1	9.0

Table V.4: Dispersion of action potential duration at 90% repolarization (msec) at the locations of maximum (□) and minimum (◇) conductance over the range of left ventricular pressures for the three models of regionally-varying stretch-dependent conductance.

imum (◇) conductances. For the $g_{ms}(E_{ff})$ model (Figure V.4) the apical midwall location of the minimum conductance was unchanged over the range of LV pressures, but the location of the the maximum conductance moved from the basal midwall at 5 mm Hg to the apical subendocardium at higher pressures. Similarly, the apical subepicardial location of the minimum conductance for the $g_{ms}(E_{cc})$ and $g_{ms}(E_{ff}, E_{cc})$ models (Figures V.5 and V.6) did not change over the pressure range. In both models, though, the maximum conductance location shifted slightly in the transmural direction toward the endocardium at pressures above 5 mm Hg, but maintained the same longitudinal position.

Dispersion of APD_{90} was computed at the locations of the maximum (□) and minimum (◇) conductance (Table V.4). For the $g_{ms}(E_{ff})$ model dispersion of APD_{90} decreased with increasing pressure, ranging from 8.3 milliseconds at 5 mm Hg to 1.1 milliseconds at 15 mm Hg. Dispersion of APD_{90} for both the $g_{ms}(E_{cc})$ and $g_{ms}(E_{ff}, E_{cc})$ models increased from 5 to 15 mm Hg pressure, from 7.2 to 11.1 milliseconds with the $g_{ms}(E_{cc})$ model and from 4.6 to 9.0 milliseconds with the $g_{ms}(E_{ff}, E_{cc})$ model.

The mean action potential amplitude for the three models of regionally varying stretch-dependent conductance (Table V.5) was consistently less than baseline (100 mV) but higher than the spatially uniform model with $g_{ms} = 25$ μS/cm^2 (69.3 mV). Over the entire range of LV pressures the standard deviation of the action

	$g_{ms}(E_{ff})$	$g_{ms}(E_{cc})$	$g_{ms}(E_{ff}, E_{cc})$
5 mm Hg	94.7 ± 0.9	95.6 ± 2.4	91.2 ± 1.0
10 mm Hg	90.0 ± 1.5	91.7 ± 4.4	83.4 ± 2.0
15 mm Hg	86.6 ± 1.9	88.7 ± 5.9	73.0 ± 4.7

Table V.5: Action potential amplitude (mean ± SD mV) over the range of left ventricular pressures for the three models of regionally-varying stretch-dependent conductance. Note that all the amplitudes are less than 100 mV, the baseline amplitude with no stretch-dependent conductance (Table V.2, second column), but greater than 69.3 mV, the amplitude with a spatially uniform stretch-dependent conductance of 25 μS/cm^2 (Table V.2, sixth column).

potential amplitude was always lowest with the $g_{ms}(E_{ff})$ model and largest with the $g_{ms}(E_{cc})$ model. At the endocardium the $g_{ms}(E_{ff})$ model consistently produced a larger action potential amplitude than the $g_{ms}(E_{cc})$ model, which in turn was larger than that of the $g_{ms}(E_{ff}, E_{cc})$ model (Table V.6). In a pseudo-mathematical form the relationship between the action potential amplitude produced by the different models can be expressed as:

$$\text{at endocardium: } A\left[g_{ms}(E_{ff}, E_{cc})\right] < A\left[g_{ms}(E_{cc})\right] < A\left[g_{ms}(E_{ff})\right]$$

for the range of left ventricular pressures. At the epicardial site the $g_{ms}(E_{ff}, E_{cc})$ model still produced the lowest action potential amplitude, but the $g_{ms}(E_{cc})$ model produced the largest:

$$\text{at epicardium: } A\left[g_{ms}(E_{ff}, E_{cc})\right] < A\left[g_{ms}(E_{ff})\right] < A\left[g_{ms}(E_{cc})\right]$$

When the stretch-dependent conductance was modulated by the regional strains, the action potential amplitude also varied spatially (Figures V.4 through V.6). The action potential amplitudes and the endocardial and epicardial locations (labeled $\triangle$ and $\bigcirc$ in Figures V.4 through V.6) are shown in Table V.6. Spatial variation of the action potential amplitude from the $g_{ms}(E_{ff})$ and $g_{ms}(E_{cc})$ models

LV	$g_{ms}(E_{ff})$		
pressure	endo	epi	ratio
5 mm Hg	93.8	95.2	0.985
10 mm Hg	88.4	91.6	0.965
15 mm Hg	84.6	88.8	0.953

LV	$g_{ms}(E_{cc})$		
pressure	endo	epi	ratio
5 mm Hg	91.0	98.5	0.924
10 mm Hg	83.4	97.2	0.858
15 mm Hg	77.5	96.2	0.806

LV	$g_{ms}(E_{ff}, E_{cc})$		
pressure	endo	epi	ratio
5 mm Hg	89.4	92.0	0.972
10 mm Hg	79.5	85.2	0.933
15 mm Hg	65.3	76.6	0.852

Table V.6: Action potential amplitude (mV) at the endocardial ($\triangle$) and epicardial ($\bigcirc$) locations in Figures V.4 through V.6. The last column is the ratio of endocardial to epicardial action potential amplitude at the same left ventricular pressure.

closely followed that of the fiber or cross fiber strain, respectively, with smaller action potential amplitudes associated with higher strains and larger amplitudes associated with lower strains (Figures V.2 and V.4 - V.5). For the $g_{ms}(E_{ff})$ model the smallest action potential amplitude was located at the midwall, extending longitudinally from the basal boundary toward the apex; the largest amplitude was located at the subepicardium, also extending from the basal boundary toward the apex. Results from the $g_{ms}(E_{cc})$ model show a similar inverse relationship between action potential amplitude and cross fiber strain. The smallest amplitude, like the largest cross fiber strain, was consistently located near the apical boundary at the endocardium; the largest amplitude was at apical boundary at the epicardium. A positive gradient in action potential amplitude extended transmurally from the endocardium toward the epicardium. The action potential amplitudes from the $g_{ms}(E_{ff}, E_{cc})$ model showed characteristics similar to the amplitudes from both the $g_{ms}(E_{ff})$ and $g_{ms}(E_{cc})$ models. The largest amplitude was located at the epicardium, similar to the $g_{ms}(E_{ff})$ model, but the spatial variation was oriented more in the transmural direction than longitudinally. Like the $g_{ms}(E_{cc})$ model the smallest amplitude is near the apical boundary at the endocardium, and the gradient increases from endocardium to epicardium, though the gradient was most distinct at 15 mm Hg. At lower pressures the action potential amplitudes appear more transmurally uniform, with a difference of approximately 2 mV across the wall at 5 mm Hg.

V.E Discussion

We have conducted simulations of the effects of regional transmural fiber and cross fiber strain on the action potential amplitude in a realistically deformed model of the rabbit ventricles. The transmembrane voltage was simulated using the Beeler-Reuter model of ventricular action potential. To this we added a parallel transmembrane current with a stretch-dependent conductance. Two general models of the stretch-dependent conductance were investigated: the first was a spatially

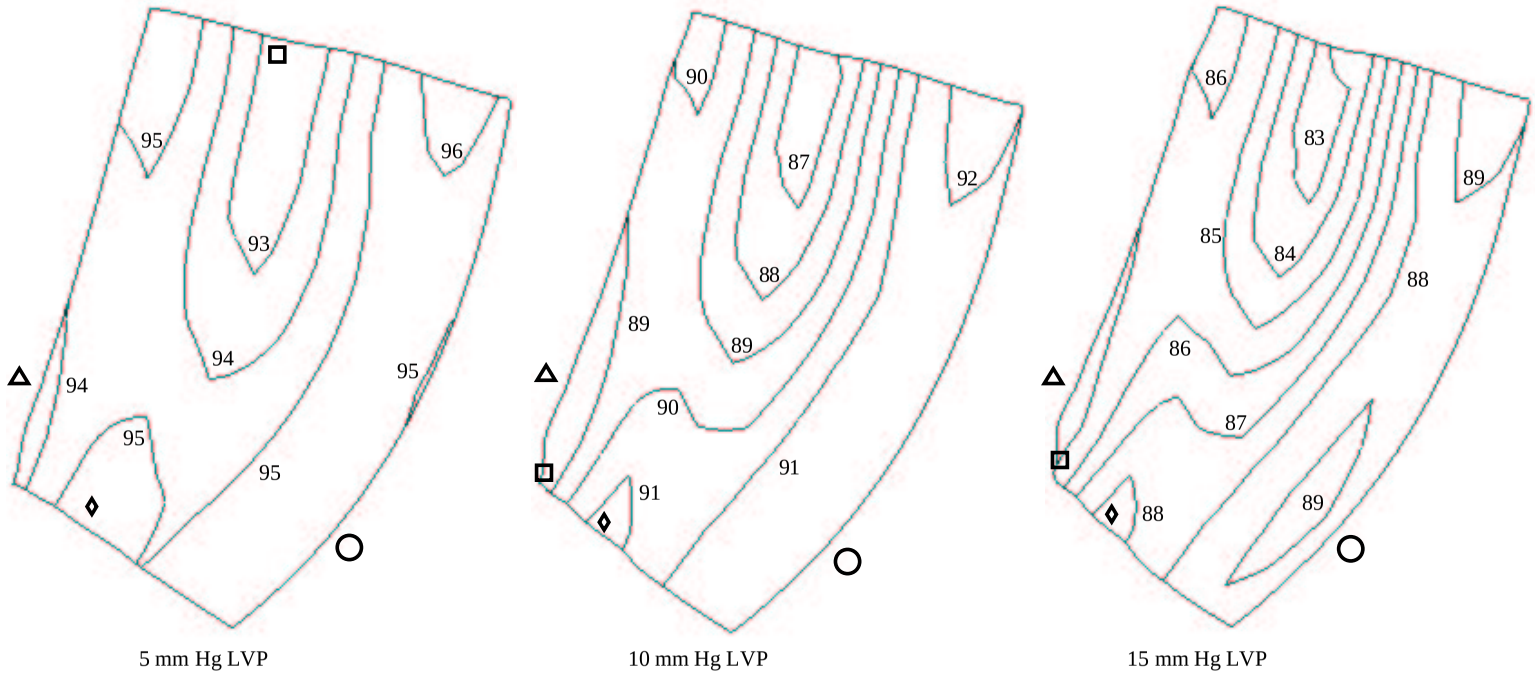

Figure V.4: Maps of action potential amplitude at 5, 10, and 15 mm Hg LV pressure. Mechanosensitive conductance model was $g_{ms}(E_f f)$. Contours are drawn at every 1 mV. Action potential amplitudes at the endocardium (△) and epicardium (◯) are listed in Table V.6. Maximum (□) and minimum (◇) conductances are listed in Table V.3.

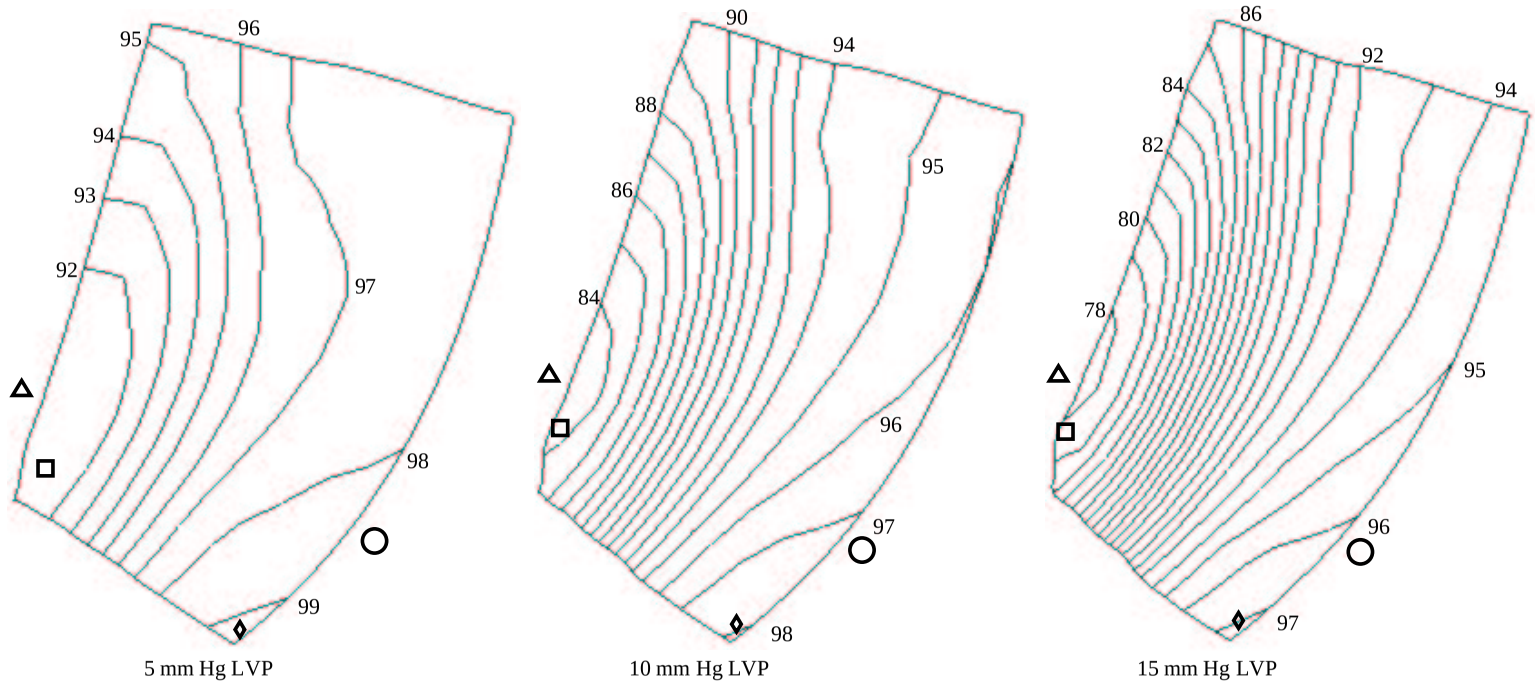

Figure V.5: Maps of action potential amplitude at 5, 10, and 15 mm Hg LV pressure. Mechanosensitive conductance model was $g_{ms}(E_c{}^c)$. Contours are drawn at every 1 mV. Action potential amplitudes at the endocardium (△) and epicardium (◯) are listed in Table V.6. Maximum (□) and minimum (◇) conductances are listed in Table V.3. Not all contours are labeled for clarity.

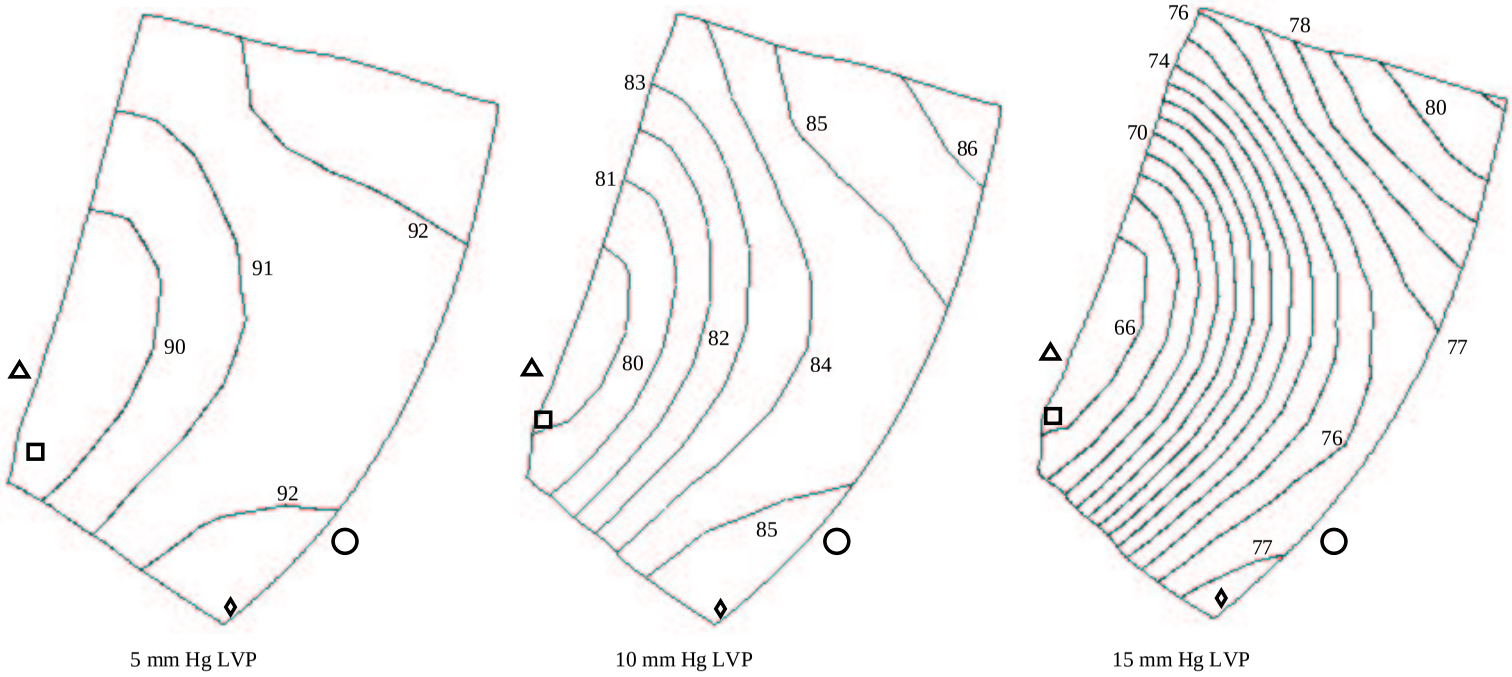

Figure V.6: Maps of action potential amplitude at 5, 10, and 15 mm Hg LV pressure. Mechanosensitive conductance model was $g_{ms}(E_f, E_{cc})$. Contours are drawn at every 1 mV. Action potential amplitudes at the endocardium (△) and epicardium (◯) are listed in Table V.6. Maximum (□) and minimum (◇) conductances are listed in Table V.3. Not all contours are labeled for clarity.

constant conductance, the second varied the conductance linearly with regionally heterogeneous myocardial strains.

V.E.1 Spatially Uniform Stretch-Dependent Conductance

The linear relationship between the constant stretch-dependent current and the rest potential (Equation V.3) is not surprising since the conductance model we used is ohmic with no time dependence. The time of intersection between the stretched potentials and baseline occurred earlier and the potential increased with increasing g_{ms} (Figure V.3). The increasing potential with g_{ms} is to be expected because, once the transmembrane potential drops below the reverse potential of the stretch current, a larger value of g_{ms} provides more inward current, slowing the rate of repolarization. That the intersection occurs earlier with increasing g_{ms} merely emphasizes the relative increase in repolarization rate. Similar to the findings reported by Zabel et al. (1996), the potential at which the action potential under stretch crosses the baseline action potential is lower than the reverse potential of the mechanosensitive channel. However, our results show the crossover potential becomes more positive with increasing stretch-dependent current, whereas no change in the crossover potential was reported by Zabel et al. (1996). This is likely due to the different models of action potential and mechanosensitive conductance we used, although we would expect the variation in crossover potential to correlate with variations in stretch-dependent current. The variation in action potential amplitude provided by the spatially uniform stretch-dependent conductance is qualitatively similar to those measured in the canine and rabbit hearts [15, 54], but this model does not provide the transmural gradient in potential changes observed by Lekven et al. (1979).

V.E.2 Regionally Varying Stretch-Dependent Conductance

With the regionally varying stretch-dependent conductance model we examined three types of mechanical stimulus that may govern the mechanosensitive

conductance. The model based on cross fiber strain (E_{cc}) stimulus always provided a lower minimum and mean conductance than the models based on either fiber strain (E_{ff}) or the cross fiber strain and mean fiber strain ($E_{cc}, \overline{E}_{ff}$) stimuli. This was not surprising since the cross fiber strain was always less than the fiber strain at the epicardium, and the cross fiber strain increases transmurally (Figure V.2). Conversely, the maximum conductance was always provided by the fiber strain stimulus for LV pressures of 5 and 10 mm Hg. This was unexpected since the fiber strain is less than the cross fiber strain at the endocardium for the range of left ventricular pressures we used (5 to 15 mm Hg). This may be due to the maximum 30 μS/cm^2 value of the conductance established for the three models at 15 mm Hg. If the maximum conductance were established differently (say, set to the minimum value where propagation failed) the maximum conductance would likely be given by the cross fiber strain stimulus instead of the fiber strain stimulus.

Using a Langendorff-perfused rabbit heart, Zabel et al. (1996) applied a sustained 75% increase in LV volume which reduced the epicardial action potential amplitude to 72.3 $\pm$ 15% of baseline. Lekven et al. (1979), using working canine hearts, increased LV end-diastolic diameter by 11% and measured reductions in the epicardial and endocardial unipolar potential to 85.3% and 72.2% of baseline, respectively. The stretch-dependent conductance model based on fiber strain, $g_{ms}(E_{ff})$, reduced the epicardial action potential amplitude to 88.8% of baseline; this is similar in magnitude to the reduction in epicardial potential reported by Lekven et al. (1979), but the model does not reproduce the transmural gradient, providing only a 84.6% reduction at the endocardium. The conductance model based on cross fiber strain, $g_{ms}(E_{cc})$, does reproduce the transmural gradient: epicardial and endocardial action potential amplitudes are reduced to 96.2% and 77.5% of baseline, respectively. This model does not, however, show sufficient reduction in the action potential amplitude at the epicardium. Thus either of the two stretch-dependent conductance models based on exclusively on fiber strain or cross fiber strain did not simultaneously reproduce the magnitude of reduction in the epicardial and endocar-

dial action potential amplitudes observed experimentally. Only the model based on both fiber and cross fiber strains resulted in a large reduction of the epicardial action potential amplitude with an even greater reduction of the endocardial potential. At the epicardium the $g_{ms}(E_{ff}, E_{cc})$ model produced an action potential with 76.6% of the baseline amplitude, and a corresponding endocardial amplitude that was 65.3% of baseline.

Zabel et al. (1996), using an isolated rabbit heart, reported that increasing left ventricular volume by 1 milliliter from a neutral volume increased the dispersion of APD_{70} from 27 to 38 milliseconds on the epicardium. The $g_{ms}(E_{ff})$ model showed a decrease in APD_{90} from 8.8 to 1.1 milliseconds. The models based on either cross fiber strain alone or both fiber strain and cross fiber strain showed an increase in APD_{90} with increasing LV pressure.

This result suggests that the stretch-dependent conductance is not a function of fiber or cross fiber strain alone, because fiber strain (and hence the conductance obtained from the the $g_{ms}(E_{ff})$ model) is relatively uniform across the wall and fails to provide a transmural gradient of conductance. Similarly, the $g_{ms}(E_{cc})$ model cannot reproduce the magnitude of epicardial action potential amplitude reduction since cross fiber strain is relatively small at the epicardium but increases almost monotonically to a maximum value at the subendocardium. Only the model incorporating tensile strains in both the fiber and cross direction reproduced the magnitude of action potential amplitude reduction at the corresponding transmural locations.

The $g_{ms}(E_{ff}, E_{cc})$ model relates cellular transmembrane stretch-dependent conductivities to the multidimensional deformation of myocardium. We used fiber and/or cross fiber strains as the mechanical stimulus because these are the primary non-negative deformations of intact myocardium under passive loading [35]. Radial strain was omitted from the models because it is compressive (negative) throughout the LV during passive loading, and stretch-inactivated channels have not been identified in cardiac cells [53]. Similarly, we omitted any influence of shear strain

because no experimental evidence suggests mechanosensitive channels respond to shear deformation. Time-dependent characteristics of mechanosensitive channels such as adaptation [20] and slow deactivation [24, 46] were also not incorporated into our stretch-dependent conductivity models.

A large body of experimental results do, however, suggest that the mechanical stimulus is much more complex than we have proposed here. It is unclear whether mechanosensitive channels are activated by tension in the sarcolemma or stresses in the cytoskeletal proteins (or a combination of these) [20, 43]. Mechanosensitive channel activity has been measured in absence of a cytoskeleton in membrane patches from *Escherichia coli* embedded in artificial bilayers [3, 11]. In contrast, results from a series of patch-clamp experiments by Ruknudin et al. (1991) suggest that mechanosensitive channels are in series with some component of the cytoskeleton, possibly spectrin or fondrin [43]. It has recently been suggested that mechanosensitive channels may not be located in the cell membrane, but in the intracellular organelles [45].

Other experiments suggest the conductivity of a mechanosensitive channel may be affected by curvature of the membrane [4, 31]. If a cardiac myocyte is assumed to be a circular cylinder that longitudinally lengthens and radially contracts as the ventricle is filled, the mechanosensitive channel activity would increase under passive loading based solely on the decrease in cross-sectional diameter. This scenario is further complicated by the data of Gerdes et al. (1994) which shows the cross section of human LV myocytes is not circular but elliptical, with the major diameter more than twice the minor diameter. They collected additional data from the rat LV showing that 77% of the epimyocardial cells were oriented such that the major diameter is within 45 degrees of the epicardial tangent plane. Thus, curvature-sensitive channels may demonstrate conductivity that changes not only with LV pressure but also with their location on the circumference of the cell. Hence, the models proposed here are extreme simplifications of the complex relationships between the deformation of intact myocardium, the biophysics of mechanosensitive channels, and

their combined effect on action potential morphology. Nevertheless, we have related regional changes in action potential amplitude to realistic heterogeneous strains of intact myocardium in a computationally tractable model.

Our choice of a maximum 30 μS/cm^2 for the stretch-dependent conductance did not block propagation of the action potential in any of the simulations performed. In all the simulations the area of maximum stretch-dependent conductance ($g_{ms} = 30$ μS/cm^2) was isolated to a small region (Figures V.4 through V.6). The surrounding regions were capable of propagation and hence provided sufficient source current through the spatial coupling of the conductivity tensor to exceed the excitation threshold in the small regions of high conductance.

All of the action potentials generated by the three models with regionally varying mechanical stimuli had amplitudes less than the baseline amplitude because the stretch-dependent current will tend to move the resting potential to a more depolarized quiescent state (i.e., V_{rest} will increase) and repolarize the cell during the plateau phase, decreasing the dome potential. The magnitude of these effects, however, will vary with the reverse potential of the mechanosensitive channel: a more negative reverse potential results in a smaller quiescent stretch-dependent current and a smaller increase in resting potential, but a larger decrease in the dome potential [38].

V.E.3 Limitations

Our results must be viewed in light of the limitations of the models. Action potential morphology is known to vary between epicardial, M, and endocardial cells [32, 28]. We did not model this transmural variation though other investigators have done so successfully [6]. Fedida and Giles (1991) have measured electrophysiological characteristics in rabbit ventricular cells and found the rest potential to be -80 mV; we used -84.5 mV, the value in the Beeler-Reuter model [2]. The Beeler-Reuter model is also not specific to the rabbit but is instead derived from the analysis of mammalian ventricular cells from several species. More detailed

ventricular action potential models exist; the most popular models improve upon the Beeler-Reuter representation of the sodium and potassium currents and include the effects of ion pumps, exchangers, and intracellular calcium transport [30, 29]. These mechanisms, though important for an essential description of cellular electrophysiology and analyses involving specific ionic currents, may not be fundamental to the regional analysis of mechanoelectrical coupling we have conducted here. We have assumed that mechanoelectric feedback in intact myocardium is governed by the activity of mechanosensitive channels, although it is not known whether these channels or alterations in intracellular calcium cycling, or the two combined, are the primary feedback mechanisms governing the electrical response to stretch [5]. It has been observed, however, that free cytosolic calcium is relatively low during diastole, thus the effect of stretch on the diastolic ventricle is likely dominated by mechanosensitive channel activity [49].

It has been shown that accurately modeling the spatial variation of cellular electrophysiological events requires a resolution on the order of 50 μm using a finite difference method [25]. A less refined discretization can result in significant errors in the fidelity of the action potential model [1]. Our model, with a spatial resolution on the order of 760 micrometers (the distance between two collocation points within a finite element), does demonstrate some of these errors. The effect of the suboptimal spatial resolution is evident in the baseline action potential Figure V.3: the maximum upstroke potential is only 16.3 mV compared with with 28 mV of the original model [2]. The action potential duration at 90% repolarization is slightly longer than that in the original model (287.3 versus 285 milliseconds). The oscillations occurring immediately before and after the upstroke (Figure V.3) are likely caused by the cubic Hermite interpolation functions required by the collocation-Galerkin finite element method [41, 1]. Rogers et al. (1997) showed that a high-order finite element method converged comparably to a finite difference method at substantially higher spatial discretization for the FitzHugh-Nagumo (FHN) equations [13, 33], suggesting that our 760 μm resolution may be equivalent to a more resolved finite

difference grid, but this analysis has not yet been conducted using an ionic model. Regardless, the errors described above are localized to a time interval that did not contribute to the results presented here, therefore we believe their presence is of little consequence to our analysis.

The myocardium is a transversely isotropic conducting medium for the action potential, with the greatest conductivity occurring in the direction of long axis of the myofibers [26, 7]. Here we have modeled the conductivity across the wall as isotropic, though this is only correct near the midwall region where the fibers are oriented in the circumferential direction, perpendicular to the transmural plane. At the epicardium and endocardium the conductivity is greater than what we have assumed because the fibers are more longitudinally oriented in these regions. For the simulations we have performed the smaller conductivity has the effect of reducing the stimulus current provided by the spatial coupling of the conductivity tensor, which could potentially lead to a subthreshold stimulus and failed propagation. With the spatially uniform stretch-dependent conductance model, propagation was blocked when g_{ms}= 30 μS/cm^2 (Figure V.3). We did not observe failed propagation when using the regionally-varying stretch-dependent conductance model, and the action potential with the lowest amplitude (approximately 66 mV at 15 mm Hg, Figure V.6) had a morphology similar to the g_{ms} = 25 μS/cm^2 action potential (Figure V.3), suggesting all the propagated action potentials using this conductance model had adequate stimulus current. The isotropic conductivity tensor does not, however, allow for transmural variations in propagation velocity due to the transmural rotation of the fiber rotation, hence we did not investigate this aspect of the model.

The unloaded reference state for the model contained no residual stress, though residual stress is known to exist in the unloaded heart [8, 17, 34] and affect resting sarcomere length [39]. The data of Costa et al. (1997) shows that residual strain is primarily tensile at the epicardium and compressive at the endocardium. Transformation of their data yields fiber strain of 0.038 at the epicardium, decreasing

to zero at approximately 40% wall depth; cross fiber strain is 0.052 at the epicardium, decreasing to zero at 20% depth. While it is not known if residual strain gives rise to stretch-dependent currents in the intact myocardium, present models of stretch-dependent conductance (including those proposed here) predict that the residual strain should increase the transmembrane rest potential of epicardial cells in the intact unloaded ventricle. The same cells should exhibit a reduced rest potential in the stress-free state. Though this hypothesis may be straightforward to verify experimentally, including residual strain in simulations like those presented here is difficult because the deformation is not additive.

V.F Conclusions

We have conducted simulations of the effects of realistic myocardial strains on the action potential amplitude using different models of the mechanosensitive conductance. Conductance models based on fiber strain or cross fiber strain alone provided results similar to those observed experimentally, but failed to yield either the transmural gradient in action potential amplitude reduction or sufficient magnitude of the reduction at the epicardium. Only a model based on both fiber and cross fiber strains simulated both effects. The results suggest that the activity of mechanosensitive channels in the intact myocardium may be more complex than previously thought, with the channels responding to deformation other than lengthening along the long axis of the myocyte.

V.G Appendix: Computational Hardware and Software

Platform	SGI Octane
address	`lawson.ucsd.edu`
OS	IRIX64 6.5
Processor	225 MHz IP30
FPU	MIPS R10010 rev. 0.0
CPU	MIPS R10000 rev. 3.4
main memory	1664 Mb
data cache	32 Kb
instruction cache	32 Kb
secondary cache	1 Mb

Libraries: Y12 matrix subroutines [36]

UMFPACK 2.2 matrix subroutines [10]

RKSUITE 1.0 ODE integrator [47]

ODEPACK collection of ODE integrators [22]

Compilers and options:

`f77`: Fortran 77, 7.2.1

```
FFLAGS = -O2 -col120 -static -r8 -DRENDER_MESH -DCOLLOCATION -DGENSOL_ALLOC
```

`cc`: C, 7.2.1

```
CFLAGS = -O2 -DDOUBLE_REAL -lm -DRENDER_MESH -DCOLLOCATION
                                        -DGENSOL_ALLOC -I../include -I.
```

References

[1] J. Beaumont, N. Davidenko, J. Davidenko, and J. Jalife. Self-sustaining spiral wave activity in a two-dimensional ionic model of cardiac ventricular muscle. In *Computer Simulations in Biomedicine*, pages 75–85. Computational Mechanics Publications, Boston, 1995.

[2] G. W. Beeler and H. Reuter. Reconstruction of the action potential of ventricular myocardial fibres. *J Physiol*, 268(1):177–210, Jun 1977.

[3] C. Berrier, A. Coulombe, C. Houssin, and A. Ghazi. A patch-clamp study of ion channels of inner and outer membranes and of contact zones of *E. coli*, fused into giant liposomes: Pressure-activated channels are localized in the inner membrane. *FEBS Lett*, 259(1):27–32, 18 December 1989.

[4] C. L. Bowman and J. W. Lohr. Curvature-sensitive mechanosensitive ion channels and osmotically-evoked movements of the patch membrane (abstract). *Biophys J*, 70(2):A365, Feb 1996. Abstract Supplement for the Biophysical Society 40rd Annual Meeting, February 17–21, 1996, Baltimore, Maryland.

[5] S. C. Calaghan and E. White. The role of calcium in the response of cardiac muscle to stretch. *Prog Biophys Mol Biol*, 71:59–90, 1999.

[6] A. W. Cates and A. E. Pollard. A model study of intramural dispersion of action potential duration in the canine pulmonary conus. *Ann Biomed Eng*, 26(4):567–576, July-August 1998.

[7] L. Clerc. Directional differences of impulse spread in trabecular muscle from mammalian heart. *J Physiol*, 255(1):335–346, Feb 1975.

[8] K. D. Costa, K. May-Newman, D. Farr, W. G. O'Dell, A. D. McCulloch, and J. H. Omens. Three-dimensional residual strain in midanterior canine left ventricle. *Am J Physiol*, 273(Heart Circ. Physiol. 42):H1968–H1976, 1997.

[9] W. Craelius. Stretch-activation of rat cardiac myocytes. *Exp Physiol*, 78(3):411–423, May 1993.

[10] T. A. Davis and I. S. Duff. An unsymmetric-pattern multifrontal method for sparse LU factorization. *SIAM J Matrix Anal Appl*, 18(1):140–158, Jan 1997.

[11] A. H. Delcour, B. Martinac, J. Adler, and C. Kung. Voltage-sensitive ion channel of *Escherichia coli*. *J Membr Biol*, 112(3):267–275, Dec 1989.

[12] D. Fedida and W. R. Giles. Regional variations in action potentials and transient outward current in myocytes isolated from rabbit left ventricle. *J Physiol*, 442:191–209, Oct 1991.

[13] R. FitzHugh. Impulses and physiological states in theoretical models of nerve membrane. *Biophys J*, 1:445–466, Jul 1961.

[14] M. R. Franz. Current status of monophasic action potential recording: theories, measurements and interpretations. *Cardiovasc Res*, 41:25–40, 1999.

[15] M. R. Franz, D. Burkhoff, D. T. Yue, and K. Sagawa. Mechanically induced action potential changes and arrhythmia in isolated and in situ canine hearts. *Cardiovasc Res*, 23(3):213–223, Mar 1989.

[16] M. R. Franz, R. Cima, D. Wang, D. Profitt, and R. Kurz. Electrophysiological effects of myocardial stretch and mechanical determinants of stretch-activated arrhythmias. *Circulation*, 86(3):968–978, Sep 1992. Published erratum appears in Circulation 1992 Nov, 86(5):1663.

[17] Y.-C. Fung. *Biodynamics: Circulation*. Springer-Verlag, New York, 1984.

[18] A. M. Gallagher, J. H. Omens, L. L. Chu, and J. W. Covell. Alterations in collagen fibrillar structure and mechanical properties of the healing scar following myocardial infarction. *Cardiovasc Pathobiol*, 2(1):25–36, 1997.

[19] A. M. Gerdes, S. E. Kellerman, K. B. Malec, and D. D. Schocken. Transverse shape characteristics of cardiac myocytes from rats and humans. *Cardioscience*, 5(1):31–36, Mar 1994. Published erratum appears in Cardioscience 1994 Jun;5(2): preceding 63.

[20] O. P. Hamill and D. W. McBride, Jr. Rapid adaptation of single mechanosensitive channels in *Xenopus* oocytes. *Proc Natl Acad Sci USA*, 89(16):7462–7466, 15 August 1992.

[21] D. E. Hansen, M. Borganelli, G. P. Stacy, Jr., and L. K. Taylor. Dose-dependent inhibition of stretch-induced arrhythmias by gadolinium in isolated canine ventricles. Evidence for a unique mode of antiarrhythmic action. *Circ Res*, 69(3):820–831, Sep 1991.

[22] A. C. Hindmarsh. ODEPACK, a systematized collection of ODE solvers. In R. S. Stepleman, editor, *Scientific Computing: Applications of Mathematics and Computing to the Physical Sciences*, volume 1 of *IMACS Transactions on Scientific Computation*, pages 55–64. North-Holland, New York, 1983. Based on papers presented at the Tenth IMACS World Congress on System Simulation and Scientific Computation, held in Montreal, Canada, August 8-13, 1982.

[23] J. W. Holmes, J. A. Nuñez, and J. W. Covell. Functional implications of myocardial scar structure. *Am J Physiol*, 272(Heart Circ. Physiol. 41):H2123–H2130, May 1997.

[24] H. Hu and F. Sachs. Mechanically activated currents in chick heart cells. *J Membr Biol*, 154(3):205–216, Dec 1996.

[25] R. W. Joyner. Effects of the discrete pattern of electrical coupling on propagation through an electrical syncytium. *Circ Res*, 50(2):192–200, Feb 1982.

[26] S. B. Knisley and B. C. Hill. Effects of bipolar point and line stimulation in anisotropic rabbit epicardium: Assessment of the critical radius of curvature for longitudinal block. *IEEE Trans Biomed Eng*, 42(10):957–966, Oct 1995.

[27] J. Lekven, K. Chatterjee, J. V. Tyberg, and W. W. Parmley. Reduction in ventricular endocardial and epicardial potentials during acute increments in left ventricular dimensions. *American Heart Journal*, 98(2):200–206, Aug 1979.

[28] D. W. Liu and C. Antzelevitch. Characteristics of the delayed rectifier current (I_{Kr} and I_{Ks}) in canine ventricular epicardial, midmyocardial, and endocardial myocytes: A weaker I_{Ks} contributes to the longer action potential of the M cell. *Circ Res*, 76(3):351–365, Mar 1995.

[29] C.-H. Luo and Y. Rudy. A model of the ventricular cardiac action potential: Depolarization, repolarization, and their interaction. *Circ Res*, 68(6):1501–1526, Jun 1991.

[30] C.-H. Luo and Y. Rudy. A dynamic model of the cardiac ventricular action potential. I. Simulations of ionic currents and concentration changes. *Circ Res*, 74(6):1071–1096, Jun 1994.

[31] B. Martinac, J. Adler, and C. Kung. Mechanosensitive ion channels of *E. coli* activated by amphipaths. *Nature*, 348(6298):261–263, 15 November 1990.

[32] M. Näbauer, D. J. Beuckelmann, P. Überfuhr, and G. Steinbeck. Regional differences in current density and rate-dependent properties of the transient outward current in subepicardial and subendocardial myocytes of human left ventricle. *Circulation*, 93(1):168–177, 1 January 1996.

[33] J. Nagumo, S. Arimoto, and S. Yoshizawa. An active pulse transmission simulating nerve axon. *Proc IRE*, pages 2061–2070, Oct 1962.

[34] J. H. Omens and Y. C. Fung. Residual strain in rat left ventricle. *Circ Res*, 66(1):37–45, Jan 1990.

[35] J. H. Omens, K. D. May, and A. D. McCulloch. Transmural distribution of three-dimensional strain in the isolated arrested canine left ventricle. *Am J Physiol*, 261(Heart Circ. Physiol. 30):H918–H928, Sep 1991.

[36] O. Østerby and Z. Zlatev. *Direct Methods for Sparse Matrices*, volume 157 of *Lecture Notes in Computer Science*. Springer-Verlag, New York, 1983.

[37] J. J. Rice, R. L. Winslow, J. Dekanski, and E. McVeigh. Model studies of the role of mechano-sensitive currents in the generation of cardiac arrhythmias. *J Theor Biol*, 190(4):295–312, February 21 1998.

[38] T. L. Riemer, E. A. Sobie, and L. Tung. Stretch-induced changes in arrhythmogensis and excitability in experiementally based heart cell models. *Am J Physiol*, 275(Heart Circ. Physiol. 44):H431–H442, 1998.

[39] E. K. Rodriguez, J. H. Omens, L. K. Waldman, and A. D. McCulloch. Effect of residual stress on transmural sarcomere length distributions in rat left ventricle. *Am J Physiol*, 264(Heart Circ. Physiol. 33):H1048–H1056, Apr 1993.

[40] J. M. Rogers, M. S. Courtemenche, and A. D. McCulloch. Finite element methods for modelling impulse propagation in the heart. In A. V. Panfilov and A. V. Holden, editors, *Computational Biology of the Heart*, chapter 7, pages 217–234. J. Wiley & Sons Ltd., West Sussex, England, 1997.

[41] J. M. Rogers and A. D. McCulloch. A collocation-Galerkin finite element model of cardiac action potential propagation. *IEEE Trans Biomed Eng*, 41(8):743–757, Aug 1994.

[42] A. Ruknudin, M. J. Song, and F. Sachs. The ultrastructure of patch-clamped membranes: A study using high voltage electron microscopy. *J Cell Biology*, 112(1):125–134, Jan 1991.

[43] F. Sachs. Stretch-sensitive ion channels: An update. In D. P. Corey and S. D. Roper, editors, *Sensory Transduction*, volume 47 of *Society of General Physiologists Series*, chapter 15, pages 241–260. Rockefeller University Press, New York, 1992. Society of General Physiologists, 45th annual symposium, Marine Biological Laboratory, Woods Hole, Massachusetts, 5–8 September 1991.

[44] F. Sachs. Modeling mechanical-electrical transduction in the heart. In V. C. Mow, F. Guilak, R. M. Hochmuth, and R. Tran-Son-Tay, editors, *Cell Mechanics and Cellular Engineering*, chapter 18, pages 308–328. Springer-Verlag, New York, 1994.

[45] F. Sachs. Mechanosensitive channels: Lost in space (abstract). *Biophys J*, 76(1):A3, Jan 1998. Abstract Supplement for the Biophysical Society 43rd Annual Meeting, February 13–17, 1999, Baltimore, Maryland.

[46] N. Sasaki, T. Mitsuiye, and A. Noma. Effects of mechanical stretch on membrane currents of single ventricular myocytes of guinea-pig heart. *Japanese Journal of Physiology*, 42(6):957–970, 1992.

[47] L. F. Shampine. *Numerical Solution of Ordinary Differential Equations*. Chapman & Hall, New York, 1994.

[48] G. P. Stacy, Jr., R. L. Jobe, L. K. Taylor, and D. E. Hansen. Stretch-induced depolarizations as a trigger of arrhythmias in isolated canine left ventricles. *Am J Physiol*, 263(Heart Circ. Physiol. 32):H613–H621, Aug 1992.

[49] P. Taggart and P. M. I. Sutton. Cardiac mechano-electric feedback in man: clinical relevance. *Prog Biophys Mol Biol*, 71:139–154, 1999.

[50] S. L. Van Leuven, L. K. Waldman, A. D. McCulloch, and J. W. Covell. Gradients of epicardial strain across the perfusion boundary during acute myocardial ischemia. *Am J Physiol*, 267(Heart Circ. Physiol. 36):H2348–H2362, Dec 1994.

[51] L. K. Waldman, Y. C. Fung, and J. W. Covell. Transmural myocardial deformation in the canine left ventricle: Normal in vivo three-dimensional finite strains. *Circ Res*, 57(1):152–163, Jul 1985.

[52] L. K. Waldman, D. Nosan, F. Villarreal, and J. W. Covell. Relation between transmural deformation and local myofiber direction in canine left ventricle. *Circ Res*, 63(3):550–62, Sep 1988.

[53] X. C. Yang and F. Sachs. Mechanically sensitive, nonselective cation channels. *Exs*, 66:79–92, 1993.

[54] M. Zabel, B. S. Koller, F. Sachs, and M. R. Franz. Stretch-induced voltage changes in the isolated beating heart: Importance of the timing of stretch and implications for stretch-activated ion channels. *Cardiovasc Res*, 32(1):120–130, July 1996.

[55] M. Zabel, S. Portnoy, and M. R. Franz. Effect of sustained load on dispersion of ventricular repolarization and conduction time in the isolated intact rabbit heart. *J Cardiovasc Electrophysiol*, 7(1):9–16, Jan 1996.

Chapter VI

Conclusions

The heart is complex three-dimensional structure with regional variations in wall thickness, curvature, and fiber orientation. The function of the heart depends on cellular processes that govern electrical propagation and mechanical deformation. The electrical and mechanical systems interact through excitation-contraction coupling and mechanoelectric feedback. We investigated how the mechanical state of the intact myocardium might affect action potential morphology of integrating models of passive ventricular mechanics, electrical propagation, cellular action potential.

Our hypothesis was that nonuniform alterations in action potential amplitude are due in part to the mechanosensitive channel response to deformation other than changes in sarcomere or myofiber length. Thus our first objective was to characterize three-dimensional diastolic strain distributions in passively loaded rabbit ventricle. We concluded that three-dimensional strains in the rabbit are qualitatively similar to those observed in the canine and porcine left ventricle, but rabbit myocardium is likely more stiff than the canine and rat. The second objective was to determine if changes in fiber length alone could account for experimentally observed nonuniform alternations in action potential amplitude in response to stretch. We concluded that changes in action potential amplitude are likely due not only to length changes along the long axis direction of the myofiber, but also to deformation in the plane normal to the long axis.

We first developed a model of the rabbit ventricles and fiber architecture. We chose the rabbit because it is a popular model model of two-dimensional mechanics, mechanoenergetics, and electrical propagation [10, 19, 36, 11, 12, 15]. New methods of acquiring geometric coordinates and fiber orientation were developed, and the resulting three-dimensional high-order finite element model of the ventricles represents over 8,000 geometric coordinates and 14,000 local fiber orientations using only 736 model variables with an accuracy of ± 0.55 mm in the geometric surfaces and ± 19 degrees in the fiber angles. Though the model lacks papillaries, atria, and laminar sheets, it captures regional variations in wall thickness, curvature, and nonuniform fiber orientations that influence distributions of stress and strain in the heart. The fiber distributions in the rabbit model are in close agreement with the the fitted distributions in a finite element model of the canine ventricles [22]. The epicardial and endocardial angles are similar in the lateral, septal, and posterior equatorial regions. Since its development, the model has been provided to investigators at other research universities.

We used the model to compute regional distributions of stress in the left ventricle validated by the two-dimensional epicardial strains measured by Gallagher et al. (1997). We estimated material parameters in a newly proposed form of the constitutive law [24], which resulted in epicardial fiber and cross fiber strains well within the accuracy of the experimental measurements. Fiber strain was consistently larger than cross fiber strain at the anterolateral region on the epicardium. The left ventricular pressure-volume curve was within 10% of the measured values [10]. Transmural distributions of strain in the left ventricle showed characteristics to those measured in the dog: fiber strain was relatively uniform across the wall, whereas cross fiber increased from epicardium to endocardium [25]. Transmural shear strains, however, were not similar to those measured in the passively inflated canine left ventricle [25], a shortcoming previously described by Costa (1996), who suggested a fully orthotropic material description may improve this result. Cauchy stresses in the left ventricle and apex were higher in the fiber direction than in the cross

fiber direction, but otherwise varied regionally without the transmural uniformity of fiber strain or positive gradient of cross fiber strain. Regional curvature of the wall, however, appeared to play a dominant role in the magnitude of stress, particularly at the subendocardium where the negative curvatures caused large gradients in the magnitudes of fiber and cross fiber stress. An analytical model of ventricular stress based on a simplified geometry showed little correlation with the mean longitudinal component of stress, but the mean circumferential stress predicted by the analytical model approximated that of the finite element model with an error of 25%.

Transmural diastolic strains in the rabbit ventricles may possibly be obtained through magnetic resonance imaging with cardiac tagging [32, 2]. Combined with confocal microscopy techniques for measuring the laminar sheet structure [39], transmural deformations would serve as another benchmark by which we could validate and improve the mechanical behavior of the model by using an orthotropic material description.

Custom finite element analysis software was ported to a scalable parallel processing computer, and performance was found to scale well with the number of processors. Previous simulations requiring 60 minutes were completed in just over five minutes [7]. The restarted GMRES iterative method was effective when used with diagonal preconditioning, and we believe that performance could be dramatically improved with a more sophisticated preconditioner.

For the first time, realistic multidimensional strains were related to regional variations in action potential amplitude. Previous mechanoelectric feedback models incorporating a stretch-dependent conductance have focused on changes in sarcomere length as the governing stimulus [16, 23, 40, 31] or have simply altered the stretch-dependent conductance without relating the changes to a physical deformation [26, 27]. We investigated three models of stretch-dependent conductance and found that only a model based on both fiber and cross fiber strain reproduced the magnitude of action potential amplitude reduction at the epicardium and the corresponding transmural gradient observed experimentally [40, 18]. A stretch-dependent

conductance model based on fiber strain alone produced a relatively uniform reduction in action potential amplitude across the wall, and thus failed to provide a larger reduction at the endocardium. Conversely, a stretch-dependent conductance modulated by only cross fiber strain provided the transmural gradient, but could not sufficiently reduce the action potential amplitude at the epicardium. In addition, dispersion of the action potential duration at 90% repolarization decreased with the stretch-dependent conductance model based on fiber strain; the stretch-dependent conductance models based on either cross fiber strain alone or both fiber strain and cross fiber strain showed increases in the dispersion of the action potential duration of 54% and 96%, respectively. These result suggests that alterations in action potential amplitude due to myocardial stretch are likely the response to the multidimensional deformation of intact myocardium.

This outcome does not conflict with patch-clamp studies of mechanosensitive channels which deform the sarcolemma in all three dimensions [29, 28, 3, 9, 8, 1]. Sachs (1991) has developed a model of the open probability of a mechanosensitive channel based on the area strain and tension of the cell membrane and the elasticity of the channel in the open and closed states. It is difficult, however, to directly relate a continuum measure of deformation such as fiber or cross fiber strain to deformation experienced by the sarcolemma. Nevertheless, we predict that under passive loading a stretch-induced depolarization should arise from the subendocardium where the myocardium undergoes the largest deformation [25]. A stretch-induced depolarization initiated at the endocardium would likely arrive at the epicardium after some finite delay after the applied stimulus because the propagated wave must either traverse the entire thickness of the ventricular wall, or excite a Purkinje fiber which would then accelerate the spread of excitation via the network of conducting fibers. This hypothesis may explain the delayed stretch-induced epicardial activation observed in the isolated canine preparation of Hansen et al. (1990).

Our analysis did not include the effects of stretch on altered intracellular

calcium cycling [5]. A recently proposed model of ventricular action potential in the canine incorporates sophisticated calcium cycling mechanisms [38], and could serve as a straightforward extension of the studies conducted here.

Regional heterogeneity in myocardial mechanics was demonstrated by McCulloch et al. (1989) in the passively inflated canine left ventricle, where the major and minor principal extensions were shown to increase significantly from the base to the apex. Similarly, passive volume loading increases heterogeneity of action potential morphology as shown by Zabel et al. (1996). Ischemia enhances mechanical and electrophysiological heterogeneity [34, 17]. A recent study by Mazhari et al. (1998) suggests that regional heterogeneity may be altered nonuniformly during ischemia. In an open chest canine preparation, they found that the width of the functional border zone (the distance from zero systolic remodeling strain to the perfusion boundary) was 2–3 times larger in the cross fiber direction that in the fiber direction. Also in the canine, Hearse et al. (1977) showed a significant elevation of the ST segment across the border zone. Thus there is significant nonuniformity in the abnormal mechanical and electrical function during ischemia.

The results presented here support the notion that mechanoelectric feedback may be arrhythmogenic. The dispersion of action potential duration increased by 96% between the 5 mm Hg and 15 mm Hg configurations using the mechanosensitive conductance model governed by fiber strain and cross fiber strain. We would expect this increase to be even more dramatic in the whole heart since our calculations were based on the action potential morphology from a region of approximately one square centimeter. A large increase in the dispersion of action potential duration will increase the excitable gap in ventricular myocardium (the region of fully excitable tissue between the front of an oncoming depolarizing excitation wave and the tail of the preceding repolarizing wave [4]). This may oppose the effect of class III anti-arrhythmic drugs used to terminate reentry by prolonging the refractory period and reducing (or eliminating) the excitable gap [37]. Depolarization of the resting potential caused by the activation of mechanosensitive channels in my-

ocardium may also present an environment favorable to the development of reentry. Singer et al. (1967) reported that phase 4 depolarization to -70 millivolts or higher in isolated canine Purkinje fibers reduced the maximum rate of rise (upstroke velocity) of the action potential, leading to slowed conduction, unidirectional or bidirectional block, and possibly unexcitability or reentry. In the abnormally stretched ventricle, potential sites of functional reentry may be localized (due to strain gradients across an ischemic region [34], for example) or global (in concordance with the increased cardiac dimensions present in congestive heart failure [35]), and the excitable gap could be enhanced by both alterations in the path length of the reentrant circuit, slowed conduction velocity, and shorter action potential duration.

References

[1] M. Akay and W. Craelius. Mechanoelectrical feedback in cardiac myocytes from stretch-activated ion channels. *IEEE Trans Biomed Eng*, 40(8):811–816, Aug 1993.

[2] E. Atalar and E. R. McVeigh. Optimum tag thickness for the measurement of motion by MRI. *IEEE Trans Med Imaging*, 13(1):152–160, Mar 1994.

[3] J. O. Bustamante, A. Ruknudin, and F. Sachs. Stretch-activated channels in heart cells: Relevance to cardiac hypertrophy. *J Cardiovasc Pharmacol*, 17(Suppl. 2):S110–S113, 1991.

[4] C. Cabo and A. L. Wit. Cellular electrophysiologic mechanisms of cardiac arrhythmias. *Cardiology Clinics*, 15(4):517–38, Nov 1997.

[5] S. C. Calaghan and E. White. The role of calcium in the response of cardiac muscle to stretch. *Prog Biophys Mol Biol*, 71:59–90, 1999.

[6] K. D. Costa. *The Structural Basis of Three-Dimensional Ventricular Mechanics*. PhD thesis, University of California, La Jolla, California, 1996.

[7] K. D. Costa, P. J. Hunter, J. M. Rogers, J. M. Guccione, L. K. Waldman, and A. D. McCulloch. A three-dimensional finite element method for large elastic deformations of ventricular myocardium: II — prolate spheroidal coordinates. *J Biomech Eng*, 118(4):464–472, Nov 1996.

[8] W. Craelius. Stretch-activation of rat cardiac myocytes. *Exp Physiol*, 78(3):411–423, May 1993.

[9] W. Craelius, V. Chen, and N. El-Sherif. Stretch activated ion channels in ventricular myocytes. *Bioscience Reports*, 8(5):407–414, Oct 1988.

[10] A. M. Gallagher, J. H. Omens, L. L. Chu, and J. W. Covell. Alterations in collagen fibrillar structure and mechanical properties of the healing scar following myocardial infarction. *Cardiovasc Pathobiol*, 2(1):25–36, 1997.

[11] Y. Goto, B. K. Slinker, and M. M. LeWinter. Similar normalized E_{max} and O_2 consumption-pressure-volume area relation in rabbit and dog. *Am J Physiol*, 255(Heart Circ. Physiol. 24):H366–H374, Aug 1988.

[12] R. A. Gray, J. Jalife, A. V. Panfilov, W. T. Baxter, C. Cabo, J. M. Davidenko, and A. M. Pertsov. Nonstationary vortexlike reentrant activity as a mechanism of polymorphic ventricular tachycardia in the isolated rabbit heart. *Circulation*, 91(9):2454–2469, May 1995.

[13] D. E. Hansen, C. S. Craig, and L. M. Hondeghem. Stretch-induced arrhythmias in the isolated canine ventricle. Evidence for the importance of mechanoelectrical feedback. *Circulation*, 81(3):1094–1105, Mar 1990.

[14] J. D. Hearse, L. H. Opie, I. E. Katzeff, W. F. Lubbe, T. J. Van der Werff, M. Peisach, and G. Boulle. Characterization of the "border zone" in acute regional ischemia in the dog. *Am J Cardiol*, 40(5):716–726, Nov 1977.

[15] S. B. Knisley. Transmembrane voltage changes during unipolar stimulation of rabbit ventricle. *Circ Res*, 77(6):1229–1239, Nov 1995.

[16] P. Kohl, K. Day, and D. Noble. Cellular mechanisms of cardiac mechano-electric feedback in a mathematical model. *Canadian Journal of Cardiology*, 14(1):111–119, Jan 1998.

[17] R. W. Kurz, R. Xiao-Lin, and M. R. Franz. Increased dispersion of ventricular repolarization and ventricular tachyarrhythmias in the globally ischaemic rabbit heart. *Eur Heart J*, 14(11):1561–1571, Nov. 1993.

[18] J. Lekven, K. Chatterjee, J. V. Tyberg, and W. W. Parmley. Reduction in ventricular endocardial and epicardial potentials during acute increments in left ventricular dimensions. *American Heart Journal*, 98(2):200–206, Aug 1979.

[19] D. H. S. Lin and F. C. P. Yin. A multiaxial constitutive law for mammalian left ventricular myocardiumin steady-state barium contracture or tetanus. *J Biomech Eng*, 120(4):504–517, Aug 1998.

[20] R. Mazhari, J. H. Omens, L. K. Waldman, and A. D. McCulloch. Regional myocardial perfusion and mechanics: a model-based method of analysis. *Ann Biomed Eng*, 26(5):743–755, Sep-Oct 1998.

[21] A. D. McCulloch, B. H. Smaill, and P. J. Hunter. Regional left ventricular epicardial deformation in the passive dog heart. *Circ Res*, 64(4):721–733, Apr 1989.

[22] P. M. F. Nielsen, I. J. LeGrice, B. H. Smaill, and P. J. Hunter. Mathematical model of geometry and fibrous structure of the heart. *Am J Physiol*, 260(Heart Circ. Physiol. 29):H1365–H1378, Apr 1991.

[23] D. Noble, A. Varghese, P. Kohl, and P. Noble. Improved guinea-pig ventricular cell model incorporating a diadic space, i_{Kr} and i_{Ks}, and length- and tension-dependent processes. *Canadian Journal of Cardiology*, 14(1):123–134, Jan 1998.

[24] W. G. O'Dell and A. D. McCulloch. A novel numerical formulation for modeling tissue compressibility. *Proc ASME*, (in press), 1998.

[25] J. H. Omens, K. D. May, and A. D. McCulloch. Transmural distribution of three-dimensional strain in the isolated arrested canine left ventricle. *Am J Physiol*, 261(Heart Circ. Physiol. 30):H918–H928, Sep 1991.

[26] J. J. Rice, R. L. Winslow, J. Dekanski, and E. McVeigh. Model studies of the role of mechano-sensitive currents in the generation of cardiac arrhythmias. *J Theor Biol*, 190(4):295–312, February 21 1998.

[27] T. L. Riemer, E. A. Sobie, and L. Tung. Stretch-induced changes in arrhythmogensis and excitability in experiementally based heart cell models. *Am J Physiol*, 275(Heart Circ. Physiol. 44):H431–H442, 1998.

[28] A. Ruknudin, F. Sachs, and J. O. Bustamante. Stretch-activated ion channels in tissue-cultured chick heart. *Am J Physiol*, 264(Heart Circ. Physiol. 33):H960–H972, Mar 1993.

[29] A. Ruknudin, M. J. Song, and F. Sachs. The ultrastructure of patch-clamped membranes: A study using high voltage electron microscopy. *J Cell Biology*, 112(1):125–134, Jan 1991.

[30] F. Sachs. Mechanical transduction by membrane ion channels: A mini review. *Mol Cell Biochem*, 104(1/2):57–60, May/June 1991.

[31] F. Sachs. Modeling mechanical-electrical transduction in the heart. In V. C. Mow, F. Guilak, R. M. Hochmuth, and R. Tran-Son-Tay, editors, *Cell Mechanics and Cellular Engineering*, chapter 18, pages 308–328. Springer-Verlag, New York, 1994.

[32] D. F. Scollan, A. Holmes, R. Winslow, and J. Forder. Histological validation of myocardial microstructure obtained from diffusion tensor magnetic resonance imaging. *Am J Physiol*, 275(Heart Circ. Physiol. 44):H2308–2318, Dec. 1998.

[33] D. H. Singer, R. Lazzara, and B. F. Hoffman. Interrelationship between automaticity and conduction in Purkinje fibers. *Circ Res*, 21(4):537–558, Oct 1967.

[34] S. L. Van Leuven, L. K. Waldman, A. D. McCulloch, and J. W. Covell. Gradients of epicardial strain across the perfusion boundary during acute myocardial ischemia. *Am J Physiol*, 267(Heart Circ. Physiol. 36):H2348–H2362, Dec 1994.

[35] Z. Wang, L. K. Taylor, W. D. Denney, and D. E. Hansen. Initiation of ventricular extrasystoles by myocardial stretch in chronically dilated and failing canine left ventricle. *Circulation*, 90(4):2022–2031, Oct 1994.

[36] M. W. Watkins, B. K. Slinker, Y. Goto, and M. M. LeWinter. 2,3-Butanedione monoxime increases contractile efficiency in the rabbit ventricle. *Am J Physiol*, 263(Heart Circ. Physiol. 32):H1811–H1818, Dec 1992.

[37] D. W. Whalley, D. J. Wendt, and A. O. Grant. Basic concepts in cellular cardiac electrophysiology: Part II: Block of ion channels by antiarrhythmic drugs. *PACE*, 18(9 Part I):1686–1704, Sep 1995.

[38] R. L. Winslow, J. Rice, S. Jafri, E. Marbán, and B. O'Rourke. Mechanisms of altered excitation-contraction coupling in canine tachycardia-induced heart failure, II model studies. *Circ Res*, 84:571–586, 19 March 1999.

[39] A. A. Young, I. J. LeGrice, M. A. Young, and B. H. Smaill. Extended confocal microscopy of myocardial laminae and collagen network. *Journal of Microscopy*, 192(Pt 2):139–150, Nov 1998.

[40] M. Zabel, B. S. Koller, F. Sachs, and M. R. Franz. Stretch-induced voltage changes in the isolated beating heart: Importance of the timing of stretch and implications for stretch-activated ion channels. *Cardiovasc Res*, 32(1):120–130, July 1996.

[41] M. Zabel, S. Portnoy, and M. R. Franz. Effect of sustained load on dispersion of ventricular repolarization and conduction time in the isolated intact rabbit heart. *J Cardiovasc Electrophysiol*, 7(1):9–16, Jan 1996.

Bibliography

[1] Akay, M. and Craelius, W. Mechanoelectrical feedback in cardiac myocytes from stretch-activated ion channels. *IEEE Trans Biomed Eng*, 40(8):811–816, Aug 1993.

[2] Allen, D. G. and Kentish, J. C. Calcium concentration in the myoplasm of skinned ferret ventricular muscle following changes in muscle length. *J Physiol*, 407:489–503, Dec 1988.

[3] Allessie, M. A., Schalij, M. J., Kirchhof, C. J., Boersma, L., Huybers, M., and Hollen, J. Experimental electrophysiology and arrhythmogenicity. Anisotropy and ventricular tachycardia. *Eur Heart J*, 10 Suppl. E:2–8, September 1989.

[4] Anderson, E., Brooks, J., Grassl, C., and Scott, S. Performance of the CRAY T3E multiprocessor. White paper, Cray Research, `http://www.cray.com/products/systems/crayt3e/1200/performace.htm` or `http://www.sgi.com/t3e/performance.html`, 22 August 1997.

[5] Antzelevitch, C., Sicouri, S., Lukas, A., Nesterenko, V. V., Liu, D.-W., and Di Diego, J. M. Regional differences in the electrophysiology of ventricular cells: Physiological and clinical implications. In Zipes and Jalife [301], chapter 23, pages 228–245.

[6] Atalar, E. and McVeigh, E. R. Optimum tag thickness for the measurement of motion by MRI. *IEEE Trans Med Imaging*, 13(1):152–160, Mar 1994.

[7] Azhari, H., Weiss, J. L., Rogers, W. J., Siu, C. O., Zerhouni, E. A., and Shapiro, E. P. Noninvasive quantification of principal strains in normal canine hearts using tagged MRI images in 3-D. *Am J Physiol*, 264(Heart Circ. Physiol. 33):H205–H216, Jan 1993.

[8] Bailie, A. H., Mitchell, R. H., and Anderson, J. M. A computer model of re-entry in cardiac tissue. *Comput Biol Med*, 20(1):47–54, 1990.

[9] Balay, S., Gropp, W. D., McInnes, L. C., and Smith, B. F. *PETSc 2.0 Users Manual*, 1998. Available from `http://www.mcs.anl.gov/petsc`.

[10] Barrett, J. S. Chest thumps and the heart beat. *N Engl J Med*, 284(7):393, 18 February 1971.

[11] Barrett, R., Berry, M., Chan, T. F., Demmel, J., Donato, J., Dongarra, J., Eijkhout, V., Pozo, R., Romine, C., and Van der Vorst, H. *Templates for the Solution of Linear Systems: Building Blocks for Iterative Methods*. SIAM, Philadelphia, 1994.

[12] Barrett, T. D., MacLeod, B. A., and Walker, M. J. A. A model of myocardial ischemia for the simultaneous assessment of electrophysiological changes and arrhythmias in intact rabbits. *Journal of Pharmacological and Toxicological Methods*, 37(1):27–36, February 1997.

[13] Bashir, Y., Sneddon, J. F., O'Nunain, S., Paul, V. E., Gibson, S., Ward, D. E., and Camm, A. J. Comparative electrophysiological effects of captopril or hydralazine combined with nitrate in patients with left ventricular dysfunction and inducible ventricular tachycardia. *Br Heart J*, 67(5):355–360, May 1992.

[14] Beaumont, J., Davidenko, N., Davidenko, J., and Jalife, J. Self-sustaining spiral wave activity in a two-dimensional ionic model of cardiac ventricular muscle. In *Computer Simulations in Biomedicine*, pages 75–85. Computational Mechanics Publications, Boston, 1995.

[15] Beeler, G. W. and Reuter, H. Reconstruction of the action potential of ventricular myocardial fibres. *J Physiol*, 268(1):177–210, Jun 1977.

[16] Behr, M., Johnson, A., Kennedy, J., Mittal, S., and Tezduyar, T. Computation of incompressible flows with implicit finite element implementations on the Connection Machine. *Comp Meth Appl Mech Eng*, 108(1–2):99–118, Sep 1993.

[17] Bendtsen, C. *ParSODES: A Parallel Stiff ODE Solver*. Danish Computer Centre for Research and Education, DTU, Bldg. 304 DK-2800 Lyngby, Denmark, 1996. Available from `http://www.netlib.org/ode/parsodes.tar.gz`.

[18] Berne, R. M., editor. *Handbook of Physiology, Section 2: The Cardiovascular System*, volume 1. American Physiological Society, Bethesda, Maryland, 1979.

[19] Berrier, C., Coulombe, A., Houssin, C., and Ghazi, A. A patch-clamp study of ion channels of inner and outer membranes and of contact zones of *E. coli*, fused into giant liposomes: Pressure-activated channels are localized in the inner membrane. *FEBS Lett*, 259(1):27–32, 18 December 1989.

[20] Bierfeld, J. L., Rodriguez-Viera, V., Aranda, J. M., Jr, C. A., Lazzara, R., and Befeler, B. Terminating ventricular fibrillation by chest thump. *Angiology*, 30(10):703–707, Oct 1979.

[21] Blackford, L. S., Choi, J., Cleary, A., D'Azevedo, E., Demmel, J., Dhillon, I., Dongarra, J., Hammarling, S., Henry, G., Petitet, A., Stanley, K., Walker, D., and Whaley, R. C. *ScaLAPACK Users Guide*. SIAM, Philadelphia, PA, 1997.

[22] Bluhm, W. F. and Lew, W. Y. W. Sarcoplasmic reticulum in cardiac length-dependent activation in rabbits. *Am J Physiol*, 269(Heart Circ. Physiol. 38):H965–H972, 1995.

[23] Bovendeerd, P. H., Arts, T., Delhaas, T., Huyghe, J. M., van Campen, D. H., and Reneman, R. S. Regional wall mechanics in the ischemic left ventricle: numerical modeling and dog experiments. *Am J Physiol*, 270(Heart Circ. Physiol. 39):H398–H410, Jan 1996.

[24] Bovendeerd, P. H., Arts, T., Huyghe, J. M., van Campen, D. H., and Reneman, R. S. Dependence of local left ventricular wall mechanics on myocardial fiber orientation: A model study. *J Biomech*, 25(10):1129–1140, Oct 1992.

[25] Bovendeerd, P. H. M., Huyghe, J. M., Arts, T., van Campen, D. H., and Reneman, R. S. Influence of endocardial-epicardial crossover of muscle fibers on left ventricular wall mechanics. *J Biomech*, 27(7):941–951, Jul 1994.

[26] Bowman, C. L. and Lohr, J. W. Curvature-sensitive mechanosensitive ion channels and osmotically-evoked movements of the patch membrane (abstract). *Biophys J*, 70(2):A365, Feb 1996. Abstract Supplement for the Biophysical Society 40rd Annual Meeting, February 17–21, 1996, Baltimore, Maryland.

[27] Bradfield, J. W. B., Beck, G., and Vecht, R. J. Left ventricular apical thin point. *Br Heart J*, 39(7):806–809, Jul 1977.

[28] Brutsaert, D. L. Nonuniformity: A physiologic modulator of contraction and relaxation of the normal heart. *J Am Coll Cardiol*, 9(2):341–348, February 1987.

[29] Bustamante, J. O., Ruknudin, A., and Sachs, F. Stretch-activated channels in heart cells: Relevance to cardiac hypertrophy. *J Cardiovasc Pharmacol*, 17(Suppl. 2):S110–S113, 1991.

[30] Cabo, C., Pertsov, A. M., Baxter, W. T., Davidenko, J. M., Gray, R. A., and Jalife, J. Wave-front curvature as a cause of slow conduction and block in isolated cardiac muscle. *Circ Res*, 75(6):1014–1028, Dec 1994.

[31] Cabo, C., Pertsov, A. M., Davidenko, J. M., Baxter, W. T., Gray, R. A., and Jalife, J. Vortex shedding as a precursor of turbulent electrical activity in cardiac muscle. *Biophys J*, 70(3):1105–1111, Mar 1996.

[32] Cabo, C. and Wit, A. L. Cellular electrophysiologic mechanisms of cardiac arrhythmias. *Cardiology Clinics*, 15(4):517–38, Nov 1997.

[33] Calaghan, S. C. and White, E. The role of calcium in the response of cardiac muscle to stretch. *Prog Biophys Mol Biol*, 71:59–90, 1999.

[34] Calkins, H., Maughan, W. L., Kass, D. A., Sagawa, K., and Levine, J. H. Electrophysiological effect of volume load in isolated canine hearts. *Am J Physiol*, 256(Heart Circ. Physiol. 25):H1697–H1706, Jun 1989.

[35] Calkins, H., Maughan, W. L., Weisman, H. F., Sugiura, S., Sagawa, K., and Levine, J. H. Effect of acute volume load on refractoriness and arrhythmia development in isolated, chronically infarcted canine hearts. *Circulation*, 79(3):687–697, Mar 1989.

[36] Cates, A. W. and Pollard, A. E. A model study of intramural dispersion of action potential duration in the canine pulmonary conus. *Ann Biomed Eng*, 26(4):567–576, July-August 1998.

[37] Caulfield, J. B. and Borg, T. K. The collagen network of the heart. *Laboratory Investigation*, 40(3):364–372, Mar 1979.

[38] Chaudhary, A. B. and Bathe, K.-J. A solution method for static and dynamic analysis of three-dimensional contact problems with friction. *Computers and Structures*, 24(6):855–873, 1986.

[39] Clerc, L. Directional differences of impulse spread in trabecular muscle from mammalian heart. *J Physiol*, 255(1):335–346, Feb 1975.

[40] Cook, S. J., Chamunorwa, J. P., Lancaster, M. K., and O'Neill, S. C. Regional differences in the regulation of intracellular sodium and in action potential configuration in rabbit left ventricle. *Pflügers Archiv. European Journal of Physiology*, 433(4):515–522, Feb 1997.

[41] Costa, K. D. *The Structural Basis of Three-Dimensional Ventricular Mechanics*. Ph.D. thesis, University of California, La Jolla, California, 1996.

[42] Costa, K. D., Hunter, P. J., Rogers, J. M., Guccione, J. M., Waldman, L. K., and McCulloch, A. D. A three-dimensional finite element method for large elastic deformations of ventricular myocardium: I — cylindrical and spherical polar coordinates. *J Biomech Eng*, 118(4):452–463, Nov 1996.

[43] Costa, K. D., Hunter, P. J., Rogers, J. M., Guccione, J. M., Waldman, L. K., and McCulloch, A. D. A three-dimensional finite element method for large elastic deformations of ventricular myocardium: II — prolate spheroidal coordinates. *J Biomech Eng*, 118(4):464–472, Nov 1996.

[44] Costa, K. D., May-Newman, K., Farr, D., O'Dell, W. G., McCulloch, A. D., and Omens, J. H. Three-dimensional residual strain in midanterior canine left ventricle. *Am J Physiol*, 273(Heart Circ. Physiol. 42):H1968–H1976, 1997.

[45] Courtemanche, M., Ramirez, R. J., and Nattel, S. Ionic mechanisms underlying human atrial action potential properties: insights from a mathematical model. *Am J Physiol*, 275(Heart Circ. Physiol. 44):H301–H321, Jul 1998.

[46] Courtemanche, M., Skaggs, W., and Winfree, A. T. Stable three-dimensional action potential circulation in the FitzHugh-Nagumo model. *Physica D*, 41(2):173–182, Mar 1990.

[47] Courtemanche, M. and Winfree, A. T. Re-entrant rotating waves in a Beeler-Reuter based model of two-dimensional cardiac electrical activity. *International Journal of Bifurcation and Chaos in Applied Sciences and Engineering*, 1(2):431–444, Jun 1991.

[48] Craelius, W. Stretch-activation of rat cardiac myocytes. *Exp Physiol*, 78(3):411–423, May 1993.

[49] Craelius, W., Chen, V., and El-Sherif, N. Stretch activated ion channels in ventricular myocytes. *Bioscience Reports*, 8(5):407–414, Oct 1988.

[50] Crisfield, M. A. *Non-linear Finite Element Analysis of Solids and Structures*, volume 2: Advanced Topics. Wiley, New York, 1997.

[51] Crozatier, B. Stretch-induced modifications of myocardial performance: from ventricular function to cellular and molecular mechanisms. *Cardiovasc Res*, 32(1):25–37, Jul 1996.

[52] Davidenko, J. M., Pertsov, A. V., Salomonsz, R., Baxter, W. T., and Jalife, J. Stationary and drifting spiral waves of excitation in isolated cardiac muscle. *Nature*, 355(6358):349–351, January 23 1992.

[53] Davidenko, J. M., Salomonsz, R., Pertsov, A. M., Baxter, W. T., and Jalife, J. Effects of pacing on stationary reentrant activity: Theoretical and experimental study. *Circ Res*, 77(6):1166–1179, Dec 1995.

[54] Davis, T. A. and Duff, I. S. An unsymmetric-pattern multifrontal method for sparse LU factorization. *SIAM J Matrix Anal Appl*, 18(1):140–158, Jan 1997.

[55] Delcour, A. H., Martinac, B., Adler, J., and Kung, C. Voltage-sensitive ion channel of *Escherichia coli*. *J Membr Biol*, 112(3):267–275, Dec 1989.

[56] Delgado, C., Steinhaus, B., Delmar, M., Chivalvo, D. R., and Jalife, J. Directional differences in excitability and margin of safety for propagation in sheep ventricular epicardial muscle. *Circ Res*, 67(1):97–110, Jul 1990.

[57] Demir, S. S., Clark, J. W., Murphey, C. R., and Giles, W. R. A mathematical model of a rabbit sinoatrial node cell. *Am J Physiol*, 266(Cell Physiol. 35):C832–C852, Mar 1994.

[58] Demiray, H. Large deformation analysis of some basic problems in biophysics. *Bull Math Biol*, 38(06):701–712, 1976.

[59] Demmel, J. W., Gilbert, J. R., and Li, X. S. *SuperLU Users Guide*, 1997. Available from `http://http.cs.berkeley.edu/~xiaoye/superlu.html`.

[60] Dias da Cunha, R. and Hopkins, T. A parallel implementation of the restarted GMRES iterative algorithm for nonsymmetric systems of linear equations. *Advances in Computational Mathematics*, 2(3):261–277, 1994.

[61] DiFrancesco, D. and Noble, D. A model of cardiac electrical activity incorporating ionic pumps and concentration changes. *Philos Trans R Soc Lond B Biol Sci*, 307(1133):353–398, January 10 1985.

[62] Dominguez, G. and Fozzard, H. A. Effect of stretch on conduction velocity and cable properties of cardiac Purkinje fibers. *Am J Physiol*, 237(3):C119–C124, Sep 1979.

[63] Durrer, D., van Dam, R. T., Freud, G. E., Janse, M. J., Meijler, F. L., and Arzbaecher, R. C. Total excitation of the isolated human heart. *Circulation*, 41(6):899–912, Jun 1970.

[64] Edwards II, C. H., Rankin, J. S., McHale, P. A., Ling, D., and Anderson, R. W. Effects of ischemia on left ventricular regional function in the conscious dog. *Am J Physiol*, 240(Heart Circ. Physiol. 9):H413–H420, Mar 1981.

[65] Efimov, I. R., Ermentrout, B., Huang, D. T., and Salama, G. Activation and repolarization patterns are governed by different structural characteristics of ventricular myocardium: Experimental study with voltage-sensitive dyes and numerical simulations. *J Cardiovasc Electrophysiol*, 7(6):512–530, Jun 1996.

[66] Efimov, I. R., Huang, D. T., Rendt, J. R. M., and Salama, G. Optical mapping of repolarization and refractoriness from intact hearts. *Circulation*, 90(3):1469–1480, Sep 1994.

[67] Emery, J. L., Omens, J. H., and McCulloch, A. D. Biaxial mechanics of the passively overstretched left ventricle. *Am J Physiol*, 272(5 Pt 2):H2299–H2305, May 1997.

[68] Emery, J. L., Omens, J. H., and McCulloch, A. D. Strain softening in rat left ventricular myocardium. *J Biomech Eng*, 119(1):6–12, Feb 1997.

[69] Fast, V. G. and Kléber, A. G. Role of wavefront curvature in propagation of cardiac impulse. *Cardiovasc Res*, 33(2):258–271, Feb 1997.

[70] Fedida, D. and Giles, W. R. Regional variations in action potentials and transient outward current in myocytes isolated from rabbit left ventricle. *J Physiol*, 442:191–209, Oct 1991.

[71] FitzHugh, R. Impulses and physiological states in theoretical models of nerve membrane. *Biophys J*, 1:445–466, Jul 1961.

[72] Franz, M. R. Stretch-activated arrhythmias. In D. P. Zipes and J. Jalife, editors, *Cardiac Electrophysiology: From Cell to Bedside*, chapter 57, pages 597–606. W. B. Saunders, Philadelphia, second edition, 1995.

[73] Franz, M. R. Mechano-electrical feedback in ventricular myocardium. *Cardiovasc Res*, 32(1):15–24, Jul 1996.

[74] Franz, M. R. Current status of monophasic action potential recording: theories, measurements and interpretations. *Cardiovasc Res*, 41:25–40, 1999.

[75] Franz, M. R., Burkhoff, D., Yue, D. T., and Sagawa, K. Mechanically induced action potential changes and arrhythmia in isolated and in situ canine hearts. *Cardiovasc Res*, 23(3):213–223, Mar 1989.

[76] Franz, M. R., Cima, R., Wang, D., Profitt, D., and Kurz, R. Electrophysiological effects of myocardial stretch and mechanical determinants of stretch-activated arrhythmias. *Circulation*, 86(3):968–978, Sep 1992. Published erratum appears in Circulation 1992 Nov, 86(5):1663.

[77] Frazier, D. W., Wolf, P. D., Wharton, J. M., Tang, A. S., Smith, W. M., and Ideker, R. E. Stimulus-induced critical point: Mechanism for electrical initiation of reentry in normal canine myocardium. *J Clin Invest*, 83(3):1039–1052, Mar 1989.

[78] Frind, E. O. and Pinder, G. F. A collocation finite element method for potential problems in irregular domains. *Int J Numer Methods Eng*, 14(5):681–701, 1979.

[79] Fung, Y.-C. *Biodynamics: Circulation*. Springer-Verlag, New York, 1984.

[80] Gallagher, A. M., Omens, J. H., Chu, L. L., and Covell, J. W. Alterations in collagen fibrillar structure and mechanical properties of the healing scar following myocardial infarction. *Cardiovasc Pathobiol*, 2(1):25–36, 1997.

[81] Gerald, C. F. and Wheatley, P. O. *Applied Numerical Analysis*. Addison-Wesley, Reading, Mass., sixth edition, 1997.

[82] Gerdes, A. M., Kellerman, S. E., Malec, K. B., and Schocken, D. D. Transverse shape characteristics of cardiac myocytes from rats and humans. *Cardioscience*, 5(1):31–36, Mar 1994. Published erratum appears in Cardioscience 1994 Jun;5(2): preceding 63.

[83] Giles, W. R. and Imaizumi, Y. Comparison of potassium currents in rabbit atrial and ventricular cells. *J Physiol*, 405:123–145, Nov 1988.

[84] Gill, P. E., Murray, W., and Wright, M. H. *Practical Optimization*. Academic Press, New York, 1981.

[85] Gillis, A. M., Kulisz, E., and Mathison, H. J. Cardiac electrophysiological variables in blood-perfused and buffer-perfused, isolated, working rabbit heart. *Am J Physiol*, 271(Heart Circ. Physiol. 40):H784–H789, August 1996.

[86] Glass, L., Hunter, P., and McCulloch, A., editors. *Theory of Heart: Biomechanics, Biophysics, and Nonlinear Dynamics of Cardiac Function*. Springer-Verlag, New York, 1991.

[87] Glowinski, R. and Le Tallec, P. *Augmented Lagrangian and operator-splitting methods in nonlinear mechanics*, volume 9 of *SIAM studies in applied mathematics*. Society for Industrial and Applied Mathematics, Philadelphia, 1989.

[88] Golub, G. H. and Van Loan, C. F. *Matrix Computations*. Johns Hopkins University Press, Baltimore, second edition, 1993.

[89] Goto, Y., Slinker, B. K., and LeWinter, M. M. Similar normalized E_{max} and O_2 consumption-pressure-volume area relation in rabbit and dog. *Am J Physiol*, 255(Heart Circ. Physiol. 24):H366–H374, Aug 1988.

[90] Gotoh, M., Uchida, T., Fan, W., Fishbein, M. C., Karagueuzian, H. S., and Chen, P.-S. Anisotropic repolarization in ventricular tissue. *Am J Physiol*, 272(Heart Circ. Physiol. 41):H107–H113, Jan 1997.

[91] Gray, R. A., Jalife, J., Panfilov, A. V., Baxter, W. T., Cabo, C., Davidenko, J. M., and Pertsov, A. M. Nonstationary vortexlike reentrant activity as a mechanism of polymorphic ventricular tachycardia in the isolated rabbit heart. *Circulation*, 91(9):2454–2469, May 1995.

[92] Green, A. E. and Adkins, J. E. *Large Elastic Deformations*. Clarendon Press, Oxford, second edition, 1970.

[93] Greenbaum, R. A., Ho, S. Y., Gibson, D. G., Becker, A. E., and Anderson, R. H. Left ventricular fibre architecture in man. *Br Heart J*, 45(3):248–263, Mar 1981.

[94] Guccione, J. M., Costa, K. D., and McCulloch, A. D. Finite element stress analysis of left ventricular mechanics in the beating dog heart. *J Biomech*, 28(10):1167–1177, Oct 1995.

[95] Guccione, J. M. and McCulloch, A. D. Finite element modeling of ventricular mechanics. In L. Glass, P. Hunter, and A. McCulloch, editors, *Theory of Heart: Biomechanics, Biophysics, and Nonlinear Dynamics of Cardiac Function*, chapter 6, pages 121–144. Springer-Verlag, New York, 1991.

[96] Guccione, J. M., McCulloch, A. D., and Waldman, L. K. Passive material properties of intact ventricular myocardium determined from a cylindrical model. *J Biomech Eng*, 113(1):42–55, Feb 1991.

[97] Hagiwara, N., Masuda, H., Shoda, M., and Irisawa, H. Stretch-activated anion currents of rabbit cardiac myocytes. *J Physiol*, 456:285–302, Oct 1992.

[98] Hamill, O. P. and McBride, Jr., D. W. Rapid adaptation of single mechanosensitive channels in *Xenopus* oocytes. *Proc Natl Acad Sci USA*, 89(16):7462–7466, 15 August 1992.

[99] Hansen, D. E. Mechanoelectrical feedback effects of altering preload, afterload, and ventricular shortening. *Am J Physiol*, 264(Heart Circ. Physiol. 33):H423–H432, Feb 1993.

[100] Hansen, D. E., Borganelli, M., Stacy, Jr., G. P., and Taylor, L. K. Dose-dependent inhibition of stretch-induced arrhythmias by gadolinium in isolated canine ventricles. Evidence for a unique mode of antiarrhythmic action. *Circ Res*, 69(3):820–831, Sep 1991.

[101] Hansen, D. E., Craig, C. S., and Hondeghem, L. M. Stretch-induced arrhythmias in the isolated canine ventricle. Evidence for the importance of mechanoelectrical feedback. *Circulation*, 81(3):1094–1105, Mar 1990.

[102] Harrild, D. M. and Henriquez, C. S. A finite volume model of cardiac propagation. *Ann Biomed Eng*, 25(2):315–334, March-April 1997.

[103] Hearse, J. D., Opie, L. H., Katzeff, I. E., Lubbe, W. F., Van der Werff, T. J., Peisach, M., and Boulle, G. Characterization of the "border zone" in acute regional ischemia in the dog. *Am J Cardiol*, 40(5):716–726, Nov 1977.

[104] Henriquez, C. S., Muzikant, A. L., and Smoak, C. K. Anisotropy, fiber curvature, and bath loading effects on activation in thin and thick cardiac tissue preparations: Simulations in a three-dimensional bidomain model. *J Cardiovasc Electrophysiol*, 7(5):424–444, May 1996.

[105] Hicks, M. N., McIntosh, M. A., Kane, K. A., Rankin, A. C., and Cobbe, S. M. The electrophysiology of rabbit hearts with left ventricular hypertrophy under normal and ischaemic conditions. *Cardiovasc Res*, 30(2):181–186, August 1995.

[106] Hill, B. C., Hunt, A. J., and Courtney, K. R. Reentrant tachycardia in a thin layer of ventricular subepicardium: Effects of d-sotalol and lidocaine. *J Cardiovasc Pharmacol*, 16(6):871–880, December 1990.

[107] Hindmarsh, A. C. ODEPACK, a systematized collection of ODE solvers. In R. S. Stepleman, editor, *Scientific Computing: Applications of Mathematics and Computing to the Physical Sciences*, volume 1 of *IMACS Transactions on Scientific Computation*, pages 55–64. North-Holland, New York, 1983. Based on papers presented at the Tenth IMACS World Congress on System Simulation and Scientific Computation, held in Montreal, Canada, August 8-13, 1982.

[108] Hodgkin, A. L. and Huxley, A. F. A quantitative description of membrane current and its application to conduction and excitation in nerve. *J Physiol*, 117:500–544, 1952.

[109] Holmes, J. W. and Covell, J. W. Collagen fiber orientation in myocardial scar tissue. *Cardiovasc Pathobiol*, 1(1):15–22, 1996.

[110] Holmes, J. W., Nuñez, J. A., and Covell, J. W. Functional implications of myocardial scar structure. *Am J Physiol*, 272(Heart Circ. Physiol. 41):H2123–H2130, May 1997.

[111] Hongo, K., Pascarel, C., Cazorla, O., Gannier, F., Le Guennec, J. Y., and White, E. Gadolinium blocks the delayed rectifier potassium current in isolated guinea-pig ventricular myocytes. *Exp Physiol*, 82(4):647–656, Jul 1997.

[112] Hort, W. Makroskopische und mikrometrische untersuchungen am myokard verschieden stark gefüllter linker kammern. *Virchows Archiv für Pathologische Anatomie und Physiologie und für Klinische Medizin*, 333:523–564, 1960.

[113] Hu, H. and Sachs, F. Mechanically activated currents in chick heart cells. *J Membr Biol*, 154(3):205–216, Dec 1996.

[114] Hughes, T. J. R., Levit, I., and Winget, J. An element-by-element solution algorithm for problems of structural and solid mechanics. *Comp Meth Appl Mech Eng*, 36:241–254, 1983.

[115] Huisman, R. M., Elzinga, G., Westerhof, N., and Sipkema, P. Measurement of left ventricular wall stress. *Cardiovasc Res*, 14(3):142–153, Mar 1980.

[116] Humphrey, J. D. and Yin, F. C. Constitutive relations and finite deformations of passive cardiac tissue II: stress analysis in the left ventricle. *Circulation Research*, 65(3):805–817, Sep 1989.

[117] Humphrey, J. D. and Yin, F. C. P. Biaxial mechanical behavior of excised epicardium. *J Biomech Eng*, 110(4):349–351, Nov 1988. Published erratum appears in J. Biomech. Eng. 1989 Aug, 111(3):227.

[118] Hunter, P. J., McCulloch, A. D., Nielsen, P. M. F., and Smaill, B. H. A finite element model of passive ventricular mechanics. In R. L. Spilker and B. R. Simon, editors, *Computational Methods in Bioengineering*, volume 9, pages 387–397. American Society of Mechanical Engineers, New York, NY, November/December 1988.

[119] Hunter, P. J. and Smaill, B. H. The analysis of cardiac function: A continuum approach. *Prog Biophys Mol Biol*, 52(2):101–164, 1988.

[120] Hutchinson, S. A., Prevost, L. V., J. N. Shadidxi and, C. H. T., and Tuminaro, R. S. *Aztec User's Guide Version 2.0*. Sandia National Laboratories, Albuquerque, NM 87185, Jul 1998. Available from `http://www.cs.sandia.gov/CRF/pspapers/Aztec_ug_2.0.ps`.

[121] Huyghe, J. M., Arts, T., van Campen, D. H., and Reneman, R. S. Porous medium finite element model of the beating left ventricle. *Am J Physiol*, 262(Heart Circ. Physiol. 31):H1256–H1267, Apr 1992.

[122] Huyghe, J. M., van Campen, D. H., Arts, T., and Heethaar, R. M. A two-phase finite element model of the diastolic left ventricle. *J Biomech*, 24(7):527–538, 1991.

[123] Janvier, N. C. and Boyett, M. R. The role of Na-Ca exchange current in the cardiac action potential. *Cardiovasc Res*, 32(1):69–84, Jul 1996.

[124] Johan, Z., Hughes, T. J. R., Mathur, K. K., and Johnsson, S. L. A data parallel finite element method for computational fluid dynamics on the Connection Machine system. *Comp Meth Appl Mech Eng*, 99(1):113–134, Aug 1992.

[125] Jones, M. T. and Plassmann, P. E. *BlockSolve95 Users Manual: Scalable Library Software for the Parallel Solution of Sparse Linear Systems*. Argonne National Laboratory, 9700 South Class Avenue, Argonne IL 60439, Jun 1997. Argonne National Laboratory Report 95/48 (revised June 1997). Available from `ftp://info.mcs.anl.gov/pub/BlockSolve95/manual.ps`.

[126] Joyner, R. W. Effects of the discrete pattern of electrical coupling on propagation through an electrical syncytium. *Circ Res*, 50(2):192–200, Feb 1982.

[127] Kanai, A. and Salama, G. Optical mapping reveals that repolarization spreads anisotropically and is guided by fiber orientation in guinea pig hearts. *Circ Res*, 77(4):784–802, Oct 1995.

[128] Keener, J. P. Wave propagation in myocardium. In L. Glass, P. Hunter, and A. McCulloch, editors, *Theory of Heart: Biomechanics, Biophysics, and Nonlinear Dynamics of Cardiac Function*, chapter 17, pages 405–436. Springer-Verlag, New York, 1991.

[129] Keller, J. B. and Givoli, D. Exact non-reflecting boundary conditions. *Journal of Computational Physics*, 82(1):172–192, May 1989.

[130] Kennedy, J., Behr, M., Kalro, V., and Tezduyar, T. Implementation of implicit finite element methods for incompressible flows on the CM–5. *Comp Meth Appl Mech Eng*, 119(1–2):95–111, Nov 1994.

[131] Knisley, S. B. Transmembrane voltage changes during unipolar stimulation of rabbit ventricle. *Circ Res*, 77(6):1229–1239, Nov 1995.

[132] Knisley, S. B. and Baynham, T. C. Line stimulation parallel to myofibers enhances regional uniformity of transmembrane voltage changes in rabbit hearts. *Circ Res*, 81(2):229–241, August 1997.

[133] Knisley, S. B. and Hill, B. C. Effects of bipolar point and line stimulation in anisotropic rabbit epicardium: Assessment of the critical radius of curvature for longitudinal block. *IEEE Trans Biomed Eng*, 42(10):957–966, Oct 1995.

[134] Knudsen, Z., Holden, A. V., and Brindley, J. Qualitative modeling of mechanoelectrical feedback in a ventricular cell. *Bull Math Biol*, 59(6):1155–1181, Nov 1997.

[135] Kohl, P., Day, K., and Noble, D. Cellular mechanisms of cardiac mechanoelectric feedback in a mathematical model. *Canadian Journal of Cardiology*, 14(1):111–119, Jan 1998.

[136] Kohl, P., Hunter, P., and Noble, D. Stretch-induced changes in heart rate and rhythm: clinical observations, experiments and mathematical models. *Prog Biophys Mol Biol*, 71:91–138, 1999.

[137] Kumar, V., Grama, A., Gupta, A., and Karypis, G. *Introduction to Parallel Computing: Design and Analysis of Algorithms*. Benjamin/Cummings, Redwood City, CA, 1994.

[138] Kuo, C. S., Reddy, C. P., Munakata, K., and Surawicz, B. Mechanism of ventricular arrhythmias caused by increased dispersion of repolarization. *Eur Heart J*, 6 Suppl. D:63–70, November 1985.

[139] Kurz, R. W., Ren, X.-L., and Franz, M. R. Dispersion and delay of electrical restitution in the globally ischaemic heart. *Eur Heart J*, 15(4):547–554, April 1994.

[140] Kurz, R. W., Xiao-Lin, R., and Franz, M. R. Increased dispersion of ventricular repolarization and ventricular tachyarrhythmias in the globally ischaemic rabbit heart. *Eur Heart J*, 14(11):1561–1571, November 1993.

[141] Lab, M. J. Transient depolarisation and action potential alterations following mechanical changes in isolated myocardium. *Cardiovasc Res*, 14(11):624–637, Dec 1980.

[142] Lab, M. J. Contraction-excitation feedback in myocardium: Physiological basis and clinical relevance. *Circ Res*, 50(6), Jun 1982.

[143] Lacampagne, A., Gannier, F., Argibay, J., Garnier, D., and Le Guennec, J. Y. The stretch-activated ion channel blocker gadolinium also blocks L-type calcium channels in isolated ventricular myocytes of the guinea-pig. *Biochimica et Biophysica Acta*, 1191(1):205–208, April 20 1994.

[144] Lee, M. C., Fung, Y. C., Shabetai, R., and LeWinter, M. M. Biaxial mechanical properties of human pericardium and canine comparisons. *Am J Physiol*, 253(Heart Circ. Physiol. 22):H75–H82, Jul 1987.

[145] LeGrice, I. J., Hunter, P. J., and Smaill, B. H. Laminar structure of the heart: A mathematical model. *Am J Physiol*, 272(Heart Circ. Physiol. 41):H2466–H2476, May 1997.

[146] LeGrice, I. J., Smaill, B. H., Chai, L. Z., Edgar, S. G., Gavin, J. B., and Hunter, P. J. Laminar structure of the heart: Ventricular myocyte arrangement and connective tissue architecture in the dog. *Am J Physiol*, 269(Heart Circ. Physiol. 38):H571–H582, Aug 1995.

[147] Lekven, J., Chatterjee, K., Tyberg, J. V., and Parmley, W. W. Reduction in ventricular endocardial and epicardial potentials during acute increments in left ventricular dimensions. *American Heart Journal*, 98(2):200–206, Aug 1979.

[148] Lerman, B. B., Burkhoff, D., Yue, D. T., Franz, M. R., and Sagawa, K. Mechanoelectrical feedback: Independent role of preload and contractility in modulation of canine ventricular excitability. *J Clin Invest*, 76(5):1843–1850, Nov 1985. Published erratum appears in J. Clin. Invest. 1986 Jun, 77(6):2053.

[149] Lesh, M. D., Pring, M., and Spear, J. F. Cellular uncoupling can unmask dispersion of action potential duration in ventricular myocardium. A computer modeling study. *Circ Res*, 65(5):1426–1440, Nov 1989.

[150] Levine, J. H., Guarnieri, T., Kadish, A. H., White, R. I., Calkins, H., and Kan, J. S. Changes in myocardial repolarization in patients undergoing balloon valvuloplasty for congenital pulmonary stenosis: evidence for contraction-excitation feedback in humans. *Circulation*, 77(1):70–77, January 1988.

[151] Lew, W. Y., Nishikawa, Y., and Su, H. Cardiac myocyte function and left ventricular strains after brief ischemia and reperfusion in rabbits. *Circulation*, 90(4):1942–1950, October 1994.

[152] Lew, W. Y. W. Influence of ischemic zone size on nonischemic area function in the canine left ventricle. *Am J Physiol*, 252(Heart Circ. Physiol. 21):H990–H997, May 1987.

[153] Lin, D. H. S. and Yin, F. C. P. A multiaxial constitutive law for mammalian left ventricular myocardiumin steady-state barium contracture or tetanus. *J Biomech Eng*, 120(4):504–517, Aug 1998.

[154] Lindblad, D. S., Murphey, C. R., Clark, J. W., and Giles, W. R. A model of the action potential and underlying membrane currents in a rabbit atrial cell. *Am J Physiol*, 271(Heart Circ. Physiol. 40):H1666–H1696, Oct 1996.

[155] Link, M. S., Wang, P. J., Pandian, N. G., Bharati, S., Udelson, J. E., Lee, M. Y., Vecchiotti, M. A., VanderBrink, B. A., Mirra, G., Maron, B. J., and Estes, III, N. A. M. An experimental model of sudden death due to low-energy chest-wall impact (commotio cordis). *N Engl J Med*, 338(25):1805–1811, June 18 1998.

[156] Liu, D. W. and Antzelevitch, C. Characteristics of the delayed rectifier current (I_{Kr} and I_{Ks}) in canine ventricular epicardial, midmyocardial, and endocardial myocytes: A weaker I_{Ks} contributes to the longer action potential of the M cell. *Circ Res*, 76(3):351–365, Mar 1995.

[157] Luo, C.-H. and Rudy, Y. A model of the ventricular cardiac action potential: Depolarization, repolarization, and their interaction. *Circ Res*, 68(6):1501–1526, Jun 1991.

[158] Luo, C.-H. and Rudy, Y. A dynamic model of the cardiac ventricular action potential. I. Simulations of ionic currents and concentration changes. *Circ Res*, 74(6):1071–1096, Jun 1994.

[159] Luo, C.-H. and Rudy, Y. A dynamic model of the cardiac ventricular action potential. II. Afterdepolarizations, triggered activity, and potentiation. *Circ Res*, 74(6):1097–1113, Jun 1994.

[160] MacKenna, D. A., Vaplon, S. M., and McCulloch, A. D. Microstructural model of perimysial collagen fibers for resting myocardial mechanics during

ventricular filling. *Am J Physiol*, 273(Heart Circ. Physiol. 42):H1576–H1586, Sep 1997.

[161] Maron, B. J., Poliac, L. C., Kaplan, J. A., and Mueller, F. O. Blunt impact to the chest leading to sudden death from cardiac arrest during sports activities. *N Engl J Med*, 333(6):337–342, Aug 1995.

[162] Martinac, B., Adler, J., and Kung, C. Mechanosensitive ion channels of *E. coli* activated by amphipaths. *Nature*, 348(6298):261–263, 15 November 1990.

[163] May-Newman, K., Omens, J. H., Pavelec, R. S., and McCulloch, A. D. Three-dimensional transmural mechanical interaction between the coronary vasculature and passive myocardium in the dog. *Circ Res*, 74(6):1166–1178, Jun 1994.

[164] Mazhari, R., Omens, J. H., Waldman, L. K., and McCulloch, A. D. Regional myocardial perfusion and mechanics: a model-based method of analysis. *Ann Biomed Eng*, 26(5):743–755, Sep-Oct 1998.

[165] McAllister, R. E., Noble, D., and Tsien, R. W. Reconstruction of the electrical activity of cardiac Purkinje fibres. *J Physiol*, 251(1):1–59, Sep 1975.

[166] McCulloch, A., Waldman, L., Rogers, J., and Guccione, J. Large-scale finite element analysis of the beating heart. *Crit Rev Biomed Eng*, 20(5–6):427–449, 1992.

[167] McCulloch, A. D. Cardiac biomechanics. In J. D. Bronzino, editor, *Biomedical Engineering Handbook*, chapter 31, pages 418–439. CRC Press: IEEE Press, Boca Raton, 1995.

[168] McCulloch, A. D. and Omens, J. H. Factors affecting the regional mechanics of the diastolic heart. In L. Glass, P. Hunter, and A. McCulloch, editors, *Theory of Heart: Biomechanics, Biophysics, and Nonlinear Dynamics of Cardiac Function*, chapter 5, pages 87–119. Springer-Verlag, New York, 1991.

[169] McCulloch, A. D. and Omens, J. H. Non-homogeneous analysis of three-dimensional transmural finite deformation in canine ventricular myocardium. *J Biomech*, 24(7):539–548, 1991.

[170] McCulloch, A. D., Smaill, B. H., and Hunter, P. J. Regional left ventricular epicardial deformation in the passive dog heart. *Circ Res*, 64(4):721–733, Apr 1989.

[171] Message Passing Interface Forum. MPI: A message-passing interface standard. *Int J Supercomp Appl*, 8(3/4):169–416, Fall-Winter 1994.

[172] Mirsky, I. Ventricular and arterial wall stresses based on large deformation analyses. *Biophys J*, 13(11):1141–1159, Nov 1973.

[173] Mirsky, I. Elastic properties of the myocardium: a quantitative approach with physiological and clinical applications. In R. M. Berne, editor, *Handbook of Physiology, Section 2: The Cardiovascular System*, volume 1, chapter 14, pages 497–531. American Physiological Society, Bethesda, Maryland, 1979.

[174] Moore, C. C., O'Dell, W. G., McVeigh, E. R., and Zerhouni, E. A. Calculation of three-dimensional left ventricular strains from biplanar tagged MR images. *Journal of Magnetic Resonance Imaging*, 2(2):165–175, March-April 1992.

[175] Morgera, T., Baldi, N., Chersevani, D., Medugno, G., and Camerini, F. Chest thump and ventricular tachycardia. *PACE*, 2(1):69–75, Jan 1979.

[176] Morris, C. E. and Sigurdson, W. J. Stretch-inactivated ion channels coexist with stretch-activated ion channels. *Science*, 243(4892):807–809, February 10 1989.

[177] Näbauer, M., Beuckelmann, D. J., Überfuhr, P., and Steinbeck, G. Regional differences in current density and rate-dependent properties of the transient outward current in subepicardial and subendocardial myocytes of human left ventricle. *Circulation*, 93(1):168–177, 1 January 1996.

[178] Nagumo, J., Arimoto, S., and Yoshizawa, S. An active pulse transmission simulating nerve axon. *Proc IRE*, pages 2061–2070, Oct 1962.

[179] Naidu, S. and Kavaler, F. Interaction of sarcomere length and excitation-contraction coupling in ventricular myocardium. *Bulletin of the New York Academy of Medicine*, 47(10):1231, Oct 1971.

[180] Nazir, S. A. and Lab, M. J. Mechanoelectric feedback in the atrium of the isolated guinea-pig heart. *Cardiovasc Res*, 32(1):112–119, Jul 1996.

[181] Nielsen, P. M. F., LeGrice, I. J., Smaill, B. H., and Hunter, P. J. Mathematical model of geometry and fibrous structure of the heart. *Am J Physiol*, 260(Heart Circ. Physiol. 29):H1365–H1378, Apr 1991.

[182] Noble, D., Varghese, A., Kohl, P., and Noble, P. Improved guinea-pig ventricular cell model incorporating a diadic space, i_{Kr} and i_{Ks}, and length- and tension-dependent processes. *Canadian Journal of Cardiology*, 14(1):123–134, Jan 1998.

[183] Nour-Omid, B. and Parlett, B. N. Element preconditioning using splitting techniques. *SIAM J Sci Stat Comput*, 6(3):761–770, Jul 1985.

[184] Novak, V. P., Yin, F. C. P., and Humphrey, J. D. Regional mechanical properties of passive myocardium. *J Biomech*, 27(4):403–412, Apr 1994.

[185] O'Dell, W. G. and McCulloch, A. D. A novel numerical formulation for modeling tissue compressibility. *Proc ASME*, (in press), 1998.

[186] Omens, J. H. and Covell, J. W. Transmural distribution of myocardial tissue growth induced by volume-overload hypertrophy in the dog. *Circulation*, 84(3):1235–1245, Sep 1991.

[187] Omens, J. H., Farr, D. D., McCulloch, A. D., and Waldman, L. K. Comparison of two techniques for measuring two-dimensional strain in rat left ventricles. *Am J Physiol*, 271(Heart Circ. Physiol. 40):H1256–H1261, Sep 1996.

[188] Omens, J. H. and Fung, Y. C. Residual strain in rat left ventricle. *Circ Res*, 66(1):37–45, Jan 1990.

[189] Omens, J. H., MacKenna, D. A., and McCulloch, A. D. Measurement of strain and analysis of stress in resting rat left ventricular myocardium. *J Biomech*, 26(6):665–676, Jun 1993.

[190] Omens, J. H., May, K. D., and McCulloch, A. D. Transmural distribution of three-dimensional strain in the isolated arrested canine left ventricle. *Am J Physiol*, 261(Heart Circ. Physiol. 30):H918–H928, Sep 1991.

[191] Opie, L. H. *The Heart: Physiology, from Cell to Circulation*. Lippincott-Raven, Philadelphia, third edition, 1998.

[192] Osaka, T., Kodama, I., Tsuboi, N., Toyama, J., and Yamada, K. Effects of activation sequence and anisotropic cellular geometry on the repolarization phase of action potential of dog ventricular muscles. *Circulation*, 76(1):226–236, July 1987.

[193] Østerby, O. and Zlatev, Z. *Direct Methods for Sparse Matrices*, volume 157 of *Lecture Notes in Computer Science*. Springer-Verlag, New York, 1983.

[194] Owens, L. M., Fralix, T. A., Murphy, E., Cascio, W. E., and Gettes, L. S. Correlation of ischemia-induced extracellular and intracellular ion changes to cell-to-cell electrical uncoupling in isolated blood-perfused rabbit. *Circulation*, 94(1):10–13, July 1 1996.

[195] Panfilov, A. V. and Keener, J. P. Generation of reentry in anisotropic myocardium. *J Cardiovasc Electrophysiol*, 4(4):412–421, Aug 1993.

[196] Panfilov, A. V. and Keener, J. P. Re-entry in an anatomical model of the heart. *Chaos, Solitons, and Fractals*, 5(3/4):681–689, March/April 1995.

[197] Papadakis, J. S. Exact, nonreflecting boundary conditions for parabolic-type approximations in underwater acoustics. *Journal of Computational Acoustics*, 2(2):83–98, Jun 1994.

[198] Papadopoulos, P., Jones, R. E., and Solberg, J. M. A novel finite element formulation for frictionless contact problems. *Int J Numer Methods Eng*, 38(15):2603–2617, 15 August 1995.

[199] Parisch, H. A consistent tangent stiffness matrix for three-dimensional nonlinear contact analysis. *Int J Numer Methods Eng*, 28(8):1803–1812, Aug 1989.

[200] Pascarel, C., Hongo, K., Cazorla, O., White, E., and Le Guennec, J. Y. Different effects of gadolinium on I_{KR}, I_{KS} and I_{K1} in guinea-pig isolated ventricular myocytes. *Br J Pharmacol*, 124(2):356–360, May 1998.

[201] Pearlman, E. S., Weber, K. T., and Janicki, J. S. Quantitative histology of the hypertrophied human heart. *Federation Proceedings*, 40(7):2042–2047, May 15 1981.

[202] Pearlman, E. S., Weber, K. T., Janicki, J. S., Pietra, G. G., and Fishman, A. P. Muscle fiber orientation and connective tissue content in the hypertrophied human heart. *Laboratory Investigation*, 46(2):158–164, Feb 1982.

[203] Penefsky, Z. J. and Hoffman, B. F. Effects of stretch on mechanical and electrical properties of cardiac muscle. *Am J Physiol*, 204(3):433–438, 1963.

[204] Pertsov, A. M., Davidenko, J. M., Salomonsz, R., Baxter, W. T., and Jalife, J. Spiral waves of excitation underlie reentrant activity in isolated cardiac muscle. *Circ Res*, 72(3):631–650, Mar 1993.

[205] Pinsky, M. R., Perlini, S., Solda, P. L., Pantaleo, P., Calciati, A., and Bernardi, L. Dynamic right and left ventricular interactions in the rabbit: simultaneous measurement of ventricular pressure-volume loops. *Journal of Critical Care*, 11(2):65–76, June 1996.

[206] Pinto, J. G. and Fung, Y. C. Mechanical properties of the heart muscle in the passive state. *J Biomech*, 6(6):597–616, Nov 1973.

[207] Plonsey, R. and Barr, R. C. Current flow patterns in two-dimensional anisotropic bisyncytia with normal and extreme conductivities. *Biophys J*, 45(3):557–571, Mar 1984.

[208] Pollard, A. E., Spitzer, K. W., and Burgess, M. J. Contributions of the specialized conduction system to the activation sequence in the canine pulmonary conus. *Am J Physiol*, 273(Heart Circ. Physiol. 42):H446–H463, Jul 1997.

[209] Province, R. A., Fishler, M. G., and Thakor, N. V. Effects of defibrillation shock energy and timing on 3-D computer model of heart. *Ann Biomed Eng*, 21(1):19–31, 1993.

[210] Pye, M. P. and Cobbe, S. M. Arrhythmogenesis in experimental models of heart failure: the role of increased load. *Cardiovasc Res*, 32(2):248–257, Aug 1996.

[211] Reiter, M. J., Synhorst, D. P., and Mann, D. E. Electrophysiological effects of acute ventricular dilatation in the isolated rabbit heart. *Circ Res*, 62(3):554–562, Mar 1988.

[212] Reiter, M. J., Zetelaki, Z., Kirchhof, C. J., Boersma, L., and Allessie, M. A. Interaction of acute ventricular dilatation and d-sotalol during sustained reentrant ventricular tachycardia around a fixed obstacle. *Circulation*, 89(1):423–431, Jan 1994.

[213] Rice, J. J., Winslow, R. L., Dekanski, J., and McVeigh, E. Model studies of the role of mechano-sensitive currents in the generation of cardiac arrhythmias. *J Theor Biol*, 190(4):295–312, February 21 1998.

[214] Riemer, T. L., Sobie, E. A., and Tung, L. Stretch-induced changes in arrhythmogensis and excitability in experiementally based heart cell models. *Am J Physiol*, 275(Heart Circ. Physiol. 44):H431–H442, 1998.

[215] Riggs, D. S., Guarnieri, J. A., and Addelman, S. Fitting straight lines when both variables are subject to error. *Life Sciences*, 22(13–15):1305–1360, April 3–17 1978.

[216] Robb, J. S. and Robb, R. C. The normal heart: Anatomy and physiology of the structural units. *American Heart Journal*, 23:455–467, 1942.

[217] Robinson, T. F., Cohen-Gould, L., and Factor, S. M. Skeletal framework of mammalian heart muscle. Arrangement of inter- and pericellular connective tissue structures. *Laboratory Investigation*, 49(4):482–498, Oct 1983.

[218] Robinson, T. F., Geraci, M. A., Sonnenblick, E. H., and Factor, S. M. Coiled perimysial fibers of papillary muscle in rat heart: morphology, distribution, and changes in configuration. *Circ Res*, 63(3):577–592, Sep 1988.

[219] Rodriguez, E. K., Omens, J. H., Waldman, L. K., and McCulloch, A. D. Effect of residual stress on transmural sarcomere length distributions in rat left ventricle. *Am J Physiol*, 264(Heart Circ. Physiol. 33):H1048–H1056, Apr 1993.

[220] Rogers, J. M., Courtemenche, M. S., and McCulloch, A. D. Finite element methods for modelling impulse propagation in the heart. In A. V. Panfilov and A. V. Holden, editors, *Computational Biology of the Heart*, chapter 7, pages 217–234. J. Wiley & Sons Ltd., West Sussex, England, 1997.

[221] Rogers, J. M. and McCulloch, A. D. A collocation-Galerkin finite element model of cardiac action potential propagation. *IEEE Trans Biomed Eng*, 41(8):743–757, Aug 1994.

[222] Rogers, J. M. and McCulloch, A. D. Nonuniform muscle fiber orientation causes spiral wave drift in a finite element model of cardiac action potential propagation. *J Cardiovasc Electrophysiol*, 5(6):496–509, Jun 1994.

[223] Ross, M. A. and Streeter, Jr., D. D. Nonuniform subendocardial fiber orientation in the normal macaque left ventricle. *European Journal of Cardiology*, 3(3):229–247, Oct 1975.

[224] Roth, B. J. How the anisotropy of the intracellular and extracellular conductivities influences stimulation of cardiac muscle. *J Math Biol*, 30(6):633–646, 1992.

[225] Rudy, Y. and Quan, W. A model study of the effects of the discrete cellular structure on electrical propagation in cardiac tissue. *Circ Res*, 61(6):815–823, Dec 1987.

[226] Ruknudin, A., Sachs, F., and Bustamante, J. O. Stretch-activated ion channels in tissue-cultured chick heart. *Am J Physiol*, 264(Heart Circ. Physiol. 33):H960–H972, Mar 1993.

[227] Ruknudin, A., Song, M. J., and Sachs, F. The ultrastructure of patch-clamped membranes: A study using high voltage electron microscopy. *J Cell Biology*, 112(1):125–134, Jan 1991.

[228] Saad, Y. Highly parallel preconditioners for general sparse matrices. In *Recent Advances in Iterative Methods*, volume 60 of *The IMA Volumes in Mathematics and its Applications*, pages 165–199. Springer-Verlag, New York, 1994. Papers from the IMA Workshop on Iterative Methods for Sparse and Structured Problems, held in Minneapolis MN, February 24–March 1, 1992.

[229] Saad, Y. *Iterative Methods for Sparse Linear Systems*. PWS Pub. Co., Boston, 1996.

[230] Saad, Y., Lo, G.-C., and Kuznetsov, S. *PSPARSLIB Users Manual: A Portable Library of parallel Sparse Iterative Solvers*. University of Minnesota, Department of Computer Science, 200 Union Street S.E., Minneapolis, MN 55455, Jan 1998. Available from `http://www.cs.umn.edu/Research/arpa/p_sparslib/psp/DOCS/manual.ps`.

[231] Sachs, F. Mechanical transduction by membrane ion channels: A mini review. *Mol Cell Biochem*, 104(1/2):57–60, May/June 1991.

[232] Sachs, F. Stretch-sensitive ion channels: An update. In D. P. Corey and S. D. Roper, editors, *Sensory Transduction*, volume 47 of *Society of General Physiologists Series*, chapter 15, pages 241–260. Rockefeller University Press, New York, 1992. Society of General Physiologists, 45th annual symposium, Marine Biological Laboratory, Woods Hole, Massachusetts, 5–8 September 1991.

[233] Sachs, F. Modeling mechanical-electrical transduction in the heart. In V. C. Mow, F. Guilak, R. M. Hochmuth, and R. Tran-Son-Tay, editors, *Cell Mechanics and Cellular Engineering*, chapter 18, pages 308–328. Springer-Verlag, New York, 1994.

[234] Sachs, F. Mechanosensitive channels: Lost in space (abstract). *Biophys J*, 76(1):A3, Jan 1998. Abstract Supplement for the Biophysical Society 43rd Annual Meeting, February 13–17, 1999, Baltimore, Maryland.

[235] Saffitz, J. E., Kanter, H. L., Green, K. G., Tolley, T. K., and Beyer, E. C. Tissue-specific determinants of anisotropic conduction velocity in canine atrial and ventricular myocardium. *Circ Res*, 74(6):1065–1070, Jun 1994.

[236] Salinger, A. G., Xiao, Q., Zhou, Y., and Derby, J. J. Massively parallel finite element computations of three-dimensional, time-dependent, incompressible flows in materials processing systems. *Comp Meth Appl Mech Eng*, 119(1–2):139–156, Nov 1994. Symposium on Parallel Finite Element Computations, Minneapolis, MN, USA; 25–27 Oct. 1993.

[237] Santamore, W. P., Lynch, P. R., Meier, G., Heckman, J., and Bove, A. A. Myocardial interaction between the ventricles. *J Appl Physiol*, 41(3):362–368, Sep 1976.

[238] Sasaki, N., Mitsuiye, T., and Noma, A. Effects of mechanical stretch on membrane currents of single ventricular myocytes of guinea-pig heart. *Japanese Journal of Physiology*, 42(6):957–970, 1992.

[239] Schalij, M. J., Lammers, W. J. E. P., Rensma, P. L., and Allessie, M. A. Anisotropic conduction and reentry in perfused epicardium of rabbit left ventricle. *Am J Physiol*, 263(Heart Circ. Physiol. 32):H1466–H1478, November 1992.

[240] Scollan, D. F., Holmes, A., Winslow, R., and Forder, J. Histological validation of myocardial microstructure obtained from diffusion tensor magnetic resonance imaging. *Am J Physiol*, 275(Heart Circ. Physiol. 44):H2308–2318, December 1998.

[241] Shampine, L. F. *Numerical Solution of Ordinary Differential Equations*. Chapman & Hall, New York, 1994.

[242] Sicouri, S. and Antzelevitch, C. Afterdepolarizations and triggered activity develop in a select population of cells (M cells) in canine ventricular myocardium: the effects of acetylstrophanthidin and Bay K 8644. *PACE*, 14(11 Part 2):1714–1720, Nov 1991.

[243] Sicouri, S. and Antzelevitch, C. Drug-induced afterdepolarizations and triggered activity occur in a discrete subpopulation of ventricular muscle cells (M cells) in the canine heart: quinidine and digitalis. *J Cardiovasc Electrophysiol*, 4(1):48–58, Feb 1993.

[244] Sideris, D. A., Toumanidis, S. T., Kostopoulos, K., Pittaras, A., Spyropoulos, G. S., Kostis, E. B., and Moulopoulos, S. D. Effect of acute ventricular pressure changes on QRS duration. *J Electrocardiol*, 27(3):199–202, Jul 1994.

[245] Sigurdson, W., Ruknudin, A., and Sachs, F. Calcium imaging of mechanically induced fluxes in tissue-cultured chick heart: Role of stretch-activated ion channels. *Am J Physiol*, 262(Heart Circ. Physiol. 31):H1110–H1115, Apr 1992.

[246] Sigurdson, W. J., Morris, C. E., Brezden, B. L., and Gardner, D. R. Stretch activation of a K^+ channel in molluscan heart cells. *Journal of Experimental Biology*, 127:191–209, Jan 1987.

[247] Silicon Graphics, Inc. CRAY T3E datasheets. Technical report, Silicon Graphics, Inc., `http://www.sgi.com/t3e/t3e_1200.html`, 1999.

[248] Singer, D. H., Lazzara, R., and Hoffman, B. F. Interrelationship between automaticity and conduction in Purkinje fibers. *Circ Res*, 21(4):537–558, Oct 1967.

[249] Smaill, B. H. and Hunter, P. J. Structure and function of the diastolic heart. In L. Glass, P. Hunter, and A. McCulloch, editors, *Theory of Heart: Biomechanics, Biophysics, and Nonlinear Dynamics of Cardiac Function*, chapter 1, pages 1–29. Springer-Verlag, New York, 1991.

[250] Sonnenblick, E. H., Ross, Jr., J., Covell, J. W., Spotnitz, H. M., and Spiro, D. The ultrastructure of the heart in systole and diastole. Changes in sarcomere length. *Circ Res*, 21(4):423–431, October 1967.

[251] Spach, M. S., Miller, III, W. T., Geselowitz, D. B., Barr, R. C., Kootsey, J. M., and Johnson, E. A. The discontinuous nature of propagation in normal canine cardiac muscle. Evidence for recurrent discontinuities of intracellular resistance that affect the membrane currents. *Circ Res*, 48(1):39–54, Jan 1981.

[252] Spencer, A. J. M. *Continuum Mechanics*. Longman, New York, 1980.

[253] Stacy, Jr., G. P., Jobe, R. L., Taylor, L. K., and Hansen, D. E. Stretch-induced depolarizations as a trigger of arrhythmias in isolated canine left ventricles. *Am J Physiol*, 263(Heart Circ. Physiol. 32):H613–H621, Aug 1992.

[254] Streeter, Jr., D. D. Gross morphology and fiber geometry of the heart. In R. M. Berne, editor, *Handbook of Physiology, Section 2: The Cardiovascular System*, volume 1, chapter 4, pages 61–112. American Physiological Society, Bethesda, Maryland, 1979.

[255] Streeter, Jr., D. D. and Bassett, D. L. An engineering analysis of myocardial fiber orientation in pig's left ventricle in systole. *Anat Rec*, 155(4):503–512, Aug 1966.

[256] Streeter, Jr., D. D. and Hanna, W. T. Engineering mechanics for successive states in canine left ventricular myocardium: I. Cavity and wall geometry. *Circ Res*, 33:639–655, Dec 1973.

[257] Streeter, Jr., D. D. and Hanna, W. T. Engineering mechanics for successive states in canine left ventricular myocardium: II. Fiber angle and sarcomere length. *Circ Res*, 33:656–664, Dec 1973.

[258] Streeter, Jr., D. D., Powers, W. E., Ross, M. A., and Torrent-Guasp, F. Three-dimensional fiber orientation in the mammalian left ventricular wall. In J. Baan, A. Noordergraaf, and J. Raines, editors, *Cardiovascular System Dynamics*, chapter 9, pages 73–84. MIT Press, Cambridge, Mass., 1978.

[259] Streeter, Jr., D. D., Spotnitz, H. M., Patel, D. P., Ross, Jr., J., and Sonnenblick, E. H. Fiber orientation in the canine left ventricle during diastole and systole. *Circ Res*, 24(3):339–347, Mar 1969.

[260] Taber, L. A. On a nonlinear theory for muscle shells: Part II — Application to the beating left ventricle. *J Biomech Eng*, 113(1):63–71, Feb 1991.

[261] Taggart, P., Sutton, P., Lab, M. J., Runnalls, M., O'Brien, W., and Treasure, T. Effect of abrupt changes in ventricular loading on repolarization induced by transient aortic occlusion in humans. *Am J Physiol*, 263(Heart Circ. Physiol. 32):H816–H823, Sep 1992.

[262] Taggart, P., Sutton, P. M., Treasure, T., Lab, M., O'Brien, W., Runnalls, M., Swanton, R. H., and Emanuel, R. W. Monophasic action potentials at discontinuation of cardiopulmonary bypass: evidence for contraction-excitation feedback in man. *Circulation*, 77(6):1266–1275, Jun 1988.

[263] Taggart, P. and Sutton, P. M. I. Cardiac mechano-electric feedback in man: clinical relevance. *Prog Biophys Mol Biol*, 71:139–154, 1999.

[264] ter Keurs, H. E., Rijnsburger, W. H., van Heuningen, R., and Nagelsmit, M. J. Tension development and sarcomere length in rat cardiac trabeculae: Evidence of length-dependent activation. *Circ Res*, 46(5):703–714, May 1980.

[265] Tezduyar, T., Behr, M., Mittal, S., and Johnson, A. A. Computation of unsteady incompressible flows with stabilized finite element methods: Space-time formulations, iterative strategies and massively parallel implementations. In P. Smolinski, editor, *New methods in Transient Analysis*, PVP-Vol. 246/AMD-Vol. 143, pages 7–24, New York, 1992. ASME. Presented at the Winter Annual Meeting of the American Society of Mechanical Engineers, Anaheim, California, November 8–13, 1992.

[266] Torrent-Guasp, F. *The Cardiac Muscle*. Publications of the Juan March Foundation. Editorial Graficas Torroba, Madrid, Spain, 1973. Translation of El musculo cardiaco.

[267] Tsadok, S. *Fiber and Sheet Strain Distributions in Ventricular Myocardium Referred to the Stress-Free State*. Master's thesis, University of California, La Jolla, California, 1998.

[268] van Gijzen, M. B. An element-by-element solution algorithm for nonsymmetric linear systems of equations. In J. F. Dijksman and F. T. M. Nieuwstadt, editors, *Integration of Theory and Applications in Applied Mechanics*, pages 295–304, Boston, 1990. Kluwer Academic Publishers. Choice of papers presented at the First National Mechanics Congress, April 2-4, 1990, Rolduc, Kerkrade, the Netherlands.

[269] Van Leuven, S. L., Waldman, L. K., McCulloch, A. D., and Covell, J. W. Gradients of epicardial strain across the perfusion boundary during acute myocardial ischemia. *Am J Physiol*, 267(Heart Circ. Physiol. 36):H2348–H2362, Dec 1994.

[270] Vesalius, A. *The Epitome of Andreas Vesalius*. M.I.T. Press, Cambridge, Mass., 1969. Translated from the Latin by L. R. Lind.

[271] Villarreal, F. J., Lew, W. Y., Waldman, L. K., and Covell, J. W. Transmural myocardial deformation in the ischemic canine left ventricle. *Circ Res*, 68(2):368–381, February 1991.

[272] Villarreal, F. J., Waldman, L. K., and Lew, W. Y. Technique for measuring regional two-dimensional finite strains in canine left ventricle. *Circ Res*, 62(4):711–721, Apr 1988.

[273] Waldman, L. K. Multidimensional measurement of regional strains in the intact heart. In L. Glass, P. Hunter, and A. McCulloch, editors, *Theory of Heart: Biomechanics, Biophysics, and Nonlinear Dynamics of Cardiac Function*, chapter 7, pages 145–174. Springer-Verlag, New York, 1991.

[274] Waldman, L. K., Fung, Y. C., and Covell, J. W. Transmural myocardial deformation in the canine left ventricle: Normal in vivo three-dimensional finite strains. *Circ Res*, 57(1):152–163, Jul 1985.

[275] Waldman, L. K., Nosan, D., Villarreal, F., and Covell, J. W. Relation between transmural deformation and local myofiber direction in canine left ventricle. *Circ Res*, 63(3):550–62, Sep 1988.

[276] Wang, Z., Taylor, L. K., Denney, W. D., and Hansen, D. E. Initiation of ventricular extrasystoles by myocardial stretch in chronically dilated and failing canine left ventricle. *Circulation*, 90(4):2022–2031, Oct 1994.

[277] Wathen, A. J. An analysis of some element-by-element techniques. *Comp Meth Appl Mech Eng*, 74(3):271–287, Sep 1989.

[278] Watkins, M. W., Higashiyama, A., Chen, Z., and LeWinter, M. M. Rapid shortening during relaxation increases activation and improves systolic performance. *Circulation*, 94(6):1475–1482, September 15 1996.

[279] Watkins, M. W., Slinker, B. K., Goto, Y., and LeWinter, M. M. 2,3-Butanedione monoxime increases contractile efficiency in the rabbit ventricle. *Am J Physiol*, 263(Heart Circ. Physiol. 32):H1811–H1818, Dec 1992.

[280] Weber, K. T. Cardiac interstitium in health and disease: The fibrillar collagen network. *J Am Coll Cardiol*, 13(7):1637–1652, Jun 1989.

[281] Whalley, D. W., Wendt, D. J., and Grant, A. O. Basic concepts in cellular cardiac electrophysiology: Part II: Block of ion channels by antiarrhythmic drugs. *PACE*, 18(9 Part I):1686–1704, Sep 1995.

[282] White, E., Le Guennec, J.-Y., Nigretto, J. M., Gannier, F., Argibay, J. A., and Garnier, D. The effects of increasing cell length on auxotonic contractions; membrane potential and intracellular calcium transients in single guinea-pig ventricular myocytes. *Exp Physiol*, 78(1):65–78, Jan 1993.

[283] Wilby, M. R., Lab, M. J., and Holden, A. V. Dynamical model of signal propagation in the heart. *J Theor Biol*, 168(4):399–406, Jun 1994.

[284] Winfree, A. T. Varieties of spiral wave behavior: An experimentalist's approach to the theory of excitable media. *Chaos*, 1(3):303–334, 1991.

[285] Winfree, A. T. Persistent tangled vortex rings in generic excitable media. *Nature*, 371(6494):233–236, September 15 1994.

[286] Winget, J. M. and Hughes, T. J. R. Solution algorithms for nonlinear transient heat conduction analysis employing element-by-element iterative strategies. *Comp Meth Appl Mech Eng*, 52:711–815, 1985.

[287] Winslow, R. L., Rice, J., Jafri, S., Marbán, E., and O'Rourke, B. Mechanisms of altered excitation-contraction coupling in canine tachycardia-induced heart failure, II model studies. *Circ Res*, 84:571–586, 19 March 1999.

[288] Yang, X.-C. and Sachs, F. Block of stretch-activated ion channels in Xenopus oocytes by gadolinium and calcium ions. *Science*, 243(4894 Part 1):1068–1071, February 24 1989.

[289] Yang, X. C. and Sachs, F. Mechanically sensitive, nonselective cation channels. *Exs*, 66:79–92, 1993.

[290] Yeckel, A. and Derby, J. J. Parallel computation of incompressible flows in materials processing: Numerical experiments in diagonal preconditioning. *Parallel Computing*, 23(9):1379–1400, Sep 1997.

[291] Yin, F. C. Ventricular wall stress. *Circ Res*, 49(4):829–842, Oct 1981.

[292] Yin, F. C. P., Chan, C. C., and Judd, R. M. Compressibility of perfused passive myocardium. *Am J Physiol*, 271(Heart Circ. Physiol. 40):H1864–H1870, Nov 1996.

[293] Yin, F. C. P., Strumpf, R. K., Chew, P. H., and Zeger, S. L. Quantification of the mechanical properties of noncontracting canine myocardium under simultaneous biaxial loading. *J Biomech*, 20(6):577–589, 1987.

[294] Young, A. A. and Axel, L. Three-dimensional motion and deformation of the heart wall: estimation with spatial modulation of magnetization — a model-based approach. *Radiology*, 185(1):241–247, Oct 1992.

[295] Young, A. A., Kramer, C. M., Ferrari, V. A., Axel, L., and Reichek, N. Three-dimensional left ventricular deformation in hypertrophic cardiomyopathy. *Circulation*, 90(2):854–867, Aug 1994.

[296] Young, A. A., LeGrice, I. J., Young, M. A., and Smaill, B. H. Extended confocal microscopy of myocardial laminae and collagen network. *Journal of Microscopy*, 192(Pt 2):139–150, Nov 1998.

[297] Zabel, M., Koller, B. S., Sachs, F., and Franz, M. R. Stretch-induced voltage changes in the isolated beating heart: Importance of the timing of stretch and implications for stretch-activated ion channels. *Cardiovasc Res*, 32(1):120–130, July 1996.

[298] Zabel, M., Portnoy, S., and Franz, M. R. Effect of sustained load on dispersion of ventricular repolarization and conduction time in the isolated intact rabbit heart. *J Cardiovasc Electrophysiol*, 7(1):9–16, Jan 1996.

[299] Zeng, J., Laurita, K. R., Rosenbaum, D. S., and Rudy, Y. Two components of the delayed rectifier K^+ current in ventricular myocytes of the guinea pig type: Theoretical formulation and their role in repolarization. *Circ Res*, 77(1):140–152, June 1995.

[300] Zhong, Z.-H. and Mackerle, J. Static contact problems — a review. *Engineering Computations*, 9:3–37, 1992.

[301] Zipes, D. P. and Jalife, J., editors. *Cardiac Electrophysiology: From Cell to Bedside*. W. B. Saunders, Philadelphia, second edition, 1995.